Nadja Rebecca Brun

Ecotoxicological Assessment of Organic Photovoltaics

DISS. ETH NO. 23256
2016

DISS. ETH NO. 23256

ECOTOXICOLOGICAL ASSESSMENT OF ORGANIC PHOTOVOLTAICS

A thesis submitted to attain the degree of

DOCTOR OF SCIENCES of ETH ZURICH

(Dr. sc. ETH Zurich)

presented by

NADJA REBECCA BRUN

MSc in Environmental Geosciences, University of Basel

born on September 16, 1984

citizen of Klingnau AG

accepted on the recommendation of

Prof. Dr. Bernhard Wehrli, examiner

Prof. Dr. Karl Fent, co-examiner

Prof. Dr. Thomas Braunbeck, co-examiner

2016

Nadja Rebecca Brun

Ecotoxicological Assessment of Organic Photovoltaics

PhD thesis ETH Zurich, Switzerland

for Norbert

ACKNOWLEDGEMENTS

CONTENTS

SUMMARY

Renewable energy sources are evolving rapidly to address today's global climate and energy challenges. And with it, the worldwide installed solar photovoltaics increased exponentially over the past years. There is a negligible risk of environmental contamination during routine operation of photovoltaics, but it remains an open question whether their decommissioning and uncontrolled disposal could pose environmental risks. Some photovoltaics contain hazardous materials such as cadmium and other heavy metals, raising environmental and human health concerns regarding the end-of-life disposal of photovoltaic panels. In this thesis, the focus was set on thin-film photovoltaics based on organic polymers, so called organic photovoltaics (OPV). This technology is still under development but predicted to gain market share in the near future due to its potential to be flexible, low cost, low weight, semi-transparent, and easily to be integrated into different applications. Ensuring an environmentally sound device must be the aim before production amount increase. Therefore, the potential ecotoxicological risks of single compounds used in OPV, as well as of product leachates of OPVs were assessed. This work contributes to a hazard and risk assessment of this new technology.

Metals including zinc, indium, and aluminum were identified as compounds of toxicological relevance but with knowledge gaps. Thus, the selected metals were screened for various toxicological activities in zebrafish embryos (*Danio rerio*) and waterfleas (*Daphnia magna*) using molecular and phenotypic endpoints. Gene expression analysis revealed new insights on molecular mode of actions. We showed in zebrafish that zinc is a potential inducer of a pro-inflammatory response while indium can trigger an endoplasmic reticulum stress (ER) response. Indications on the transcription level for an ER stress response were also found when exposing zebrafish embryos to weathering leachates from OPVs. Leachates were produced under different environmental condition to assess the consequences of OPV dumping close to lake and marine environments, or simulating acidic rain run-off from broken devices on roof tops. The lake water leached zinc only and no alterations on the abundance of assessed target genes or phenotypic effects were measured. Whereas harsher conditions such as acidic rain water leached copper and zinc inducing transcriptional changes of ER stress related genes. Seawater leachates containing silver and zinc altered several biologically relevant target genes and significantly reduced hatching success of zebrafish embryos.

Metallic compounds in electronic devices including OPVs are frequently applied in form of nanoparticles due to their unique electronic and photonic properties. The increasing use of nanotechnology in material sciences and consumer products inevitably leads to their release into the environment where they may have an impact on organisms. Uptake across cell membrane is expected to be facilitated and occur through diffusion or endocytosis. Thus, different cellular compartments or mode of actions might be affected in comparison to soluble metals which are taken up through ion transporters. In the work presented here, ZnO and ITO nanoparticles and corresponding concentrations of released zinc and indium were compared on molecular and morphological level for its toxicity. Moreover, it

is recognized that nanoparticles may have unusual physico-chemical properties and behaviors in water, which was addressed with an adapted exposure set up in this thesis.

OPVs and electronic waste in general are likely to contaminate the environment with a mixture of metals, if not handled properly. Therefore, mixture toxicity of indium and aluminum was investigated in detail in *Daphnia magna*. It is a generally accepted mixture concept that effects of two single compounds simply can be added up to predict its mixture toxicity. However, it becomes more and more evident that compounds in a mixture might interact chemically with each other or at molecular level by affecting additional pathways. In collaboration with the University of Birmingham (UK) and the University of Basel (Switzerland), we chose a global transcriptional profiling to explore differentially expressed genes after exposure to single metals, compared it to affected genes in the mixture treatment, and related it to adverse phenotypic response in chronic exposures. The target gene approach used throughout this work allows early detection of affected functional pathways. However, the predictive power is not fully understood and thus needs to be causally linked to events at different levels of biological organization. This concept was applied in this last study.

This thesis makes an important contribution to the scientific basis for the ecotoxicological risk assessment of OPVs. Novel molecular responses (e.g. ER stress) of single metals are described potentially serving as early marker for metal contaminated ecosystems in the near future. In the comparative assessment of ZnO nanoparticles and soluble zinc no differences in effects could be shown, suggesting effects mainly related to released soluble zinc. Furthermore, a metal mixture was shown to activate additional pathways suggesting that effect concentrations are likely to be underestimated for compounds occurring in mixtures in the environment. Phenotypic effects are described and used to predict potential adverse outcome at organism level allowing a risk evaluation, although not comprehensive. Metals leaching from OPVs at their end-of-life might exhibit ecotoxicological implications if dumped in larger quantities close to marine environments or exposed to acidic rain. Promising is that in comparison to another commercially available thin-film photovoltaic, OPV was shown to be of lesser environmental concern. The results presented in this thesis strongly suggest to reduce inorganic contents in photovoltaics and to promote take-back obligations and metal recycling from photovoltaics and e-waste in general.

ZUSAMMENFASSUNG

Die Klimaerwärmung zusammen mit den limitierten fossilen Energieressourcen treibt die Entwicklung neuer Technologien zur Nutzung erneuerbarer Energien an. Damit geht auch ein exponentieller Anstieg der weltweit installierten Photovoltaikanlagen über die letzten Jahre einher. Zwar werden während des Betriebs von Photovoltaik keine Emissionen in die Umwelt erwartet, jedoch bleibt die Frage nach dem potentiellen Umweltrisiko bei der unkontrollierten Entsorgung und Stilllegung von Anlagen offen. Einige Photovoltaik Typen enthalten gefährlich Stoffe wie Cadmium und andere Schwermetalle, welche Bedenken bezüglich der Umweltbelastung und menschlicher Gesundheit wecken. In der hier vorliegenden Dissertation richtet sich der Fokus auf die organische Solarzelle, basierend auf leitfähigen, organischen Materialien. Diese Technologie steckt zwar noch in der Entwicklung, ist jedoch besonders zukunftsträchtig: Geringe Energie- und Rohstoffkosten in der Herstellung sowie neue Anwendungsmöglichkeiten dank ihrer Flexibilität und Transparenz. Bevor es aber in die Grossproduktion geht, muss die Umweltfreundlichkeit dieses Produkts gewährleistet sein. Deshalb wurden in dieser Arbeit die potentiellen ökotoxikologischen Risiken von einzelnen Komponenten der organischen Solarzelle, als auch deren Auswaschungen untersucht. Damit trägt diese Arbeit wesentlich zur Gefahren- und Risikobewertung dieser neuen Technologie bei.

Metalle wie Zink, Indium, und Aluminium wurden als Komponenten von toxikologischer Relevanz, jedoch mit limitierten Kenntnissen, identifiziert. Daher wurden diese Metalle hinsichtlich verschiedener toxikologischer Aktivitäten in Embryonen des Zebrabärblings (*Danio rerio*) und Wasserflöhen (*Daphnia magna*), mittels molekularer und phänotypischer Endpunkte geprüft. In Zebrabärblingen haben wir gezeigt, dass Zink ein entzündungsförderndes Potential aufweist, während Indium eine Stressreaktion im endoplasmatischen Retikulum (ER) auslöst. Ebenfalls wurde erhöhte Transkription von ER-Stress Genen in Embryonen des Zebrabärblings gemessen, welche den Auswaschungen aus organischen Solarzellen exponiert wurden. Bei der Herstellung der Auswaschungen wurden unterschiedliche Umweltbedingungen berücksichtigt, um einerseits die Konsequenzen von unsachgemässer Entsorgung organischer Solarzellen in der Nähe von Süss- und Meerwasser sowie andererseits den Einfluss sauren Regens auf stillgelegte Anlagen zu simulieren. Das Süsswasser wusch nur Zink aus und hatte keinen Einfluss auf die Abundanz der Transkripte der untersuchten Ziel-Gene oder die phänotypischen Endpunkte in den exponierten Embryonen. Im Gegensatz dazu führten rauere Bedingungen wie saurer Regen zur Auswaschung von Kupfer und Zink, was die transkriptionelle Aktivität von ER-Stress Genen veränderte. Die Meerwasser Auswaschung enthielt Silber und Zink, was die Regulierung mehrere Gene aus biologisch relevanten Prozessen beeinflusste und die Schlupfrate der Embryonen des Zebrabärblings signifikant reduzierte.

In elektronischen Geräten wie organischen Solarzellen werden metallische Komponenten oft in Form von Nanopartikeln integriert, auf Grund ihrer einzigartigen elektronischen und photonischen Eigenschaften. Die zunehmende Verwendung von Nanopartikeln in Materialwissenschaften und Konsumgütern führt zwangsläufig zu deren Freisetzung in

die Umwelt, wo sie Auswirkungen auf die Organismen haben können. Es ist zu erwarten, dass die Aufnahme über die Zellmembran vereinfacht ist und durch Diffusion oder Endozytose stattfindet. Daher könnten andere Zellkompartimente betroffen oder molekulare Prozesse beeinflusst sein als bei kationischen Metallen, welche über Ionentransporter aufgenommen werden. Darüber hinaus ist bekannt, dass Nanopartikel ungewöhnliche physikalisch-chemische Eigenschaften, auch in Bezug auf ihr Verhalten im Wasser, mit sich bringen, was für die Expositionen in dieser Arbeit berücksichtigt wurde.

Es kann davon ausgegangen werden, dass unsachgemäss entsorgte organische Solarzellen sowie Elektronikschrott im Allgemeinen, die Umwelt zukünftig mit Metallmischungen belasten werden. Aus diesem Grund wurde im Rahmen von dieser Dissertation die Mischungstoxizität von Indium und Aluminium auf *Daphnia magna* untersucht. Es ist allgemein anerkannt, dass die Effekte zweier Einzelsubstanzen addiert werden können um deren Mischungstoxizität vorauszusagen. Allerdings häufen sich Studien die zeigen, dass Substanzen in Mischungen miteinander interagieren oder zusätzliche Signalwege aktivieren. In Kollaboration mit der Universität Birmingham (UK) und der Universität Basel (Schweiz) haben wir mittels genomweiter Transkriptionsprofile unterschiedlich exprimierte Gene nach Exposition mit Einzelmetallen mit jenen aus der Metallmischung verglichen und einige der gemessenen Effekte mit phänotypischen Auswirkungen aus der chronischen Exposition in Beziehung gebracht. Der in dieser Arbeit verwendete Zielgen-Ansatz erlaubt Früherkennung von betroffenen biologisch wichtigen Signalwegen. Jedoch gilt es zu beachten, dass die Voraussagekraft bezüglich nachteiliger Folgen für den Organismus noch nicht vollständig geklärt ist und daher ist die Verbindung von Genexpression und phänotypischen Auswirkungen notwendig. Dieses Konzept wurde in der letzten Studie angewendet.

Diese Dissertation leistet einen wichtigen Beitrag für die wissenschaftliche Grundlage der ökotoxikologischen Risikobewertung organischer Solarzellen. Bisher unbekannte biologische Aktivitäten von Einzelmetallen wurden beschrieben, die möglicherweise in naher Zukunft als Biomarker für metallkontaminierte Ökosysteme eingesetzt werden könnten. Die vergleichende Beurteilung von ZnO Nanopartikeln und löslichem Zink zeigte keine unterschiedlichen Effekte, was auf Effekte induziert von löslichem Zink hindeutet. Ausserdem verstärken die synergistisch wirkenden Metallmischungen den Verdacht, dass Effektkonzentrationen von Einzelsubstanzen oftmals unterschätzt werden wenn sie in Mischungen in der Umwelt vorkommen. Die Genexpressionsdaten wurden, wenn möglich, mit phänotypischen Effekten ergänzt, was die Vorhersage nachteiliger Folgen für Organismen und damit eine Risikobeurteilung ermöglicht, wenn auch nicht vollständig. Metalle die von organischen Solarzellen nach ihrem Gebrauch ausgewaschen werden, können ökotoxikologische Folgen mit sich bringen wenn sie in grösseren Mengen in mariner Umgebung entsorgt oder saurem Regen ausgesetzt werden. Es kann jedoch durchaus positiv gewertet werden, dass im Vergleich zu einer anderen bereits kommerziell produzierten Solarzelle, die organische Solarzelle ökologisch weniger bedenklich ist. Die Resultate dieser Dissertation geben starken Anlass zur Empfehlung, dass in Solarzellen anorganische Komponenten reduziert werden und Rücknahmepflicht sowie Metall-Recycling aus Photovoltaik und Elektroschrott im Generellen gefördert werden soll.

1

INTRODUCTION

1.1 Rationale

Renewable energy sources are the solution to overcome the worldwide increasing thirst for energy. Fossil fuels, including coal, oil, and natural gas, are limited. Current estimates assume that reserves will be exhausted in 35 to 245 years (Cho, 2010). Additionally, a problem caused by fossil fuels is the CO_2 emission, being the most important actor for global warming. Recent climate change-related extremes include droughts, floods, cyclones, and wildfires causing alterations in ecosystems, disruption of food production, and water supply (IPCC, 2014). Measured on final energy consumption, electricity production is the largest contributor of greenhouse gases and therefore global warming (IPCC, 2007).

Taking advantage of the nearly endless supply, solar energy is an important part of the renewable and clean energy solution. Photovoltaics (PVs) are particularly useful to generate power in rural areas where grid-connected power is not always reliable (e.g. for water pumping and street lighting in developing countries) and find increasing use in a wide range of consumer products. The installed photovoltaic current capacity of nearly 200 gigawatts will double or even triple by 2020 to up to 700 gigawatts (IEA 2015; Fraunhofer ISE 2015). PVs are considered a clean energy source and indeed, during its use phase no release of harmful compounds to climate or the living environment is expected. However, a major unknown variable is the fate and effects PV panels have after use. This thesis focuses on the ecotoxicological effects of a specific PV taking into account its compounds used and released (Figure 1.1).

Learning from the past, it is our responsibility to manufacture a product which is safe for human health and environment throughout its lifecycle. Under any circumstances, further contribution to our unsolved electronic waste problem has to be prevented. Despite the Basel Convention stating that electronic waste containing hazardous elements may not be exported to developing countries for disposal (UNEP 1995), electronic waste is current-ly shipped to the poorest parts of the world where recycling techniques are primitive and of major concern to environmental and human health. To avoid that in 20 years PV waste is disassembled in developing countries, a recycling plan for a safe end-of-life PV disposal has to be the common goal of stakeholders, producers, and governments worldwide. Even more important is the production of PV panels which do not contain hazardous compo-nents and thus represent a real green technology.
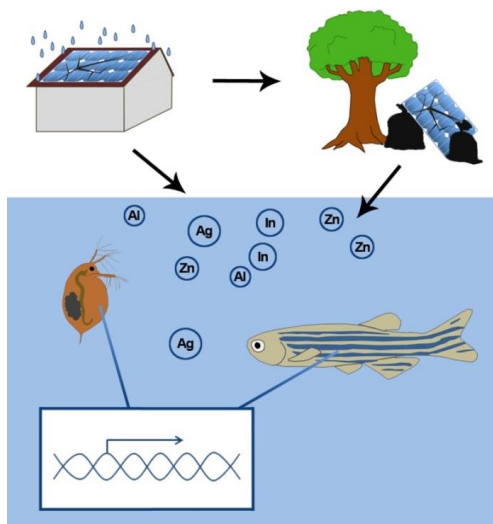
Figure 1.1 Conceptual figure illustrating the research questions addressed in this thesis on ecotoxicological assessment of organic photo-voltaics (OPVs). Production or end-of-life sce-narios (such as decommissioning and improper disposal) results in release of potentially toxic leachates. Especially metals are of concern. Ef-fects of single metals, a binary mixture, and leachates from OPV were investigated for their toxic potential in the aquatic organisms *Danio rerio* (embryos and liver cell line) and *Daphnia magna*. Phenotypic endpoints (e.g. growth or hatching) as well as molecular endpoints (e.g. gene expression) were applied. Ultimately, the potential risk for affected ecosystems was eval-uated.

1.2   Photovoltaic Technologies

To date, technologies used for the power conversion of solar energy into electric energy are basically divided into two categories: wafer-based PV (also called first generation PV) and thin-film PV. The first generation, crystalline silicon-based photovoltaic cells, are applied since more than 70 years (Chapin et al., 1954) and still are the dominant technology with a market share of about 80%. These first generation photovoltaics profit from ease of fabri-cation, high stability, and longevity, being the most expensive solar cells in terms of initial cost (Miles et al., 2005; Razykov et al., 2011). They reach a theoretically maximum efficien-cy of ~33%, as calculated by Shockley-Queisser thermodynamics (Shockley and Queisser, 1961). However, practical module efficiencies always tend to be lower due to solar cell re-sistance, solar radiation reflection, and metal contacts available on the top side, resulting in efficiencies of 15 to 18% in typical commercial crystalline silicon PVs (Saga, 2010). In search for more efficient and cost effective PV technology, second generation technologies

have been developed: amorphous silicon (a-Si), cadmium telluride (CdTe), copper indium gallium selenide (CIS or CIGS), gallium arsenide (GaAs), dye-sensitized (DSSC), quantum dot (QD), perovskite, and organic (OPV) photovoltaics. They come with advantages of semi-transparency, shape and bending flexibility, as well as low weight, and therefore a whole new set of consumer applications (e.g. building-integrated PVs, portable consumer electronics, integration into textiles; Roes et al., 2009). They allow high power output even under weak light conditions, and lower production costs than the first generation PVs. With a thickness of 1 to 20 μm they are generally referred to as thin-films. In comparison, crystalline silicon wafers make use of 200 to 300 μm (El Chaar et al., 2011). The main limitation of thin-film modules to overcome is the lower efficiency of 10.5% for a-Si (Ahn et al., 2012), 16.1% for CdTe (Gloeckler et al., 2013), and 14.4% for CIGS (Herrmann et al., 2014). GaAs module efficiency reaches 23.5 % (Mattos et al., 2012), but production costs are very expensive. Some thin-film technologies are still in the research or development phase, hence are classified as emerging photovoltaics. Among them are DSSC, QD, perovskite, and OPV. Rapid progress in the development of new materials and device optimization has brought commercialization of OPV closer to reality, with reported power conversion efficiencies of 10.6% (You et al., 2013). Efficiencies reached in the laboratory of all technologies are collected and frequently updated by the National Renewable Energy Laboratory (for further information see NREL, 2015).

Additional drawbacks of GaAs, CdTe, CIGS, and QD photovoltaics are the use of scarce raw materials such as tellurium and indium and raised toxicity concerns as cadmium is an inherent part. The European Parliament discussed in May 2015 stronger regulations regarding products containing cadmium. Based on the Restriction of Hazardous Substances Directive (RoHS, also known as Directive 2002/95/EC) the use of cadmium in electronic devices (e.g. TV and computers) is only allowed until a reliable technical alternative is available. For now, the PV modules will continue to remain exempt from the RoHS directive. However, this may not hold for long and then can result in a major change of the thin-film PV market in Europe boosting the production of a-Si, DSSC, perovskite, and OPV photovoltaics.

1.3   Organic Photovoltaic (OPV)

This thesis focuses on OPV, due to its potential wide scale deployment in future and existing knowledge gaps on environmental risks. The development of a sustainable energy technology implies the evaluation of the ecotoxicological properties of the main materials used.

The OPV cell has a layered structure (Figure 1.2). In terms of materials a transparent PET coating is protecting the cell from oxygen, moisture, and degradative UV light. The PET is blended with UV filters and phthalates. It covers the transparent anode commonly made of indium tin oxide (ITO) coated on a buffer layer made of a polymer mixture (PEDOT:PSS). Theoretically, the indium layer could be replaced with a silver grid or carbon nanotubes

(Emmott et al., 2012) but it is practically not yet feasible due to the reduction of lifetime and efficiency. After the anode, the sunlight hits the photoactive layer where it is absorbed by a blend of organic polymer (PEDOT:PSS as donor) and a fullerene (PCBM as acceptor) to generate photocurrents. The structure is followed by a metallic cathode made of silver, zinc oxide, or aluminum nanoparticles (NPs) and completed with a protection layer made of PET (Bao et al., 2014; Eo et al., 2009; Galagan and Andriessen, 2012; Griffith et al., 2015; Lin et al., 2010).

To absorb light at a broader spectrum of wavelengths and therefore increase the overall efficiency, two active sub-cells can be stacked to a so-called tandem solar cell. Altogether, the tandem cell has a thickness of no more than half a millimetre (Zimmermann et al., 2012).
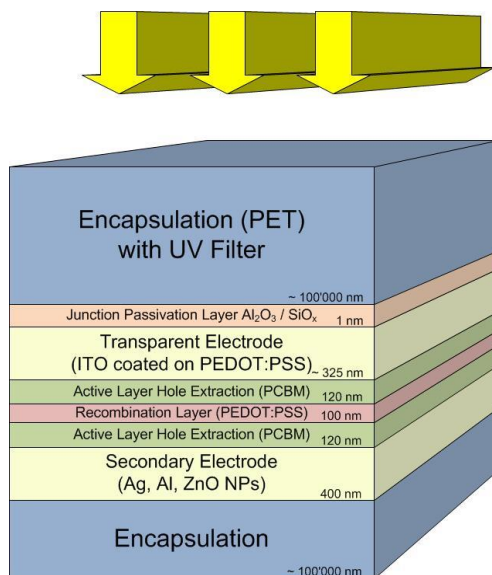
Figure 1.2 Layered structure of a typical organic photovoltaic (OPV) cell according to description in literature (Galagan and Andriessen, 2012).

1.4 Compounds of Ecotoxicological Concern

With the encapsulation of the OPV, the release of harmful substances is prevented as long as the layer structure is intact. Ageing processes such as UV irradiation, pollutants, high surface temperatures, hot-cold and dry-wet cycles, as well as mechanical damage will eventually lead to leachates that contain critical compounds (Manceau et al., 2011). After use, improper disposal, shredding or burning result in a release of potentially hazardous substances into the environment.

Life cycle assessments (LCAs) analyse both the energy use and environmental impacts associated with a product over its full life cycle and are also conducted for OPVs (Lizin et al., 2013; Tsang et al., 2016). The ecotoxicity database relies on EC_{50} values and in case experimental data on ecotoxicology are scarce, values are estimated by extrapolating data from non-target ecosystems or organisms (Haye et al., 2007). Many compounds have not been assessed at all for their ecotoxic potential. For some of them, including indium, more knowledge is urgently needed. Indium is the most successful transparent electrode material not just in photovoltaics but moreover in every smartphone, TV and PC displays, and light-emitting diodes (LED; Hecht et al., 2011).

Basically, the OPV cell consists of organic and inorganic components. Three metals were elucidated as compounds of high ecotoxicological relevance: zinc, indium, and alumi-

num. They all have in common that relatively little is known on their toxicity on aquatic organisms despite the increasing use, as in case of indium and aluminum. A scientific discussion on distinct nanoparticle effects has just been launched on ZnO and ITO NPs and with this work I can contribute to it. Silver is a major compound and of potential concern regarding its toxicity. However, it has been extensively studied and therefore was not prioritized. All the organic compounds (PET, phthalates, Tinuvin 360, Tinuvin 1577, PEDOT:PSS, TQ1, P2000, PC60BM, PC70BM) were considered as not being of major environmental concern. In the following a more detailed reasoning for not selecting these compounds in the ecotoxicological assessment is given.

Silver. In the past years, silver and silver NPs are found in an expanding range of consumer products including food packaging materials, odor-resistant textiles, washing machine, medicine, cosmetics, and toothpastes, inevitably leading to their release into the environment (Benn and Westerhoff, 2008; Farkas et al., 2011). Modelled and experimental data suggest that concentrations present in surface waters are in the ng L^{-1} range and exponential increases are predicted due to increase in usage (Gottschalk et al., 2009). Therefore silver has received considerable attention and has been extensively studied regarding its (eco)toxicity. In addition to its antibacterial properties, it also exhibits toxic activity towards organisms like algae, *Daphnia*, and fish (Fabrega et al., 2011). The highest concentration exhibiting no effect to the exposed organism referred to as "no observed effect concentration" (NOEC) for freshwater and seawater algae is between 2 and 2000 µg L^{-1} (Ratte, 1999), for *Daphnia* spp 0.001 µg L^{-1} (Bielmyer et al., 2002), and for fish 0.37 µg L^{-1} (Holcombe et al., 1983). As waterfleas are affected at predicted environmental concentrations, their populations are potentially at risk, which could also affect ecosystems.

In fish embryos, Ag NPs affect spinal cord deformities, cardiac arrhythmia, hatching success, and survival. In our lab, induction of reactive oxygen species (ROS) was shown by Ag NP. Moreover, an endoplasmic reticulum (ER) stress response in zebrafish liver cells and embryos was shown for the first time (Christen et al., 2013a). The activation of the ER stress response can lead to activation of apoptotic (programmed cell death) and inflammatory pathways.

Organic Compounds. Organic molecules applied in OPV can be divided in polymers and associated chemicals such as plasticizers and organic chemicals. The organic polymers were considered as not having critical environmental implications, mostly due to their low concentration. For example, PET is far more applied in other products. It is very resistant to environmental degradation including biodegradation (Nicholson, 2012), hence large volumes of persistent waste are created. Usually, PET will be taken under a process of fragmentation (by heat, oxidation, light, ionic radiation, hydrolysis, and mechanical shear) into smaller pieces down to sizes below 5 mm, called microplastics (Barnes et al., 2009). Transport across biological membranes of PET polymers is limited due to their large size (Anastas et al., 2000). Therefore they are not considered as directly toxic. Nevertheless, effects from ingestion of microplastic, including suffocation or blocking of digestive tract causing death, have been documented for fish (Boerger et al., 2010), birds, turtles, and marine mammals (Gregory, 2009). Additionally, persistent organic pollutants are absorbed

and concentrated in microplastics (Endo et al., 2005). Ingested microplastic waste are translocated from the gut to the circulatory system in mussels and transported to hemo-cytes (Browne et al., 2008). PET is used very widespread, produced in enormous amounts, and OPVs will not make a major contribution to the potential environmental implications.

Similar holds for other organic polymers such as PEDOT:PSS, P3HT, TQ1, and P2000 used in OPVs. Polymers are generally too big in size to be taken up into the cell, therefore toxic effects are not expected by these polymers. However, UV-irradiation and degradation mechanisms (Hintz et al. 2011) could lead to smaller-sized molecules (e.g. its monomers), which may have a potential for ecotoxicological risks.

Benzotriazole UV-stabilizers such as Tinuvin 360 are integrated to protect from UV degradation. Acute toxic potential for *Daphnia* is in the high mg L^{-1} range (Kim et al., 2011), however they have the potential to bioaccumulate in aquatic biota due to high lipophilicity and persistence (Nakata et al., 2009). Estrogenic activity was suggested as potential mode of action (Liang et al., 2014), whereas in our lab the analysis of a series of UV stabilizers did not show any estrogenic or androgenic activity (Fent et al., 2014). Phthalates used as plas-ticizers were shown to have anti-androgenic activity, but at concentrations much higher than expected to leach from OPVs (Christen et al., 2012).

PC60BM and PC70BM are fullerenes involving different numbers of carbon atoms. The initial size of a PCBM cluster used for P3HT/PCBM donor/acceptor material in polymer solar cells is 20 nm, but after thermal annealing of the P3HT:PCBM nanocomposites, nee-dle-like PCBM crystals were formed with a size of up to 20 μm (Karagiannidis et al., 2011). They may occur at 0.018-0.19 ng L^{-1} in surface waters and 3.69-25.1 ng L^{-1} in sewage treatment effluents (Gottschalk et al., 2009), but are highly insoluble in water (Heymann, 1996). Ecotoxicological effects of the C60 fullerene were assessed in a variety of organisms showing no acute toxicity up to very high concentrations of several mg L^{-1} range in *E. coli* and *B. subtilis* (Xia et al., 2010), *Daphnia magna* (Baun et al., 2008), and zebrafish embryos (Henry et al., 2007). Thus, although fullerenes might have adverse effects at high concen-tration, they are not of priority in this ecotoxicological assessment.

1.5   Nanoparticles

The ecotoxicological risk assessment presented in this thesis, focused on the metal com-pounds of the OPV cell. These compounds are frequently applied in form of nanoparticles. With their unique features significantly enhancing light absorption and electrical proper-ties, metallic nanoparticles have recently been identified as a breakthrough route for effi-ciency enhancement of OPVs (Stratakis and Kymakis, 2013).

Metallic NPs might be accidentally discharged into the environment during produc-tion (Nowack and Bucheli, 2007). To what extent, they are released from devices at their end-of-life remains to be investigated. A general concern has risen, that nanomaterials are taken up by organisms through ingestion, inhalation, skin lesion, or gills in fish (Handy et al., 2008b; Larese et al., 2009). These organs may also be sinks for nanoparticles, but

through transport other tissues can be affected as well, including the brain (Oberdörster, 2004). In zebrafish embryos, uptake rates through the chorion into the perivitelline space (surrounding the unhatched embryos), appeared to be up to 8 times higher for CuO NPs than for dissolved Cu (Muller et al., 2015). In chorion pore canals, having a diameter between 0.5-0.7 μm, uptake of individual NPs may occur via passive diffusion (Lee et al., 2007) and high osmotic pressure of the protein rich fluid (Xia et al., 2011), while in the gut and other tissues vesicular uptake (endocytosis) may be equally important (Moore, 2006). Intracellular distribution of ZnO NPs was demonstrated to be different from ionic zinc. ZnO NPs were mainly found in organelles and the cytosol, whereas ionic zinc was distributed in cell membranes and tissues suggesting that ZnO NPs cross membranes (L.-Z. Li et al., 2011). Toxicological modes of action involved in adverse outcome of NPs include generation of reactive oxygen species, which ultimately can lead to alteration of transcriptional gene expression and induction of apoptosis and necrosis (Nel et al., 2006; Xia et al., 2008). Other effect that have been ascribe to metal NPs include inflammatory reactions (Gojova et al., 2007; Xia et al., 2008) induction of DNA damage (Valdiglesias et al., 2013; Yin et al., 2010) and ER stress (R. Chen et al., 2014; Christen et al., 2013a).

Although NPs are routinely defined to have a dimension between 1 and 100 nm, Auffan et al. (2009) point out that many particles undergo dramatic changes in crystalline structure at a size of 30 nm or less, suggesting to focus on this smaller set of NPs when conducting toxicity studies. Indeed, different studies have shown that particle size is closely correlated with toxicity, as shown by increased uptake of smaller Ag NPs in *Daphnia magna* (Zhao and Wang, 2012) and decreased feeding rate of smaller ZnO NPs exposed *Daphnia magna* (Lopes et al., 2014), while smaller Cu NPs induce higher mortality rate in zebrafish embryos (Hua et al., 2014). Initial particle sizes used in OPV are less than 10 nm (Bao et al., 2014; Hong et al., 2008).

Ecotoxicological effects of metal NPs have been described in aquatic and terrestrial organisms, but such studies mainly focused on acute toxicity to various species, whereas molecular effects at lower concentrations remain to be further explored. Additionally, knowledge on the ecotoxic potential of ITO NPs is generally lacking. Only two studies exposed indium nitrate and ITO NPs, respectively, to several taxonomic groups of aquatic organisms and found acute toxicity at concentrations lower than 5 mg L^{-1} with the most sensitive response of *Hydra attenuata* (EC$_{50}$ = 0.1-1 mg L^{-1}, 96 h exposure; Blaise et al., 2008; Zurita et al., 2007). Up to the work presented in this thesis, the toxicity of ITO to fish and its molecular or cellular mode of action were unknown.

1.6 Model Organisms and Cellular Model

A wide range of model organisms are commonly used in aquatic toxicology including *Vibrio fischeri* (aquatic bacteria), *Chlorella vulgaris* and *Pseudokirchneriella subcapitata* (microalgae), *Lumbriculus variegatus* (annelid), *Daphnia* sp. (crustaceans), *Mytilus sp.* and oyster (molluscs), *Xenopus* sp. (amphibia), and many different fish species. The choice of organism

depends on the problems to be addressed and the available experimental techniques. In this thesis, the zebrafish (*Danio rerio*) embryos and the waterflea *Daphnia magna* were used as model organisms as well as the zebrafish liver (ZFL) cell line as cellular model (Figure 1.3).

The zebrafish is a widely used species in biomedical research and has been extended for assessing adverse effects of environmental contaminants. It is an ideal model system for

Figure 1.3 Model organisms and cellular model used in this thesis. (A) Zebrafish embryo developing stages at 24, 48, and 96 hours post fertilisation (hpf), (B) adult *Daphnia magna*, (C) ZFL cells.

genetic analysis due to its qualities such as high fecundity, almost translucent embryo development, short generation time (3 - 4 months from fertilization to sexual maturity), and ease of husbandry (Westerfield, 1995). Moreover, rapid searches for conspicuous phenotypes can be done by a simple visual screening using a microscope. As a vertebrate organism, it has many organs and cell types similar to those of mammals. From the zebrafish liver, the ZFL cell line has been established (Ghosh et al., 1994) inheriting the general hepatocyte characteristics (Eide et al., 2014). The liver represents a key organ for detoxification and contains a number targets for environmental contaminants such as the cytochrome P450 enzymes, aryl hydrocarbon receptor, and nuclear receptors. Having these useful attributes for toxicological studies, the ZFL cell line has been applied to assess alterations in gene transcription following exposure to many environmental contaminants including different metal ions (Y. Y. Chen et al., 2014; Cheuk et al., 2008; Sandrini et al., 2009; Wan et al., 2009) and metal NPs (Chen et al., 2011; Christen et al., 2014a). The use of a cell model is a necessary alternative for *in vivo* exposures not just as it allows cell specific and high-throughput of environmental contaminants assessment, but also due to ethical considerations going along with the 3Rs (Russell and Burch, 1959).

The key strength of the zebrafish is the well documented development and broadly conserved nature of developmental mechanism and signalling pathways across all vertebrates, allowing its use for insights into human disease processes. Its genome has been entirely sequenced, revealing that about 70% of human genes have counterparts in zebrafish (Howe et al., 2013). Despite the depth of knowledge on developmental and genetic mechanisms in zebrafish, the species remains underexploited for behavioural, ecological, and evolutionary studies (Engeszer et al., 2007). Its natural history - coming from the tributaries of

the Ganges river in India and Bangladesh and therefore not well suited for environmental studies in temperate environments - is often neglected.

This is not the case for *Daphnia*. They are keystone pelagic filter feeders in the food webs of many continental ponds and lakes. Hence, they are of great ecological importance. It entails advantages of an experimental model organism such as ease of culturing and short generation time (7-12 days from fertilization to sexual maturity). The use of *Daphnia* across various biological disciplines including evolutionary biology, resurrection ecology, aquatic ecology, ecotoxicology, and biomedical research is rapidly expanding. Its outstanding feature is the parthenogenetic life cycle (Ebert, 2005; Lampert, 2011). The use of genetic clones enables to distinguish between environmental factors and genetic variation. Likewise in zebrafish, both, the *Daphnia pulex* genome and recently the *Daphnia magna* genome have been completely sequenced. The *Daphnia pulex* genome revealed that more than one-third of all genes do not occur in the sequenced vertebrates. Among these *Daphnia*-specific genes are the most responsive genes to ecological challenges, suggesting that *Daphnia* may respond to environmental stress by gene duplication (Colbourne et al., 2011).

Daphnia have been an important model system for assessing effects of metals on freshwater ecosystems. Elevated concentrations of metals can adversely affect individual development, population growth rate, longevity, and reproduction (Connon et al., 2008; De Schamphelaere et al., 2004; Knops et al., 2001). In the past few years, global transcriptional alterations using microarrays have been applied revealing distinct expression profiles in response to metal and metal NP contaminants including copper, cadmium, lead, nickel, and zinc (Garcia-Reyero et al., 2009; Poynton et al., 2011, 2007; Vandegehuchte et al., 2010b). Known biomarkers of exposure such as metallothioneins and oxidative stress related genes were validated and extended with novel mode of actions such as the zinc inhibition of chitinase activity (Poynton et al., 2007). These genes are related to exoskeleton maintenance and molting. A reduced activity can thus be linked to reduced reproduction, as daphnids must molt in order to release a new brood.

1.7 Transcriptomics

Cells adapt to their environment by fine-tuning their transcriptome. Gene expression is a widely used technique for assessing ecotoxicological effects and it is in particular useful in combination with organisms of which the genome is well studied (Nikinmaa and Rytkönen, 2011). Zebrafish and *Daphnia*, are such aquatic organisms with extensively studied developmental genetic pathways (Amsterdam et al., 2004; Patton and Zon, 2001) and ecological interaction with genes (Connon et al., 2008; Heckmann et al., 2008; Miner et al., 2012). Using transcriptomic methods, insights into the contaminants mode of action are gained beyond traditional end points of growth, reproduction, and death. Once the connection between molecular response and adverse outcome is established, these genes can be used as early markers. Heckmann et al. (2008) and Connon et al. (2008) successfully linked molecular stress response with chronic consequences at population level in *Daphnia magna*. And

the mixture of endocrine disruptive chemicals in fish were shown to elicit a distinct transcriptomic fingerprint which could be related to physiological and behavioural responses (Garcia-Reyero et al., 2011; Zhao et al., 2015; Zucchi et al., 2014). Throughout the following chapters of this thesis, variations in gene expression were determined. New modes of actions were discovered and adverse effects predicted by specifically looking at stress related and biologically relevant biomarkers.

Extensive transcriptomic tools such as quantitative reverse transcription PCR (RT-qPCR), DNA microarrays, and high-throughput sequencing have been developed to explore how toxicologically relevant stressors affect molecular pathways and biological processes (Snape et al., 2004). RT-qPCR enables detection and measurement of selected target genes, whereas microarray and high-throughput sequencing assess transcriptional alterations of thousands of genes or even the whole transcriptome, respectively (Wang et al., 2009). DNA microarray is the most prominent technique to identify genes that respond to environmental contaminants. This technique is now outperformed by high-throughput sequencing which allows a transcriptome-wide investigation of all differentially expressed genes, is sensitive to genes of low abundance, and differentiates between isoforms (Wilhelm and Landry, 2009).

Although transcriptomic analysis allow a better understanding of the molecular mechanisms involved in the organisms response to toxicants, some limitations have to be taken into account to avoid misinterpretation of the results. The response is likely to be different in chronic versus acute effects, as the organism might adapt to change in the environmental condition. One has to keep in mind, that gene expression analyses give only a snapshot in time of the expression. Furthermore, it is highly recommended to evaluate environmentally realistic concentrations of contaminants, as high doses will represent acute toxicity mechanism mainly leading to apoptosis and cellular death. One of the main aims that should not be missed is the link of the observed molecular effects with adverse effects at cellular, tissue, individual, or population level (Fent and Sumpter, 2011). As mRNA expression does not necessarily reflect protein expression (Nikinmaa and Rytkönen, 2011), the translation of transcript expression to physiological effects is the proof of principal (Furlong, 2011; Nikinmaa and Rytkönen, 2011).

1.8 Scope of the Thesis

Research Questions. This thesis seeks to explore the ecotoxicological effects and associated potential hazards and risks of compounds used in and released from OPV cells. Knowledge gaps hamper a confident OPV risk assessment and need to be filled. To meet this objective, the toxic potential and toxicological properties of single compounds used for the production as well as leachates from end-of-life tests are investigated. The research aims to identify toxic components, as well as environmental implications of OPV weathering, and ultimately, to yield an ecotoxicological hazard and risk assessment of this new technology.

The PhD thesis has the following specific objectives:

(1) to identify acute toxic potential of selected metallic components (Al, In, Zn) used in different OPV layers,

(2) to analyse selected components for various toxicological activities using biomarkers of exposure for oxidative stress, apoptosis, inflammation, and ER stress,

(3) to compare nanoparticulate effects with ionic metals,

(4) to assess metal mixture toxicity and compare it to single metal exposure,

(5) to analyse the potential toxicity of OPV leachates and assess the consequences of different environmental conditions on leaching behaviour and toxicity.

Approach and Thesis Overview. To address these objectives, compounds of interest were identified after a careful literature review (see above and chapters 2 to 5): zinc, indium, and aluminum. Selected compounds, especially ZnO nanoparticles, went through an in-depth characterisation to describe initial shape and size and behaviour such as shedding of metal ions and aggregation in different exposure media. Potential effects of the selected single compounds, one mixture thereof, and OPV leachates were assessed *in vivo* in the aquatic organisms *Danio rerio* and *Daphnia magna* and *in vitro* in a fish liver cell line system. The investigation of the single compounds prepared the basis to analyse the OPV leachates. By using the same biomarkers it was aimed at elucidating biologically active compounds in the leachate mixture. When working with the fish system, the compounds were first assessed for their biological activity *in vitro* before investigating the observed effects in zebrafish embryos. Gene expression analysis is an appropriate approach to assess molecular effect, particularly when mechanisms of action are unknown. Throughout the three studies with zebrafish, the well-established SYBR-Green based RT-qPCR technology was used to examine differences in gene expression between exposed and non-exposed cells or organisms. In the metal mixture study with *Daphnia magna* the cutting-edge technology high-throughput RNA sequencing was performed. All the compounds and leachates were tested not only for molecular but also phenotypic effects to achieve a comprehensive picture of the toxic potential. Furthermore, bioaccumulation of the three metals was assessed using the laser-ablation ICP-MS technique.

The main part of the thesis is organized in four chapters, which are individual research articles, followed by a concluding chapter. An outlook over chapters 2 to 5 is given below.

Chapter 2 presents an ecotoxicological comparison of ZnO NPs and dissolved zinc using zebrafish embryos. First, a profound physico-chemical characterisation of ZnO NPs used in OPVs was performed. ZnO NPs had an initial size of 9.4 nm, but upon contact with zebrafish exposure media, considerable particle aggregation was observed, which could be reduced by supplementing the media with alginic acid sodium salt. Quantitative ICP-MS analysis revealed that Zn(II) dissolution rate from ZnO NPs was rapid and high. This was taken into account for the zebrafish embryo experimental design, were embryos were exposed to

three different ZnO NP and corresponding free Zn(II) concentrations to investigate nano-particulate effects. Neither was a statistically significant difference found regarding observed inhibited hatching, nor was there a difference in uptake and internal organ distribution visible. Gene expression analysis showed that transcripts of oxidative stress related genes and metallothionein were significantly altered. For the first time, we could show that excessive zinc stimulates an inflammatory immune response in fish. Besides exploring a new targeted pathway, the data visualizes zinc uptake in zebrafish embryos as not seen before, and contributes to the current discussion of potential metal nanoparticle effects.

Chapter 3 provides first evidence of a molecular pathway induced by indium. Indium, but not the nanoparticle form indium tin oxide (ITO), triggered an endoplasmic reticulum (ER) stress response and associated apoptotic reaction *in vitro* in ZFL cells an *in vivo* in zebrafish embryos. The ER stress response was shown on mRNA and protein level. Furthermore, induction of inflammatory reactions and reactive oxygen species (ROS) were measured on gene expression level, latter as well by a free radical sensor fluorescent dye. According to the chemical analysis hardly any indium was released from ITO. As ITO NPs did not induce ER stress, this is suggesting that ITO NPs may not be incorporated into cells and that the observed ER stress is induced by soluble indium rather than the NPs. This study indicates that ER stress and oxidative stress can be used as biomarkers of exposure when assessing contaminated sites.

Chapter 4 focuses on the ecotoxicological implications of OPV leachates and compares it to an already established thin-film technology, the copper indium gallium selenide (CIGS) cell. Assuming that photovoltaic cells may be dumped next to aquatic ecosystems or remain broken on roof tops, leachates were produced by physically damaging the cells and exposing it to three environmentally relevant model waters: mesotrophic lake water, seawater, and acidic rain water. The inorganic content of the different leachates was measured by ICP-MS. Zebrafish embryos were then exposed to these leachates and effects compared. CIGS leachates produced under acidic rain water, as well as CIGS and OPV leachates produced under seawater conditions resulted in a significant hatching delay. However, addition of the metal chelator ethylenediaminetetraacetic acid (EDTA) allowed the zebrafish embryos to hatch normally. The same effect was observed, when assessing transcriptional alterations of biomarker genes indicative for oxidative stress, hormonal activity, metallothionein, ER stress, and apoptosis. Depending on the model water and photovoltaic cell, different genes were up-regulated, whereas addition of EDTA protected the embryo from molecular effects. These results suggest that metals leaching from the photovoltaic cells may pose a potential environmental risk. However, when comparing the two thin-film technologies regarding their ecotoxicological potential, the OPV cells are of lesser concern.

Chapter 5 contains the results from the metal mixture exposure in *Daphnia magna*. In contaminated aquatic environments toxicants predominantly occur as mixtures, which is a realistic scenario when photovoltaics are disposed incorrectly. However, toxicological effects of metal mixtures are still poorly understood. While it is expected that metals will share common uptake routes, they are likely to interact with different biological pathways within cells. Therefore, mixture effects are often not just predictable by adding up respons-

es of single chemicals, but show either less- or more-than-additive effects. Aluminum and indium, both compounds in OPV, were assessed individually and as equi-effective mixtures for phenotypic responses and their global transcriptomic profiles. Depending on the phenotypic endpoint, synergistic effects were found, such as for total number of neonates per adult and age at maturity. On the other hand, molting and specific growth rate exhibited more of an additive behaviour in the mixture. The transcriptomic analysis of the mixture revealed additional affected genes in comparison to the single metals, however they belonged to similar biological mechanisms. This is indicative for an interactive molecular response leading to the observed synergistic phenotypic effects. The study will be completed with a pathway analysis and a multivariate analysis on the mixture activity, which is not part of this thesis. It is hypothesized that the two metals will affect similar pathways in the mixture as in the single compound exposure, but additional transcripts will be regulated in the mixture. We will look more closely for a molecular reasoning to anchor the observed phenotypic effects. This modern genome-wide approach has the potential to unravel the complex nature of mixture toxicity.

2

COMPARATIVE EFFECTS OF ZINC OXIDE NANOPARTICLES AND DISSOLVED ZINC ON ZEBRAFISH EMBRYOS AND ELEUTHERO-EMBRYOS: IMPORTANCE OF ZINC IONS

Nadja Rebecca Brun, Markus Lenz, Bernhard Wehrli, Karl Fent

Abstract

The increasing use of zinc oxide nanoparticles (nZnO) and their associated environmental occurrence make it necessary to assess their potential effects on aquatic organisms. Upon water contact, nZnO dissolve partially to zinc (Zn(II)). To date it is not yet completely understood, whether effects of nZnO are solely or partly due to dissolved Zn(II). Here we compare potential effects of 0.2, 1 and 5 mg L^{-1} nZnO and corresponding concentrations of released Zn(II) by water soluble $ZnCl_2$ to two development stages of zebrafish, embryos and eleuthero-embryos, by analysing expressional changes by RT-qPCR. Another objective was to assess uptake and tissue distribution of Zn(II). Laser ablation-ICP-MS analysis demonstrated that uptake and tissue distribution of Zn(II) were identical for nZnO and

ZnCl$_2$ in eleuthero-embryos. Zn(II)was found particularly in the retina/pigment layer of eyes and brain. Both nZnO and dissolved Zn(II) derived from ZnCl$_2$ had similar inhibiting effects on hatching, and they induced similar expressional changes of target genes. At 72 hours post fertilization (hpf), both nZnO and Zn(II) delayed hatching at all doses, and inhibited hatching at 1 and 5 mg L^{-1} at 96 hpf. Both nZnO and Zn(II) lead to induction of metallothionein (*mt2*) in both embryos and eleuthero-embryos at all concentrations. Transcripts of oxidative stress related genes *cat* and *Cu/Zn sod* were also altered. Moreover, we show for the first time that nZnO exposure results in transcriptional changes of pro-inflammatory cytokines *il-1b* and *tnf-a*. Overall, transcriptional alterations were higher in embryos than eleuthero-embryos. The similarities of the effects lead to the conclusion that effects of nZnO are mainly related to the release of Zn(II).

2.1 Introduction

Metal-based nanoparticles are increasingly implemented in materials, cosmetics and technical applications. Consequently, they may be ultimately released into the environment during production, use and disposal at the end of their life. Zinc oxide nanoparticles (nZnO) are widely used in semiconductors, (organic) solar panel devices (Zimmermann et al., 2012), paints, personal care products (sunscreens) and even in waste water treatment. Nanoparticles might have different physico-chemical properties or behaviours in contrast to bulk materials, making prediction of their fate challenging (Li et al., 2014, 2013). Their state of aggregation, and consequently their settling to sediments, depend on surface properties, abiotic factors and the presence of dissolved organic matter in surrounding media (Shaw and Handy, 2011; Zhou and Keller, 2010). Most (nano)particles in aquatic environments are covered by adsorbed layers of natural organic material, such as humic substances and polysaccharides, which can influence stability of inorganic nanoparticle suspensions (Hyung et al., 2007) and provide potential binding sites for trace elements (Buffle et al., 1990).

Zinc is an essential trace element for organisms but induces toxicity at elevated concentrations. Partially but relatively quickly, nZnO dissolve in water, and the release of free zinc ions has been previously shown to be the primary source of toxicity (Blinova et al., 2010; Buerki-Thurnherr et al., 2013; Franklin et al., 2007). However, in other studies nZnO showed higher toxicity (Bai et al., 2010; Fernández et al., 2013; Hu et al., 2009), or induced additional effects (Poynton et al., 2011) than dissolved Zn(II) alone. Thus, there are conflicting observations and therefore further research is needed to resolve these discrepancies.

In organisms, cellular zinc ion fluctuations are mainly regulated by zinc binding metallothioneins (MT). Both, Zn(II) and nZnO induce reactive oxygen species (ROS) formation (Dineley et al., 2003; Heng et al., 2010; Sensi et al., 1999). ROS induction triggering an oxidative stress response has become a widely accepted paradigm for cellular effects of nanoparticles (Nel et al., 2006; Sharma et al., 2012; Song et al., 2010; Zhu et al., 2009). Ex-

cessive production of ROS can induce pro-inflammatory and cytotoxic effects (Nel et al., 2006). nZnO and associated released Zn(II) may ultimately lead to apoptosis (Buerki-Thurnherr et al., 2013) and acute toxicity at high concentrations. In zebrafish, adverse effects of nZnO include reduced hatching of embryos and ROS production (Bai et al., 2010; George et al., 2011; Ong et al., 2013; Xia et al., 2011; Zhao et al., 2013; Zhu et al., 2009). However, induction of inflammatory responses has not yet been investigated in fish.

In our present study we compare effects of nZnO and equal concentrations of released Zn(II) (derived from $ZnCl_2$) in experimental exposures of embryos and hatched zebrafish eleuthero-embryos in environmentally relevant media. Naturally occurring alginate, a polysaccharide-based organic material, was chosen as a supplement to stabilize nanoparticles and reduce their aggregation rate (George et al., 2012, 2011). We hypothesize that effects in embryos and eleuthero-embryos are similar, because they are induced by released Zn(II). This is assumed because agglomerated nanoparticles might not pass the pores in the chorion (Fent et al., 2010), but rather act as "delivery vehicle" for zinc ions when attached to the chorion (Handy et al., 2008a). The aims of our present work were to (1) evaluate the role of the protective egg chorion; (2) compare the influence of nZnO and released Zn(II); (3) determine the uptake of zinc by embryos and eleuthero-embryos using ICP-MS analysis, and its distribution into tissues by laser-ablation ICP-MS imaging; and (4) to assess the effects of nZnO and Zn(II) on the expression of target genes including pro-inflammatory genes. Our results indicate a fast dissolution of zinc from nZnO in water, making the free metal ions the primary source of the observed effects.

2.2 Materials and Methods

Nanoparticle characterisation. Zinc oxide nanoparticles (nZnO) were supplied by Genes'Ink (France). The specific surface area was analysed by BET method (Brunauer et al., 1938) on a Gemini model 2380 (Micromeritics Instrument Corp., U.S.A.). In addition, the zeta potential of nZnO in the exposure medium was measured using a Malvern Zetasizer Nano ZS (Malvern Instruments ltd., Malvern, U.K.). In the electric field, the electrophoretic mobility of charged nanoparticles was determined at 25 °C. Automatic measurements (10–100 runs) were performed with triplicates and the Smoluchowski'smodel was applied for analysis.

For scanning electron microscopy (SEM; Carl Zeiss Supra 40 VP, Germany) nZnO were dispersed in H_2O, ultrasonicated for 5 min at a frequency of 37 kHz (Elmasonic S 30, Germany) and air dried. The working distance was set on 4 mm, and an acceleration voltage of 5 kV was used.

Mean size of single particles was determined by tracking the scattered light using the NanoSight LM10 (NanoSight Ltd., U.K.) followed by evaluation using the Nanoparticle Tracking Analysis (NTA) software. The system relies on the Brownian motion and records a multitude of particles over a period of time generating a subsequent size distribution and mean size. Each concentration of nZnO and $ZnCl_2$, as well as controls, were analysed three

times independently by NTA at 0 h and 24 h after preparation. Each sample was injected three times and analysed in triplicate calculating the arithmetic average thereof. Standard deviations were determined from mean size obtained from replicate runs.

Inductively-Coupled-Plasma Mass-Spectrometry (ICP-MS). The zinc ion dissolution of nZnO in Holtfreter's Media at 0 h and 24 h after sample preparation was quantified using ICP-MS. Samples were centrifuged for 30 min at 30,000 g and the concentrations of the zinc isotopes (using ^{64}Zn and ^{66}Zn) in the supernatant were determined using an ICP-MS system (Agilent 7500cx, Basel, Switzerland) equipped with an Octopole Reaction System, pressurized with an optimized helium flow of 5 mL min^{-1}. Supernatants were diluted 1:100 in 1% HNO_3. Rubidium was used as internal standard. ICP-MS measurements were performed to determine the corresponding concentration of dissolved zinc released by $ZnCl_2$ (Sigma-Aldrich, Switzerland). Here, strictly speaking, the dissolved Zn(II) species is not pure. The main dissolved species is $Zn^{2+}_{(aq)}$, followed by minor amounts of $ZnCl^+_{(aq)}$ and $Zn(OH)^+_{(aq)}$. The concentrations of soluble Zn(II) released by suspended nZnO at exposure concentrations of 0.2, 1 and 5 mg L^{-1} correspond to Zn(II) concentrations of 0.1, 0.5, and 2.2 mg L^{-1}, respectively.

At each sampling time point, 3 embryos of each of the 4 replicates were washed twice in 1mM EDTA and individually dissolved in 300 μL aqua regia (3:1 HCl:HNO_3) for two days. If not hatched, additional 3 embryos per replicate were dechorionated, and chorion as well as dechorionated embryos dissolved in aqua regia separately. Samples were diluted 1:20 in HPLC-grade Nanopure water. Quality control measures included the use of procedural blanks.

Laser-Ablation Inductively-Coupled-Plasma Mass-Spectrometry (LA-ICP-MS) Imaging. At each time point, embryos of the highest dose groups and controls were dehydrated and embedded in agarose according to the protocol of Sabaliauskas et al. (2006). A microtome (SM2010R, Leica, Germany) was used to prepare embryo cross sections with a flat surface. A NWR213 laser ablation system (ESI, U.S.A.) was coupled to the above ICP-MS system for bioimaging, yet without using helium as collision gas. This allowed the qualitative assessment of element distribution in zebrafish embryo cross sections. The laser was operated at 50% of its maximal energy (fluence of 6.8 J cm^{-2}), at 20 Hz firing rate, at an ablation rate of 25 μm s^{-1}, and with a focussed spot size of 20 μm. Single lines (3.6 mm long) were recorded with a line spacing of 20 μm. All embryos of the same time point were run in the same analysis to ensure relative comparison. The measured isotope data of zinc (^{66}Zn for mapping; ^{64}Zn for verification of mapping results) and calcium (^{43}Ca) were exported and converted into images using the Iolite software running on IGOR Pro 6 (WaveMetrics, U.S.A.). The development of a reliable quantification strategy would go beyond the scope of this study (Becker, 2013), yet the technique allowed the determination of the spatial element distribution and comparison of the relative intensities of exposed embryos and eleuthero-embryos to controls.

Experimental Design. Zebrafish eggs were supplied by Harland Laboratories (Switzerland). Fertilized eggs were washed twice with autoclaved Holtfreter's medium. Embryos in the blastula stage were selected for subsequent control and exposure experiments in cov-

ered glass beakers containing 250 mL of Holtfreter's medium (3.5 g NaCl, 0.2 g NaHCO$_3$, 0.05 g KCl, 0.12 g CaCl$_2$ and 0.1 g alginic acid per litre at pH 7). The supplementation of alginic acid leads to smaller and more stable nanoparticle aggregate sizes, as assessed in a previous pilot study (George et al., 2011). Stock solutions of nZnO and ZnCl$_2$ (both 1 mg mL^{-1}) were prepared in Nanopure water, stirred for 30 min and ultrasonicated for 5 min before dispersing in the media. To ensure homogenous nanoparticle dispersion, each beaker was aerated with a glass pipet. Throughout the experiments a 16 h light:8 h dark photoperiod was used.

A static-renewal procedure was applied with complete water exchange every 24 h, by carefully transferring the embryos to new beakers containing medium and the appropriate concentrations of nZnO and ZnCl$_2$, respectively. Two exposure scenarios have been chosen. First, embryos were exposed from 0 to 96 hour post fertilization (hpf). The embryos were protected by the chorion. Second, newly hatched eleuthero-embryos were exposed from 72 to 168 hpf. Embryos and eleuthero-embryos were exposed for the same period of time to 0.2, 1, 5 mg L^{-1} nZnO, as well as to the corresponding concentrations of 0.27, 1.30, 5.74 mg L^{-1} ZnCl$_2$. All of the three nZnO and ZnCl$_2$ concentrations have similar free zinc ion concentrations as determined by ICP-MS (0.1, 1 and 2.2 mg L^{-1} Zn(II)). Controls (media without nZnO or ZnCl$_2$) and each exposure concentration consisted of 240 embryos and eleuthero-embryos in total, respectively. Each dose-group consisted of four replicates with 60 embryos each. For each exposure scenario, embryos and eleuthero-embryos, respectively, were sampled at two time points; 30 embryos from each of the 4 replicates were sampled at 48 and 96 hpf, 30 eleuthero-embryos from each of the 4 replicates at 120 and 168 hpf.

RNA Isolation, Reverse Transcription, and Quantitative Real Time PCR (RT-qPCR). Total RNA was isolated from pools of 25–30 zebrafish embryos using RNeasy Mini Kit (Qiagen, Switzerland). The RNA extraction procedure included a DNase I (Qiagen, Switzerland) treatment step to remove any contaminating genomic DNA. RNA concentrations and purity were measured spectrophotometrically using a NanoDrop ND-1000 Spectrophotometer (Nanodrop Technologies Inc., U.S.A.). The RNA integrity was verified by visual inspection after agarose gel electrophoresis.

One microgram total RNA was reverse-transcribed using Moloney murine leukemia virus reverse transcriptase (Promega Biosciences Inc., Switzerland) in the presence of random hexamers (Roche, Switzerland) and deoxynucleoside triphosphate (Sigma-Aldrich, Switzerland). The reaction mixture was incubated for 5 min at 70 °C, 1 h at 37 °C, and the reaction was stopped by heating up to 95 °C for 5 min.

Quantitative real-time PCR was performed with cDNAs and gene-specific primer pairs (Table 2.1) mixed with SYBR Green (FastStart Universal SYBR Green Master, Roche, Switzerland). The samples were denatured for 10 min at 95 °C and then amplified using 40 cycles of 15 s at 95 °C and 1 min at 58 °C or 60 °C (depending on transcript target), respectively, followed by quantitation using a melting curve analysis post run.

Table 2.1   Primer sequences for quantitative real-time PCR analysis

Target gene	Primer sequence (5' to 3')	Accession no.[a]
rpL13a	Forward: AGC TCA AGA TGG CAA CAC AG	NM_198143
	Reverse: AAG TTC TTC TCG TCC TCC	
cat	Forward: AGG GCA ACT GGG ATC TTA CA	NM_130912
	Reverse: TTT ATG GGA CCA GAC CTT GG	
Cu/Zn-sod	Forward: GGC CAA CCG ATA GTG TTA GA	NM_131294
	Reverse: CCA GCG TTG CCA GTT TTT AG	
mt2	Forward: AAA TGG ACC CCT GCG AAT	NM_001131053
	Reverse: TTG CAG GTA GCA CCA CAG TT	
tnf-a	Forward: ACC AGG CCT TTT CTT CAG GT	NM_212859
	Reverse: TGC CCA GTC TGT CTC CTT CT	
il-1b	Forward: CAT TTG CAG GCC GTC ACA	NM_212844
	Reverse: GGA CAT GCT GAA GCG CAC TT	
c-jun	Forward: ACG TGG GAC TTC TCA AAC TG	NM_199987
	Reverse: TCT TGG GAC ACA GAA ACT GG	
mxa	Forward: GAT CCC AAT GGT GAT CCG CTA C	NM_182942
	Reverse: TCA CAG TCC TCT TTA AGC AGG TTG TC	
stat1a	Forward: TCA AAG GAG GAC CTG AAC CGC	NM_131480
	Reverse: CAA CAC CTC GGA CAT CTG ACT AAT C	

[a] GeneBank accession number (http://www.ncbi.nlm.nih.gov).

For calculating expression levels of selected genes, mRNA normalization was performed against the housekeeping gene (*rpl13a*), shown to be stable during the exposure period (Zucchi et al., 2012). The ΔC_T values were calibrated against the control ΔC_T values for all target genes. All reactions were run in duplicate using the BioRad CFX96 Real Time PCR Detection System (BioRad, Switzerland). The amount of transcripts of selected target genes was expressed as fold change (log2) according to the formula: $2\text{^}(\Delta C_T$ untreated$-\Delta C_T$ treated).

Statistical Analyses. The data were graphically illustrated with GraphPad Prism 5 (GraphPad Software, U.S.A.). Significant differences between treatments were assessed by one way ANOVA followed by a Bonferroni post hoc test ($p \leq 0.05$) to compare treatment means of nanoparticulate exposure with Zn(II) exposure as well as treatment means with respective controls. Results are given as mean± standard deviation of mean (SD). Differences were considered statistically significant at $p \leq 0.05$.

2.3 Results

Characterization of nZnO. The mean surface area used nZnO was 68.7102 $m^2\,g^{-1}$, which is equivalent to a particle size of 9.4

nm (assuming a spherical shape), as determined under dry conditions by Brunauer–Emmet–Teller (BET) analysis (Table 2.2). Scanning electron microscopy (SEM) further confirmed the small size of the nZnO (Figure 2.1). However, considerable particle aggregation was observed, when measuring the size distribution of nZnO in the medium using nanoparticle tracking analysis (NTA). The larger hydro-dynamic diameter, compared to BET, can be attributed to the tendency of particles to aggregate in the aqueous state. Addition of alginic acid sodium salt (100 mg L^{-1}) to media resulted in a significantly reduced agglomeration size (Table 2.2). In Holtfreter's medium with alginate, the zeta potential was found to be -28.2 mV, in contrast to a potential around zero for media without such addition. The negatively charged natural acids will bind to the positively charged nanoparticles, which ultimately leads to a reduction in surface charge and to improved dispersion. ICP-MS analysis was performed to quantify zinc ions released from nZnO and dissolved from $ZnCl_2$ in Holtfreter's media, respectively. For each of the nZnO concentration, the equivalent soluble Zn(II) concentration was prepared with appropriate concentrations of $ZnCl_2$. Dissolved Zn(II) concentrations were high upon contact with medium (average of $50.8\% \pm 3.7\%$ of initial Zn) and stayed stable over 24 h ($52.7\pm8.1\%$ in average), demonstrating a rapid release of Zn(II) from nZnO. A fast dissolution reaching the equilibrium within 3 h
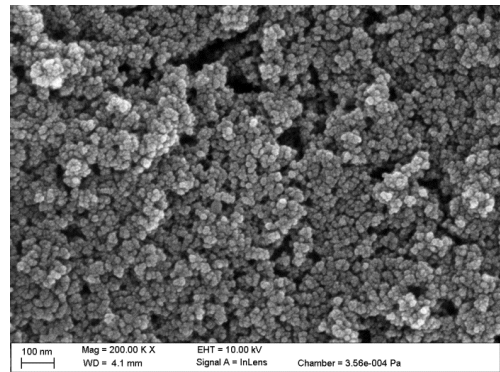
Figure 2.1 Scanning electron microscopic (SEM) image of ZnO nanoparticles. Scale bar 100 nm.
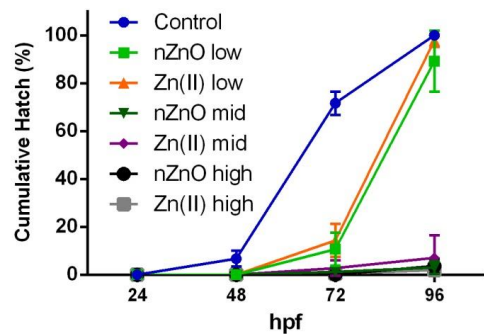
Figure 2.2 Cumulative percentage of hatched zebrafish embryos exposed different concentrations of nZnO and Zn(II). The hatching rate significantly decreased with increasing doses of nZnO and Zn(II); low refers to 0.1, mid to 0.5 and high to 2.2 mg L^{-1} dissolved zinc in exposure group with nanoparticulate ZnO (nZnO) and without (Zn(II)). Average value was calculated for a total of 120 embryos from four replicates with 30 embryos in each. Error bars represent standard deviation (SD). All exposed embryos at 72 hpf, and mid and high dose groups at 96 hpf show significant differences ($p < 0.05$) compared to control group.

(Xia et al., 2008) or 6 h (Mudunkotuwa and Grassian, 2011) is already described and accounted for the presence of biological components and small particle size. The characteristics of used nZnO are summarized in Table 2.2.

Table 2.2   Characteristics of nZnO

	0 h	24 h
Zeta potential ζ[1]		
Holtfreter's medium without alginate	2.3 mV	-[2]
Holtfreter's medium with alginate	- 27.2 mV	- 28.2 mV
Average Agglomeration Size (NTA)		
5 mg/L without alginate	218 ± 36 nm	336 ± 38 nm
0.2 mg/L with alginate	196 ± 13 nm	211 ± 23 nm
1 mg/L with alginate	214 ± 23 nm	236 ± 19 nm
5 mg/L with alginate	223 ± 12 nm	242 ± 17 nm
Zn(II) release (ICP-MS)		
nZnO low (0.2 mg L^{-1})	0.106 ± 0.014 mg L^{-1}	0.116 ± 0.018 mg L^{-1}
$ZnCl_2$ low (0.27 mg L^{-1})	0.092 ± 0.010 mg L^{-1}	0.097 ± 0.013 mg L^{-1}
nZnO mid (1 mg L^{-1})	0.530 ± 0.061 mg L^{-1}	0.567 ± 0.098 mg L^{-1}
$ZnCl_2$ mid (1.30 mg L^{-1})	0.508 ± 0.055 mg L^{-1}	0.501 ± 0.070 mg L^{-1}
nZnO high (5 mg L^{-1})	2.327 ± 0.245 mg L^{-1}	2.169 ± 0.172 mg L^{-1}
$ZnCl_2$ high (5.75 mg L^{-1})	2.249 ± 0.122 mg L^{-1}	2.192 ± 0.206 mg L^{-1}
Surface area (BET)	68.71 $m^2 g^{-1}$	

[1] measured at pH 7 and 25 °C

[2] not measureable, particle precipitations clearly visible

Effect of nZnO and Dissolved Zn(II) on Hatching. At 72 hpf, hatching was significantly delayed in exposed embryos at all doses of nZnO and Zn(II) compared to controls (Figure 2.2). At 96 hpf, almost all individuals (89.1± 12.7% nZnO and 97.8±2.6% Zn(II)) of the lowest dose groups (0.2 mg L^{-1} nZnO and 0.27 Zn(II)) hatched, whereas only a few embryos (3.1 ± 2.7% and 3.75 ± 3.1% nZnO; 7.1 ± 9.4% and 2 ± 2.7% Zn(II)) hatched in the mid and high dose groups (1 and 5 mg L^{-1} nZnO; 0.5, and 2.2 mg L^{-1} Zn(II)). No significant differences occurred between nZnO and corresponding Zn(II) concentrations. Therefore, we conclude the dissolution of Zn(II) from nZnO is the key determinant for the delayed and inhibited hatching.

Uptake of Zinc Into Embryos and Eleuthero-Embryos. Embryos and eleuthero-embryos were exposed separately, and both were sampled after an exposure period of 48 and 96 h. The uptake of zinc by embryos, dechorionated embryos and chorion was compared. A dose-dependent increase in Zn content occurred in embryos and eleuthero-embryos (Fig-

ure 2.3). The content of Zn was also determined in the chorion, where a slight increase in zinc was observed with exposure concentration at 48 and 96 hpf. Highest zinc accumulation occurred in embryos and eleuthero-embryos at the highest exposure concentrations. There was no significant difference in Zn(II) uptake between nZnO and $ZnCl_2$ exposures.
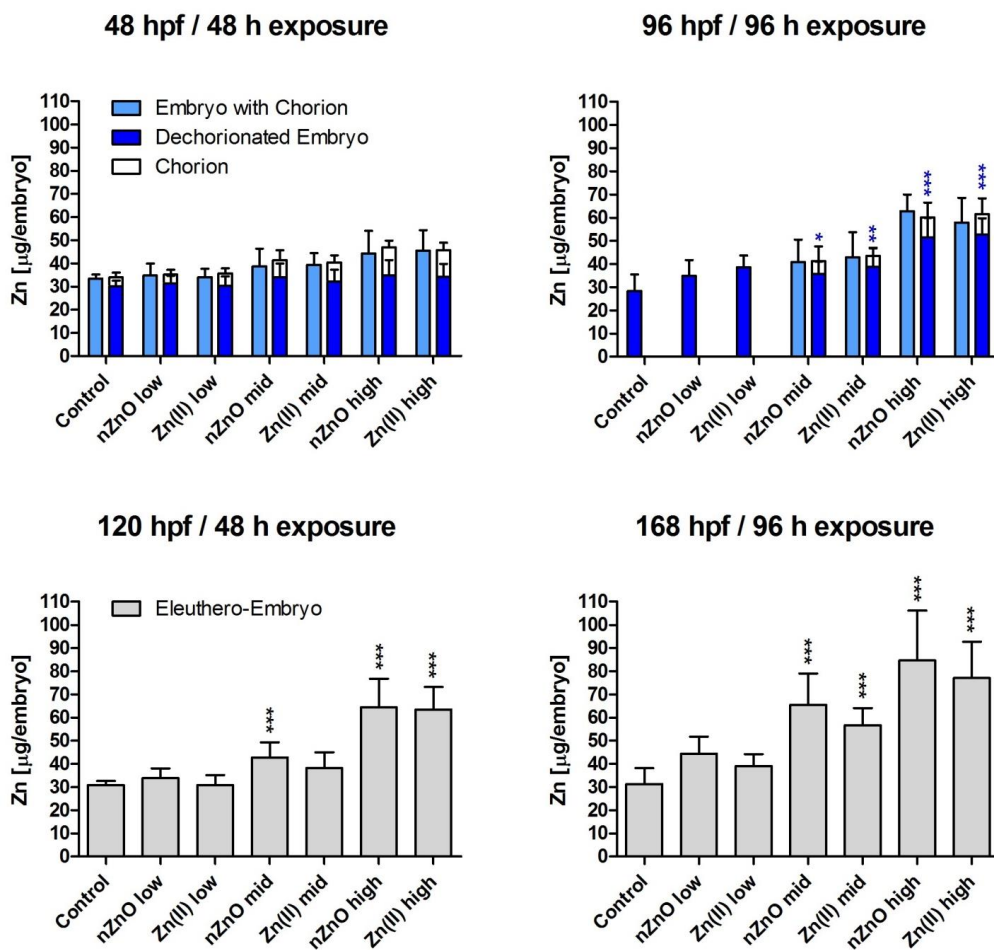
Figure 2.3 Total Zn content in zebrafish embryos (48 and 96 hpf), dechorionated embryos and chorions in µg per embryo, as well as in eleuthero-embryos (120 and 168 hpf). Both nZnO and Zn(II) exposures result in a similar dose-related uptake of ^{66}Zn into embryos and eleuthero-embryos. Low refers to 0.1, mid to 0.5 and high to 2.2 mg L^{-1} dissolved zinc in exposure group with nanoparticulate ZnO (nZnO) and without (Zn(II)). At 96 hpf embryos of control and 0.1 mg L^{-1} (low dose group) were hatched. Asterisks indicate significant differences of dechorionated embryos or eleuthero-embryos to controls (*$p < 0.05$, **$p < 0.01$, and ***$p < 0.001$). Error bars are + standard deviation (SD) of measured values for each exposure group consisting of 4 replicates (per replicate 3 embryos measured).

LA-ICP-MS profiles of embryos verified that Zn was accumulated and distributed across organs and tissues, rather than just adsorbed on the skin surface (Figure 2.4). At 48 hpf in nZnO exposed embryo and at 96 hpf, 120 hpf (48 h exposure) and 168 hpf (96 h exposure) in both nZnO and Zn(II) exposed embryos accumulation of Zn and its distribution in different tissues is clearly visible. Both nZnO and Zn(II) lead to comparably high Zn concentrations in the retina and pigment layers of the eyes, as well as in some parts of the brain, in the yolk sack and in the spinal cord. The cutting of the thin spinal cord was challenging and in some of the eleuthero-embryos even not possible. The distribution of ^{66}Zn (Figure 2.4) and of ^{64}Zn (Fig. S2.1, supplementary information) were consistent, thus only ^{66}Zn is shown in Figure 2.4. In contrast to the Zn, Ca concentrations at 120 hpf and 168 hpf were decreased in the inner ear of exposed embryos as compared to controls.

Alteration of Gene Expression. Expressional changes of selected target genes were analysed after exposure to nZnO and Zn(II) for 48 h and 96 h in both embryos and eleuthero-embryos, respectively. In both stages, mRNA levels of genes related to oxidative stress including *cat* and *Cu/Zn-sod*, metallothionein (*mt2*), and immune responsive and pro-inflammatory genes (*tnf-a*, *il-1b*, *c-jun*, *stat1a*, *mxa*) were determined by RT-qPCR. Expression of *cat* and *Cu/Zn-sod* showed a similar temporal pattern for both nZnO and Zn(II) with an up-regulation at 48 hpf in embryos and a down-regulation at 96 hpf at the highest concentrations (Figure 2.5). In eleuthero-embryo exposures *cat* and *Cu/Zn-sod* showed a down-regulation after 48 h of exposure at 120 hpf, whereas no alterations occurred at 168 hpf after 96 h of exposure (Figure 2.5). Transcripts of *mt2* were significantly up-regulated in embryos at 48 hpf and 96 hpf at almost all nZnO and Zn(II) concentrations, and at 5 mg L^{-1} nZnO and 2.2 mg L^{-1} Zn(II) in eleuthero-embryos at 120 and 168 hpf (Figure 2.5). Transcripts of the pro-inflammatory cytokines, tumor necrosis factor-α (*tnf-a*) and interleukin-1β (*il-1b*), showed a different pattern in the embryo than eleuthero-embryo-exposures. A tendency for down-regulation of *tnf-a* occurred in the embryo exposures (particularly at 96 hpf) after Zn(II) and nZnO treatment, while an induction occurred in eleuthero-embryo exposures at 120 hpf for both nZnO and Zn(II) (Figure 2.6). The expression pattern of *il-1b* was similar, showing an up-regulation in eleuthero-embryo exposures, mainly after nZnO treatment. Additionally, the jun proto-oncogene (*c-jun*) was significantly up-regulated at 96 hpf in embryo exposures at mid and high doses of nZnO and Zn(II), but was not altered in eleuthero-embryo exposures (Figure 2.6). Both nZnO and Zn(II) exposures resulted in a significant down-regulation of the anti-viral and immune-related gene Myxovirus resistance A (*mxa*), while the signal transduction and activation of transcription 1a (*stat1a*) remained unaffected (Figure 2.7). Overall, the nZnO and Zn(II) induced expressional changes were more pronounced in embryo exposures than in eleuthero-embryo exposures. This suggests that embryos at an early stage, although protected by the chorion, react more sensitively to nZnO and Zn(II) than hatched eleuthero-embryos.
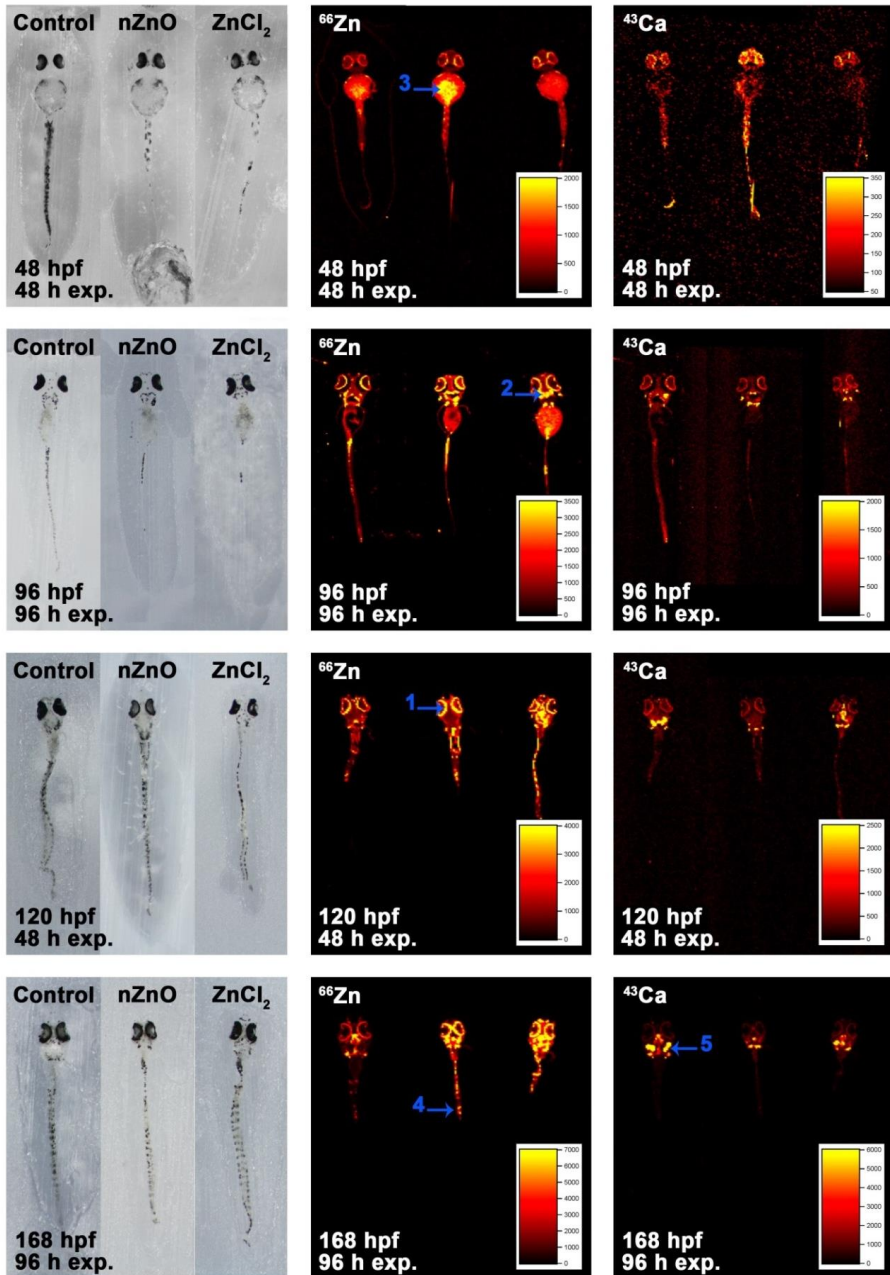
Figure 2.4 Pictures showing the embedded dechorionated embryos and eleuthero-embryos before LA-ICP-MS analysis (left) and Zn and Ca organ distribution measured by LA-ICP-MS (centre and right). In each picture coronal zebrafish embryo sections of controls (embryo on the left), nZnO high (centre) and Zn(II) high (right) exposure groups at different time points (48 hpf, 96 hpf, 120 hpf, 168 hpf) and exposure times (48 and 96 h, respectively) are shown. Spots of accumulation are labelled as (1) retina and pigment layers of the eyes, (2) brain, (3) yolk sack, (4) spinal cord, (5) inner ear. Colour bars show the intensity in counts per seconds.
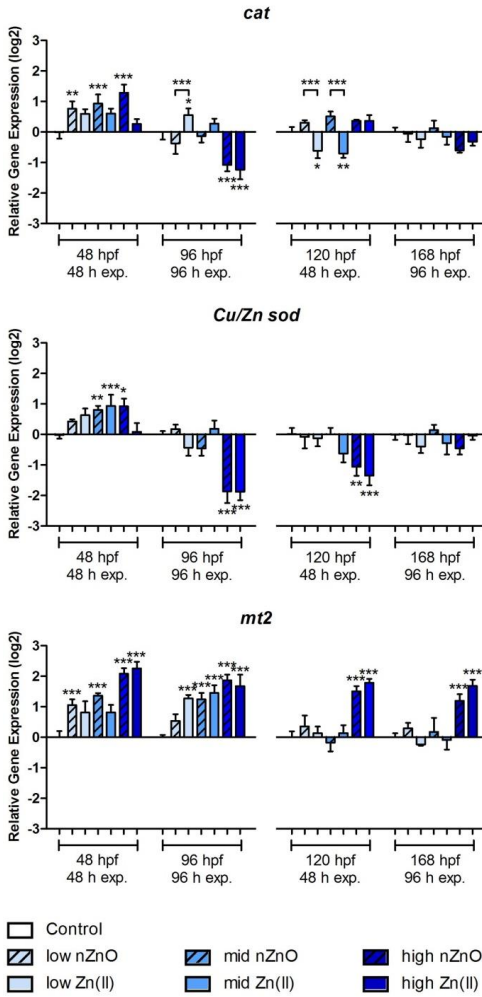
Figure 2.5 Transcriptional alterations of oxidative stress related genes catalase (*cat*), Cu/Zn superoxide dismutase (*Cu/Zn sod*) and metallothionein (*mt2*) in zebrafish embryos (at 48 and 96 hpf or 48 and 96 h exposure, left) and eleuthero-embryos (at 120 and 168 hpf or 48 and 96 h exposure, right), respectively, exposed to 0.1, 0.5 and 2.2 mg L^{-1} of dissolved zinc in exposure groups with nanoparticulate ZnO (nZnO) and without (Zn(II)). Asterisks indicate significant differences to controls (*p < 0.05, **p < 0.01, and ***p < 0.001). Values are presented as mean ± SD (n=4).
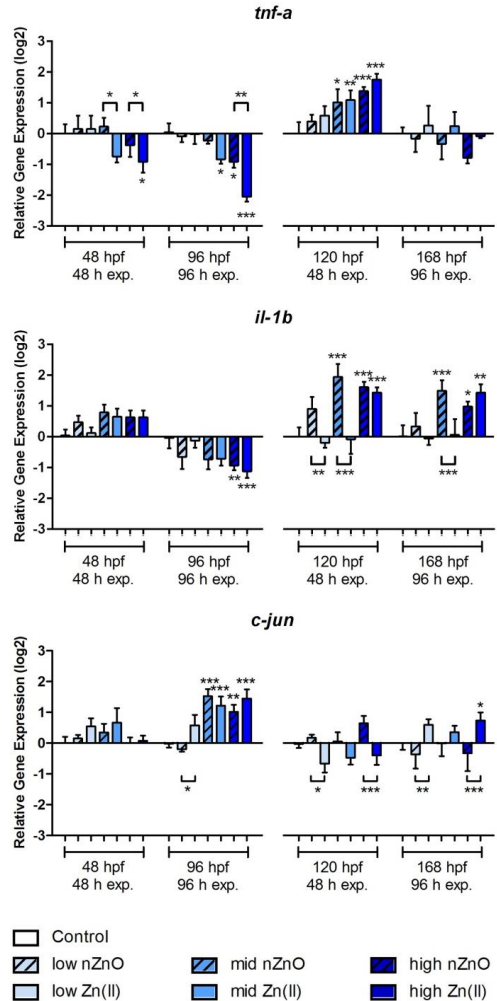
Figure 2.6 Transcriptional alteration of innate immune system related genes *tnf-a*, *il-1b* and of *c-jun* in zebrafish embryos (at 48 and 96 hpf or 48 and 96 h exposure, left) and eleuthero-embryos (at 120 and 168 hpf or 48 and 96 h exposure, right), respectively, exposed to 0.1, 0.5 and 2.2 mg L^{-1} of dissolved zinc in exposure groups with nanoparticulate ZnO (nZnO) and without (Zn(II)). Asterisks indicate significant differences to controls (*p < 0.05, **p < 0.01, and ***p < 0.001). Values are presented as a mean ± SD (n=4).

2.4 Discussion

The present study demonstrates dose-dependent effects of nZnO at individual size of 9.4 nm (BET), which tend to agglomerate in medium to a size of 196–242 nm (NanoSight, Table 2.2). Exposure of zebrafish embryos and eleuthero-embryos lead to an accumulation of zinc (Figure 2.3). Dose-dependent adverse effects on hatching (Figure 2.2) and expressional changes of genes associated with oxidative stress (Figure 2.5) and inflammation reaction (Figures 2.6, 2.7) occurred. Our data confirm previous reports on inhibitory effect of nZnO on hatching of embryos (Bai et al., 2010; Zhao et al., 2013), and they contribute to the understanding of the causes behind their effects. The effects were mainly related to the release of Zn(II) from nanoparticles, and they were more pronounced in embryos than eleuthero-embryos. There is still a debate on this question, as there are supporting reports (Buerki-Thurnherr et al., 2013; Song et al., 2010), as well as reports showing that zinc ions only partly contributed to the effects of nZnO (Bai et al., 2010; Ong et al., 2013; Zhao et al., 2013; Zhu et al., 2009).

        Alginate added to the medium resulted in a stabilization of particles suspension, as indicated by NTA and Zeta potential measurements. Particles with a zeta potential greater than 30 mV, or lower than −30mV, tend to repel each other, and are therefore considered to be a stable colloidal

Figure 2.7 Transcriptional alteration of interferon- and virus-inducible genes including *mxa* and *stat1a* in zebrafish embryos (at 48 and 96 hpf or 48 and 96 h exposure, left) and eleuthero-embryos (at 120 and 168 hpf or 48 and 96 h exposure, right), respectively, exposed to 0.1, 0.5 and 2.2mg L^{-1} of dissolved zinc in exposure groups with nanoparticulate ZnO (nZnO) and without (Zn(II)). Asterisks indicate significant differences to controls (*p < 0.05, **p < 0.01, and ***p < 0.001). Values are presented as a mean ± SD (n=4).

system (Webb and Orr, 1997). This indicates increased particle mobility under environmentally relevant conditions. Enhanced particle stability by dissolved natural organic matter (NOM), Suwannee River humic acid or biogenic molecules (proteins) is also found to crucially determine particle fate/transport for other nanoparticles (Chen et al., 2006; Hyung et al., 2007; Mohd Omar et al., 2014; Zhou and Keller, 2010). An increased negative surface charge of nanoparticles occurs in NOM-fortified medium, whereas a negative charge can be neutralized by adding counter cations (Zhang et al., 2009). Although Holt-
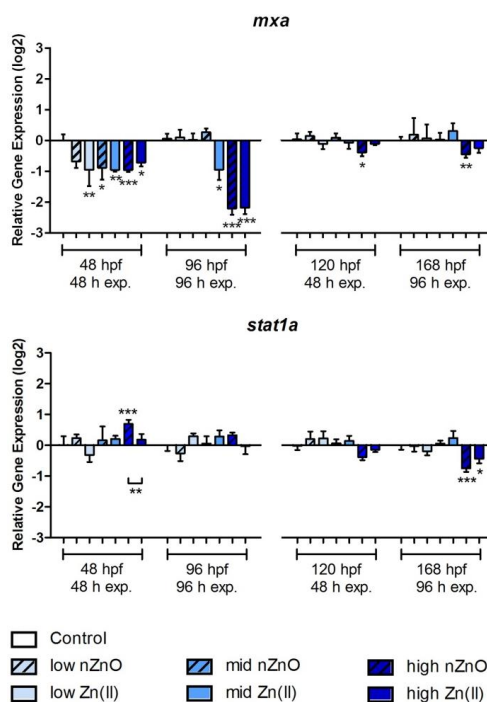
freter's medium used in our study contains a rather high salt concentration, and therefore having a relatively high ionic strength, we could not observe the counteraction of the multivalent cations. The solubility of nZnO is highly dependent on the matrix in which they are suspended; a quicker and higher zinc dissolution occurs in complex cell culture media, or in presence of serum albumin compared with nanopure or moderately hard water (Reed et al., 2012). Furthermore, the presence of anions (e.g. Cl^-) can serve as Zn^{2+} binding ligands, and thus accelerate nZnO dissolution. The small initial particle size of 9.4 nm might promote dissolution, considered to be proportional to the specific surface area of nanoparticles (Borm et al., 2006). Increasing solubility with decreasing nZnO size has been reported (Reed et al., 2012). In addition, the solubility of nZnO is highly pH-dependent. Over a pH range of 7 to 8, $Zn^{2+}_{(aq)}$ is the dominant species with $Zn(OH)^+_{(aq)}$ being present as well (Reichle et al., 1975).

The free metal ions are the bioavailable species and therefore mostly responsible for the here observed effects. Our study demonstrates that Zn(II) released from nZnO became accumulated in zebrafish embryos and eleuthero-embryos (Figures 2.3, 2.4). In the first 48 h after fertilization, the chorion seems to protect the embryo by adsorption of nZnO and associated Zn(II) or blocking its transport through the pore canals. In contrast, after 96 h an increased uptake of zinc was measured in embryos, indicating an uptake of nZnO and/or Zn(II). In such embryos, uptake and transport of Zn(II) are mediated by zinc–iron related transporter proteins (ZIP) in the plasma membrane involved in the regulation of intracellular zinc level (Gaither and Eide, 2001). Possibly, binding sites on the chorion are fully occupied and zinc is starting to trespass the chorion after 48 hpf, and concomitant with the need for oxygen and minerals from the aquatic environment zinc was taken up. Although chorion pore canals are approximately 500–700 nm in diameter (Lee et al., 2007), agglomerates of nanoparticles of about 200 nm (as is the case for nZnO of this study, Table 2.2) can be already too large to be incorporated. This is based on the fact that not only the size but also the surface charge is a determining factor for uptake (Fent et al., 2010).

Our LA-ICP-MS analysis shows for the first time the uptake and embryonic tissue distribution pattern of zinc after exposure to nZnO and Zn(II) (Figure 2.4). Due to known interference of zinc divalent cations with calcium, both elements were monitored and compared. The distribution patterns of zinc and calcium were strikingly different. We suggest that higher uptake occurs due to the high demand of Zn, and possibly the higher activity and presence of uptake transporters in these tissues. Zinc is accumulated prominently in the retina and pigment layer of the eyes, in brain structures spinal cord and yolk sac, whereas in these tissues, calcium showed no increase (compare spots 1–5; Figure 2.4). In contrast, calcium was decreased in the inner ear. In zebrafish embryos uptake of gas and nutrients occurs mainly through the body surface. Skin chloride cells were suggested to be the main site for Ca^{2+} influx before the complete development of the gills (Van der Heijden et al., 1999). Chloride cells start to differentiate in the skin of embryos at 48 hpf and active transport of Ca^{2+} is suggested (Hwang et al., 1994). It is likely that zinc is competitive with calcium and therefore impairing its uptake. As the process is in the skin of embryos, a large surface is affected. Hence, embryos show strong zinc uptake with calcium depletion. The reason for the specific calcium loss in the inner ear remains to be investigated. Similar as in

zebrafish in our study, cellular uptake of Zn(II) caused a net loss of Ca^{2+} in brown trout fry (Sayer et al., 1991) and adult mud minnows (Sauer and Watabe, 1988).

Induction of ROS upon nZnO exposure has been reported in zebrafish embryos (Zhao et al., 2013; Zhu et al., 2009), activating or inhibiting several antioxidant enzymes. As a consequence, this may result in oxidative damage in zebrafish early life stages. To mitigate adverse effects of ROS, superoxide anions are converted to H_2O_2 by SOD, and O_2 by CAT (Valavanidis et al., 2006). In our study, exposure to nZnO and Zn(II) lead to up-regulation of both *Cu/Zn sod* and *cat* at 48 hpf, indicating a reaction to elevated ROS levels and thus, an induction of oxidative stress at 48 hpf. At 96 hpf, in contrast, *Cu/Zn sod* and *cat* were down-regulated, which may be related to a potential negative feedback mechanism at this time point in embryos. In eleuthero-embryos the down-regulation of *cat* and *Cu/Zn sod* at 120 hpf indicates an imbalance of Zn(II)-induced ROS. An increased SOD but decreased CAT enzyme activity was reported in zebrafish embryos (144 hpf) exposed to nZnO (Zhao et al., 2013). This suggests that the expressional pattern of these genes (and ROS levels) is not only related to Zn(II) concentrations, but also to the exposure time and time of sampling. The expression pattern induced by nZnO and Zn(II) was time-dependent and changed at different development stages. Similar to our study, effects of nZnO in a human cell line were mainly based on the uptake of released Zn(II), followed by apoptosis (Buerki-Thurnherr et al., 2013).

In contrast to *cat* and *Cu/Zn sod*, transcripts of *mt2* were significantly increased at all exposure times in embryos and eleuthero-embryos. Up-regulation is governed by free Zn(II) and persisted during exposure to nZnO and Zn(II) to protect against high Zn(II) concentrations and oxidative stress.

Both *tnf-a* and *il-1b* play a critical role in initiating the pro-inflammatory cytokine cascade, apoptosis, cell differentiation, and in stimulation of the adaptive immune response (Grayfer and Belosevic, 2012). Oxidative stress can activate pro-inflammatory signalling pathways (Xia et al., 2008). In human cell lines nZnO can lead to acute cytokine and chemokine generation, inducing inflammation (Feltis et al., 2012; Kermanizadeh et al., 2013). Moreover, ZnO nanoparticles and fine particles provoke similar inflammation on the rat lung exposed by inhalation (Warheit et al., 2009).

Here, we describe for the first time a down-regulation of *tnf-a* and *il-1b* in zebrafish embryos exposed to nZnO and Zn(II), and a significant up-regulation in eleuthero-embryos (Figure 2.6), which indicates a stimulation of the inflammatory immune response. Additionally, the c-jun proto-oncogene, which is a member of the c-Jun N-terminal protein kinase (JNK) signalling pathway, was significantly up-regulated. The activation of redox-sensitive JNK and pro-inflammatory cytokines, such as *tnf-a* and *il-1b*, leads to induction of genes for cytokines, chemokines and various pro-inflammatory mediators, which play an important role in the inflammatory response (Ip and Davis, 1998). We therefore conclude that exposure to nZnO and Zn(II) leads to modulation of pro-inflammatory responses in embryos and eleuthero-embryos.

2.5 Conclusion

Our present study sheds new lights on the potential effects of nZnO in zebrafish early life stages. To determine whether effects of nZnO are based on the free Zn(II) concentration, we exposed early life stages of zebrafish to nZnO and to equal concentrations of released free Zn(II) derived from $ZnCl_2$. Both nZnO and $ZnCl_2$ showed a similar hatching interference, uptake and distribution in embryos and eleuthero-embryos, and they induced similar dose-related effects on gene expression. This leads to the conclusion that the biological activity of nZnO is mainly based on the released free Zn(II) concentration. The nanoparticle nature itself contributed very little to the effects, therefore we conclude that the nanoparticulates themselves are not taken up. This is further evidenced by bioimaging. Figure 2.4 showed no evident spots of zinc, which would originate from nanoparticle accumulation. As images of nZnO and Zn(II) are similar, we conclude that Zn(II) but not nZnO do enter the embryo.

The current study adds to the existing data by exploring a series of different target molecular pathways. Novel are potential pro-inflammatory effects of nZnO and Zn(II), indicated by the up-regulation of *tnf-a* and *il-1b* in eleuthero-embryos. More pronounced expressional changes indicated higher sensitivity of embryo exposures in contrast to eleuthero-embryo exposures. Thus, embryos reacted more sensitively to nZnO and Zn(II) although potentially protected by the chorion. Reasons for the higher sensitivity are unknown but also found with other environmental pollutants (Zucchi et al., 2012). Thus, nZnO agglomerates adsorbed to the chorion are indicated to release Zn(II), which are responsible for the observed effects. The most prominent expressional changes were the induction of *mt2* and alterations in the oxidative stress related genes *sod* and *cat*. Alteration of pro-inflammatory genes *tnf-a* and *il-1b* implies that nZnO and Zn(II) result in modulation of pro-inflammatory reactions. Estimated concentrations of nZnO are expected in the range of $0.3-0.4$ μg L^{-1} in sewage treatment plant effluents (Nowack and Bucheli, 2007). Despite nZnO concentrations used in our present study are much higher, our data contribute to the understanding of the potential hazards and effects of nZnO in the aquatic environment.

2.6 Supplementary Information
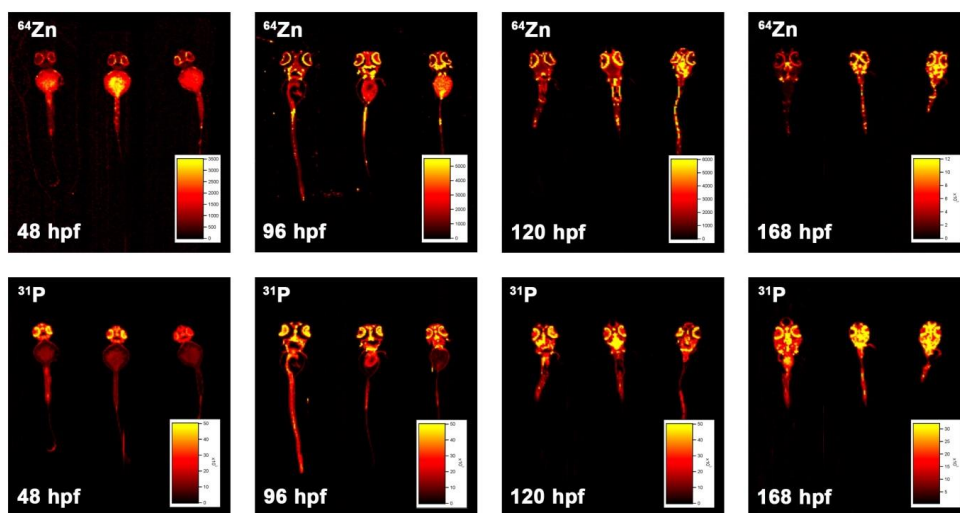
Figure S2.1 Pictures demonstrating ^{64}Zn and ^{31}P distribution in dechorionated embryos and eleuthero-embryos measured by LA-ICP-MS. Shown are coronal zebrafish embryo sections of controls (embryo on the left), 5 mg L^{-1} nZnO (middle) and 2.5 mg L^{-1} Zn(II) (right) exposure groups at different time points (48 hpf, 96 hpf, 120 hpf, 168 hpf). Colour bars show the intensity in counts per seconds. The same pattern observed for ^{66}Zn (Figure 2.4) was also seen for ^{64}Zn (this figure). This demonstrates consistency of the Zn mapping results.

3

INDIUM AND INDIUM TIN OXIDE INDUCE ENDOPLASMIC RETICULUM STRESS AND OXIDATIVE STRESS IN ZEBRAFISH (*DANIO RERIO*)

Nadja Rebecca Brun, Verena Christen, Gerhard Furrer, Karl Fent

Abstract

Indium and indium tin oxide (ITO) are extensively used in electronic technologies. They may be introduced into the environment during production, use, and leaching from electronic devices at the end of their life. At present, surprisingly little is known about potential ecotoxicological implications of indium contamination. Here, molecular effects of indium nitrate ($In(NO_3)_3$) and ITO nanoparticles were investigated *in vitro* in zebrafish liver cells (ZFL) cells and in zebrafish embryos and novel insights into their molecular effects are provided. $In(NO_3)_3$ led to induction of endoplasmic reticulum (ER) stress response, induction of reactive oxygen species (ROS) and induction of transcripts of pro-apoptotic genes and *tnf-a in vitro* at a concentration of 247 µg L^{-1}. $In(NO_3)_3$ induced the ER stress key gene BiP at mRNA and protein level, as well as *atf6*, which ultimately led to induction of the important pro-apoptotic marker gene *chop*. The activity of $In(NO_3)_3$ on ER stress induction

was much stronger than that of ITO, which is explained by differences in soluble free indium ion concentrations. The effect was also stronger in ZFL cells than in zebrafish embryos. Our study provides first evidence of ER stress and oxidative stress induction by $In(NO_3)_3$ and ITO indicating a critical toxicological profile that needs further investigation.

3.1 Introduction

Indium, and particularly indium tin oxide (ITO), are increasingly used in electronic devices. The global refinery production of indium in 2013 was 670 tons (Tolcin, 2013). Over 75% of the total indium consumption accounts for ITO (Hecht et al., 2011). ITO comes in form of nanoparticles and represents a sintered mixture of indium oxide (In_2O_3) and tin oxide (SnO_2) in a 90:10 atomic ratio. ITO has such unique physical properties including high electrical conductivity and transparency, that it became an essential compound in the electronic industry. There it is used in flat panel displays for TVs, PCs, tablets, mobile phones, and light-emitting-diode (LED), organic light-emitting diode (OLED), as well as organic and copper indium gallium selenide (CIGS) photovoltaics (Betz et al., 2006; Fthenakis, 2009).

In pristine environments and oceans indium (In^{3+}) tends to complex with hydroxide ions forming $In(OH)_3$, and is found at low concentrations with an expected upper limit of solubility at ~40 nmol L^{-1} (5 µg L^{-1}) at neutral pH (Wood and Samson, 2006). Potential industrial inputs into waters include coal burning, mining and smelting, electronics manufacture, incineration, and atmospheric deposition derived from each of these production sites. Indium concentrations of up to 75 mg kg^{-1} in river sediments were found near a smelter (Boughriet et al., 2007). Leaching from electronics, or from its incineration ashes, or from E-waste at the end-of-life-phase could result in releases to the aquatic and terrestrial environment.

At present, little is known on the toxicology of indium (Zimmermann et al., 2012). Occupational inhalation of ITO induced pulmonary fibrosis in workers (Homma et al., 2005) or pulmonary inflammation (Tanaka et al., 2002), genotoxicity, and reactive oxygen species (ROS) formation (Lison et al., 2009) in rodents. ITO particles were significantly more toxic than its single components (In_2O_3 or SnO_2) or the unsintered blend (In_2O_3 and SnO_2) and thus, ITO seems to represent a new toxicological entity (Lison et al., 2009). Cellular uptake of ITO is reported to be phagocytic and of importance in macrophages with an EC_{50} value of 400 mg L^{-1} (Gwinn et al., 2013; Lison et al., 2009). Cytotoxicity is explained by solubilization of indium ions via phagolysosomal acidification (Gwinn et al., 2013).

Surprisingly little is known on the ecotoxicology and modes of action of ITO and indium. Acute toxicity for ITO was reported in *Hydra attenuata* with an EC_{50} of 0.3 mg L^{-1} (Blaise et al., 2008). Indium nitrate ($In(NO_3)_3$) induced cytotoxicity (EC_{50} of 4.5 to 6.5 mM; 1354 to 1955 mg L^{-1}), increased metallothionein levels (EC_{50} of 3.8 mM; 1143 mg L^{-1}) and inhibited acetylcholinesterase activity (EC_{50} of 5.4 mM; 1624 mg L^{-1}) in the fish hepatoma cell line (PLHC-1; Zurita et al., 2007).

Given the extensive use of indium and associated exposure of humans and the environment, it is surprising that potential (eco)toxicological effects have only little been investigated. Consequently, in the present study, molecular and cellular effects of indium and ITO were investigated *in vitro* in zebrafish liver (ZFL) cells and *in vivo* in zebrafish embryos. The focus was set on the endoplasmic reticulum (ER) stress, which has previously shown to be induced by cadmium (Geoghegan et al., 2008), silver nanoparticles (Christen et al., 2013a), and silica nanoparticles (Christen and Fent, 2012). The ER is the subcellular organelle responsible for protein folding and maturation, and is also a major intracellular calcium reservoir. A perturbation of the ER leads to an overload with unfolded proteins. To avoid accumulation of unfolded proteins in the ER lumen, the cell activates several adaptive responses, which are known as the unfolded protein response (UPR; Ron and Walter, 2007). UPR is characterized by induction of chaperones including the binding immunoglobulin protein (BiP or GRP78), a homologue of the hsp70 heat shock proteins. BiP induction can augment the folding capacity, reduce the protein load that enters the ER, or trigger apoptosis in case of irreversible cell damage (Schröder and Kaufman, 2005).

In this study, the focus was set on important molecular and cellular reactions, including induction of ER stress, apoptosis, inflammation, and oxidative stress to evaluate little known effects of In(NO$_3$)$_3$ and ITO. As an important model organism in toxicology and ecotoxicology, zebrafish was chosen. There is a growing interest in the scientific and regulatory community to understand and be able to extrapolate *in vitro* to *in vivo* effects. To compare *in vitro* with *in vivo* activities, effects in ZFL cells were compared with those in zebrafish embryos. ITO and indium taken up from the intestine and gills are likely to reach the liver. Therefore, the frequently used ZFL cells were selected as a suitable *in vitro* model for potential effects of fish exposure, also because the liver represents a key organ for both detoxification and protein secretion and thus ER stress plays an important role (Dara et al., 2011). In both systems, the hypothesis is tested that the induction of ER stress and associated unfolded protein response by indium is linked to oxidative stress, apoptotic, and inflammatory action.

3.2 Materials and Methods

Chemicals. ITO nanoparticles (Sigma-Aldrich, Switzerland) were characterized for its specific surface area by Brunauer-Emmet-Teller method (Brunauer et al., 1938) using a Gemini model 2380 (Micromeritics Instrument Corp., U.S.A.) and for its zeta potential using a Zetasizer (Malvern Instrument Ltd., U.K.). The zeta potential of ITO nanoparticles was measured in exposure medium at 25 °C. Automatic measurements (10–100 runs) were performed in triplicates and the Smoluchowski's model was applied for analysis. The shape and size was assessed by scanning electron microscopy (SEM; Carl Zeiss Supra 40 VP, Germany). ITO nanoparticles were dispersed in H$_2$O, ultra-sonicated for 5 min at a frequency of 37 kHz using an Elmasaonic S 30 (Elma GmbH, Germany) and air-dried. Images were taken at an accelerating voltage of 5 kV and over a working distance of 4 mm. The particle

size distribution was determined by NanoSight LM10 (NanoSight Ltd., U.K.) followed by evaluation using the Nanoparticle Tracking Analysis (NTA) software according to Brun et al. (2014b). Three independent samples per concentration were taken and each sample was injected three times, calculating the arithmetic average thereof.

The amount of soluble indium in ZFL cell line culture medium and zebrafish culture medium was quantified using an ICP-MS system (Agilent 7500cx, Switzerland) equipped with an Octopole Reaction System, pressurized with an optimized helium flow of 5 mL min^{-1}. Medium samples (1 mL) were centrifuged for 30 min at 30 000 g and the concentrations of indium (^{115}In) and tin (^{118}Sn) isotopes determined in the supernatant. Supernatants were diluted 1:100 in 1% HNO$_3$. Rubidium was used as internal standard.

Cell Culture and Exposure. *Danio rerio* liver cells (ZFL; ATCC number CRL-2643) were cultured as described elsewhere (Christen et al., 2009). ZFL cells were seeded at a density of 100 000 cells per well in 96-well plates. After 24 h, cells were exposed for 24 h to different nominal concentrations (0.5 to 1000 mg L^{-1}) of In(NO$_3$)$_3$ or ITO, respectively and 504 mg L^{-1} KNO$_3$. Untreated cells served as controls. Mitochondrial activity was evaluated using the methyl tetrazolium (MTT) assay (Mosmann, 1983) and production of reactive oxygen species (ROS) using the ROS assays (Christen and Fent, 2012) as previously described. For gene expression analysis, the cells were seeded in 22.1 cm^2 tissue culture plates (TPP Techno Plastic Products AG, Switzerland). Due to hygroscopic behavior, stock solutions of In(NO$_3$)$_3$ were prepared immediately after receiving. Stock solutions of both ITO and In(NO$_3$)$_3$ (1 mg mL^{-1}) were prepared in Nanopure water, stirred for 30 min and ultrasonicated for 5 min at a frequency of 37 kHz before dispersing in the media.

MTT Assay. The cytotoxicity was determined based on the enzymatic conversion of the MTT tetrazolium salts to formazan crystals by the MTT (Mosmann, 1983) assay. After incubation with serial dilutions of In(NO$_3$)$_3$ and ITO for 24 h, 20 μL of 3-(4,5-dimethylthiazol-2-yl)-2,5-diphenyltetrazolium bromide (MTT; 5 mg mL^{-1} in PBS, Sigma-Aldrich, Switzerland) were added to each well and incubated at 28 °C for 3 h. The medium was aspirated from each well and the resulting formazan crystals were solubilized by adding 200 μL of dimethyl sulfoxide and shaking for 10 min. 25 μL of Sörensen buffer (0.1 M Glycine, 0.1 M NaCl, pH 10.5) were added to each well. After an incubation time of 5 min at room temperature, the absorbance was measured by an automatic microplate reader (Tecan Infinite M200, Tecan, Switzerland) at 570 nm. The results were expressed as percent living cells compared to untreated control cells. AgNO$_3$ served as positive control.

ROS Assay. Intracellular ROS production was determined using 2,7-dichlorofluorescein diacetate (H$_2$DCFDA in dimethyl sulfoxide; Sigma-Aldrich, Switzerland) as described before (Christen and Fent, 2012). Following the exposure, the medium was discarded, each well was washed with PBS, and incubated with H$_2$DCFDA dye (100 μM) for 30 min at 28 °C. The nonfluorescent H$_2$DCFDA passes through the plasma membrane, where it is de-esterified and may be oxidized to fluorescent 2,7-dichlorofluorescein (DCF) by ROS. The reaction mixture was replaced by PBS and fluorescence intensity (extinction at 485 nm and emission at 530 nm) measured in an automatic microplate reader (Tecan Infinite M200, Tecan, Switzerland). The results were expressed as intracellular ROS activity in percent compared

to control (cells in medium) and normalized to cell viability (assessed by MTT assay). H_2O_2 served as positive control.

RNA Isolation, Reverse Transcription and RT-qPCR. Total RNA was extracted from ZFL cells using TRIzol reagent (LuBioScience, Switzerland) and from a pool of 25 zebrafish embryos using RNeasy Mini Kit (Qiagen, Switzerland) and further purified by on-column RNase free DNase digestion (Qiagen, Switzerland) according to the manufacturer's instructions. 1000 ng thereof were reverse transcribed by Moloney murine leukemia virus reverse transcriptase in the presence of random hexamers and deoxynucleoside triphosphate, followed by RT-qPCR based on SYBR green fluorescence. The amplification conditions were 95 °C for 10 min, 40 cycles of 95 °C for 15 s, and 60 °C for 60 s. A melting curve was run afterward. To mitigate technical variability, two technical replicates per biological replicate were performed for each run using the BioRad CFX96 RealTime PCR Detection System (BioRad, Switzerland). The ribosomal protein L13α (*rpl13a*) was selected as housekeeping gene, as its expression profile did not vary neither under the experimental conditions, nor in the *in vitro* or *in vivo* study. To illustrate mRNA expression, C_T values of target gene were normalized to the C_T value of the housekeeping gene *rpl13a* (=ΔC_T) and then normalized to the untreated control (ΔC_T untreated – ΔC_T treated). Fold changes were log2 transformed to produce symmetrical values and for further data analysis. The sequences of used primers are shown in Supporting Information (SI) Table S1. Thapsigargin, which is a potent inducer of ER stress and UPR through inhibition of the ER-resident Ca^{2+}-dependent ATPase (Thastrup et al., 1990), was used as positive control in the *in vitro* study.

Preparation of Cell Extracts and Immunoblotting. ZFL cells were homogenized in cell lysis buffer (50 mM TRIS, 150 mM NaCl, 15 mM EDTA, 0.1% Triton X-100, and 1 mM phenylmethylsulfonyl fluorid), incubated for 20 min on ice, centrifuged at 14 000 g for 15 min, and the supernatant was collected. Protein concentrations were quantified using Pierce BCA protein assay kit (Fisher Scientific, Switzerland) and immunoblotting performed as previously described (Duong et al., 2004). The membrane was incubated with BiP antibody (Sigma, Switzerland), followed by incubation with an Alexa488-labled DyLight Fluor secondary antibody (Thermo Scientific, Switzerland). The protein bands were visualized using a Fujifilm FLA-900 scanner (Bucher Biotec, Switzerland). β-Actin was detected using anti-β-actin monoclonal antibody (Thermo Scientific, Switzerland). Thapsigargin was used as positive control.

Exposure of Zebrafish Embryos to In(NO₃)₃ and ITO. Zebrafish eggs from the blastula stage to 96 h post fertilization (hpf) were exposed to three nominal concentrations (0.1, 1, 10 mg L⁻¹) of In(NO₃)₃ and ITO in zebrafish culture medium (5 mM NaHCO₃, 0.5 mM KCl, 17.7 mM CaCl₂, 6.8 mM MgSO₄). A higher test concentration was not feasible as indium carbonate precipitation was visible at concentrations above 15 mg L⁻¹. Embryos from the control group were kept in zebrafish culture medium only. Embryos were kept in glass beakers and to ensure homogeneous nanoparticle dispersion, each beaker was aerated with a glass pipet. Every dose-group consisted of four replicates with 60 embryos each. Embryos were kept at a 16:8 h light/dark photoperiod at 27 ± 1 °C. A static-renewal procedure with complete water exchange every 24 h was applied. Embryos were not dechorionated and sam-

pled at 48 hpf and 96 hpf. At each time point, 25 embryos were pooled and stored in RNAlater for further molecular analysis. Isolation of total RNA, reverse transcription and RT-qPCR were conducted as described above.

Statistical Analyses. All data were graphically and statistically evaluated with GraphPad Prism 5 (GraphPad Software, CA). Significant differences between treatments were assessed by one way ANOVA followed by Bonferroni posthoc test ($p \leq 0.05$) to compare treatments with respective controls. In the *in vitro* studies, three independent experiments were conducted, using four replicates for each treatment group. In the *in vivo* study, four replicates for each treatment group were used. Results are expressed as means ± standard deviation of mean (SD). Differences were considered statistically significant at $p \leq 0.05$.

3.3 Results

Chemical Characterization. The characterization of ITO nanoparticles included SEM, Brunauer–Emmet–Teller method, zeta potential, and size distribution measurements. ITO nanoparticles were a heterogeneous, polygonal shaped mixture (SI Figure S3.1), with a specific surface area of 19.5 $m^2 g^{-1}$ and a zeta potential of −15.2 mV (500 mg L^{-1} in ZFL medium) or 6.0 mV (10 mg L^{-1} in zebrafish medium). NanoSight measurements confirmed a heterogeneous mixture of 50−300 nm sized nanoparticles in both ZFL and zebrafish medium (SI Figure S3.2). This size distribution together with a zeta potential of less than ±30 mV indicates agglomeration of nanoparticles when dispersed in both media. ICP-MS analyses demonstrated that the concentration of indium ions released from ITO after 24 h are low (SI Table S2). In ZFL culture medium, the highest measured indium concentration was 624 µg L^{-1} (5.44 µM) in the supernatant after centrifugation. This was about 1500 times lower than the nominal concentration (1000 mg L^{-1}; 3325 µM), with no significant change over 24 h. In ITO exposures, the soluble indium concentration (nominal 1000 mg L^{-1}) was 156 µg L^{-1} (1.36 µM), thus lower than in the $In(NO_3)_3$ exposures. In zebrafish medium, the concentration of soluble indium was as low as 0.12 to 9.53 µg L^{-1} for both $In(NO_3)_3$ and ITO exposures (SI Table S3.3, Figure S3.3). Due to low soluble indium concentrations in comparison to nominal concentrations and as the soluble indium is critical to toxicity, results are given in terms of measured values representing actual exposure levels.

Cytotoxicity. Cytotoxicity was investigated by MTT assay after 24 h incubation with different concentrations of $In(NO_3)_3$ and ITO. The LC_{50} value of $In(NO_3)_3$ was 310 µg L^{-1} (1.03 µM; SI Figure S3.4), whereas ITO induced no cytotoxicity up to 156 µg L^{-1} (corresponding to a nominal concentration of 1000 mg L^{-1}).

Transcriptional Alterations *In Vitro*. It was analysed whether $In(NO_3)_3$ and ITO exposure result in alterations of target gene transcripts belonging to ER stress, apoptosis, oxidative stress, and inflammatory response pathways. A nitrate effect can be excluded, as no transcriptional alterations in ZFL cells exposed to 504 mg L^{-1} KNO_3, equivalent to 500 mg L^{-1} $In(NO_3)_3$ occurred (SI Figure S3.5). To demonstrate that the ER stress response can be induced, ZFL cells were exposed to the positive control thapsigargin. A time-dependent in-

duction of major ER stress genes was observed with strongest response after 6 and 12 h of exposure (SI Figure S3.6).

For assessing the effects of In(NO$_3$)$_3$ and ITO an exposure time of 24 h was chosen, as a less rapid induction compared to the potent inducer thapsigargin was expected. Exposure of ZFL cells to noncytotoxic concentrations of 201 and 247 μg L^{-1} In(NO$_3$)$_3$ for 24 h promoted a significant activation of *bip*, activating transcription factor 6 (*atf6*), CCAAT/-enhancer-binding protein homologous protein (*chop*) and synoviolin (*synv*) transcripts related to ER stress (Figure 3.1A). BiP protein was also induced at the high In(NO$_3$)$_3$ concentration (Figure 3.1B). In contrast, ITO did not significantly alter ER stress genes (Figure 3.1A), nor the BiP protein (Figure 3.1B).

Exposure to In(NO$_3$)$_3$ also altered transcripts of apoptosis related genes, including B-cell lymphoma 2 (*bcl-2*), tumor suppressor protein (*p53*), PMA induced protein 1 (*noxa*), apoptotic protease-activating factor 1 (*apaf1*), and caspase 9 (*casp9*), whereas ITO was less active as indicated by alteration of *noxa* and *casp9* (Figure 3.2A). Genes such as cyclin-dependent kinase inhibitor 1 (*p21*), E3 ubiquitin-protein ligase (*mdm2*), Bcl-2 like protein 4 (*bax*), and caspase 3 (*casp3*) were unaltered for both compounds.

To analyze for inflammatory responses, the induction of interferon regulatory factor 3 (*irf 3*), interferon regulatory factor 9 (*irf 9*), tumor necrosis facor α (*tnf-a*), and nuclear factor NF-kappa-B p50 subunit (*nfkb1/p50*) mRNA levels were deter-

Figure 3.1 (A) Transcriptional alterations of ER stress related genes in ZFL cells after incubation with indicated concentrations of In(NO$_3$)$_3$ and ITO for 24 h. Relative expression levels were normalized to *rpl13a*, calculated relatively to expression levels in control cells and are shown as log2. Asterisks indicate significant differences to controls (*p < 0.05, **p < 0.01, and ***p < 0.001). Values are presented as mean ± SD (n=3, independent experiments). (B) Representative Western blot of BiP (78 kDa) and actin (42 kDa).

mined (Figure 3.2B). In(NO$_3$)$_3$ led to a significant and strong induction of *tnf-a*, while the induction by ITO was weaker. In(NO$_3$)$_3$ solely led to alterations of *irf 3*, *irf 9*, and *nfkb1/p50* (Figure 3.2B).
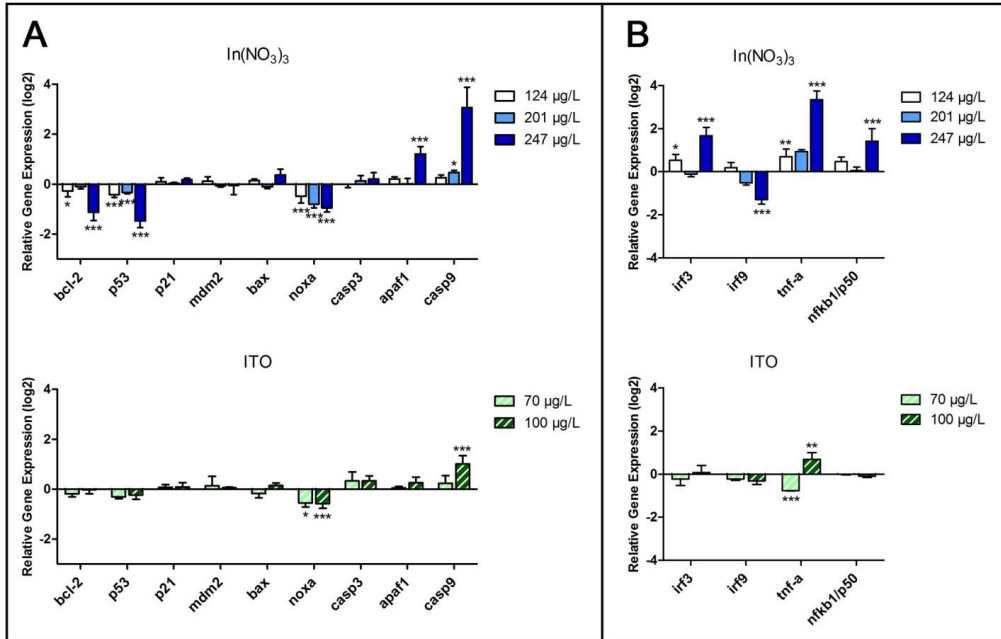
Figure 3.2 Transcriptional alterations of apoptosis (A) and innate immune system (B) related genes in ZFL cells after incubation with indicated concentrations of In(NO$_3$)$_3$ and ITO for 24 h. Relative expression levels were normalized to *rpl13a*, calculated relatively to expression levels in control cells and are shown as log2. Asterisks indicate significant differences to controls (*p < 0.05, **p < 0.01, and ***p < 0.001). Values are presented as mean ± SD (n=3, independent experiments).

Induction of ROS. In(NO$_3$)$_3$ and ITO exposure resulted in dose-related generation of reactive oxygen species (ROS; Figure 3.3A). In(NO$_3$)$_3$ induced a stronger activity than ITO. In addition, oxidative stress is indicated by transcriptional alterations of catalase (*cat*) and glutathione-S-transferase Mu 1 (*gstm1*; Figure 3.3B).

Transcriptional Alterations *In Vivo*. To analyze for *in vivo* effects, zebrafish embryos were exposed to In(NO$_3$)$_3$ and ITO up to 96 hpf. A significant up-regulation of *bip* and *atf6* transcripts was found after exposure to 1.59 and 9.53 μg L^{-1} of In(NO$_3$)$_3$ at 48 hpf and after exposure to 9.53 μg L^{-1} at 96 hpf (Figure 3.4). Exposure to ITO led to induction of *bip* and *atf6* transcripts at the highest concentration of ITO at 48 or 96 hpf, respectively. In addition, a strong induction of *tnf-a* transcripts occurred at 1.59 and 9.53 μg L^{-1} In(NO$_3$)$_3$ as well as at 1.07 and 7.93 μg L^{-1} (Figure 3.4). As found *in vitro*, the activity of In(NO$_3$)$_3$ was higher than that of ITO. Both In(NO$_3$)$_3$ and ITO led to induction of the catalase transcript at the highest concentrations. Transcripts of apoptosis related genes *casp9* and *p53* showed little alterations. Over the two sampled time points (48 hpf and 96 hpf), the expression of *bip*, *atf6*, *cat*, and *tnf-a* remained similar, whereas *casp9* and *p53* showed a tendency of up-regulation at 48 hpf and a significant down-regulation at 96 hpf.
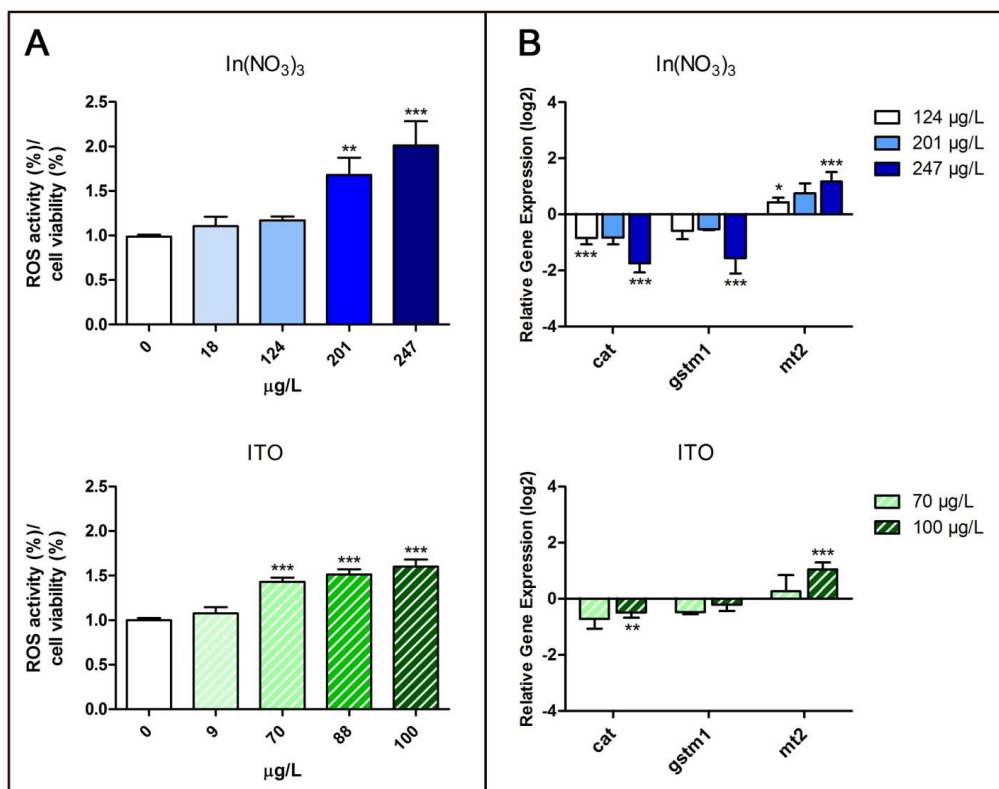
Figure 3.3 Induction of oxidative stress in ZFL cells after exposure with indicated concentrations of In(NO$_3$)$_3$ and ITO for 24 h. (A) ROS detection using H$_2$DCFDA. Changes of intracellular ROS activity shown as percent of control (cells in medium) and normalized to cell viability (assessed by MTT assay). (B) Transcriptional alterations of oxidative stress related genes (*cat*, *gst*) and metallothionein (*mt2*). Relative expression levels were normalized to *rpl13a*, calculated relatively to expression levels in control cells and are shown as log2. Asterisks indicate significant differences to controls (*p < 0.05, **p < 0.01, and ***p < 0.001).Values are presented as mean ± SD (n=3, independent experiments).
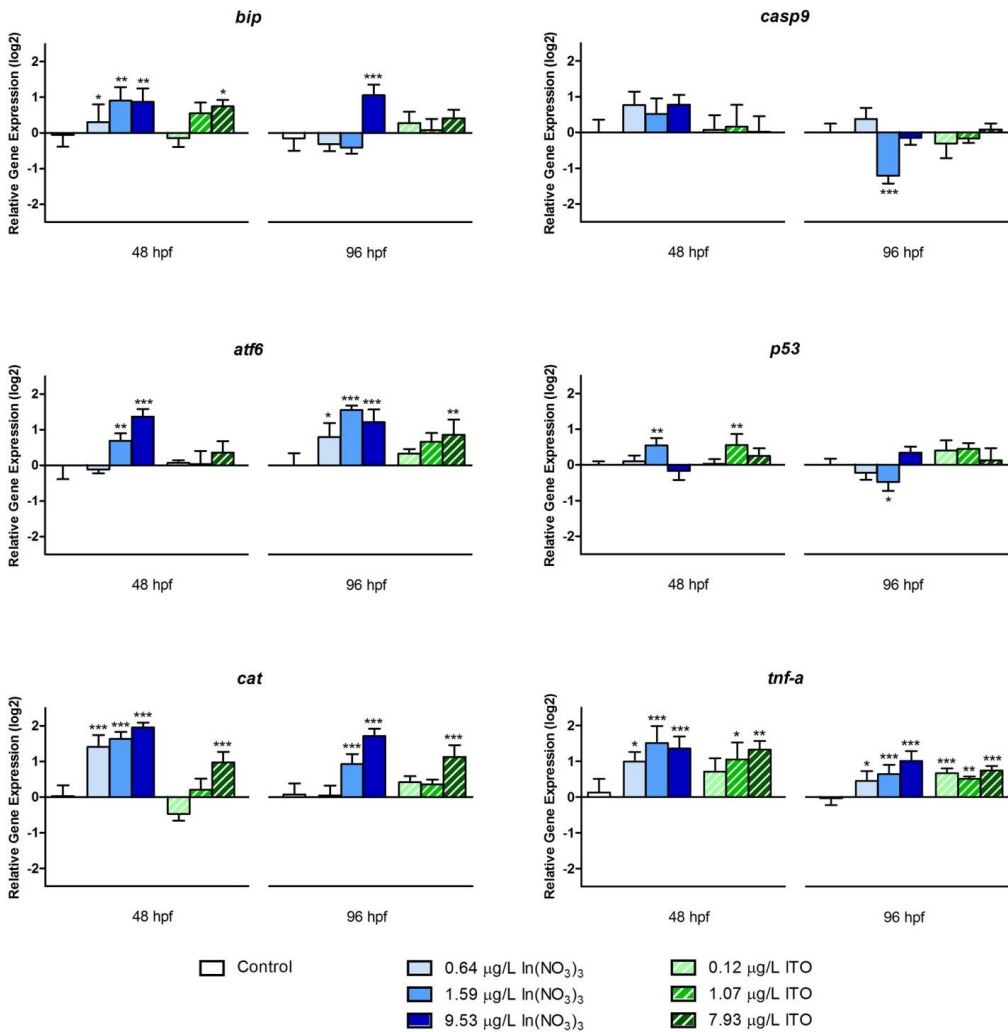
Figure 3.4 Transcriptional alterations of selected genes (*bip*, *atf6*, *cat*, *casp9*, *p53*, *tnf-a*) in zebrafish embryos after exposure to the indicated concentrations of In(NO₃)₃ and ITO until 48 and 96 hpf, respectively. Relative expression levels are normalized to *rpl13a*, calculated relatively to expression levels in control cells and shown as log2. Asterisks indicate significant differences to controls (*p < 0.05, **p < 0.01, and ***p < 0.001). Values are presented as mean ± SD (n=4).

3.4 Discussion

Our data demonstrate that $In(NO_3)_3$ and ITO induce ER stress *in vitro* and *in vivo*. The ER stress response was related to apoptosis, oxidative stress, and inflammation at high tested concentrations. The effects of $In(NO_3)_3$ were much stronger than those of ITO, both *in vitro* and *in vivo*. On the basis of the higher concentrations of soluble free indium ions in $In(NO_3)_3$ exposures, it is suggested that the toxic moiety is ionic indium.

Indium Solubility. The solubility of indium $(In(OH)_3(s))$ is expected to have its upper limit at circumneutral pH at a concentration of ~5 µg L^{-1} (40 nM; Wood and Samson, 2006). In solution, In^{3+} preferentially forms complexes with hard bases such as OH^-, F^-, acetate (Wood and Samson, 2006), and in particular with small organic molecules (Martell and Smith, 1977; White and Hemond, 2012). Hence, indium prevails in the form of $In(OH)_3^0$ in natural waters. In ZFL culture medium, the amino acid concentration is 8.73 mM and there-fore exceeds the highest added indium concentration of 624 µg L^{-1} (5.44 µM). It is suggest-ed that soluble free indium build complexes with amino acids, thus becoming more soluble. Although indium had a higher solubility in cell culture medium compared to the zebrafish culture medium, effects in ZFL cells occurred at higher soluble indium concentrations than in zebrafish embryos. This means that embryos had a higher sensitivity to indium than ZFL cells.

ER Stress. ER stress induction is determined by a targeted gene expression approach fo-cusing on key genes related to ER stress. Our data clearly show that BiP is induced by $In(NO_3)_3$. The prominent ER chaperone BiP binds to the stress sensors inositol-requiring kinase 1α (IRE1α), double-stranded RNA-activated protein kinase-like ER kinase (PERK), and activating transcription factor 6 (ATF6) under nonstressed conditions, whereas it is released and binds to unfolded or misfolded proteins, when such proteins are accumulated in the ER. Upon ER stress three different UPR signaling cascades can be activated through IRE1α, PERK, or ATF6 (Hetz, 2012). While PERK reduces the translocation of proteins into the ER lumen, IRE1α and ATF6 mediate the transcription of genes that increase the protein folding, including BiP. To evaluate the effects of $In(NO_3)_3$ and ITO, marker genes from each of the signaling cascades were analyzed. Activation of PERK would lead to phosphorylation of the eukaryotic translation initiation factor eIF2α, which causes induction of activating transcription factor 4 (ATF4), while IRE1α would initiate X-box binding protein (*xbp-1*) mRNA splicing, and ATF6 would lead to transport to the Golgi complex with further trans-location to the nucleus where it induces transcription of several genes including *bip* and *chop* (Todd et al., 2008). Figure 3.1 shows that $In(NO_3)_3$ promoted a selective activation of ATF6 leading to an increased induction of *bip* and *chop* in ZFL cells. However, $In(NO_3)_3$ and ITO did not lead to induction of *atf4b1* and spliced form of *xbp-1* (*xbp-1s*), and therefore the PERK and IRE1α pathways were not remarkably activated.

Transcription analysis indicated that the induction of ER stress response by $In(NO_3)_3$ was potentially followed by apoptosis. Chop has been implicated in repressing transcription of the anti-apoptotic Bcl-2 protein (Cullough et al., 2001; Kim et al., 2006), which leads to enhanced oxidant injury and apoptosis. Pyati et al. (2011) showed in

zebrafish that ER stress-induced cell death can be blocked by overexpression of mRNA encoding Bcl-2 and proved that *chop* is ER stress responsive. The Bcl-2 family includes members which suppress apoptosis (e.g., Bcl-2 and Bcl-xL), and other which enhance apoptosis (e.g., Bax; Adams, 1998). Although one would expect an up-regulation of the pro-apoptotic gene bax, several studies observe a coordinate down-regulation of Bcl-2 and Bax proteins, as Bcl-2 may bind Bax and form heterodimers which leads to inhibited Bax activity (Mengubas et al., 1996; Wang et al., 1998).

During ER stress, Ca^{2+} is released to the cytoplasm (Deniaud et al., 2008). Increased cytosolic Ca^{2+} can activate both mitochondria-dependent and -independent caspase cascades (Rao et al., 2002). Ca^{2+} released from ER also enters mitochondria to depolarize the inner membrane, promoting cytochrome c release and activating Apaf-1, then caspase 9, caspase 3 and finally leading to apoptosis (Li et al., 1997). Indium nitrate led to induction of *apaf-1* and *casp9* transcripts (Figure 3.2A), indicating induction of apoptosis. However, genes required for most forms of apoptosis such as bcl-2 or *noxa* were down-regulated and bax was not altered. The significant down-regulation of the *p53* transcript may not be due to the *p53* inactivator *mdm2* (as it is not up-regulated), but rather due to *synv*. Synoviolin, a representative of ER-resident E3 ubiquitin ligase, is up-regulated to protect against ER stress-induced apoptosis (Kaneko et al., 2002). Moreover, synoviolin inhibits *p53* expression in the cytosol and ubiquinates it (Yamasaki et al., 2007a, 2007b).

ITO exposure altered none of the transcripts of investigated ER stress genes in ZFL cells, including BiP protein (Figure 3.1B). Regarding apoptosis related genes, ITO altered the transcript of *noxa*, which is not necessarily associated with ER stress. Thus, ER stress is indicated to be induced by the concentration of soluble free indium ions, as $In(NO_3)_3$ but not ITO (with less free indium) led to transcriptional induction of ER stress key genes.

Oxidative Stress. Our results show a significant ROS generation by both $In(NO_3)_3$ and ITO, induction of metallothionein-2 (*mt2*) and down-regulation of *cat* and *gstm1*. Catalase is a major ROS-scavenging enzyme, metabolizing hydrogen peroxide to water while glutathione-S-transferases are primarily involved in detoxification and protection against oxidative stress. The presence of excessive ROS is indicated by the ROS assay and *mt2* transcripts, while down-regulation of *cat* and *gstm1* suggests an autoregulatory negative feedback loop suppressing further transcription.

The complex interaction between protein misfolding and oxidative stress is incompletely characterized but there is growing evidence that activating of either one will affect the other (Malhotra et al., 2008; Zhang, 2010). Increased ROS can result in depletion of calcium stores in the ER (Zhang, 2010) or in accumulation of oxidatively damaged proteins (Finkel and Holbrook, 2000), in particular ROS scavenging and heat shock proteins, as well as chaperones (Godon et al., 1998). The increased cytosolic calcium subsequently stimulates the mitochondria metabolism to produce more ROS while the activation of the protective PERK signaling cascade can up-regulate genes involved in resistance to oxidative stress (Cano et al., 2014; Harding et al., 2003). Finally, both oxidative stress and unresolved ER stress can initiate multiple pathways of cell death including expression of Chop and activation of caspases (Malhotra and Kaufman, 2007).

Innate Immune Response. By assessing mRNA expression levels of the interferon-stimulated genes *irf3* and *irf9*, TNF-α, and NF-κB family member *nfkb1/p50*, effects on the innate immune system in particular by In(NO$_3$)$_3$ were demonstrated. Furthermore, this response is suggested to be associated with ER stress. Calcium release, ROS production, and accumulation of proteins in the ER potently triggers activation of transcription factor NF-κB (Hung et al., 2004; Lin et al., 2012; Pahl and Baeuerle, 1995), leading to the expression of type 1 interferons and tumor necrosis factor alpha (Akira et al., 2006; Christen et al., 2013b; Martinon and Glimcher, 2011; Zhang and Kaufman, 2008). Yamazaki et al. (2009) demonstrated that UPR-mediated activation of NF-κB is selectively depending on the ATF6 pathway. Therefore, it is suggested that there is a potential link between the activation of the ATF6 pathway and the up-regulation of *nfkb1/p50* by indium. However, previous reports showed that NF-κB can also be activated through PERK, IRE1α, and ATF6 pathways, depending on varying time courses in response to ER stress (Lin et al., 2007) or cell types (Deng et al., 2004). The pro-inflammatory cytokine TNF-α was induced by ER stress depending on NF-κB (Hu et al., 2006). Indium containing compounds are known for their inflammatory effects, which are thought to be due to oxidative stress (Gottschling et al., 2001). Our present data indicate that the inflammatory reaction of indium is related to ER stress.

In Vivo **Exposure.** ER stress was also induced by In(NO$_3$)$_3$ and ITO in zebrafish embryos as indicated by *bip* and *atf6* induction. In addition, the *tnf-a* transcript was induced, similar as *in vitro*, but there were also some differences, such as induction of *cat* and lack of alteration of apoptosis related gene *casp9*. The weaker ER stress induction in zebrafish embryos in comparison to *in vitro* may be related to differences in dissolved indium concentrations, as indicated by ICP-MS analysis (dissolved indium concentration of highest exposure group is about 20-times higher in the *in vitro* study; SI Figure S3.3). The amino acids in the cell culture medium are suggested to complex free indium, and thus increase its solubility. Further, the ZFL cell line is derived from adult zebrafish liver, a key organ for protein secretion, and therefore ER stress marker genes are likely to be induced relatively stronger than in whole zebrafish embryos. A weaker ER stress induction in zebrafish embryos could also be caused by differential uptake and bioaccumulation.

Comparison *In Vitro* and *In Vivo*. Effects such as induction of ER stress, oxidative stress as well as TNF-α occurred in both the ZFL cells and zebrafish embryos. Thus, the *in vitro* system has a predictive power for these effects. The ZFL cells turned out to be more resistant than embryos in terms of exposure concentrations exhibiting these effects. This means that higher concentrations were needed for induction of transcriptional alterations in ZFL cells than in embryos. This finding is in accordance with previous studies with other compounds, where the combination of zebrafish embryos and ZFL cells was shown to be useful for determining molecular effects. Also in these studies ZFL cells were less sensitive than zebrafish embryos (Chen et al., 2011; Christen et al., 2013a). One reason for the often reported higher effect levels in *in vitro* systems lies in the fact that no measurement of actual exposure concentrations were performed. However, in the present study soluble indium exposure levels were measured both in cell culture and embryo culture medium.

Other reasons may account for the lower sensitivity of the *in vitro* system. The uptake mechanisms may be more efficient in embryos than in the cell culture system. The liver is the primary organ for metabolism and detoxification, hence ZFL liver cells may have a higher tolerance (including induction of metallothioneins) compared to whole embryos.

Collectively, this study indicates that the ZFL *in vitro* system is suitable to predict molecular effects of indium. For a more comprehensive investigation, the effects of indium on gill cells or macrophages could be of interest. However, the ZFL cells are less suitable compared to zebrafish embryos to derive effect levels that may be used for quality assessment of water bodies or regulatory purposes. The data of this study may also reveal potential effects of indium to human health. On the molecular level zebrafish and humans exhibit many common mechanisms and therefore, the zebrafish has become a widely accepted model in toxicology and for studying human diseases (Aleström et al., 2006; Schartl, 2014).

In conclusion, our data demonstrate that $In(NO_3)_3$ and ITO lead to induction of oxidative stress, ER stress, and associated UPR *in vitro* and *in vivo*. ER stress induction was associated with apoptotic and inflammatory reactions, similar to silica nanoparticles (Christen and Fent, 2012). The combination of an *in vitro* system (ZFL cells) and zebrafish embryos allowed to elucidate potential molecular effects and mode of actions of indium. The physiological and toxicological implications of our data should further be investigated to assess the ecotoxicological consequences of indium contamination.

3.5 Supplementary Information

Table S3.1   Primer sequences used for quantitative real-time PCR analysis

Target gene	Primer sequence (5' to 3')	Accession no.[a]
rpl13a	fw: AGC TCA AGA TGG CAA CAC AG	NM_198143
	rv: AAG TTC TTC TCG TCC TCC	
bip	fw: CGA AGA AGC CAG ATA TCG ATG A	NM_213058
	rv: ACG GCT CTT TTC CGT TGA AC	
xbp-1	fw: GGG TTG GAT ACC TTG GAA A	NM_131874
	rv: AGG GCC AGG GCT GTG AGT A	
xbp-1s	fw: TGT TGC GAG ACA AGA CGA	XM_003199171
	rv: CCT GCA CCT GCT GCG GAC T	
atf6	fw: CTG TGG TGA AAC CTC CAC CT	NM_001110519
	rv: CAT GGT GAC CAC AGG AGA TG	
atf4b1	fw: CTT TCT CTC CTC CTG CTT CT	NM_213233
	rv: GAG TCA CAC GAC CCA ATC A	
chop	fw: GAG TTG GAG GCG TGG TAT GA	NM_001082825
	rv: CCT TGG TGG CGA TTG TGT AA	
syvn	fw: ACC GAC AAT GTG TGC ATC ATC T	NM_212735
	rv: AAC CAT GAG CGA AGG CAA CT	
bcl-2	fw: TCA CTC GTT CAG ACC CTC AT	NM_001030253
	rv: ACG CTT TCC ACG CAC AT	
p53	fw: GCT TGT CAC AGG GGT CAT TT	NM_131327
	rv: ACA AAG TCC CAG TGG AGT G	
p21	fw: GGA AAG ATG ACC GAT GAG GA	NM_001002717
	rv: GAC GCA CCT TGT CCA ATT TT	
mdm2	fw: TGA CAA CGA GAA ACT GGT AAG A	NM_131364
	rv: AAA CAT AAC CTC CTT CAT GGT	
bax	fw: ACA GGG ATG CTG AAG TGA CC	NM_131562
	rv: GAA AAG CGC CAC AAC TCT TC	
noxa	fw: ATG GCG AAG AAA GAG CAA AC	NM_001045474
	rv: CGC TTC CCC TCC ATT TGT AT	
casp3	fw: CCG CTG CCC ATC ACT A	NM_131877
	rv: ATC CTT TCA CGA CCA TCT	
casp9	fw: AAA TAC ATA GCA AGG CAA CC	NM_001007404
	rv: CAC AGG GAA TCA AGA AAG G	
apaf-1	fw: TTC TAC AGT AAA CGC CCA CC	NM_131608
	rv: TAT CTA GTA TTT CCC CAT ATT CC	
irf3	fw: CAA AAC CGC TGT TCG TGC C	NM_001143904
	rv: CAT CGT CGC TGT TGG AGT CCT	

irf9	fw: AAG GCT TGG GCG GCG TTT	NM_205710
	rv: GGC ACA TCG AAG GCG TGT T	
tnf-a	fw: ACC AGG CCT TTT CTT CAG GT	NM_212859
	rv: TGC CCA GTC TGT CTC CTT CT	
nfkb1/ p50	fw: AGT CAG CCT CAG ATC CGT GTG TTT	XM_003199975
	rv: TTG TAA GCA AGG CCC ATC AAC TGC	
cat	fw: AGG GCA ACT GGG ATC TTA CA	NM_130912
	rv: TTT ATG GGA CCA GAC CTT GG	
gstm1	fw: CTA TAC ATG CGG CGA AGC T	NM_212676
	rv: GGC ATT GCT CTG GAC GAT	
mt2	fw: AAA TGG ACC CCT GCG AAT	NM_001131053
	rv: TTG CAG GTA GCA CCA CAG TT	

[a] GeneBank accession number (http://www.ncbi.nlm.nih.gov).

Table S3.2   Nominal concentrations and concentrations measured by ICP-MS in ZFL culture medium after 24 h of exposure

Nominal		Measured	
mg L^{-1}	μM	μg L^{-1}	μM
50 In(NO$_3$)$_3$	166 In(NO$_3$)$_3$	124 ± 10 In	1.08 ± 0.09 In
200 In(NO$_3$)$_3$	664 In(NO$_3$)$_3$	201 ± 81 In	1.75 ± 0.71 In
500 In(NO$_3$)$_3$	1662 In(NO$_3$)$_3$	247 ± 43 In	2.15 ± 0.38 In
1000 In(NO$_3$)$_3$	3325 In(NO$_3$)$_3$	624 ± 148 In	5.44 ± 1.29 In
50 ITO	340 ITO	70 ± 33 In	0.61 ± 0.29 In
200 ITO	1359 ITO	88 ± 11 In	0.77 ± 0.10 In
500 ITO	3397 ITO	100 ± 22 In	0.87 ± 0.19 In
1000 ITO	6794 ITO	156 ± 36 In	1.36 ± 0.31 In

Table S3.3   Nominal concentrations and concentrations measured by ICP-MS in zebrafish embryo culture medium after 24 h of exposure

Nominal		Measured	
mg L^{-1}	μM	μg L^{-1}	μM
0.1 In(NO$_3$)$_3$	0.332 In(NO$_3$)$_3$	0.64 ± 0.26 In	4.36 ± 1.75 In
1 In(NO$_3$)$_3$	3.325 In(NO$_3$)$_3$	1.59 ± 1.63 In	5.27 ± 5.42 In
10 In(NO$_3$)$_3$	33.245 In(NO$_3$)$_3$	9.53 ± 0.01 In	31.69 ± 0.02 In
0.1 ITO	0.679 ITO	0.12 ± 0.02 In	0.39 ± 0.06 In
1 ITO	6.798 ITO	1.07 ± 0.82 In	7.24 ± 5.58 In
10 ITO	67.981 ITO	7.93 ± 2.52 In	53.89 ± 17.11 In
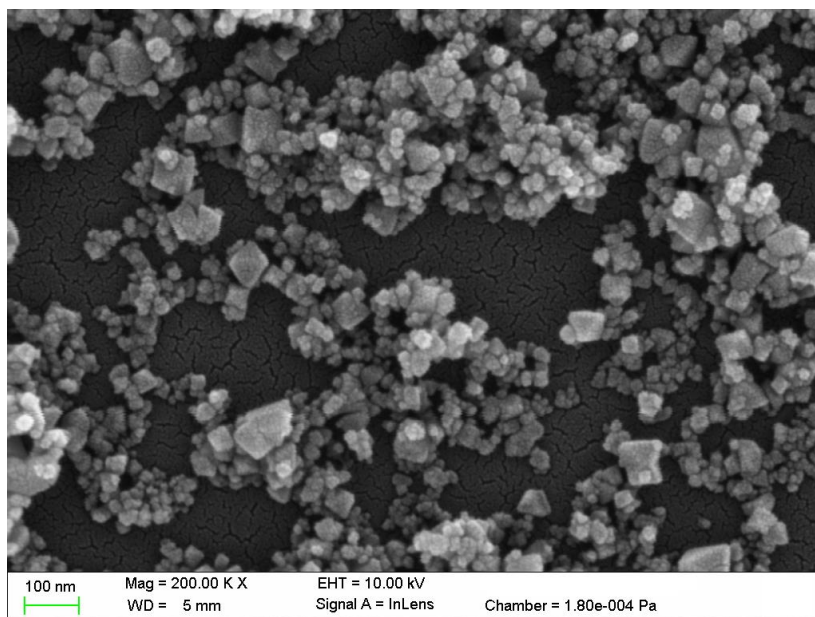
Figure S3.1 Scanning electron microscopic (SEM) image of ITO nanoparticles.
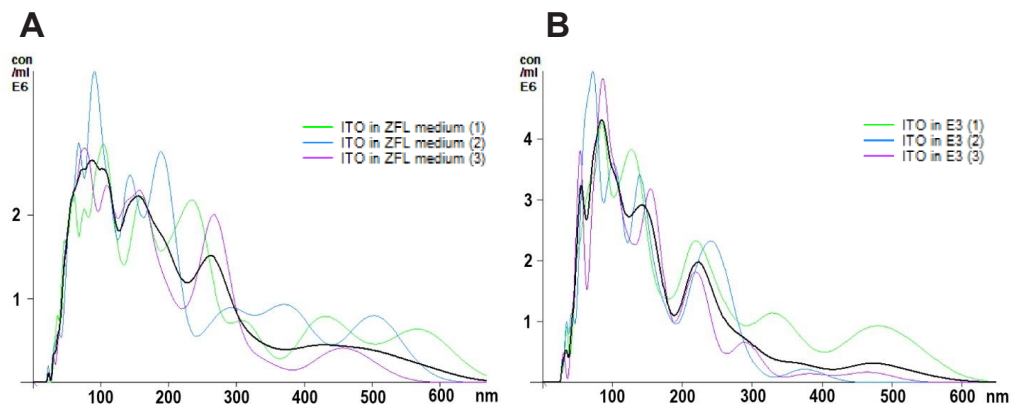
Figure S3.2 Mean ITO nanoparticle size in ZFL culture medium (A) and zebrafish culture medium (B) measured by NanoSight LM10. Coloured lines show three independent measurements, black line shows mean of three independent measurements.

A ZFL culture medium

B ZFL culture medium

C zebrafish medium

D zebrafish medium

In(NO$_3$)$_3$ 0 h   In(NO$_3$)$_3$ 24 h   ITO 0 h   ITO 24 h
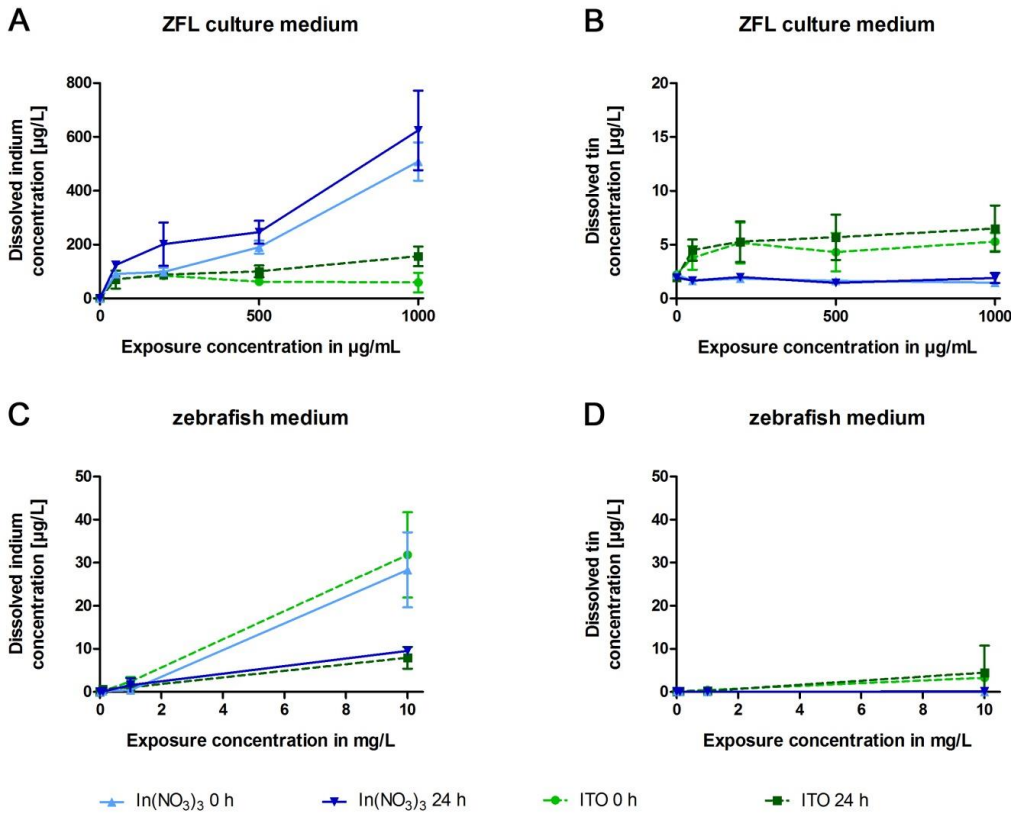
Figure S3.3 Measured concentrations by ICP-MS of total In and Sn in ZFL culture medium (A and B), and In and Sn in zebrafish culture medium (C and D) after 0 h and 24 h exposure expressed as µg L^{-1}.
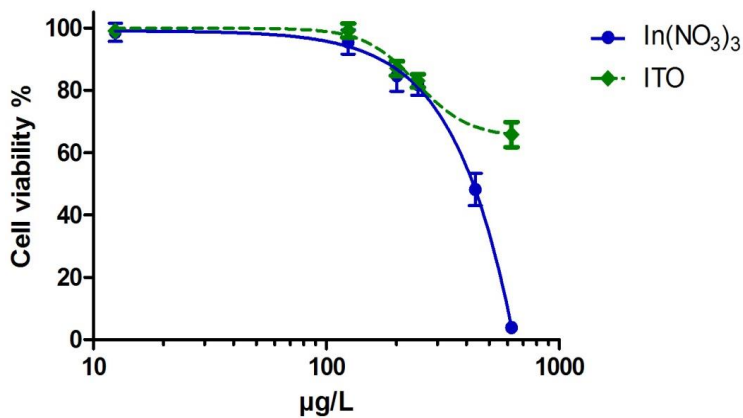
In(NO$_3$)$_3$ ITO

Figure S3.4 Cytotoxicity in ZFL cells measured by MTT assay after incubation for 24 h with indicated concentrations of ITO and In(NO$_3$)$_3$. Data are normalized to controls and expressed as mean ± SD (n=3, independent experiments). EC$_{50}$ of In(NO$_3$)$_3$ is 310 µg L^{-1} (1.031 µM).
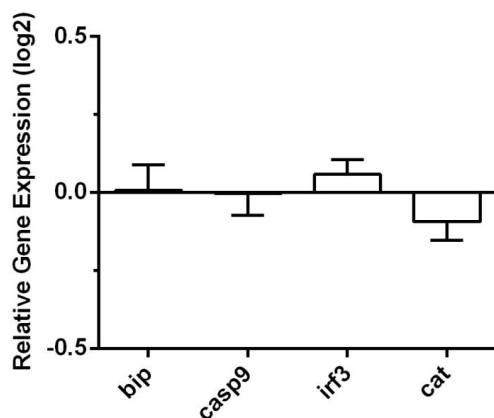
Figure S3.5 Transcriptional alterations in ZFL cells exposed to 5 mM (504 mg L^{-1}) KNO$_3$, equivalent to highest In(NO$_3$)$_3$ concentration (500 mg L^{-1}). No significant transcriptional alterations of ER stress (*bip*), apoptosis (*casp9*), oxidative stress (*cat*), innate immune system (*irf3*) related genes are demonstrating the importance of an indium effect, rather than the effect of nitrate. Values as mean ± SD (n=3, independent experiments).
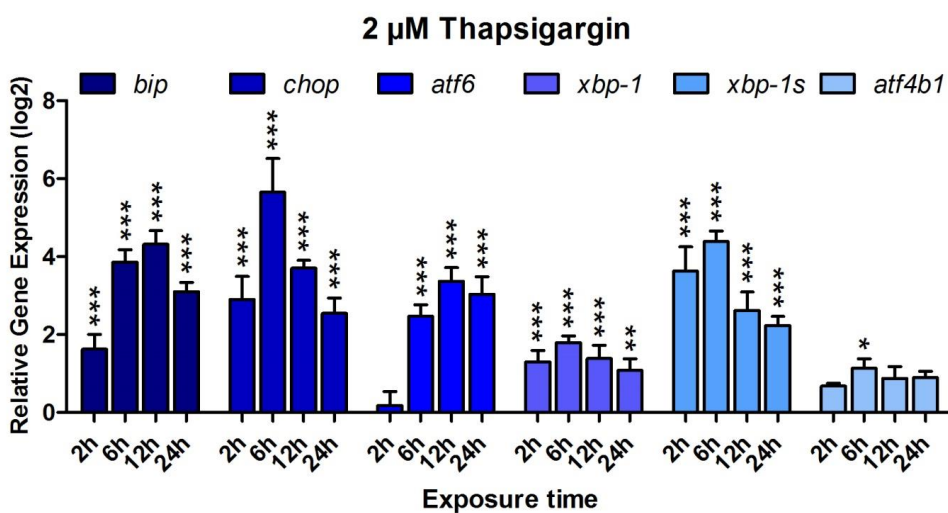
Figure S3.6 Transcriptional alterations of ER stress related genes in ZFL cells exposed to 2 μM thapsigargin, used as positive control for ER stress. Expression varies with exposure time. Asterisks indicate significant differences to controls (*p < 0.05, **p < 0.01, and ***p < 0.001). Values as mean ± SD (n=3, independent experiments).

4

Ecotoxicological Assessment of Solar Cell Leachates: Copper Indium Gallium Selenide (CIGS) Cells Show Higher Activity Than Organic Photovoltaic (OPV) Cells

Nadja Rebecca Brun, Bernhard Wehrli, Karl Fent

Abstract

Despite the increasing use of photovoltaics their potential environmental risks are poorly understood. Here, we compared ecotoxicological effects of two thin-film photovoltaics: established copper indium gallium selenide (CIGS) and organic photovoltaic (OPV) cells. Leachates were produced by exposing photovoltaics to UV light, physical damage, and exposure to environmentally relevant model waters, representing mesotrophic lake water, acidic rain, and seawater. CIGS cell leachates contained 583 µg L^{-1} molybdenum at lake water, whereas at acidic rain and seawater conditions, iron, copper, zinc, molybdenum, cadmium, silver, and tin were present up to 7219 µg L^{-1}. From OPV, copper (14 µg L^{-1}), zinc (87 µg L^{-1}) and silver (78 µg L^{-1}) leached. Zebrafish embryos were exposed until 120 hours post

fertilization to these extracts. CIGS leachates produced under acidic rain, as well as CIGS and OPV leachates produced under seawater conditions resulted in a marked hatching delay and increase in heart edema. Depending on model water and solar cell, transcriptional alterations occurred in genes involved in oxidative stress (*cat*), hormonal activity (*vtg1*, *ar*), metallothionein (*mt2*), ER stress (*bip, chop*), and apoptosis (*casp9*). The effects were dependent on the concentrations of cationic metals in leachates. Addition of ethylenediaminetetraacetic acid protected zebrafish embryos from morphological and molecular effects. Our study suggests that metals leaching from damaged CIGS cells may pose a potential environmental risk.

4.1 Introduction

Photovoltaics are renewable energy sources used in a wide range of consumer products. The actual installed global photovoltaic capacity of nearly 200 gigawatts is expected to triple by 2020 to nearly 700 GW (IEA, 2015). Photovoltaics are thought to cause no environmental contamination during use. The question arises, however, whether their decommissioning and disposal could pose environmental risks. Life cycle assessment (LCA) methods are widely applied on various types of photovoltaics taking into consideration environmental impacts during production, installation, and demolition phases, as well as greenhouse gas emissions, energy consumption, and labour accidents (Laleman et al., 2011; Tsoutsos et al., 2005). Several studies pointed out the potential risks to human and environmental health associated with disposal of large quantities of photovoltaic panels on landfills (Cyrs et al., 2014; Fthenakis, 2004; Raugei and Fthenakis, 2010). However, the potential ecotoxicological burden is rarely addressed due to the lack of ecotoxicological investigations.

Photovoltaics can be classified into cells based on crystalline silicon and thin films. The latter brings the advantage of flexibility and semi-transparency, but bears lower power conversion efficiency. The market share was about 20% in 2012 (Edoff, 2012). Efficiency depends on the energy bandgap of the compound semiconductors, which in case of thin-film photovoltaics, are most commonly made of amorphous silicon (αSi), cadmium telluride (CdTe), copper indium gallium selenide (CIGS), or organic polymers. Organic photovoltaic (OPV) cells are lagging behind metal(loid) based thin film technology in terms of lifetime (3-5 years; Brabec et al., 2010), energy payback times (2-4 years; García-Valverde et al., 2010), and efficiency (García-Valverde et al., 2010), but have the advantage of avoiding toxic materials such as cadmium (Cd) by using organic polymers as light-absorbing layers. During use, no release of potentially harmful compounds is expected, as all photovoltaics are tightly encapsulated in glass or polymeric layer protecting from UV light, moisture, and oxygen. However prolonged UV exposure may lead to aging of the polymeric encapsulation. Improper disposal can impair the physical integrity of the cell, resulting in release of previously encapsulated material into the environment. The layered structure of an OPV and a CIGS is shown in Figure 4.1. Leaching of metal(loids) such as zinc (Zn), molybdenum (Mo), Cd, selenium (Se), and silver (Ag) from OPV and CIGS was previously assessed in model

natural waters (seawater, mesotrophic lake water, and acidic rain). Thereby predicted environmental concentrations (PECs) were estimated (Zimmermann et al., 2013). Estimated PECs for Cd from CIGS cells in acidic rain (PEC in arid climate: 173.4 µg L^{-1}, in humid climate 32.5 µg L^{-1}) exceeded acute toxicity for *Daphnia magna* (LC_{50} = 25.5 µg L^{-1}) and PECs for Se (9.4 µg L^{-1}) exceeded adverse effect levels for fish and birds (>5 µg L^{-1}), and as well PEC for Cd from CIGS cells in seawater (55.4 µg L-1) was in the acutely toxic range for marine phytoplankton (IC_{50} = 7.9 µg L^{-1}), while in all scenarios for OPV cells PECs did not reach toxic levels.

Some heavy metals have a considerable toxicity and can disrupt various signaling pathways in organisms. Cd is well known to induce apoptosis (Chan and Cheng, 2003) and to cause developmental malformations such as heart edema in zebrafish embryos (Cheng and Wai, 2000). Copper (Cu) in excess can target gills, gut, and sensory system affecting fish behavior (De Boeck et al., 2006; Shaw and Handy, 2006). Cu, Zn, and iron (Fe) can lead to hatching delay (Brun et al., 2014b; Johnson et al., 2007; Zhu et al., 2012). Zn and Se can induce reactive oxygen species (ROS) formation potentially leading to pro-inflammatory and cytotoxic effects at elevated concentrations in fish (Brun et al., 2014b; Monteiro et al., 2009). Ag has a propensity to bioconcentrate in (marine) organisms (Wang et al., 2014), and affects oxidative phosphorylation and protein synthesis on the transcription level in zebrafish (Aerle et al., 2013). Furthermore, Ag nanoparticles and indium (In) were shown to induce endoplasmic reticulum (ER) stress in zebrafish embryos (Brun et al., 2014a; Christen et al., 2013a). Mo is relatively non-toxic to fish with an LC_{50} of more than 100 mg L^{-1} in chinook salmon (Hamilton and Buhl, 1990). Overall, the toxic potential of some heavy metals in certain types of photovoltaics, including Cd, thus raise environmental concerns, in particular when leached at their end of life. In case of OPV cells, organic compounds such as UV stabilizers and phthalates, known to exhibit endocrine activities (Fent et al., 2014; Lyche et al., 2009), may potentially pose an environmental risk too.

In this study, we assessed the ecotoxicological activity of two thin film photovoltaics leachates in zebrafish (*D. rerio*) embryos. The aim was to compare effects of CIGS cell leachates with those of OPV. We hypothesize that CIGS photovoltaics may represent a potential ecotoxicological risk at their end of life under harsh environmental conditions, as several metals could leach into water and soil and would trigger ecotoxicological activity. Here, we produced three different leachates from damaged OPV and CIGS cells under different conditions: (1) mesotrophic lake water with pH 8.4 representing dumping in freshwater environments, (2) acidic rain water at pH 4.0 representing an acidic rain-runoff scenario for damaged roof-top and building integrated PV, and (3) artificial seawater with pH 7.9 representing dumpsites adjacent to marine environments to test leaching behavior under normal condition and under harsh acidic and saline conditions. To this end, we compared their ecotoxicological implications on a morphological and molecular level in zebrafish eleuthero-embryos. Teratogenic effects such as reduced hatching can indicate general adverse effects, while changes in mRNA abundance of selected target genes allow identification of molecular effects and mode of actions.
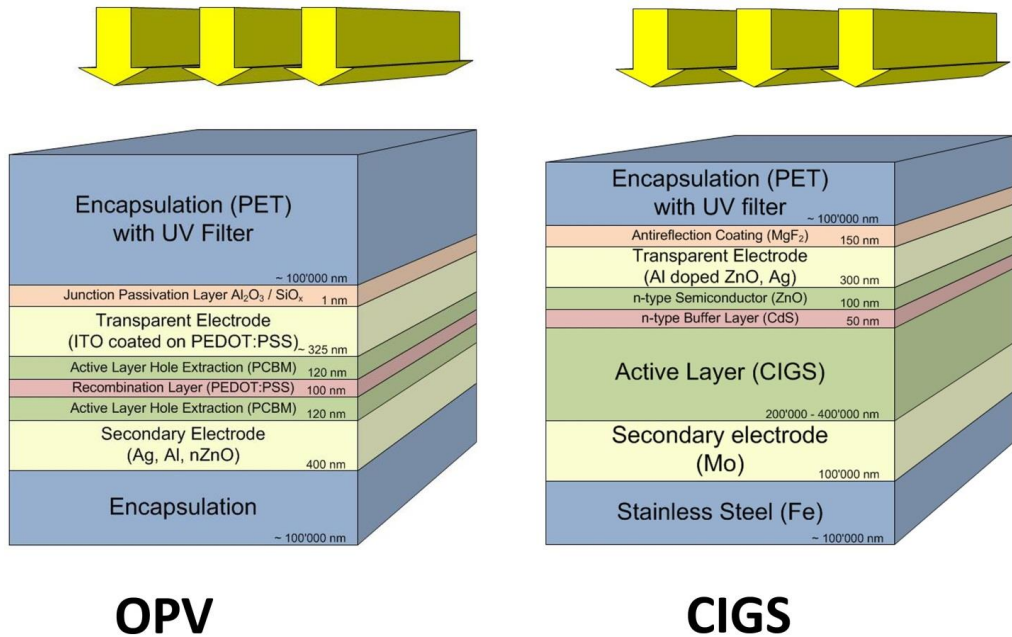
Figure 4.1 Multilayer structure of OPV and CIGS cells studied here, adapted from materials commonly in use (Miles et al., 2005; Zimmermann et al., 2012).

4.2 Materials and Methods

Solar Cells and Sample Preparation. Two different types of solar cells were investigated; a commercially available CIGS cell (Sunload 12 Wp Solar Panel from Sunload Mobile Solutions GmbH, Berlin, Germany, article no. 301.120) and an OPV cell provided by BELECTRIC OPV GmbH (Nuremberg, Germany). Detailed description of multilayer structure from both photovoltaics can be found in Figure 4.1 and in literature (Miles et al., 2005; Zimmermann et al., 2012). In brief, metals such as aluminum (Al), Cd, Cu, gallium (Ga), In, Fe, Mo, Se, Ag, and Zn are part of the multilayer structured CIGS cell. Al, In, Ag, tin (Sn), and Zn are metals incorporated in OPV cells. In central Europe, irradiance levels can be expected to vary from 600 to 1000 W m^{-2} on summer days with clear sky, whereas its only between 50 to 150 W m^{-2} on foggy winter days (Leal Filho and Kotter, 2015). Both cells were exposed to UV radiation in a solar simulator Suntest XLS+ (Atlas, Germany) set on maximum power (765 W m^{-2}) for 1000 h and afterwards cut in pieces of 1.5 cm x 3.0 cm, simulating shredding of solar cells on dumping sites or damaged cells on roof tops. Ten pieces were added to 250 mL acid cleaned brown glass flasks and filled up with 200 mL of model freshwater (representing mesotrophic lake water, pH 8.4; Zotina et al., 2003), acidic rainwater (pH 4; Smith et al., 2002), and seawater (pH 7.9; Kester et al., 1967); see Table S4.1 in the supplementary in-

formation, SI, for more details). The flasks were shaken at room temperature at 130 rpm for 123 days until sampling according to the protocol by Zimmermann et al. (2013).

Chemical Analysis of Metals. Elemental analysis of different leachates was performed using inductively-coupled-plasma mass-spectrometry (ICP-MS). Leachates used in embryonic exposure were diluted 1:20 to a solution containing a final concentration of 5% aqua regia and elements were quantified using a calibration solution with multi-element standards (Sigma-Aldrich, Switzerland) containing 5% aqua regia. Isotopes [7]Li, [27]Al, [47]Ti, [56]Fe, [60]Ni, [63]Cu, [64]Zn, [66]Zn, [69]Ga, [75]As, [78]Se, [98]Mo, [106]Cd, [107]Ag, [113]In, [115]In, [118]Sn, [121]Sb, and [208]Pb were analyzed on an Agilent 7500cx ICP-MS (Agilent Technologies AG, Basel, Switzerland) equipped with an Octopole Reaction System, pressurized with an optimized helium flow of 5 mL min^{-1} or 4.7 mL min^{-1} hydrogen for [78]Se, respectively, using a dwell time of 0.3 s per isotope. Rubidium was used as internal standard.

Discrimination Between Dissolved and Nanoparticulate Species. Instrumental settings for the Time-Resolved Single-Particle ICP-MS analysis (TRSP-ICP-MS) were the same as for the ICP-MS with exception of a dwell time of 0.03 s. While dissolved species were detected as small peaks of similar low intensity, particulates were detected as distinct peaks of high intensity, as particles arrive at irregular intervals at the detector. To discriminate dissolved species from nanoparticles, Gaussian distribution was fitted to the plotted signal frequency versus intensity. R^2 of > 0.95 was defined to represent dissolved species. A value R^2 of < 0.95 was taken as an indication of the presence of nanoparticles according to an established protocol (Zimmermann et al., 2013). Extreme values of $R^2 < 0.8$ were interpreted as an indicator for a major fraction of particulate material and therefore no further soluble speciation was calculated. Presence of nanoparticles was confirmed using a NanoSight LM10 (Malvern Instruments Ltd, UK) followed by evaluation using the Nanoparticle Tracking Analysis (NTA) software. Five independent samples per concentration were injected, calculating the arithmetic average thereof.

Modeling of Metal Speciation. Visual MINTEQ software ver. 3.1 (Jon Petter Gustafsson, Sweden 2014) was used to determine major speciation of Al, Ag, Cd, Cu, Fe, Ga, In, Mo, Se, Sn, and Zn in each exposure water based on metal concentrations as determined by ICP-MS. It was assumed that CO_2 present in the air was equilibrated with the aqueous phase. The temperature was set to 27 °C as used in the embryo exposure.

Early Life Stage Toxicity Assessment. Zebrafish embryos from the blastula stage to 120 hours post fertilization (hpf) were exposed to a 1:10 dilution of the different OPV and CIGS leachates. This dilution factor is based on the concentrations determined by chemical analysis, from which we expected that a 1:10 dilution would not lead to mortality. Due to high Cd content in CIGS leachates representing acid rain conditions, a 1:100 dilution was chosen. Mesotrophic lake water and acidic rain water leachates were diluted with freshly prepared zebrafish culture media (5 mM NaHCO$_3$, 0.5 mM KCl, 17.7 mM CaCl$_2$, 6.8 mM MgSO$_4$), while sea water leachates were diluted with nanopure water to reach appropriate salt concentrations. Embryos from the control group were kept in mesotrophic lake water/zebrafish culture media (1:10), acidic rain water/zebrafish culture media (1:10), or seawater/nanopure (1:10) only. For all groups, pH was adjusted to 7.2 ± 0.1 before expo-

sure started, as this is the recommended pH for embryo exposure (Westerfield, 1995). Every group included four replicates with 30 embryos each. Embryos were kept in polystyrene 48-well dishes (Greiner Bio-One, Germany), at a 16:8 h light/dark photoperiod at 27 ± 1 °C. Embryos and hatched eleuthero-embryos were observed individually under a stereomicroscope (Discovery V8; Zeiss, Germany) every 24 h in order to assess hatching rate, mortality, and morphological abnormalities including pericardial edema, lack of pigmentation, and delayed development. By the end of exposure at 120 hpf, 25 embryos were pooled and stored in RNA later for further molecular analysis.

For the exposure with leachate and added ethylenediaminetetraacetic acid (EDTA), the molarity of cationic metals with a Me-EDTA stability constant above 14 (Al, Cd, Cu, Fe, Ga, In, Ni, Pb, Sn, Zn) present in the leachate was calculated. Accordingly, this amount of EDTA was added to the leachate (lake water OPV = 0.5 μM, lake water CIGS = 0.7 μM, acidic rain water OPV = 0.2 μM, acidic rain water CIGS = 5 μM, seawater OPV = 0.2 μM, seawater CIGS = 300 μM). Ca^{2+} and Mg^{2+} with a stability constant of 10.7 and 8.69, respectively, should not be bound by EDTA. The stability constants were found in literature (Anderegg, 1977). Unbound high EDTA concentrations of 2.7 mM and more can affect sodium, calcium, glucose, potassium, chloride, and iron homeostasis, and toxic values were shown for rainbow trout (LC_{50} = 7.6 mM, after 96 h; Mohammad et al., 2012). The leachate with added EDTA was allowed to equilibrate for two hours before diluted 1:10 with respective water and used in the assay.

Gene Expression Analysis. Total RNA was extracted from pools of 25 zebrafish embryos and eleuthero-embryos, respectively, using the RNeasy Mini Kit (Qiagen, Switzerland) and further purified by on-column RNase free DNase digestion (Qiagen, Switzerland) to remove genomic DNA. RNA purity and concentration were evaluated using the NanoDrop spectrophotometer (NanoDrop Technologies, Germany) and integrity checked using agarose gel electrophoresis (Figure S4.1, SI), reverse transcription, and quantitative real-time PCR (RT-qPCR) for assessing mRNA abundance of selected genes based on SYBR green fluorescence was conducted as described in detail previously (Brun et al., 2014a). The sequences of used primers are shown in Table S4.2 in SI.

Estrogenic Activity. The estrogenic and antiestrogenic activity of the different leachates was assessed using the yeast estrogen screen (YES) according to Routledge and Sumpter (1996). Briefly, serial dilutions of all leachates and standards were prepared, diluted 1:1 in ETOH, added to a microtiter plate and then allowed to evaporate to dryness. After incubation time of 72 h absorbance was read at 540 nm and plotted against the concentration for graphical illustration. 17β-estradiol (E2) served as estrogen standard and assayed alongside each batch of samples together with the solvent controls and blank.

Statistical Analyses. The data were graphically illustrated with GraphPad Prism 6 (GraphPadSoftware, U.S.A.). Variance homogeneity of the data was assessed with the Bartlett's test. Significant differences between treatments were assessed by one way ANOVA followed by a Bonferroni posthoc test ($p \leq 0.05$) to compare treatment means with respective controls. In *in vivo* toxicity studies four replicates for each treatment group were tested. In the YES assay chemicals were tested in triplicate and two independent experiments

were conducted. Results are expressed as means ± standard deviation of mean (SD). Differences were considered statistically significant at $p \leq 0.05$. Principal component analysis (PCA) using SIMCA 14 (Umetrics, Sweden) was applied to measured activity including differentially expressed genes, hatching rate, and edema, combined with measured metal contents.

4.3 Results

Leachate Characterization. The leaching experiment, lasted over four months (123 days) and revealed specific patterns of leached metals for the different types of water and solar cell fragments (Figure 4.2). Under mesotrophic lake water conditions, Mo leached from CIGS cells in high amounts and Cd, Se, and Zn in minor amounts. Only Zn was detected in the OPV cell leachate. From CIGS cells in acid rain condition, Cu, Mo, and Zn leached in highest amounts, and furthermore, Al, Cd, Fe, Ga, In, and Sn were found in concentrations above detection limit. From OPV cells, only Cu and Zn leached at notable concentrations. Under seawater condition, CIGS cells released high amounts of Fe, which was oxidized and present as visible particles, giving rise to concentration variability represented by high standard deviation. Additionally, higher amounts of Sn and Mo were released compared to Ag, Cd, Cu, Ga, In, Ni, Se, and Zn. In the OPV cell leachate, Ag and Zn were detected at elevated concentration.

TRSP-ICP-MS analysis showed some elements leaching from CIGS cells under acidic rain water conditions were present at least partially as (nano- and micro-) particles (Figure 4.2, Table S4.3, SI). This was the case for Cu, In, Fe, and Mo. Under seawater conditions Cu, Se, and Sn showed a tendency to be present as particles, whereas Fe, In, Mo, and Zn were very likely present in particulate form due to their low R^2 value. No particulates were detected under lake water conditions, and in general, in OPV cell leachates. As modelled by Visual MINTEQ, the thermodynamically prevalent and favoured metal species were the ionic forms (Table S4.3, SI). This was the case for Cd and Zn under lake water condition, Al, Cd, Cu, Ga, In, Fe, and Zn under acidic rain condition, Cu, Ni, and Zn (for OPV only) under seawater condition. Presence of particles in CIGS cells under seawater condition was confirmed using NanoSight. Particle concentration was at least one order of magnitude higher than in other samples and particles in the range of 20-600 nm were detected, with the highest concentration below 100 nm (Figure 4.3).

Metal concentrations and corresponding observed effects among all leachates are summarized in Figure 4.2. A multivariate analysis revealed that CIGS in acidic rain and seawater, and OPV in seawater separate from the rest along PC1, accounting for more than 50% of the variation in the data (Figure S4.3, SI).

	Concentration in $\mu g\,L^{-1}$	Main Speciation	Hatching	Heart Edema	Oxidative Stress	Metallothionein	Hormonal Signalling	Phase I Enzyme Activity	ER Stress	Apoptosis
Mesotrophic Lake	Cd: 9 ± 1	Cd^{2+}								
	Mo: 583 ± 24	MoO_4^{2-}								
	Se: 11 ± 1	SeO_4^{2-}								
	Zn: 63 ± 7	Zn^{2+}								
	Zn: 60 ± 4	Zn^{2+}								
Acidic Rain	Al: 10 ± 1	Al^{3+}								
	Cd: 21 ± 1	Cd^{2+}								
	Cu: 14 ± 2	Cu^{2+}								
	Cu: 57 ± 3	Cu^{2+}								
	Fe: 12 ± 5	Fe^{3+}								
	Ga: 13 ± 0	Ga^{3+}								
	In: 9 ± 1	In^{3+}								
	Mo: 59 ± 2	MoO_4^{2-}								
	Sn: 12 ± 14	$Sn(OH)_6^{2-}$								
	Zn: 87 ± 7	Zn^{2+}								
	Zn: 52 ± 10	Zn^{2+}								
Seawater	Ag: 78 ± 7	$AgCl_2^-$, $AgCl_3^{2-}$								
	Ag: 50 ± 18	$AgCl_2^-$, $AgCl_3^{2-}$								
	Cd: 61 ± 5	$CdCl^+$, $CdCl_2$ (aq)								
	Cu: 122 ± 31	Cu^{2+}								
	Fe: 7219 ± 1949	Particulate Fe								
	Ga: 10 ± 1	$Ga(OH)_4^-$								
	In: 15 ± 4	Particulate In								
	Mo: 483 ± 118	Particulate Mo								
	Ni: 9 ± 0	Ni^{2+}								
	Se: 42 ± 11	$HSeO_3^-$								
	Sn: 691 ± 389	$Sn(OH)_2$								
	Zn: 17 ± 1	Zn^{2+}								
	Zn: 43 ± 9	Particulate Zn								

(Column group headers: Chemistry — Hatching, Heart Edema; Embryo toxicity — Oxidative Stress, Metallothionein; Affected Pathways — Hormonal Signalling, Phase I Enzyme Activity, ER Stress, Apoptosis. Logo: OPV CIGS.)

Figure 4.2 Presence or absence of nanoparticles in different leachates measured by NanoSight LM10. Coloured lines show five independent measurements, black line shows mean thereof. Y-axis shows particle concentration and exact values are given in the legend.

Embryotoxicity. Toxicity endpoints in zebrafish embryos included scoring of hatching success, mortality rates, and appearance of abnormal morphological features, such as pericardial edema. Figure 4.4 demonstrates that CIGS cell leachates, produced under acidic rain and seawater conditions, inhibited hatching of embryos until the end of the assay at 120 hpf. By employing EDTA as metal chelating agent, exposure groups all developed normally. This indicates that cationic metals were mainly responsible for reduced hatching. This does not account for OPV cell leachates produced under seawater conditions. Despite addition of EDTA hatching of embryos was delayed. Pericardial edema occurred in zebrafish embryos exposed to CIGS cell leachates produced under acidic rain and seawater conditions from 48 hpf onwards, although not statistically significant (Figure 4.4). In exposed embryos, no oth-

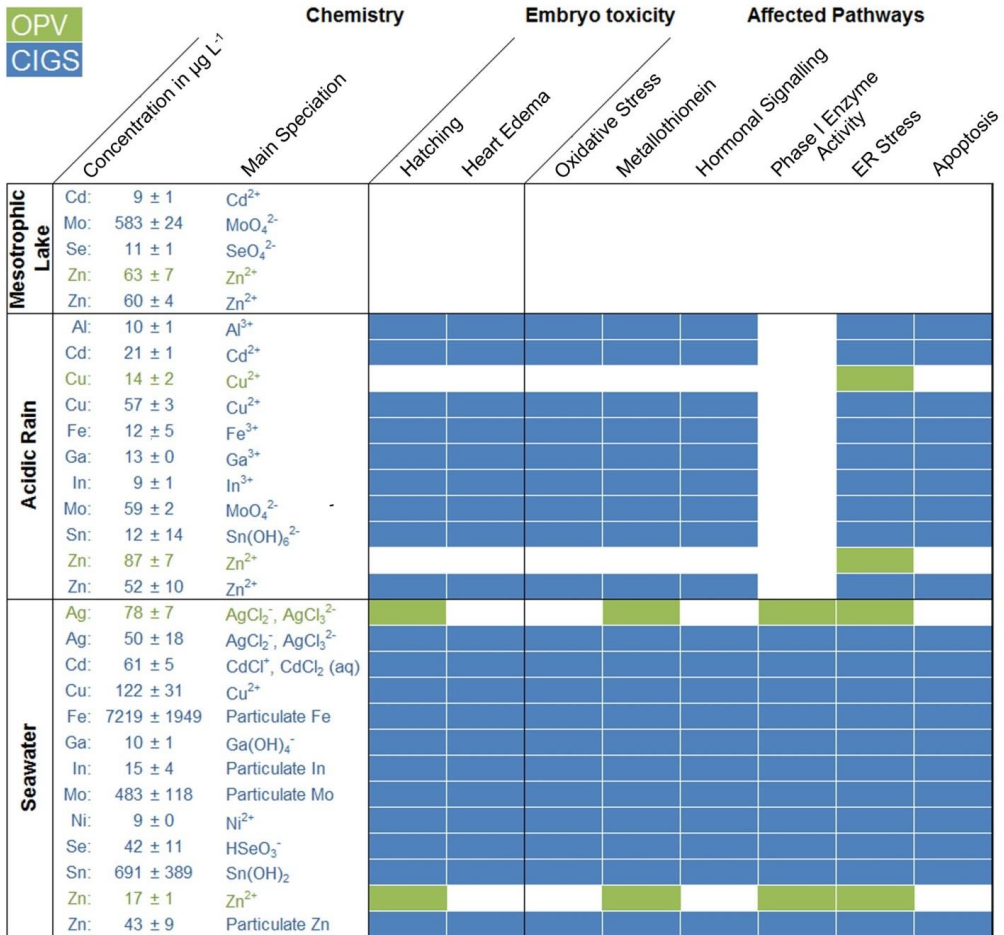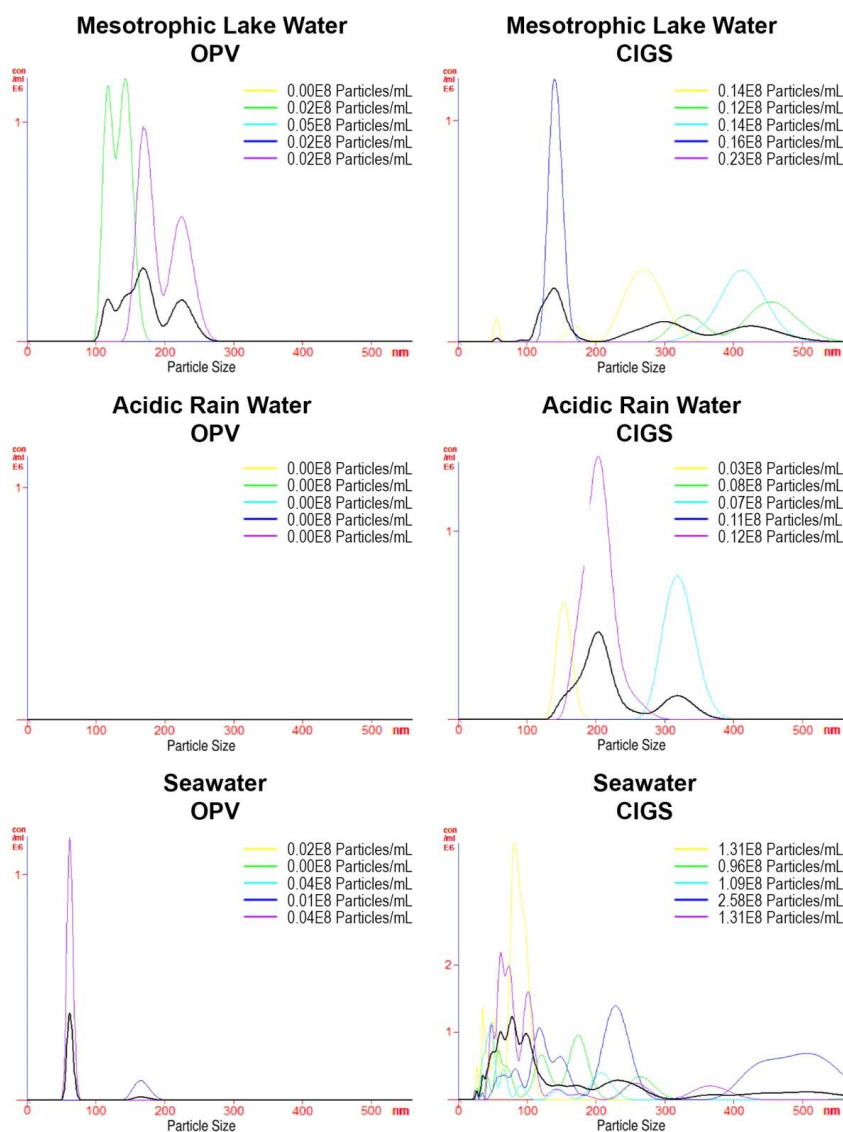**Figure 4.3** The presence or absence of nanoparticles in different leachates measured by NanoSight LM10. Colored lines show five independent measurements, and black line shows mean thereof. Y-axis shows particle concentration and exact values are given in the legend.

er signs of toxicity, including effects on pigmentation, heartbeat, eye development, malformation (Table 4.1), or survival were observed (Figure 4.5A).

Transcriptional Alterations. By choosing target genes from different stress pathways we aimed at elucidating molecular effects and modes of action of metals and chemicals present in the different leachates. Target genes belonging to pathways, including oxidative stress, adaptive response against bivalent metals (metallothionein), hormonal signalling, ER stress response, and apoptosis were analysed.

Exposure to leachates in mesotrophic lake water did not lead to alteration of abundance of any transcripts. Leachates of CIGS cells produced under acidic rain conditions promoted a significant increase in transcript abundance of genes involved in oxidative stress (*cat*), metallothionein (*mt2*), hormonal pathway (*vtg1*), ER stress (*chop*), as well as apoptosis (*casp9*; Figure 4.6). Leachates of OPV cells produced under the same acidic rain condition led to reduction of transcripts of *bip*, a key gene indicative of ER stress, in 120 hpf eleuthero-embryos. Seawater leachates from CIGS cells induced significant transcriptional alterations of *cat*, *mt2*, *vtg1*, *ar*, *cyp1a*, *p53*, *bip*, and *casp9*, whereas OPV cells led to alterations of *mt2*, *cyp1a*, and *bip*. Addition of EDTA to leachates resulted in a decrease of transcript levels or equal levels as in control zebrafish eleuthero-embryos (Figure 4.6).

Assessment of Estrogenicity. In order to assess estrogenic activity of the photovoltaic leachates, a yeast screen assay (YES) was performed. Neither OPV, nor CIGS cell leachates showed estrogenic or antiestrogenic activity (Figure S4.2, SI).

Table 4.1   Developmental endpoints adapted from OECD guidelines 236 (percentage of effect; 100% means normal except for malformation, where 0% means normal) recorded in zebrafish embryos during exposure to different leachates.

Group	Detached tail at 24 hpf (%)	Normal development of eyes at 24 hpf (%)	Heartbeat at 48 hpf (%)	Pigmentation at 48 hpf (%)	Malformation at 48 hpf (%)
Mesotrophic Lake Water					
Control	100	100	100	100	0
OPV	100	100	100	97.7 ± 3.1	0
CIGS	100	100	100	94.5 ± 4.5	4.95 ± 3.2
Acidic Rain Water					
Control	100	100	100	100	1.7 ± 1.9
OPV	100	100	100	97.0 ± 3.5	0.8 ± 1.5
CIGS	100	100	100	100	0.8 ± 1.6
Seawater					
Control	100	100	95.8 ± 6.1	98.5 ± 1.7	0.7 ± 1.5
OPV	100	100	100	99.2 ± 1.6	1.7 ± 2.0
CIGS	100	100	100	95.8 ± 6.1	0
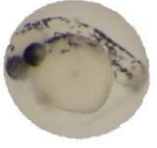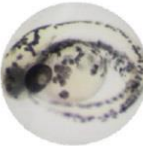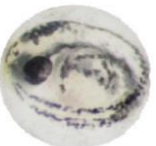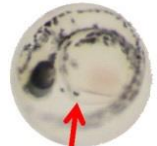
Figure 4.4 Morphological effects of different leachates in zebrafish embryos, and hatched eleuthe-ro-embryos compared to controls. Left lateral view images of representative embryos from all treatment groups. Arrow indicates pericardial edema. Brownish color on unhatched embryos in extracts produced under seawater condition stems from dissolved iron and iron nanoparticles.
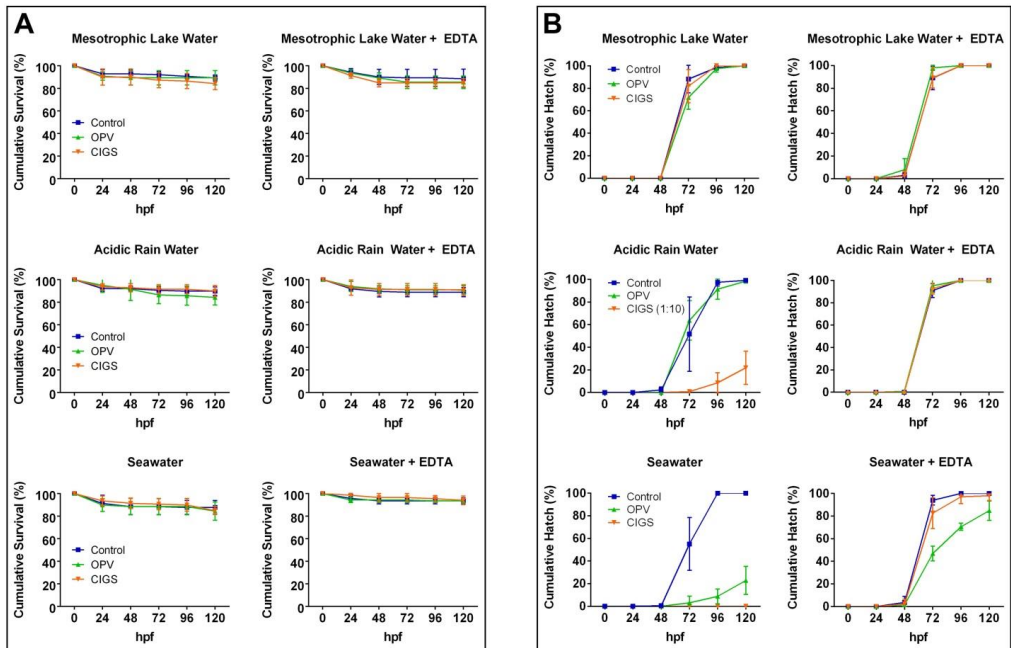
Figure 4.5 Cumulative percentage of survival (A) and hatching (B) of zebrafish embryos exposed to leachates from OPV and CIGS cell in different model waters and leachates with addition of appropriate amounts of EDTA. Error bars represent standard deviation (SD) of four replicates with 25 embryos in each.
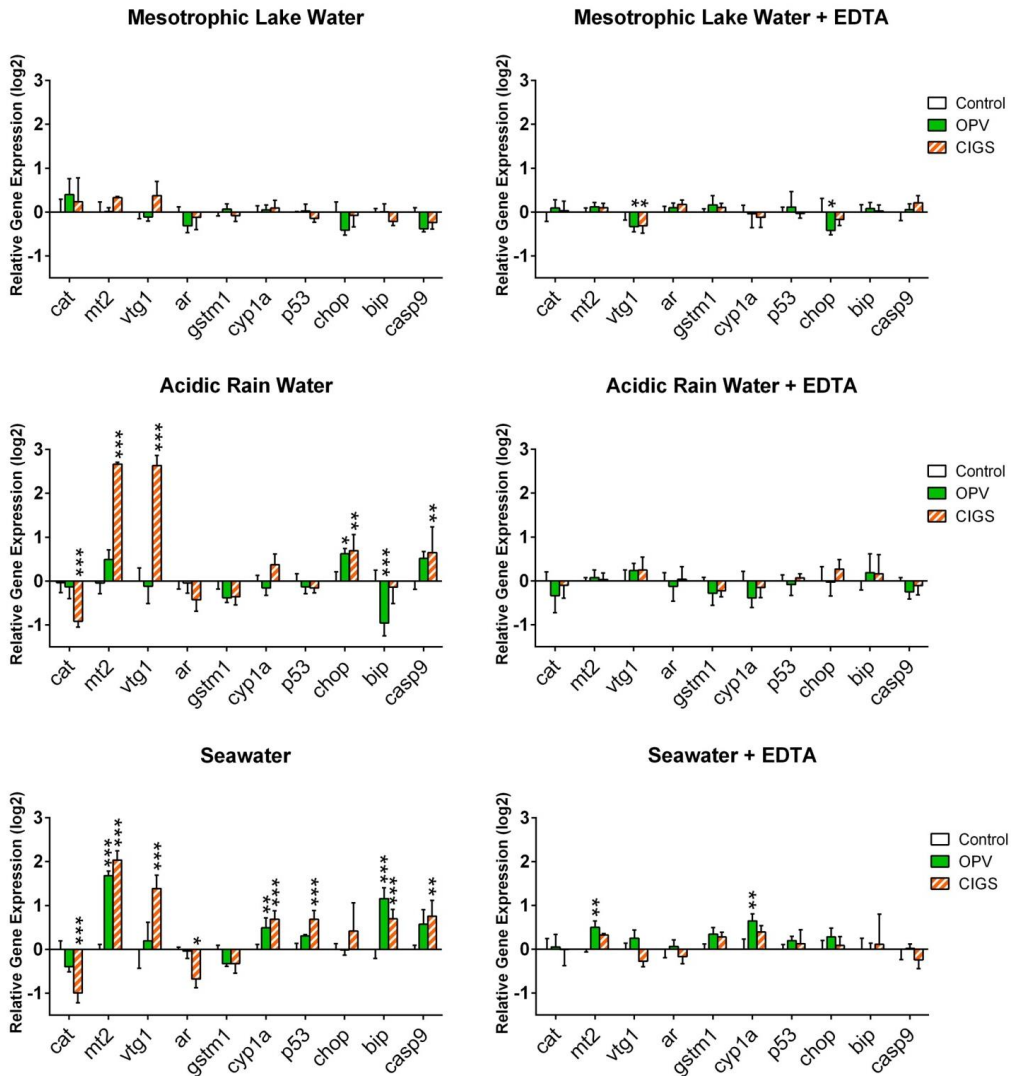
Figure 4.6 Transcriptional alterations of 10 marker genes for oxidative stress (*cat*), metallothionein (*mt2*), hormonal pathway (*vtg1*, *ar*), phase I enzyme activity (cytochrome P4501a, *cyp1a*), phase II enzyme activity (glutathione s-transferase, *gst*), apoptosis (*p53*, caspase 9 *casp9*), and ER stress (binding immunoglobulin protein *bip*, C/EBP homologous protein *chop*). Relative expression levels were normalized to *rpl13a*, calculated relatively to expression levels in control embryos and are shown on a log2 scale. Asterisks indicate significant differences to controls (*p < 0.05, **p < 0.01, and ***p < 0.001). Values are presented as mean ± SD (n=4).

4.4   Discussion

In our study, we compared two types of thin-film photovoltaics, CIGS and OPV, for their leaching behavior in three environmentally relevant model waters and their associated ecotoxicological activities. The results show leaching of metal mixtures, in particular from CIGS cells, which induced toxicity in zebrafish eleuthero-embryos. Physiological (hatching delay, morphological alterations) and molecular (alteration in mRNA abundance) effects were observed that are well-established measures to assess ecotoxicological implications of the leachates. Three leachates (from CIGS under acidic rain and seawater conditions, and OPV under seawater conditions) reduced or inhibited hatching success. Effects were induced by mixtures of cationic dissolved metal ions. Morphological abnormalities including pericardial edema occurred at much lower metal concentrations than expected from lowest observed effect levels of single metals. Furthermore, distinct alterations of transcripts of target genes indicative of metal exposure, involved in ER stress, oxidative stress, and apoptosis were induced by CIGS cell leachates, but little by OPV cell leachates. This suggests that damaged OPV cells pose lower environmental risks than CIGS cells.

Leaching experiments were based on a previous set-up (Zimmermann et al., 2013), and the comparison with our data suggests the following. We confirmed that among the three environmental conditions, Cd and Se leached in highest amounts in seawater, and Mo in lake water. Both studies indicated that Ag leached to a higher extent from OPV than CIGS, especially in seawater. None of the metals from CIGS in lake water were considered as of concern based on estimates of predicted environmental concentrations (PEC; Zimmermann et al., 2013). Although leachates used in our exposures were relatively highly concentrated and Cd exceeded the WHO limit (3 μg L^{-1}; WHO, 2008), the presence of Cd (9 μg L^{-1}), Mo (583 μg L^{-1}), and Se (11 μg L^{-1}) in lake water indeed did not affect zebrafish embryo development. In acidic rain, leached Cd, Mo, and Se were assumed to be of environmental concern (Zimmermann et al., 2013). Our ecotoxicological data suggest that a combination of Cd, Cu, and Zn negatively affected embryo hatching and development. In the marine water dumping scenario of Zimmermann et al. (2013), PECs for Cd and Se were thought to exceed toxicity for different freshwater and marine species. Based on data of our zebrafish toxicity study, Sn additionally contributed to toxicity. As related to OPV, both studies agree on potential adverse effects to aquatic organisms by leached Ag.

Cationic Metals Responsible for Effects (Reduced Hatching, Heart Edema, and Gene Expression Alterations). To analyse for the influence of dissolved cationic metals, we performed experiments without and with the addition of EDTA as a metal chelating agent. EDTA chelates cationic Al, Cd, Cu, Fe, Pb, Ni, and Zn. Leachates from CIGS cells under acidic rain condition and from CIGS and OPV cells under seawater condition severely inhibited hatching success. Hatching success of embryos, exposed to OPV leachates produced under seawater condition, was increased with addition of EDTA though still delayed. This can be related to higher binding affinity of ETDA to calcium and magnesium than Ag or Se (Stumm and Morgan, 1981). Hence, Ag present in OPV leachate from seawater might be unbound and still bioavailable, thus delaying hatching. It is rather unlikely that EDTA affected em-

bryo development by reducing essential cations such as calcium and magnesium, as the appropriate amount of EDTA was added to bind metals with a stronger binding affinity than calcium and magnesium. In addition to morphological effects, EDTA supplement also reduced molecular effects. The comparison between leachates without and with EDTA on transcriptional alterations confirms that also these effects were based on cationic metal concentrations.

Metal Mixtures in Leachates and Ecotoxicological Implications. Three different conditions were chosen to produce leachates from OPV and CIGS photovoltaics: (1) mesotrophic lake water with pH 8.4 representing dumping in freshwater environments, (2) acidic rain water at pH 4.0 representing an acidic rain-runoff scenario for damaged roof-top and building integrated PV, and (3) artificial sea water with pH 7.9 representing dumpsites adjacent to marine environments. Throughout all conditions Mo leached from CIGS pieces as its thermodynamically favoured species molybdate (MoO_4^{2-}), which is its bioavailable form (Schwarz et al., 2009). Mo is a trace element essential for enzymes catalyzing redox reactions and is one of the least toxic metals. The most sensitive marine species reported was *M. edulis* (48 h-EC_{10} of 10 mg L^{-1}; Heijerick et al., 2012). Mo is considered non-toxic to fish with an LC_{50} of more than 100 mg L^{-1} in chinook salmon (Hamilton and Buhl, 1990). With Mo being the only metal leaching in lake water from CIGS cells in high amounts (583 µg L^{-1}) and Cd (9 µg L^{-1}), Se (11 µg L^{-1}), and Zn (60 µg L^{-1}) at low concentrations, and as Zn (63 µg L^{-1}) was the only metal leaching from OPV, lake water condition can be considered as of low risk for contamination with metals originating from photovoltaics.

Acidic conditions may provoke increased mobility of some metals. Indeed, Al, Cd, Cu, Fe, Ga, In, Mo, Sn, and Zn leached at considerable amounts from damaged CIGS cells, whereas solely Zn leached from OPV cells. Most of the metals are present in their ionic form and thus bioavailable. It is suggested that even though none of the metals were present in excessive amount, the combination of several cationic metals may have led to the observed effects. At elevated concentrations of 53 µg L^{-1}, Cu was reported to inhibit hatching of zebrafish embryos (Johnson et al., 2007), and 15 µg L^{-1} can induce oxidative stress marker genes such as catalase and lead to accumulation in gill and liver of adult fish (Craig et al., 2007). Likewise, we showed in a previous study that excessive Zn reduced hatching of zebrafish embryos and triggered an oxidative stress response leading to pro-inflammatory effects and apoptosis starting from 100 µg L^{-1} (Brun et al., 2014b). Moreover, Cd can delay hatching starting from 371 µg L^{-1} (Fraysse et al., 2006), induce apoptosis at 11200 µg L^{-1} (Chan and Cheng, 2003), and reactive oxygen species at 5000 µg L^{-1} (Basha and Rani, 2003) in fish. Therefore, the observed hatching delay in the CIGS cell leachate cannot be attributed to a specific metal, but is a likely consequence of the combination of metal mixtures containing Cd (21 µg L^{-1}), Cu (57 µg L^{-1}) and Zn (52 µg L^{-1}).

Under seawater condition considerable amounts of Ag, Cd, Cu, Fe, Ga, In, Mo, Ni, Se, Sn, and Zn leached from CIGS cells, and Ag and Zn from OPV cells. At 6000 µg L^{-1} Sn induced teratogenic effects including pericardial edema in zebrafish embryos, which is well above our Sn exposure concentration (691 µg L^{-1}). Cd induced pericardial edema in zebrafish embryos at 5000 µg L^{-1} ($CdCl_2$) and higher (Cheng and Wai, 2000; Hallare et al., 2005), de-

creased hatchability in fish at 800 μg L^{-1}, and morphological abnormality starting at 400 μg L^{-1} CdCl$_2$ (Cao et al., 2009). Mean Cd concentration in our leachate was 61 μg L^{-1} and thus below this effect level. Se can induce pericardial edema at concentrations of 722 μg L^{-1}, mainly attributed to the SeO$_3^{2-}$ species (Wiecinski et al., 2013). Also Se exposure concentration in CIGS seawater leachate was much lower (42 μg L^{-1}) with HSeO$_3^{1-}$ as the predominant species. As each single metal was below the effect concentration, the observed pericardial edema in our study are suggested to be induced by the mixture of Sn, Cd, and Se.

Hatching was significantly decreased in embryos exposed to CIGS in acidic rain, as well as OPV and CIGS in seawater. This effect induced by toxicants has far-reaching consequences for embryos. However, the chorion also acts as protective barrier layer to prevent free passage to the embryo of particles of 60 nm in size (Fent, 2010). Our nanoparticle analysis showed that in particular nanoparticles of around 50 to 100 nm were present in CIGS leachate from seawater. Hence, they are not expected to pass through the chorion. In this study, the majority of gene expressional changes were measured in embryos that were affected by reduced hatching. Therefore, we conclude that mainly the soluble metal fraction, rather than the particles, induced the transcriptional changes.

Although the leachates were produced under different pH conditions, the embryo exposure was conducted at pH 7.2, ensuring no pH effect on embryo development. Furthermore, exposure of fish in the environment is likely to be downstream of dumping sites, where pH is expected to be more equilibrated. The results show that in this comparison of two photovoltaics in environmentally relevant model waters, mainly CIGS leachates induced toxicity. Morphological abnormalities in zebrafish embryos occurred at much lower metal concentrations than expected from reported lowest observed effect levels (LOEL) of single metals. This suggests that the effects of single metals jointly acted together in the metal mixture, thus inducing toxicity despite the individual metal was below the LOEL. Hatching delay observed in three leachates (CIGS cells under acidic rain and seawater condition, and OPV cells under seawater condition) may imply adverse consequences for embryos (starvation, predation) in natural environments.

Leachates Activate Metallothionein and Pathways of Oxidative Stress, Apoptosis, and ER Stress. Possible effects of different leachates on expression of marker genes related to oxidative stress, metallothionein induction, hormonal pathway, phase I and phase II, apoptosis, and ER stress were investigated to identify potential molecular effects of the leachates.

Under **lake water condition** mainly Mo leached from CIGS cells and none of the selected gene transcripts from different pathways were altered in their abundance. This confirms the morphological data thus CIGS or OPV cell leachates in lake water conditions can be considered as environmentally safe.

When leached under **acidic rain condition**, OPV cells released mainly Zn, while CIGS cells mainly released Cd, Cu, Mo, and Zn as potentially toxic metals. OPV cell leachate altered the *bip* transcript, indicating a disturbed protein folding and ER stress response, which can lead to induction of *chop* to trigger apoptosis in case of irreversible cell damage (R. Chen et al., 2014; Schröder and Kaufman, 2005).

Several studies have attributed the effect of Cu (Rola et al., 2014), Zn (Brun et al., 2014b), Cd (Galán et al., 2001; Wang et al., 2004), and other metals to their capacity to induce ROS, a general stress marker for metals. In CIGS cell leachates produced under acidic condition, transcripts of catalase were downregulated. This suggests a potential auto-regulatory negative feedback mechanism, suppressing further transcription of this enzyme after an increased production in reaction to excess ROS. Induction of metallothionein is an important biomarker for divalent metal exposure. Metallothioneins sequester and detoxify cytosolic cationic Cu, Zn, and Cd fluctuations and counter ROS induced by exposure (Chen et al., 2007, 2004). The binding affinity of metallothionein for Cu was shown to be higher than for Cd and Zn (Funk et al., 1987). Besides the non-toxic Mo, Cu is present in the highest amount in the acidic condition, hence the metallothioneins might sequester primarily excessive Cu, while Zn and Cd still contribute to toxic effects. In our study, significant induction was observed in CIGS cell leachate, which is suggested to be a result of dissolved cationic metal mixtures, in particular Cu.

Seawater exposure led to leaching of Ag and Zn from OPV cells and Fe, Cu, Mo, and Sn (as well as low amounts of Ag, Cd, Ga, In, Ni, Se, and Zn) from CIGS cells. The leachate originating from OPV cells led to significant up-regulation of *mt2*, *bip*, and *cyp1a*. We previously showed induction of *mt2* and ER stress response (induction of *bip*) mRNA transcript by Ag and Ag nanoparticles (Christen et al., 2013a), thus Ag in the leachate may have caused these alterations. Not only is the observed gene expression pattern supported by literature, but also by the found amelioration of induction by EDTA. On the other hand, induction of *cyp1a* is probably related to unknown aryl hydrocarbon receptor-activating organic compounds such as benzotriazoles used as UV-stabilizer in the encapsulation or degraded polymers used in the light-absorbing layer (Fent et al., 2014).

CIGS cells released a high amount of oxidised Fe, which is implicated in ROS induction (Sant'Anna et al., 2011). However, as the evaluation for nanoparticles indicate, Fe was not present in bioavailable form, thus alteration of *cat* transcription could be related to other cationic metals. Similarly, Mo is not expected to be responsible for measured gene alterations due to its generally low toxicity. Sn is present in a relative high concentration of 691 µg L^{-1} and its toxicity is largely based on genotoxicity (Şişman, 2009). Accumulation of Cu and Cd are known to induce apoptosis in zebrafish embryos (Blechinger et al., 2007; Hernández et al., 2006) and production of metallothionein at lower concentrations (Hart et al., 2001). We measured induction of genes from the apoptosis pathway such as *casp9* and *p53*, as well as a high induction of *mt2*. Ag and Se were present in the leachate too, which can contribute to an ER stress response (Christen et al., 2013a; Kupsco and Schlenk, 2014).

Genes from every pathway investigated, except *gstm1*, were altered thus, we suggest that this is an effect of a mixture of Ag, Cd, Cu, Se, Sn, and Zn, rather than from one metal alone. Metal mixtures are likely to interact with each other affecting uptake and toxicity. Often, they exhibit less than additive or protective effects as shown in adult zebrafish, where co-administration of Zn and Se revoked oxidative stress and metallothionein induced by Cd (Banni et al., 2011). Bioaccumulation of Cd was inhibited by Cu, Pb, and Zn (Komjarova and Blust, 2009), and gill-metal binding of Cd was reduced by both Zn and Cu

(Niyogi et al., 2015). It is generally accepted, that metals can displace each other from common binding sites, resulting in reduced activity. On the other hand, synergistic effects were also shown in fish by consistently higher metallothionein concentrations (Kamunde and MacPhail, 2011) or acute toxic endpoints (Zhu et al., 2011) than in single metal exposures.

Differences among the leachates regarding their molecular and morphological effects and metal concentration were determined by PCA. CIGS in acidic rain and seawater, and OPV in seawater separated from the rest, confirming that these are the leachates of concern. Furthermore, these three leachates are distinct from each other, indicating different mechanisms of action and metal concentrations.

Estrogenic Activity. Vitellogenin transcripts have been shown to be induced upon Cd exposure, though it was suggested to be mediated indirectly (Murphy et al., 2005; Williams et al., 2006), while others reported inhibition (Hwang et al., 2000) or no alteration (Chang et al., 2011). Exposure of goldfish to 22 μg L^{-1} $CdCl_2$ did not significantly change plasma vitellogenin (Palermo et al., 2008), whereas 10 μg L^{-1} $CdCl_2$ induced gene expression in zebrafish larvae (Chen et al., 2010). As *vtg1* expression was not induced when EDTA was added in our study, we suggest that Cd was responsible for *vtg1* induction at exposure concentration of 21 μg L^{-1}. Moreover, an effect caused by Cd might indicate that metallothioneins did not cope with the cationic metal overload, or sequestered Cu or Zn first.

Previously it was found that Cd, Cu, and Zn did not show any estrogenic activity in the YES assay, but lead to a reduction of effects in combination with E2 (Silva et al., 2006), while in other studies Cd, Pb, and Cu showed estrogenic activity *in vitro* (Chang et al., 2011; Isidori et al., 2010), and Pb and Cu *in vivo* (Isidori et al., 2010). Our YES data do not indicate any estrogenic activity in any leachate, even though *vtg1*was induced at a lower leachate dilution (1:10 versus 1:2 in the YES). Lack of responsiveness in recombinant yeast was previously found, possibly as Cd is unable to directly activate the estrogen response element in recombinant yeast (Chen et al., 2010; Denier et al., 2009). Therefore, we suggest that Cd was responsible for induction of the *vtg1* transcript.

Conclusion. Taken together, our results show that damaged CIGS cells pose a significantly higher risk to the environment than the OPV cells. Conditions simulating roof-top acidic rain run-off and disposal in marine water environment indicate leaching of multiple metals with a prevalence of Ag, Cd, Cu, Fe, Mo, Sn, and Zn. In contrast, disposal of these cells after their use in freshwater environments are of less concern than other environmental conditions. Our data suggest that the metal cations in the mixture added up to a joint activity in the leachate and affected multiple pathways. Cd is suggested to be responsible for *vtg1* induction, Ag, Se, or Zn for induction of ER stress response, and Ag, Cd, Cu, and Zn for hatching delay. Reducing inorganic content in photovoltaics should be an aim for stakeholders and producers, as well as adopting recycling policies for governments worldwide.

4.5   Supplementary Information

Table S4.1   Composition of model waters (modified after Kester et al., 1967; Smith et al., 2002; Zotina et al., 2003)

Water	Compound	[mg L^{-1}]	pH[1]	Ionic strength	Original source
Mesotrophic lake	$NaHCO_3$	168	8.4	0.00334	Zotina et al. (2003)
	KNO_3	3			
	$MgSO_4$ x 7 H_2O	49.3			
	$CaCl_2$ x 2 H_2O	5.88			
	$CaSO_4$ x 2 H_2O	27.6			
Acidic rain	NaCl	4.266	4.0	0.000425	Smith et al. (2002)
	$MgCl_2$ x 7 H_2O	7.255			
	$CaCl_2$ x 6 H_2O	6.123			
	KCl	0.746			
	$NaNO_3$	3.06			
	Na_2SO_4	5.965			
Seawater 35.00‰	NaCl	23926	7.9	0.5645	Kester et al. (1967)
	Na_2SO_4	4008			
	KCl	677			
	$NaHCO_3$	196			
	KBr	98			
	H_3BO_3	26			
	NaF	3			
	$MgCl_2$ x 7 H_2O	11735			
	$CaCl_2$ x 2 H_2O	1519			

[1]   pH was set in the beginning of the experiment

Table S4.2   Primer sequences used for quantitative real-time PCR analysis

Target gene	Primer sequence (5' to 3')	Accession no.[a]
rpl13a	fw: AGC TCA AGA TGG CAA CAC AG	NM_198143
	rv: AAG TTC TTC TCG TCC TCC	
cat	fw: AGG GCA ACT GGG ATC TTA CA	NM_130912
	rv: TTT ATG GGA CCA GAC CTT GG	
mt2	fw: AAA TGG ACC CCT GCG AAT	NM_001131053
	rv: TTG CAG GTA GCA CCA CAG TT	
vtg1	fw: AGC TGC TGA GAG GCT TGT TA	NM_001044897
	rv: GTC CAG GAT TTC CCT CAG T	
ar	fw: CAC TAC GGA GCC CTC ACT TGC GGA	NM_001083123.1
	rv: GCC CTG AAC TGC TCC GAC CTC	
gstm1	fw: CTA TAC ATG CGG CGA AGC T	NM_212676.1
	rv: GGC ATT GCT CTG GAC GAT	
cyp1a	fw: GCA TTA CGA TAC GTT CGA TAA GGA C	NM_131879.1
	rv: GCT CCG AAT AGG TCA TTG ACG AT	
p53	fw: GCT TGT CAC AGG GGT CAT TT	NM_131327
	rv: ACA AAG GTC CCA GTG GAG TG	
chop	fw: GAG TTG GAG GCG TGG TAT GA	NM_001082825
	rv: CCT TGG TGG CGA TTG GTG AA	
bip	fw: CGA AGA AGC CAG ATA TCG ATG A	NM_213058
	rv: ACG GCT CTT TTC CGT TGA AC	
casp9	fw: AAA TAC ATA GCA AGG CAA CC	NM_001007404
	rv: CAC AGG GAA TCA AGA AAG G	

[a]   GeneBank accession number (http://www.ncbi.nlm.nih.gov).

Table S4.3 Main elements in leachates from OPV and CIGS cell fragments used in embryo exposure determined by TRSP-ICP-MS, speciation calculated by MINTEQ

Element	Photo-voltaic	Model Water[1]	Particulate (R[2])[2]	Speciation[3]
Ag	OPV	Seawater	No (0.9797)	57% $AgCl_2^-$, 42% $AgCl_3^{2-}$, 1% AgCl (aq)
	CIGS	Seawater	No (0.9834)	57% $AgCl_2^-$, 42% $AgCl_3^{2-}$, 1% AgCl (aq)
Al	CIGS	Acidic Rain Water	No (0.9870)	82% Al^{3+}, 18% $AlSO_4^+$
Cd	CIGS	Lake Water	No (0.999)	91% Cd^{2+}, 4% $CdHCO_3^+$, 2% $CdCO_3$ (aq), 2% $CdSeO_4$ (aq), 1% $CdCl^+$
		Acidic Rain Water	No (0.9819)	97% Cd^{2+}, 2% $CdCl^+$, 1% $CdSO_4$ (aq)
		Seawater	No (0.9823)	49% $CdCl^+$, 47% $CdCl_2$ (aq), 4% Cd^{2+}, 1% $CdSO_4$ (aq)
Cu	OPV	Acidic Rain Water	No (0.9781)	99% Cu^{2+}, 1% $CuSO_4$ (aq)
	CIGS	Acidic Rain Water	Some (0.9404)	99% Cu^{2+}, 1% $CuSO_4$ (aq)
		Seawater	Some (0.8737)	63% Cu^{2+}, 18% $CuCl^+$, 14% $CuSO_4$ (aq), 1% $CuCl_2$ (aq), 1% $CuCO_3$ (aq), 1% $CuHCO_3^+$, 1% $CuOH^+$
Fe	CIGS	Acidic Rain Water	Some (0.9233)	63% Fe^{3+}, 37% $FeSO_4^+$
		Seawater	**Yes** (0.5351)	Particulate
Ga	CIGS	Acidic Rain Water	No (0.9858)	100% Ga^{3+}
		Seawater	Some (0.8991)	98% $Ga(OH)_4^-$, 2% $Ga(OH)_2^+$
In	CIGS	Acidic Rain Water	Some (0.8090)	80% In^{3+}, 17% $InCl_2^+$, 3% $InSO_4^+$
		Seawater	**Yes** (0.5214)	Particulate
Mo	CIGS	Lake Water	No (0.9729)	85% MoO_4^{2-}, 11% $MgMoO_4$(aq), 4% $CaMoO_4$(aq)
		Acidic Rain Water	Some (0.8982)	97% MoO_4^{2-}, 3% $MgMoO_4$(aq)
		Seawater	**Yes** (0.6313)	Particulate
Ni	CIGS	Seawater	No (0.9738)	79% Ni^{2+}, 15% $NiSO_4$ (aq), 4% $NiCl^+$, 2% $NiHCO_3^+$
Se	CIGS	Lake Water	No (1.000)	99% SeO_4^{2-}, 1% $CaSeO_4$ (aq)
		Seawater	Some (0.9427)	99% $HSeO_3^-$, 1% SeO_3^{2-}
Sn	CIGS	Acidic Rain Water	No (0.9589)	99% $Sn(OH)_6^{2-}$, 1% SnO_3^{2-}
		Seawater	Some (0.9082)	99% $Sn(OH)_2$, 1% $SnOH^+$
Zn	OPV	Lake Water	No (0.9731)	87% Zn^{2+}, 5% $ZnCO_3$ (aq), 1% $ZnOH^+$, 4% $ZnHCO_3^+$, 2% $ZnSeO_4$ (aq)
		Acidic Rain Water	Some (0.9552)	99% Zn^{2+}, 1% $ZnSO_4$ (aq)
		Seawater	No (0.9872)	54% Zn^{2+}, 22% $ZnCl^+$, 12% $ZnSO_4$ (aq), 5% $ZnCl_2$ (aq), 3% $ZnCl_3^-$, 1% $Zn(SO_4)_2^{2-}$, 1% $ZnCl_4^{2-}$

CIGS	Lake Water	No (0.9884)	87% Zn^{2+}, 5% $ZnCO_3$ (aq), 4% $ZnHCO_3^+$, 2% $ZnSeO_4$ (aq), 1% $ZnOH^+$
	Acidic Rain Water	No (0.9589)	99% Zn^{2+}, 1% $ZnSO_4$ (aq)
	Seawater	**Yes** (0.7610)	Particulate

[1] Model waters used: mesotrophic lake water (pH 8.4), acidic rain water (pH 4.0), artificial sea-water (pH 7.9). (see Table S4.1 for composition) with adjusted pH 7.2 for embryo exposure. Original OPV leachates from mesotrophic lake water and acidic rain water were diluted 1:10 with zebrafish culture medium, CIGS leachate from mesotrophic lake water 1:10 and from acidic rain water 1:100 with zebrafish culture medium, OPV and CIGS leachates in artificial sea water were diluted 1:10 with nanopure water.

[2] R^2 values for particulate species determined by TRSP-ICP-MS of > 0.95 was defined to represent dissolved species, whereas R^2 of 0.8-0.95 was defined to represent partially as particulate elements, and R^2 of < 0.8 as particles. Model calculations were not carried out for particles.

[3] Species modeled by Visual Minteq. Listed are species with an abundance of > 1%.
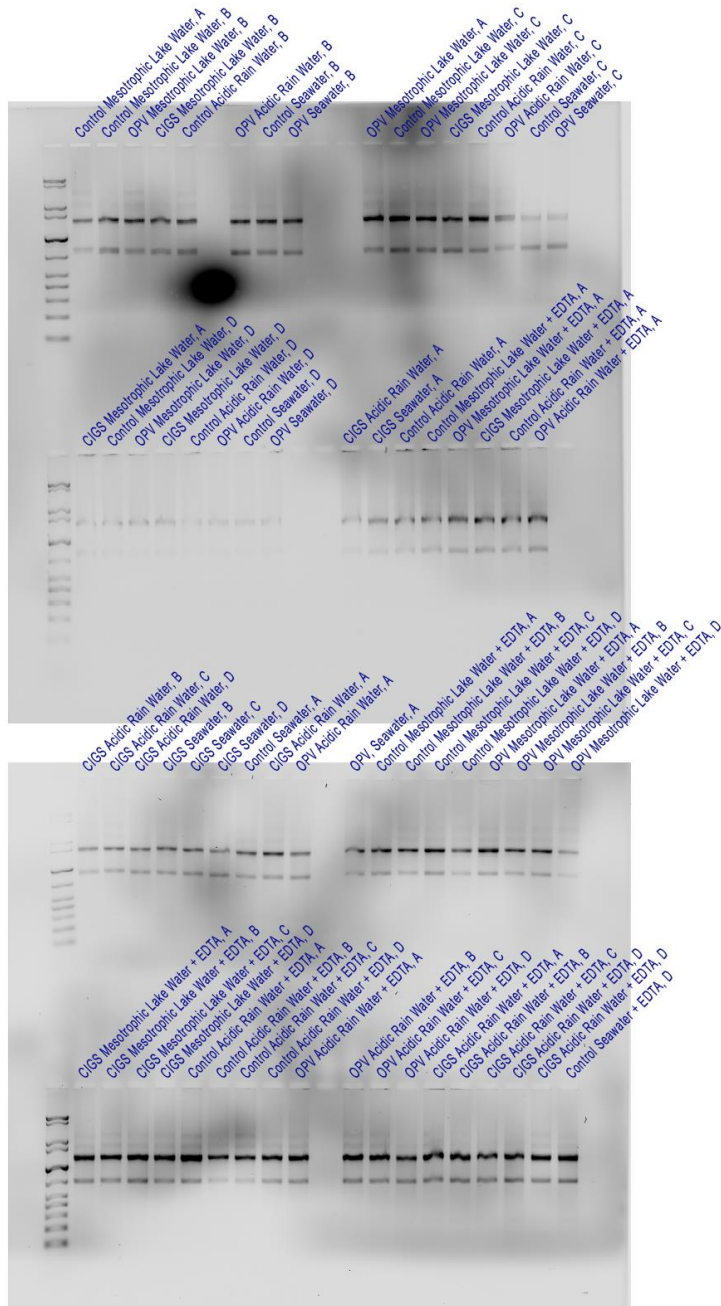
Figure S4.1 RNA quality analysis by agarose gel electrophoresis. A ratio of approximately 2:1 of 28S:18S rRNA bands are indicating intact RNA.
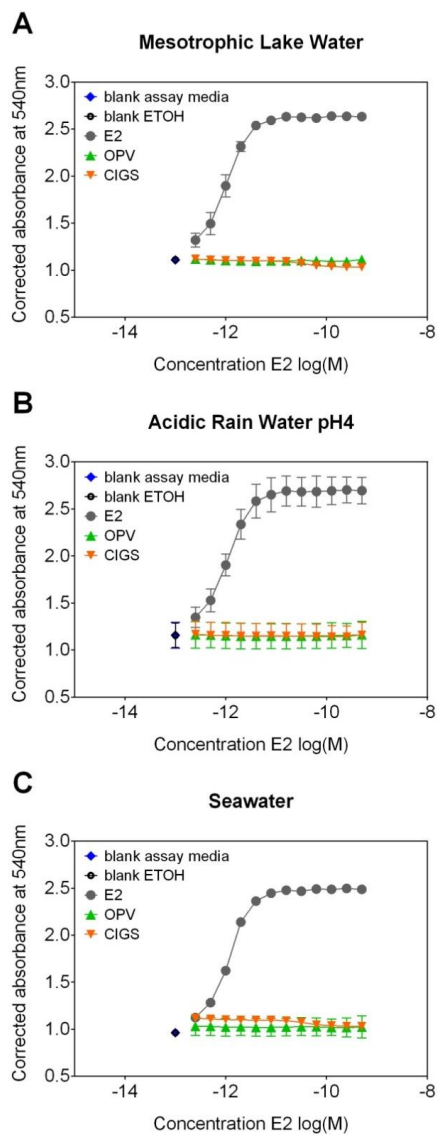
Figure S4.2 *In vitro* activity of OPV and CIGS leachates from three different model waters (meso-trophic lake water, acidic rain water, seawater) in the recombinant yeast estrogen screen (YES) assay. A 2-fold dilution series of the original leachate with ethanol was prepared. Positive control 17β-estradiol (E2) shows estrogenic activity, but no leachate extracts. Values as mean ± SD (n=2, independent experiments).
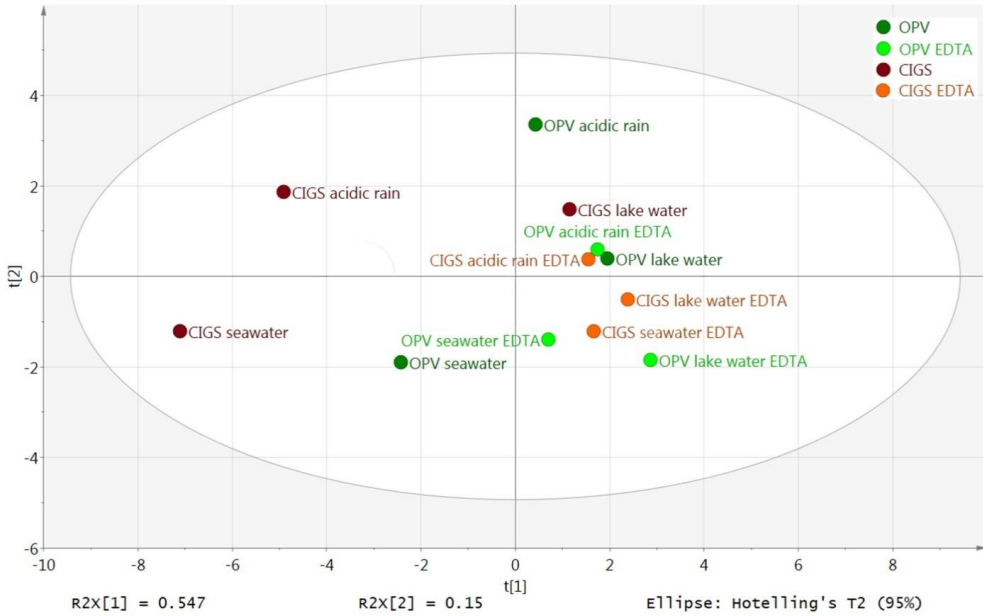
Figure S4.3 Principal Component Analysis (PCA). Relationships between the transcription of the 10 target genes, hatching rate, edema, and metal contents. Scores for the principal components 1 and 2 were 54.7% and 15%, respectively. The tolerance ellipse is drawn based on Hotelling's T2.

5

SYNERGISTIC ACTIVITY OF BINARY MIXTURES OF ALUMINUM AND INDIUM IN *DAPHNIA MAGNA* IN PHENOTYPIC AND TOXICOGENOMIC RESPONSES

Nadja Rebecca Brun, Peter Fields, John K. Colbourne, Dieter Ebert, Karl Fent

Manuscript in preparation

Abstract

We evaluated the phenotypic responses of *Daphnia magna* to aluminum (Al) and indium (In), as well as their equi-effective mixtures in parallel with global transcriptomic profiling by transcriptome next-generation sequencing (RNA-seq) at nominal concentrations between 28.54 and 45.84 mg L^{-1} (measured: 0.59 - 12.25 mg L^{-1}). Both metals were accumulated in gut and limbs of *Daphnia*, as shown by bioimaging using LA-ICP-MS. Both Al and In led to dose-dependent adverse effects on growth and reproduction. The equi-effective mixtures exhibited synergistic phenotypic responses. Al and In showed specific transcription profiles with 130 and 75 expressed genes, respectively. Although affected gene transcripts were different, they belong to similar biological pathways, including lipid and sugar metabolism, exoskeleton maintenance, transmembrane transport, and metal binding. In the mixture, a markedly higher number of transcriptional changes (368 genes) occurred, indicative

for an interactive molecular response and the observed synergistic phenotypic effects. The global transcriptome expression pattern support known mechanisms of metal toxicity, but also reveal novel modes of action, including ageing and muscle related disruptions demonstrating the power of this analysis.

5.1   Introduction

In surface waters, excessive heavy metal loads originate from anthropogenic activities. Although generally there is a good knowledge on potential toxicity of frequently used metals, effects of rare metals are poorly known. This also holds true for mixtures of metals that often occur as such in the environment. Aluminum (Al) is a ubiquitous metal in soil and water, affecting aquatic ecosystems subjected to acidification (Driscoll et al., 2001; Herkovits et al., 2015). Reported total Al concentrations in lakes vary from 12.5 - 85.5 μg L^{-1} or 10 - 104 μg L^{-1} in undisturbed lake systems in the Ukraine or U.K., respectively (Linnik et al., 2012; Quiroz-Vazquez et al., 2008) and 8.4 - 396.3 ug L^{-1} in lakes influenced by acidic deposition across the northeastern U.S. (Warby et al., 2008).

Excess Al in waters may induce toxic effects in aquatic organisms, including mortality. Genotoxic effects were measured in mussel gills close to aluminum smelters (Baršienė et al., 2010). Al can affect crustaceans immunity, as shown for crayfish (Ward et al., 2006). Al may be transferred in food webs (freshwater snails to crayfish); in crayfish Al accumulated in soft tissues, especially in the green gland, gut, and hepatopancreas (Walton et al., 2010). In *Daphnia*, Al$_2$O$_3$ nanoparticles inhibited growth and disrupted the energy budget (M. Li et al., 2011). Co-exposure of Al$_2$O$_3$ nanoparticles with As(V) in *Daphnia* led to synergistic effects in mortality (Wang et al., 2011). In *Daphnia magna*, LC$_{50}$ values vary between 9.89 and 54.29 mg L^{-1} Al^{3+}, depending on water conductivity (Jancula et al., 2011). In fish, Al bioaccumulated predominantly in gills (Grassie et al., 2013) and muscle tissue (Sivakumar et al., 2012), but was also found in kidneys, brain, and liver. Acute toxic Al^{3+} doses for fish are in the range of 0.004 to 0.178 mg L^{-1} (Roy and Campbell, 1995).

Molecular effects of Al in fish include induction of oxidative stress and genotoxicity (García-Medina et al., 2013; Pereira et al., 2013). Al induced neurotoxicity in carp (Fernández-Dávila et al., 2012; Razo-Estrada et al., 2013), and reduced expression of NeuroD1 transcript levels in the forebrain of salmon related to impaired learning performance (Grassie et al., 2013). Al also led to alteration of thyroid hormone levels in neotropical freshwater fish (Vieira et al., 2013) starting from 0.05 mg L^{-1}. Global gene expression analysis in zebrafish showed that AlCl$_3$ affected transcripts of 105 genes, including down-regulation of genes involved in cell cycle regulation and inhibition of apoptosis. Furthermore, effects on gill morphology and Na+, K+-ATPase activity was shown in zebrafish (Griffitt et al., 2011).

In contrast to aluminum, indium (In) has rarely been regarded in the environment and knowledge about its (eco)toxicity is very limited, in particular in aquatic organisms. Many of today's electronics including smart phones, flat panel displays, and light emitting

diodes (LEDs) rely on indium's unique properties of high electrical conductivity and transparency. Reported In concentrations in natural system were up to 5 µg L^{-1} (White and Hemond, 2012), and concentrations of up to 75 mg kg^{-1} are found in river sediments near smelters (Boughriet et al., 2007). Indium induced adverse effects, including inflammatory reactions, genotoxicity, production of reactive oxygen species (Lison et al., 2009), induction of metallothionein and inhibition of acetylcholine esterase activity (Zurita et al., 2007). Moreover, we found that In induced endoplasmic reticulum (ER) stress in zebrafish (Brun et al., 2014a). Besides, adverse effects of In are poorly known, nothing is known in *Daphnia*.

Although Al and In have their specific toxicological profiles, both of them also share some common molecular effects, including genotoxicity and oxidative stress. Therefore, mixtures of Al and In may have common toxicological targets. This alone makes a mixture study interesting, as the joint activity of both metals on these common targets can be evaluated. Moreover, we have shown that among additional metals Al and In occur together in leachates of damaged photovoltaic cells (Brun et al. 2016), or they may be found together in leachates of electronic waste. Another reason for analysing mixtures of Al and In is that trivalent Al^{3+} and In^{3+} can compete with divalent metals in binding with biomolecules and binding sites (Conner et al., 1995; Martin, 1986). Thus, some similar effects for trivalent In^{3+} and Al^{3+} could be expected. These reasons prompted us to investigate the joint activity of Al and In mixtures and as single compounds for their phenotypic and molecular effects.

It is generally accepted that compound mixtures acting through the same molecular target can be exchanged for other compounds with equally effective concentration without changing the overall mixture toxicity (Loewe and Muischnek, 1926), thus, the compounds act by concentration addition in a mixture. In contrast, substances with dissimilar mode of actions in a mixture interact with different target sites, and thus, joint effects can be estimated by response addition , also known as independent action (Bliss, 1939). Generally, activity of two compounds together can be additive or lead to a greater (synergism) or lesser (antagonism) activity than expected from that of the individual substances. Deviation from additivity may be explained by chemical, receptor, or cofactor interactions. We have shown both additive, synergistic and antagonistic interactions for endocrine active organic compounds *in vitro* (Christen et al., 2014b, 2012) and *in vivo* in fish (Kunz and Fent, 2009). Also for metal mixtures, additivity, synergism, and antagonism have been observed (Cooper et al., 2009; Meyer et al., 2015; Nys et al., 2015). Still, a challenge remains the mechanistic explanation for the mixture activity.

The cladoceran *Daphnia magna* has been extensively used as model organism in aquatic toxicology and freshwater ecology. Causal relationships between metals effects on somatic growth, reproduction and transcriptional responses in *Daphnia* have been suggested (Poynton et al., 2007). In response to metals, *Daphnia magna* genotypes can vary in their sensitivity (Baird et al., 1991; Barata et al., 1998). Another reason to select *Daphnia magna* for assessing effects of Al and In is the fact that the reference genome has recently been sequenced (DGC, 2015). Transcriptome next-generation sequencing (RNA-seq) is the cutting-edge method for gaining mechanistic insights into the organism's response to chemical exposures. It enables the assembly of full transcripts and thereby allowing relia-

ble and reproducible quantification over a wide range of gene expression levels (Mortazavi et al., 2008).

Here, we investigated phenotypic and molecular effects of Al and In as single metals, and subsequently, in equi-effective binary mixtures to evaluate their joint activity. First, we assessed acute and adverse chronic effects, including reproduction and growth, followed by transcriptomic analysis in neonates from acute exposure to unveil molecular mechanisms of these metals. This is particularly relevant as the mode of action of In as well as of the mixture is currently poorly known (Brun et al. 2014). By linking transcriptional initiating events with observed phenotypic responses, a comprehensive analysis of the activity of In and Al can be obtained. This concept is also known as phenotypic anchoring (Paules, 2003) and recently has been extended to the so called adverse outcome pathway (AOP; Ankley et al., 2010). Furthermore, we aimed at identifying biomarkers of exposure to aluminum, indium, and their mixture. Our study demonstrates that while these metals target different genes, they are involved in the same biological function, including lipid and sugar metabolism, exoskeleton maintenance, transmembrane transport, and metal binding. Overall, the equi-effective mixture affected substantially more genes, and the mixtures induced synergistic phenotypic responses.

5.2   Materials and Methods

Metals. Aluminum sulfate ($Al_2(SO_4)_3$), 99.99% trace metals basis) and indium (III) chloride ($InCl_3$; anhydrous, 99.999% trace metals basis) were obtained from Sigma Aldrich (Gillingham, UK).

Experimental Organism. We used a genotype with inherited alleles from parents with a different phenotypic and environmental background. The *Daphnia magna* genotype IXF originates of two parental clones (Xinb3 and Iinb1) with large phenotypic differences (Routtu et al., 2010). While the ancestors of the mother (Xinb3; also used in the genome sequencing project to produce a reference genome assembly; Routtu et al., 2014) came from a small rock pool from Tvärminne, Finland, those from the father (Iinb1) came from a carp breeding pond connected to the outlet of the largest wastewater plant in Munich, Germany. Xinb3 was self-crossed for three generations and Iinb1 for one generation before crossing.

All culture and experiments were conducted in ADaM medium (see Supporting Information ,SI, Table S5.1; Ebert, 2006; Klüttgen et al., 1994) at pH of 7.75 ± 0.01 in a climate controlled chamber (20 ± 1 °C) under artificial light:dark photoperiod of 16:8 h. The bicarbonate (HCO_3^-) content in the media acts as natural pH buffer. At least six generations were cultivated under these conditions in the laboratory before neonates from the third clutch were used for exposure. *Daphnia* were fed daily with the algae *Chlorella vulgaris* (0.5 mg carbon mL^{-1} at OD 0.8) and medium was renewed every 3rd day.

Experimental Design. Experiments were designed according to an equi-effective protocol, where metals were compared for their equal mortality. This allows the comparison of re-

sponses of the single metals Al and In at equi-effective doses with those of mixture exposures. Effect concentrations (EC) based on mortality were determined by conducting an acute 48 h dose-response experiment of single compounds.

In a next step, equi-effective concentrations of both metals were applied in metal mixtures to determine mixture activity of $EC_{0.625}$, $EC_{1.25}$, $EC_{2.5}$, EC_5, EC_{10}, EC_{20}, EC_{40}, EC_{80}. Basis of this experimental mixture design was the effect additivity concept. Thus, it was based on the assumption that, for example, the mixture of $EC5_{compound\ A}$ and $EC5_{compound\ B}$ would lead to an overall effect of 10% in the mixture. To determine the onset of mortality during the exposure time, mortality was recorded continuously over 48 hours. According to this time-course study, more than 80% of the *Daphnia* survived the first ten hours in the $EC_5 + EC_5$ mixture. Therefore, the equi-effective mixture of $EC_5 + EC_5$ and the single metal concentration of EC_{10} were assessed after exposure for 10 h for the transcriptome study using RNA-seq. Acute exposure was chosen for RNA-seq to determine initiating molecular events leading to chronic effects. After exposure, surviving *Daphnia* were immediately snap frozen in liquid nitrogen and stored at -80 °C until RNA extraction.

During acute exposures, *Daphnia magna* were kept at a density of ten organisms per 200 mL ADaM medium without feeding. For each treatment group, four biological replicates were set up in beakers containing ten individuals per 200 mL. In chronic exposures, 1 organism per 60 mL ADaM was kept and fed daily. A total of ten replicates per dose group were set up. At higher concentrations, $Al_2(SO_4)_3$ led to lowering of the pH due to production of H_2SO_4. To maintain a stable pH during exposure, pH was adjusted using sodium hydroxide before starting the exposures.

Molting, Growth, and Reproduction. Chronic exposures were performed using a 5-, 10-, and 20-fold dilution of the EC_{10} of the single metal, and $EC_5 + EC_5$ of the metal mixture. Daphnids were exposed until the release of the third brood or 21 day at maximum. Daphnids were monitored daily for molting frequency, time of sexual maturity (defined as the first appearance of eggs in the brood chamber), number of juveniles produced, and mortality. Every other day (starting at 24 h), pictures were taken under a microscope (Nikon SMZ800 with C-Mount camera) to measure daphnid size using ImageJ software (Abràmoff et al., 2004). Every third day, the test solution was refreshed. The length of carapace of daphnid was defined as distance from the top of the eye to the base of the caudal spine, and used as indicator for growth.

Juvenile growth rate (JGR) was calculated as follows:

$$JGR = \frac{\ln(x_{t=sexual\ maturity}) - \ln(x_{t=1})}{\#\ of\ days\ until\ sexual\ maturity} \times 100\%$$

(2)

where $x_{t=sexual\ maturity}$ is the carapace length of the daphnid at the day when reaching sexual maturity, and $x_{t=1}$ is the length of the daphnid at the start of the experiment. The same formula was used to calculate the specific growth rate (SGR) over 20 days.

Inductively-Coupled Plasma Mass-Spectrometry (ICP-MS) Analyses. Concentrations of the soluble fraction of aluminum (^{26}Al) and indium (^{115}In) isotopes in exposure media were quantified by inductively-coupled-plasma mass-spectrometry (ICP-MS; Agilent 7500cx, Switzerland) equipped with an Octopole Reaction System, pressurized with an optimized helium flow of 5 mL min^{-1}. Medium samples were filtered through a 0.45 μm membrane, acidified to 1% HNO$_3$ before analysis. Rubidium was used as internal standard.

Bioimaging Using Laser-Ablation ICP-MS (LA-ICP-MS). For elemental mapping, 6 days old *Daphnia* were chosen, as they are larger in size than 24 h old neonates. This facilitated embedding and visualisation, needed for LA-ICP-MS analysis. At this time point, egg development had not yet started, and therefore, uptake was assumed to be similar as in neonates. *Daphnia* were exposed for ten hours to the EC$_{10}$ of aluminum, the EC$_{10}$ of indium, and the EC$_5$ + EC$_5$ of the mixture. Following exposure, *Daphnia* were rinsed with 1 μmol L^{-1} of EDTA, and subsequently with deionized water. Formaldehyde 4% was used as fixation reagent overnight at 4 °C. *Daphnia* were then dehydrated by increasing concentrations of ethanol (80%, 2x 90%, 2x 96%, 2x isopropanol, Roti-Histol; 1 hour each, then Roti-Histol overnight and another exchange for 4 h), and embedded in paraffin overnight. *Daphnia* were cut sagittally using a microtome.

LA-ICP-MS technique was applied for bio-imaging the elemental distribution within *Daphnia*. For this, a NWR213 laser ablation system (ESI, Portland, USA) was coupled to the above described ICP-MS system as previously described (Brun et al. 2014). The laser was operated at 50% of its maximum energy, at a repetition rate of 20 Hz, a spot size of 25 μm, and a stage translation velocity of 25 μm sec^{-1}. Successive lines were spaced 25 μm apart. Isotopes recorded via the Masshunter workstation software (Agilent) were ^{27}Al, ^{31}P, ^{43}Ca, ^{113}In, ^{115}In. Data processing was performed within the Iolite freeware environment (Paton et al., 2011) running in Igor Pro (Wavemetrics).

RNA Extraction, Library Preparation, and Sequencing. RNA of 20 neonates of each of the four replicates was extracted using the RNeasy Mini Kit (Qiagen) following the manufacturer's instructions. *Daphnia* were homogenized using the 2010 Geno/Grinder (SPEX SamplePrep, UK; 1750 rpm for ten sec). RNA quantity was measured using a Nanodrop 8000 (Thermo Scientific, US), and integrity verified on a 2200 TapeStation system (Agilent Technologies, US). Only samples with an RNA integrity number (RIN) higher than 7 were used for further analysis. Poly(A)+ RNA was enriched using a NEBNext Poly(A) mRNA Magnetic Isolation Module. After reverse transcription, a complementary cDNA library was constructed using the NEBnext Ultra Directional RNA Library Prep Kit (New England Biolabs, U.S.).

Briefly, mRNA was further purified by exploiting the poly-A tails using NEBNext Oligo d(T) beads. Then, mRNA was fragmented to suitable lengths, which were subsequently converted into cDNA by reverse transcriptase. The fragmented cDNA were purified using AMPure XP beads, bound by oligonucleotide adaptor, followed by PCR library enrichment. After library production, QC was performed using the TapeStation system with a High-Sensitivity D1000 tape, confirming the size of the library. Quantitation was performed using the Kapa Library Quantitation Kit (Kapa Biosystems Ltd, UK) for Illumina Platforms,

and equal molar quantities of each library mixed to produce a pooled library sample. These pooled samples were tested again by the same procedures. A 2 nM pooled library sample was denatured using NaOH (per Illumina protocols), and loaded onto a Rapid-Run v2 slide using the Illumina cBot instrument at a 12pM concentration. The cDNA was sequenced in paired-end sequencing-mode with 50 bp read length on an Illumina HiSeq 2500 machine using a v2 Rapid-Run SBS kit.

Statistical Analyses. The phenotypic data were graphically illustrated with GraphPad Prism 6 (GraphPadSoftware Inc., USA). For EC calculations, raw data were logarithmically transformed, normalized, and curves fitted using the four-parameter logistic equation (variable Hill slope).

First, the data was tested for normality and homogeneity of variance. Then, significant differences in phenotypic response between treatments or respective controls were assessed by one way ANOVA followed by a Bonferroni posthoc test ($p \leq 0.05$). In the toxicity studies, four replicates for each treatment group were used. Results are expressed as means ± standard deviation of mean (SD). Differences were considered statistically significant at $p \leq 0.05$.

5.3 Results

Exposure Concentrations. ICP-MS analysis was performed to quantify the soluble fraction of Al and In in exposure medium of the transcriptomic experiment. Measured concentrations of the soluble fraction were significantly lower for both metals, of which Al was 45-times, and In 4-times lower than nominal. This suggests significant precipitation of the metals, particularly of Al. Furthermore, a tendency of a decrease over exposure time from 5 to 10 h can be seen, probably due to sorption to and incorporation of metals in daphnids (Table 5.1). All nominal EC values are listed in Table S5.2 in the SI.

Table 5.1 Nominal concentrations and concentrations measured by ICP-MS in ADaM after 5 h and 10 h of exposure to $Al_2(SO_4)_3$, $InCl_3$, and their binary mixture. Nominal concentrations are calculated for single metals only (without sulphate or chloride) to make the comparison to measured concentrations detecting the signal for ^{27}Al and ^{115}In isotopes using ICP-MS. Each value represents the mean of four replicates.

		Nominal		Measured	
		mg L^{-1}	µM	mg L^{-1}	µM
Al EC$_{10}$	5 h	30.31	88.59	0.664	24.61
	10 h	30.31	88.59	0.606	22.46
In EC$_{10}$	5 h	45.84	207.25	12.248	106.67
	10 h	45.84	207.25	10.822	94.25
Al EC$_5$ + In EC$_5$	5 h	28.54 + 43.30	83.41 + 195.77	0.606 + 9.891	22.46 + 86.14
	10 h	28.54 + 43.30	83.41 + 195.77	0.586 + 8.300	21.72 + 72.29

Effects on Survival - Acute Exposure. The dose-response curve for mortality produced a steep hill slope (Al: 12.73, In: 12.62) for both metals with an EC_{50} value of 35.91 mg L^{-1} and 54.49 mg L^{-1} for Al and In, respectively (Figure 5.1A). The EC_5 and EC_{10} values were relatively close to each other due to the steep hill slope. The experimentally assessed mixture effect revealed a greater effect than predicted from the combination of the individual effects. Mortality started to increase after ten hours for both metals (at lower concentrations), and even earlier (6 h) at higher concentrations (mixture: Figure 5.1B; single metals: Figure S5.1, SI). The metal mixture of EC_5 + EC_5 induced an average mortality rate of 10% after ten hours. Consequently, a ten hour exposure and a combination of EC_5 + EC_5 and EC_{10} for single compounds were chosen for transcription analysis.
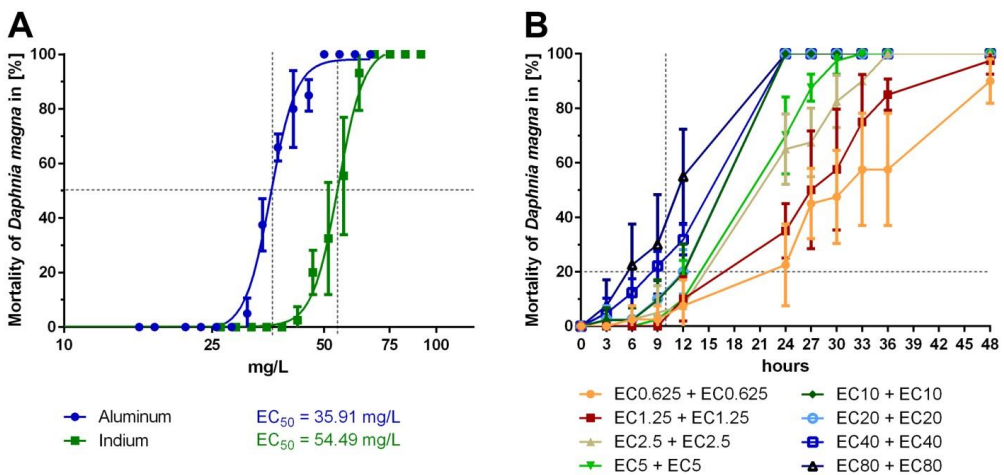
Figure 5.1 (A) Mortality of *Daphnia magna* neonates exposed for 48 h to aluminum (Al$_2$(SO$_4$)$_3$) or indium (InCl$_3$), respectively. X-axis shows nominal concentrations. Dose-response curves were the basis to assess equi-effective concentrations for mixture experiments. Hill slope for aluminum and indium is 12.73 and 12.62, respectively. (B) Mortality of neonates to equi-effective mixtures of aluminium and indium. In the mixture of EC_5 + EC_5 more than 80% of *Daphnia magna* survived the first ten hours, and therefore, this exposure time was set in the transcriptomics study. Error bars represent the standard error of each exposure group (four replicates, ten individuals in each).

Effects on Molting, Growth, and Reproduction - Chronic Exposure. Concentrations used for chronic exposures are listed in Table 5.2. Molting was recorded daily and plotted cumulative against time (Figure 5.2). High aluminum concentration significantly decreased molting. This effect did not appear in the binary mixture. However, both compounds (mid and high) and the mixture (low, mid, and high) clearly decreased the amount of juveniles produced (Figure 5.3A), suggesting reproduction effects. When comparing the mixture effect with effects of the single metals at equal toxicity, a difference for the low and mid dose was noted. The high doses could not be compared as two groups did not produce any neonates.

Table 5.2 Nominal concentrations used in chronic exposures. Low is corresponding to a 20-fold, mid to a 10-fold, and high to a 5-fold dilution of the EC_{10} of the single compound and $EC_5 + EC_5$ of the mixture.

	Low	Mid	High
Aluminum (mg L^{-1})	1.52	3.03	6.06
Indium (mg L^{-1})	2.29	4.58	9.17
Aluminum + Indium (mg L^{-1})	1.43 + 2.17	2.85 + 4.33	5.71 + 8.66

Brood sizes increased from the first to the third brood in controls and single metals exposures (low and mid doses), whereas the high indium and mid mixture doses showed a decrease in the third brood size (Figure S5.2A, SI). A similar pattern of greater effect in the mixture can be seen, when comparing the divergence in age at maturity of different exposure groups (Figure S5.2B, SI). Both metal exposures and the mixture reduced daphnid growth in the first ten days in the low concentration in a similar way. Whereas the middle concentration induced a stronger growth reduction over time in the mixture and in the highest concentration, growth was already minimal in the aluminum exposure, therefore no further reduction in the mixture exposure could be expected. A significant decrease in growth was measured after starting from day 2 on. Over all time points, daphnids were smaller than controls showing a concentration-dependent decrease (Figure 5.3C).

Juvenile growth rate until sexual maturity (Figure 5.3B), population growth rate (Figure S5.3A, SI) and specific growth rate over 20 days (Figure S5.3B, SI) was calculated. The population growth rate was significantly reduced in all mid and high exposure groups, and the specific growth rate in all high exposure groups. While juvenile growth rates were significantly decreased in all exposure groups, indicating a greater effect on developmental stages.
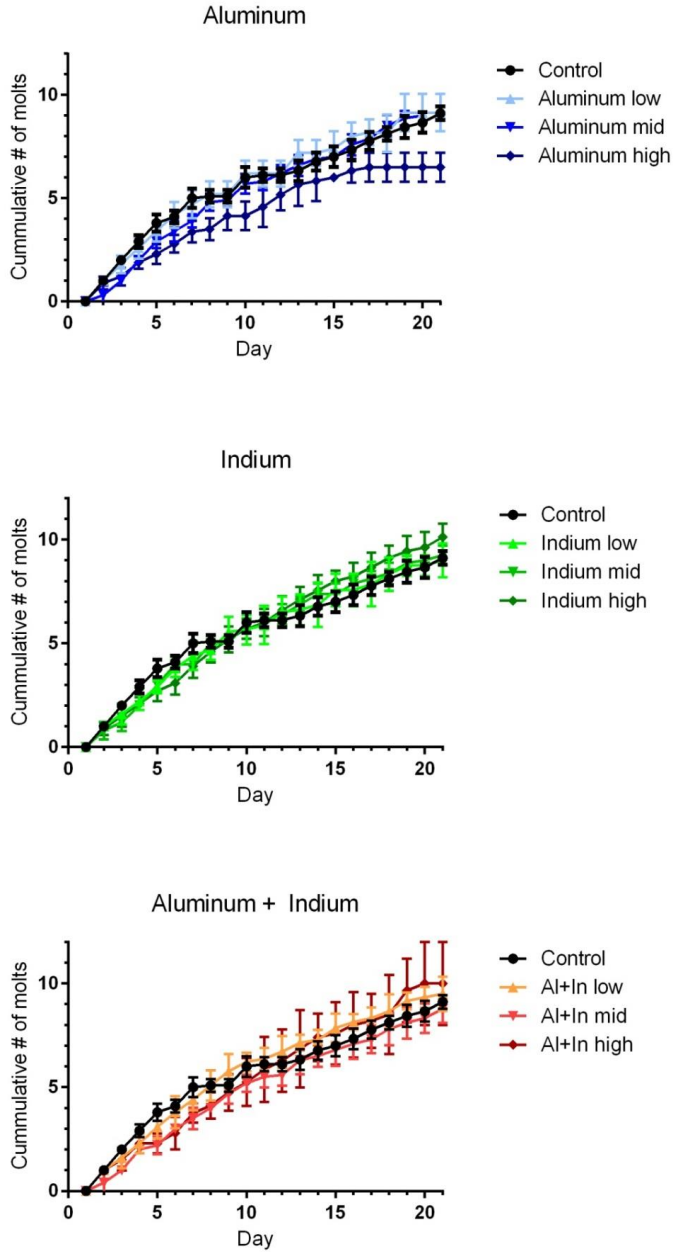
Figure 5.2 Cumulative number of molts of *Daphnia magna* exposed to nominal aluminum (low:1.52, mid: 3.03, high, 6.06 mg L^{-1}), indium (low: 2.29, mid: 4.58, high: 9.17 mg L^{-1}), and their equi-effective binary mixture (Al + In low: 1.43 + 2.17, mid: 2.85 + 4.33, high: 5.71 + 8.66 mg L^{-1}) over 21 days. Number of molts in the aluminum high treatment is significantly different from control.
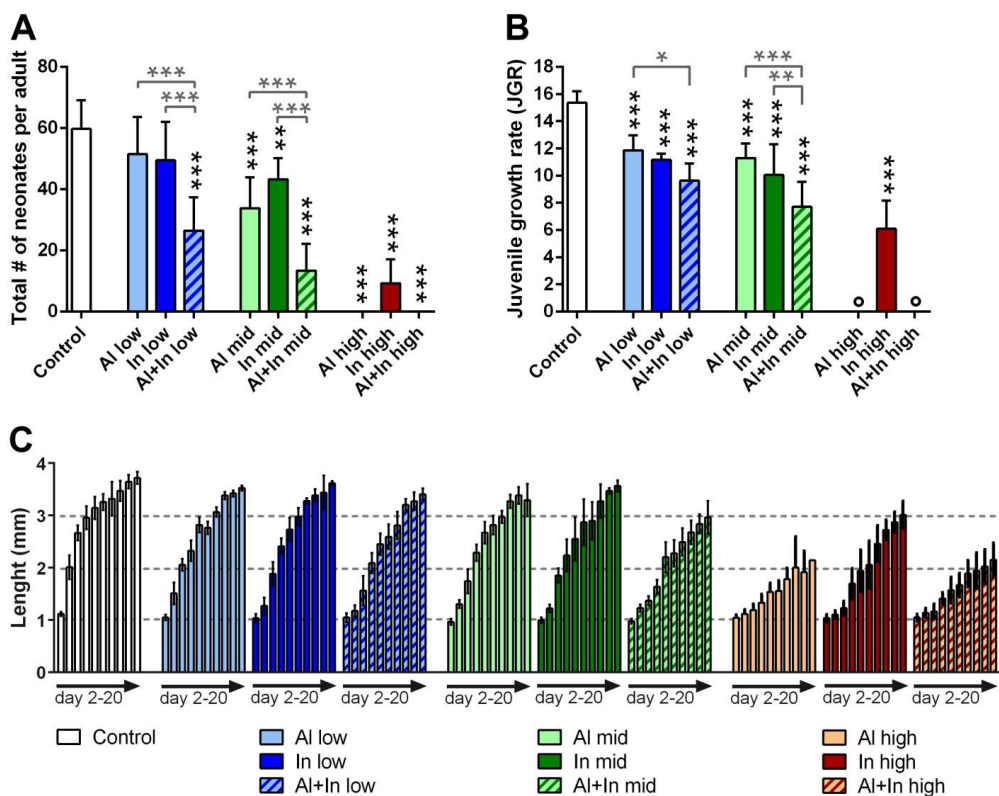
Figure 5.3 Fecundity, growth rate and length of *Daphnia magna* from day 2 to 20 exposed to three doses of aluminium (Al), indium (In), and their equi-effective mixture concentration (Al+In). (A) Fecundity of *Daphnia* in controls and exposure groups. Total number of neonates after 3 brood releases or 21 days maximal. (B) Juvenile somatic growth rates from day 2 to maturity. Circles indicate that, due to toxicity, none of the individuals in the group reached maturity within 21 days, and therefore, were not included in statistical analysis. (C) Growth based on carapace length over 20 days. Mean ± SD. Black asterisks indicate significantly different to control, grey asterisks indicate difference between single compound and equi-effective mixture (n=10). Nominal concentrations are for Al 1.52 (low), 3.03 (mid), 6.06 (high) mg L^{-1}, for In 2.29 (low), 4.58 (mid), 9.17 mg L^{-1} (high), and for Al + In 1.43 + 2.17 (low), 2.85 + 4.33 (mid), 5.71 + 8.66 mg L^{-1} (high).

Uptake of Aluminum and Indium. We determined LA-ICP-MS profiles of embedded *Daphnia* of all dose groups to assess the distribution of aluminum and indium in the organisms after single and single exposures and in the mixture-exposed *Daphnia* on the carapace. Furthermore, aluminum accumulation was mainly displayed in the blind gut and midgut, as well as in the thoracic limbs, carrying the filtering screens. A minor distribution of aluminum is measurable in controls and indium exposed daphnids as aluminum is an essential
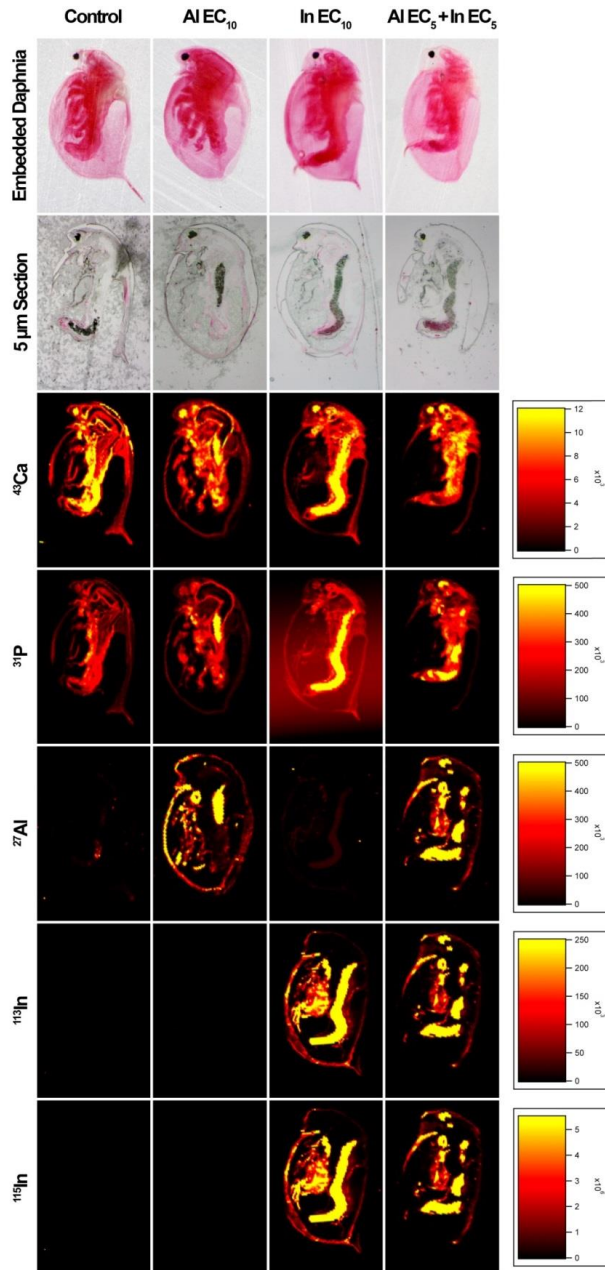
Figure 5.4 Laser-ablation ICP-MS elemental mapping of aluminium, indium, and calcium in 6 days old *Daphnia magna* after a ten hour exposure to nominal 30.31 mg L^{-1} aluminium, 45.84 mg L^{-1} indium, or equi-effective mixture 28.54 and 43.30 mg L^{-1} thereof. First row: paraffin embedded *Daphnia magna*; second row: 5 µm section; third to seventh row: LA-ICP-MS images of elements indicated on the left. Colour bars show the intensity in counts per seconds. The intensity for [113]In and [115]In are related with a factor of 22 to each other, which equals to its isotope ratio.

trace element (Quiroz-Vázquez et al., 2010). Both [113]In and [115]In are shown and their intensity is displayed according to its isotope ratio of 22. Both isotopes reveal similar images and intensity, therefore interferences between them can be ruled out. Indium showed a similar, if not almost identical accumulation as aluminum in the carapace, thoracic limbs and gut. The pattern of these metals is distinctly different from calcium and mixture exposures after ten hours (Figure 5.4). Clearly visible is the adsorption of aluminum in phosphorus that are found in the gut, but also in eyes and blind gut (caecum) in case of calcium.

Transcriptomic Profiles of *D. magna*. RNA-seq data resulted in a set of *de novo* assembled transcripts. The statistically significantly up- or down-regulated transcript clusters were then aligned to the *D. magna* genome using the BLAST tool from the wFleaBase (gene set: 09.2014, and genome assembly: 22.04.2010). Sequences were annotated if they had a BLAST hit with an E value below 10^{-5} and a score above 100. Homology search was performed against UniProt, GenBank (NCBI) and GeneCards. The list of statistically significantly up- or down-regulated transcripts, and predicted involvement in biological processes is listed in Table 5.3. Each metal had a unique expression profile, with only a few genes shared among the treatment groups. Exposure to Al and In resulted in differential expression of 130 and 75 transcripts, respectively. In the mixture substantially more genes (368) were differentially expressed than in the single treatment, with 323 transcripts uniquely differentially expressed in the mixture (Figure 5.5).
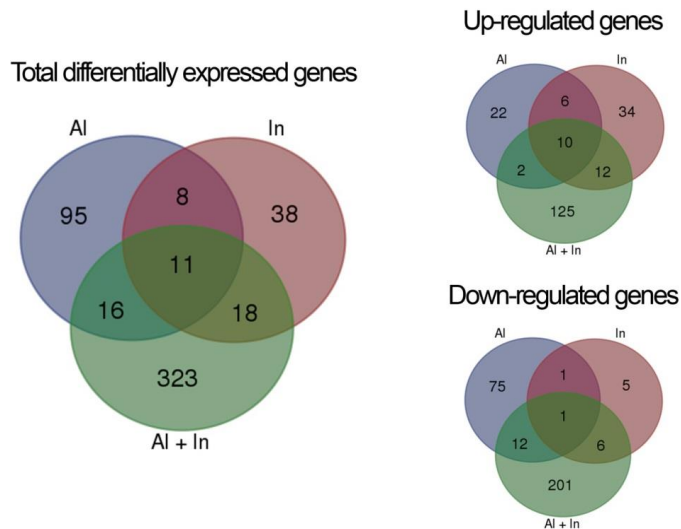
Figure 5.5 (A) Venn diagram of all differentially expressed genes determined by RNA-seq in *Daphnia magna* after exposure to nominal 30.31 mg L^{-1} aluminum, 45.84 mg L^{-1} indium, and equi-effective mixture of aluminum and indium (28.54 and 43.30 mg L^{-1}), respectively, compared to non-exposed control. Overlapping planes share differentially expressed genes.

Among the aluminum-specific genes that were down-regulated are several fragments coding for protein folding, lipid and sugar metabolism, and muscle development. Genes that were specifically up-regulated by indium were complement C1q protein 4 and

defense protein 1(2)34Fc, which is related to an immune response and glioma pathogenesis-related protein related to sugar metabolism. The only gene down-regulated by both single treatments, as well as the mixture is involved in ageing. Of the 10 transcripts significantly up-regulated among all three treatment groups were cathepsin o and muscle-specific protein as the only two identified transcripts. Additionally, several "unknown" gene fragments were commonly altered.

The expression data were further analysed for patterns that could be predictive for biological processes and pathways. Transcriptional changes can be ascribed to six major processes and mechanisms for both metals, while disruption of protein folding, maturation, and degradation was affected by Al. Following six processes were affected by both Al and In: (1) lipid metabolism, (2) sugar metabolism, (3) chitin metabolism, (4) nervous system function, (5), metal binding, and (6) ionic transmembrane transport.

Table 5.3 Statistically significantly up- (red) or down-regulated (green) transcripts in *Daphnia magna* after exposure to nominal 30.31 mg L^{-1} aluminum, 45.84 mg L^{-1} indium, and mixtures of 28.54 mg L^{-1} aluminum and 43.30 mg L^{-1} indium.

Biological function / molecular process	Gene ID	Gene description	Al	In	Al + In
Response to unfolded protein	Dapma7bEVm001168t2	F-box only protein	green		green
	Dapma7bEVm001168t1	F-box only protein			green
	Dapma7bEVm011816t1	F-box only protein			green
	Dapma7bEVm003637t5	Eukaryotic translation initiation factor 2-alpha kinase	green		
	Dapma7bEVm009686t8	Calnexin			
	Dapma7bEVm009686t1	Calnexin	red		
	Dapma7bEVm009686t4	Calnexin			green
	Disulfide-isomerase	Disulfide-isomerase	green		
	Dapma7bEVm000493t10	O-mannosyl-transferase			
	Dapma7bEVm004347t5	Cathepsin o	red	red	red
	Dapma7bEVm010239t4	Cathepsin o			red
	Dapma7bEVm000991t1	Cathepsin o			red
	Dapma7bEVm001908t1	Cathepsin o			red
	Dapma7bEVm010576t9	Heat shock protein HSP 90-alpha			green
	Dapma7bEVm003115t1/3	Heat shock 70 kDa protein cognate			green
	Dapma7bEVm004111t2/3/4/5/6	Disulfide-isomerase A4			green
	Dapma7bEVm001525t1	Calreticulin			green
	Dapma7bEVm000493t10	O-mannosyl-transferase	green		
	Dapma7bEVm000493t4/5	O-mannosyl-transferase			
	Dapma7bEVm002784t4	phosphatidylinositol-4-phosphate type-2 alpha			green
Detoxification	Dapma7bEVm010990t2	glutathione s-transferase			
Lipid metabolism	Dapma7bEVm027617t2	phosphatidate phosphatase/ARP2_G1315	green		
	Dapma7bEVm001623t1	Lipid phosphate phosphohydrolase	green		
	Dapma7bEVm003505t1	Pyruvate carboxylase, mitochondrial			
	Dapma7bEVm003505t6	Pyruvate carboxylase, mitochondrial			green
	Dapma7bEVm002776t1	Transmembrane protein 120B	red		
	Dapma7bEVm005944t1	Gastric triacylglycerol lipase precursor	red		
	Dapma7bEVm005643t1	Phospholipase A2 isozyme PA4			
	Dapma7bEVm028496t1	Glioma pathogenesis-related protein		red	
	Dapma7bEVm009928t8	Glioma pathogenesis-related protein		red	
	Dapma7bEVm002062t5	Apolipoprotein D/sw			green
	Dapma7bEVm010378t1	Z9 acyl-CoA desaturase B			red
	Dapma7bEVm001546t6	Z9 acyl-CoA desaturase B			red
Sugar metabolism	Dapma7bEVm001990t2	dTDP-D-glucose 4,6-dehydratase	green		
	Dapma7bEVm015291t5	Sugar transporter			green
	Dapma7bEVm015291t3/8/12	Sugar transporter			green
	Dapma7bEVm015028t2/3/4/8/6/14	Sugar transporter			green
	Dapma7bEVm015445t1	Sugar transporter			green
	Dapma7bEVm004695t2/1/5	Sugar transporter			red
	Dapma7bEVm003185t5/3	Sugar transporter			red
	Dapma7bEVm006765t2/3	Sugar transporter			red

Category	ID	Description
	Dapma7bEVm000493t10	O-mannosyl-transferase
	Dapma7bEVm000493t4/5	O-mannosyl-transferase
	Dapma7bEVm003505t1	Pyruvate carboxylase, mitochondrial
	Dapma7bEVm003505t6	Pyruvate carboxylase, mitochondrial
	Dapma7bEVm000151t2/1/3	NUAK family SNF1 kinase 2
	Dapma7bEVm002820t2	Mitochondrial 2-oxoglutarate/malate carrier protein
	Dapma7bEVm010938t2/3	Alpha1,3fucosyltransferase
	Dapma7bEVm005865t4/6/1	Phosphoenolpyruvate carboxykinase, cytosolic (GTP)
	Dapma7bEVm001990t2	dTDP-D-glucose 4,6-dehydratase
	Dapma7bEVm001990t5/15	GDP-mannose 4,6 dehydratase
Exoskeleton related	Dapma7bEVm028798t1	Cuticular protein 65Eb
	Dapma7bEVm001606t9	Cuticular protein
	Dapma7bEVm001606t3	Cuticular protein
	Dapma7bEVm001605t3	Cuticular protein
	Dapma7bEVm001605t4	Cuticular protein
	Dapma7bEVm004406t1	Cuticular protein 30B, RT03304p
	Dapma7bEVm004981t1	Cuticular protein analogous to peritrophins 1-D
	Dapma7bEVm005109t4	Nuclear receptor subfamily 4 group A member
	Dapma7bEVm005611t4	Larval cuticle protein
	Dapma7bEVm005890t2	Chitin deacetylase 3 precursor
	Dapma7bEVm001337t9/5/8/7/6	Brain chitinase and chia
	Dapma7bEVm006242t3	Brain chitinase and chia
	Dapma7bEVm009864t8	Chitin synthase variant
Ectysis	Dapma7bEVm004624t2	Ecdysone-induced protein 78C
Neurogenesis/ Nervous system/ Morphogenesis	Dapma7bEVm006117t1	Ninjurin a
	Dapma7bEVm000904t4	Spastin
	Dapma7bEVm015104t2	BAI1-associated protein
	Dapma7bEVm009881t8	Periaxin
	Dapma7bEVm009881t9/11	Periaxin
	Dapma7bEVm028473t7	neurexin IV/ARP2_G19
	Dapma7bEVm009504t7	Multiple PDZ domain protein
	Dapma7bEVm003505t1	Pyruvate carboxylase, mitochondrial
	Dapma7bEVm000640t10	Neural cell adhesion molecule
	Dapma7bEVm001263t4	Neurexin IV
	Dapma7bEVm018535t1	Glutamate receptor, ionotropic kainate
	Dapma7bEVm000640t10	Neural cell adhesion molecule
	Dapma7bEVm000671t5	Sodium- and chloride-dependent GABA transporter
	Dapma7bEVm000671t6/2/9/7	Sodium- and chloride-dependent GABA transporter
	Dapma7bEVm003073t4/5/2	Sodium- and chloride-dependent GABA transporter
	Dapma7bEVm018721t2	Neurocalcin-delta B
	Dapma7bEVm003933t1	Reeler
	Dapma7bEVm006029t4/1	Neuroguidin
	Dapma7bEVm010144t2	Headcase protein
	Dapma7bEVm004192t1/5	4-aminobutyrate aminotransferase, mitochondrial
	Dapma7bEVm018658t3/11/12/10/6/7/9/1/8/4	Single-minded
	Dapma7bEVm011097t5	Glutamine synthetase 2 cytoplasmic
Immune response	Dapma7bEVm010318t5	Complement C1q protein 4/sw
	Dapma7bEVm010318t1/3/4/8	Complement C1q protein 4/sw
	Dapma7bEVm003933t3	Defense protein l(2)34Fc
	Dapma7bEVm010256t1	Complement C1q tumor necrosis factor-related protein 3/sw
ATP binding	Dapma7bEVm002623t11	DNA mismatch repair protein Mlh3
	Dapma7bEVm000904t4	Spastin
	Dapma7bEVm001113t5	ATP-binding cassette sub-family B member 8, mitochondrial
	Dapma7bEVm018714t4	Helicase c-terminal domain containing protein
	Dapma7bEVm003505t1	Pyruvate carboxylase, mitochondrial
	Dapma7bEVm000654t4	Threonine--tRNA ligase 2, cytoplasmic
	Dapma7bEVm003637t4	Eukaryotic translation initiation factor 2-alpha kinase
	Dapma7bEVm005677t4/2/1	Serine/threonine-protein kinase Nek7
	Dapma7bEVm001056t2/6/4/8/7	L-fucose kinase
	Dapma7bEVm001754t4/5/3/8	Lymphoid-specific helicase
	Dapma7bEVm006959t3/1	Multidrug resistance-associated protein lethal(2)03659
	Dapma7bEVm010711t4/7/3/6/5	Molybdenum cofactor synthesis protein cinnamon
Ageing	Dapma7bEVm012054t1	Methionine-r-sulfoxide reductase
	Dapma7bEVm002062t5	Apolipoprotein D/sw
	Dapma7bEVm009708t8	Copper-zinc cu-zn superoxide dismutase.
Zinc ion binding	Dapma7bEVm018381t1	Remodeling and spacing factor
	Dapma7bEVm005011t2	Nardilysin
	Dapma7bEVm000463t1	Protease m1 zinc metalloprotease
	Dapma7bEVm001569t4	Zinc carboxypeptidase
	Dapma7bEVm018787t1	Retrovirus-related Pol polyprotein from transposon TNT 1-94
	Dapma7bEVm001285t2	High choriolytic enzyme
	Dapma7bEVm001285t5/9/3/4	High choriolytic enzyme
	Dapma7bEVm000495t5	High choriolytic enzyme
	Dapma7bEVm004914t5	Low choriolytic enzyme
	Dapma7bEVm004624t2	Ecdysone-induced protein 78C
	Dapma7bEVm000285t9/6/8/4/7/11	Cytosolic carboxypeptidase
	Dapma7bEVm005109t4	Nuclear receptor subfamily 4 group A member
	Dapma7bEVm001489t4	RING finger and SPRY domain-containing protein
	Dapma7bEVm001472t2	Matrix metalloproteinase-15
	Dapma7bEVm009708t8	Copper-zinc cu-zn superoxide dismutase.
Iron ion binding	Dapma7bEVm010043t8	NADPH--cytochrome P450 reductase protein
	Dapma7bEVm003637t4	Eukaryotic translation initiation factor 2-alpha kinase
	Dapma7bEVm002353t1/3	Epsilon-trimethyllysine dioxygenase

Category	ID	Description
Calcium ion binding	Dapma7bEVm003448t4	Calcyphosin protein
	Dapma7bEVm001075t6	Sushi, von Willebrand factor type A, EGF and pentraxin domain-containing protein
	Dapma7bEVm023196t1	Kinesin calmodulin-binding protein
	Dapma7bEVm023994t2	Double oxidase: two peroxidase domains
	Dapma7bEVm004682t7	Double oxidase: two peroxidase domains
	Dapma7bEVm010695t3	Double oxidase: two peroxidase domains
	Dapma7bEVm005643t1	Phospholipase A2 isozyme PA4
	Dapma7bEVm001469t6	SPARC-related modular calcium-binding protein
	Dapma7bEVm018721t2	Neurocalcin-delta B
	Dapma7bEVm001576t2	Collagen and calcium-binding EGF domain-containing protein
	Dapma7bEVm001525t1	Calreticulin
	Dapma7bEVm002606t1	RalBP1-associated Eps domain-containing protein
	Dapma7bEVm002338t3	Annexin-B9
Ca channel	Dapma7bEVm008410t1	Calcium channel flower
Mg ion binding	Dapma7bEVm000151t2/1/3	NUAK family SNF1 kinase 2
Metal ion binding	Dapma7bEVm029456t2	dna-directed rna polymerase ii largest subunit/ARP2_G207
	Dapma7bEVm003505t1	Pyruvate carboxylase, mitochondrial
	Dapma7bEVm000493t10	O-mannosyl-transferase
	Dapma7bEVm000493t4/5	O-mannosyl-transferase
	Dapma7bEVm010711t4/7/3/6/5	Molybdenum cofactor synthesis protein cinnamon
	Dapma7bEVm006542t5/1	Galactosylgalactosylxylosylprotein 3-beta-glucuronosyltransferase P
Cellular response to potassium ion starvation	Dapma7bEVm005865t4/6/1	Phosphoenolpyruvate carboxykinase, cytosolic (GTP)
Oxygen transport	Dapma7bEVm015299t5	di-domain 94aemoglobin precursor
	Dapma7bEVm015367t12	di-domain 94aemoglobin precursor
	Dapma7bEVm015299t3	di-domain 94aemoglobin precursor
Oxidative stress	Dapma7bEVm005234t1	Iodotyrosine dehalogenase
	Dapma7bEVm009708t8	Copper-zinc cu-zn superoxide dismutase.
	Dapma7bEVm010990t2	glutathione s-transferase
Transmembrane transporter / solute carrier	Dapma7bEVm004715t7	Ammonium transporter Rh type C
	Dapma7bEVm024032t6	Sulfate transporter
	Dapma7bEVm029187t5	sulfate transporter/ARP2_G713
	Dapma7bEVm024032t1	Sulfate transporter
	Dapma7bEVm000671t11	high affinity gaba transporter/ARP2_G8233
	Dapma7bEVm000671t5	Sodium- and chloride-dependent GABA transporter
	Dapma7bEVm000671t6/2/9/7	Sodium- and chloride-dependent GABA transporter
	Dapma7bEVm003073t4/5/2	Sodium- and chloride-dependent GABA transporter
	Dapma7bEVm001228t7	Solute carrier family 25 member 36-A
	Dapma7bEVm009947t4/16/12/8/7/6/5/22/21/9/10/11/2/20/24	Bumetanide-sensitive na-k-cl cotransport protein
	Dapma7bEVm000220t3/19/20/6/8/5/21/9/3/6/11/2	Bumetanide-sensitive na-k-cl cotransport protein
	Dapma7bEVm009542t17/6/1/13	Bumetanide-sensitive na-k-cl cotransport protein
	Dapma7bEVm006959t3/1	Multidrug resistance-associated protein lethal(2)03659
	Dapma7bEVm001302t5/2/1	V-type proton ATPase subunit D
	Dapma7bEVm023722t1	Bestrophin
	Dapma7bEVm010966t1/2	Voltage-gated potassium channel subunit beta-2
	Dapma7bEVm015372t2	H(+)/Cl(-) exchange transporter
	Dapma7bEVm010045t12	Natural resistance-associated macrophage protein
Na+/K+ -ATPase	Dapma7bEVm002578t1	Sodium/potassium-transporting ATPase alpha-3 chain protein
	Dapma7bEVm002578t9/17	Sodium/potassium-transporting ATPase alpha-3 chain protein
Intracellular transport	Dapma7bEVm010163t1	Innexin inx2
	Dapma7bEVm010376t4	Innexin inx3
Locomotion	Dapma7bEVm000493t10	O-mannosyl-transferase
	Dapma7bEVm000493t4/5	O-mannosyl-transferase
	Dapma7bEVm018399t37	myosin-2 heavy chain/ARP2_G8
	Dapma7bEVm009447t6	myosin light chain kinase/ARP2_G892
	Dapma7bEVm003974t4/26	Unconventional myosin-X
	Dapma7bEVm000039t41	Unconventional myosin-XV
	Dapma7bEVm003974t18	Unconventional myosin-X
	Dapma7bEVm004909t5	Muscle-specific protein

5.4 Discussion

Aluminum and indium are increasingly used and released into the environment through diverse industrial and manufacturing processes, weathering of photovoltaics, and electronic waste operations. So far, the ecotoxicological effects of indium are poorly known (Brun et al. 2014), while aluminum was fairly well studied for effects in aquatic organisms before the turn of the millennium due to the topic of acidic precipitation (Gensemer and Playle, 1999). These two toxicants occur in leachates of photovoltaic devices (Brun et al. 2016), belong to the same group in the periodic table and are classified as metalloids. This prompted us to study these metals as single compounds and equi-effective mixtures for their phenotypic and molecular effects. We assessed the gene expression profile of *Daphnia magna* exposed to EC_{10} levels of Al and In determined by acute toxicity (immobility), and equi-effective $EC_5 + EC_5$ levels in the mixture at a time point below acute lethality. Therefore, a stress response indicative for chronic effects was expected. We were specifically interested in exploring affected functional biological processes by linking acute gene expression responses assessed by RNA-seq to adverse phenotypic responses. Our transcriptomic results underline that reduced growth and reproduction is likely to be the combination of several mechanisms, including glucose and lipid metabolism, affecting the energy budget. Chronic equi-effective mixture exposures exhibited synergistic effects in endpoints such as age at maturity, growth, and reproduction. While on the transcription level, substantially more genes were affected, possibly explaining the stronger effect on growth and reproduction. Already the alteration of a few genes, as shown in the indium exposure, can affect adverse outcome. Thereby, the amount of biologically important genes could be narrowed down. Nevertheless, the function of these genes and their linkage to adverse phenotypic outcome need to be better understood. Based on these results, we conclude that the two metals primarily act through similar molecular modes of action. Genes encoding for cathepsin o (protein folding) and methionine-r-sulfoxide reductase (ageing) were identified to be upregulated among all treatment groups and thus suggested as potentially new biomarkers. Furthermore, the divalent metal transporter-1 is suggested to transport Al and In across cell membranes.

Bioaccumulation and Uptake. Bioimaging showed that areas of highest uptake of Al and In are in the midgut, which is in line with other studies on metal uptake in *D. magna* (Komjarova and Blust, 2008). Additionally, both metals, were accumulated in the carapace and filtering screens, possibly physically hindering a constant flow of algae and thus reduce net energy and growth. As shown already by the micro-XRF technique (De Samber et al., 2008), calcium has a distinct presence in the carapace and the tissue in the head part. Particularly in the carapace, Al and In could compete with calcium deposition. This needs further investigation, as the resolution of LA-ICP-MS is not high enough to detect a competitive effect. The internal accumulation of Al and In are strikingly similar and deviate from those of calcium and phosphorus. This implies that Al and In do not compete with calcium deposition within the body.

Uptake studies with metals showed that multi-metal exposure mostly leads to decreased uptake rates, even at low concentrations, suggesting competitive inhibition at common uptake sites (Komjarova and Blust, 2008). Metals including Al and In are likely to cross intracellular and plasma membranes by metal ion transporters, also termed solute carriers. Our global transcription analysis revealed a number of transmembrane transporters affected, especially in the mixture of Al and In. Among them is the natural resistance-associated macrophage protein (also known as divalent metal transporter-1), which is an intestinal iron transporter in fish (Kwong et al., 2013), but also has the potential to transport a range of other divalent metals including cadmium and copper (Komjarova and Bury, 2014). In *c. elegans*, divalent metal transporter-1 homologue is predicted to transport Al across intracellular membranes (Vanduyn et al., 2013). Thus, it is suggested that in *Daphnia* the natural resistance-associated macrophage protein might mediate uptake and intracellular distribution. The up-regulation observed in our mixture exposure indicates that more metals are transported into and across the cell, if the increased gene expression is also manifested on the protein level.

It is striking that the number of differentially expressed transporter genes in the Al and In mixture clearly exceeds the number of the single compound treatments, suggesting that the metal mixture triggers a more than additive response. Similar observations in molecular activity of mixtures have been described in microarrays studies (Finne et al., 2007; Vandenbrouck et al., 2009). In this case, this is suggesting that intracellular ion transport and thus disturbed homeostasis is of higher relevance in the mixture. On the other hand, divalent ion binding is more pronounced in single metal exposure in comparison to the mixture.

Growth- and Reproduction-Related and Transcriptional Responses. Aluminum and indium exhibited similar phenotypic responses, regarding all the endpoints measured including growth and reproduction. The only deviations were found (1) in population growth rate and age at maturity, where In induced a stronger effect than Al in the low concentration, and (2) in molting and growth, were Al had a stronger effect than In in the high concentration. In the following, predicted toxic modes of actions (lipid metabolism, exoskeleton maintenance, sugar metabolism) and its relation to the phenotypic responses are discussed.

Growth reduction in daphnids is a common effect observed for metals (De Schamphelaere et al., 2004), and likewise for organic compounds (Vandegehuchte et al., 2010a). Also Al and In reduced growth in a concentration-dependent manner. This is assumed to be related to depleted lipid reserves already in the first two days, affecting the net energy budget of the organism (De Coen and Janssen, 2003; M. Li et al., 2011; Soetaert et al., 2007). Similarly here, growth is affected already after the first measurement in the chronic exposure. Our transcriptomics responses after ten hours displayed effects on the lipid metabolism by Al, In, and their mixtures. Thus, the gene-families related to lipid metabolism are suggested to serve as early markers for growth reduction at a later stage. Although, all exposures affected gene expression of genes active in lipid metabolism, none of

them were shared among the treatment groups. Nevertheless, being active in the same biological process, they are expected to exhibit similar effects on growth.

RNA-seq analysis revealed a set of eight mainly down-regulated genes induced by Al, In, and the mixture, which all are involved in transcription of cuticular proteins. These proteins are important structural components of the exoskeleton (Muthukrishnan et al., 2012) and thus a down-regulation could be the reason for the observed growth inhibition. Furthermore, altered mRNA abundance of cuticula related fragments were related to molting behavior (De Schamphelaere et al., 2008). However, molting frequency was not affected, except for the highest Al exposure. With each molting, arthropods gain in size, but the increase under stressed conditions is not as much as under unstressed condition (independent from numbers of molting). Furthermore, molting behaviour as well as reproduction of arthropods is regulated by ecdysteroid hormones (Rodríguez Moreno et al., 2003; Sumiya et al., 2014). Solely In reduced mRNA abundance of the ecdysone-induced protein 78c, but this was not related to the number of moltings or reproduction, as it was equally affected in all the treatment groups. Thus, it is suggested that ecdysteroid related gene fragments would be expressed at a later stage of exposure and development, or that reproductive success is coupled to size. Because bigger daphnids have a higher feeding rate, more energy, and can contain more eggs than smaller ones, the size is consequently related to the reduced reproduction success observed (Jager et al., 2010).

A major composite material of the cuticula is chitin. Genes involved in chitin metabolism were shown to be altered in several metal exposure studies (De Schamphelaere et al., 2008; Poynton et al., 2007; Vandenbrouck et al., 2009). Likewise, the mixture of Al and In in this study altered chitin-related mRNA expression levels. This additional affected component of the exoskeleton could be a reason for the stronger effect in growth reduction in the mixture. Chitin is a polysaccharide. The altered mRNA fragments related to sugar metabolism after ten hours of exposure to Al, In, and their mixture might potentially disrupt chitin synthesis at a later stage.

Overall, the altered transcripts of sugar and lipids related genes likely mirror the organisms elevated need for energy (stored in form of macromolecules such as lipids and glycogen) to confront the stress situation. Ultimately, energy demanding processes including reproduction and growth are reduced. However, the upstream events remain to be explored, as growth and reproduction are of high ecological relevance.

Reproduction-Related Responses. Reproductive traits were evaluated during a 21 day chronic exposure. Total amount of neonates was significantly reduced in mid and high concentrations of single metal exposures and in all concentrations of the mixture. Previous studies have shown that metal can decrease fecundity of *Daphnia* (Poynton et al., 2008). As no hormone related transcriptional alterations were detected in our transcriptomics study, impaired reproduction is most likely a consequence of depleted energy reserves and reduced size. However, gene expression studies with juveniles and with short term exposures tend to miss predictive genes for reproduction.

Age at maturity was significantly delayed in all exposure groups (except Al low) suggesting an effect on early life stages. This becomes even more obvious, when comparing

juvenile growth rate (taking into account growth until sexual maturity) with specific growth rate (taking into account growth until day 21). Juvenile growth rate was reduced in all treatment groups and doses, whereas specific growth rate was reduced in the highest dose group only.

However, the commonly used general stress related gene vitellogenin showed no alteration in mRNA abundance. Vitellogenin would serve as storage proteins providing nutrients to the developing embryo. Thus, its down-regulation is a marker for lack of energy during development (Vandenbrouck et al., 2009), but its use for general stress response was not confirmed here.

Effects of Single Compounds. Exposures to Al or In affected similar functional groups of genes except for protein folding, immune response, and heme binding whch gene families distinctively activated by either Al or In. Disrupted protein folding and its aggregation in the endoplasmic reticulum, also called ER stress, is mainly affected by Al, and to an even higher extent in the mixture. However, ER stress was suggested to be a targeted pathway for both metals in higher organisms (Brun et al., 2014a; Mustafa Rizvi et al., 2014). Furthermore, genes coding for cathepsin and heatshock proteins were shown to be induced in *Daphnia* by several other (divalent) metals (Tang et al., 2014; Vandenbrouck et al., 2009). Thus, disrupted protein folding might be a conserved pathway targeted by various metals. Its adverse outcome was related to reduced lipid content in fish (Song et al., 2015).

The gene coding for di-domain haemoglobin precursor involved in heme binding and oxygen transport was down-regulated in the In and mixture exposure. The same gene was down-regulated in *Daphnia magna* exposed to cadmium (Soetaert et al., 2007), and another hemoglobin related gene by zinc (Vandegehuchte et al., 2010c). In mammals, In^{3+} can compete with Zn^{2+} for binding sites leading to inhibition of heme synthesis (Conner et al., 1995; Rocha et al., 2004). Hemoglobin genes of *Daphnia magna* are among the well characterized genes and found to be altered under hypoxic conditions (Nunes et al., 2005). The repressed transcription of this gene suggests a conserved metal related response resulting in reduced oxygen transport in *Daphnia*, which could be an energy-saving mechanism.

In altered the expression of fewer genes than Al or the mixture exposure. Still, the alteration of these In-specific genes led to adverse outcome regarding reproduction and growth. According to the snapshot after ten hours of exposure and the so far identified gene fragments this would imply that the following few genes are involved by increased expression of this severe response: cathepsin o (protein degradation and turnover), glioma pathogenesis-related protein (lipid metabolic process), sugar transporter, cuticular protein, two immune response proteins, three nervous system related genes, zinc-, calcium-, and magnesium-binding genes, and the muscle-specific protein. However, at later stages of development, other genes might be switched on, which remains to be investigated in future studies.

Effects of Mixtures. When comparing the equi-effective binary mixture at phenotypic effect levels with the single compounds of equal toxicity, greater effects on mortality, reproduction (number of neonates), maturity, and growth was noted. Interestingly, synergistic

effects were also reported for daphnid mortality in mixture exposure of nano-Al_2O_3 and As(V) (Wang et al., 2011).

The combination of two compounds with similar modes of actions is generally assumed to be additive. However, evidences from toxicogenomic studies pile up, showing that mixture expression profiles represent not merely the additive sum of individual compounds fingerprint (Vandenbrouck et al., 2009; Zucchi et al., 2014). Converging pathways can be activated leading to a faster and/or stronger response. This could be relevant in processes related to cation binding, transmembrane transport, exoskeleton maintenance, lipid and sugar metabolism. The latter three may be involved in stronger phenotypic response.

Transcripts of genes related to oxidative stress pathway, including glutathione-s-transferase and superoxide dismutase (Barata et al., 2005), were altered in the mixture treatment only. In contrast to our data in *Daphnia*, Al reduced superoxide dismutase activity in the brain of mammals (Kumar et al., 2009) and in blood of fish (García-Medina et al., 2013), which could be explained by the long exposure times applied in these studies. Al and In did not induce these biomarker genes, but nevertheless lead to reduced growth (which is frequently observed in metal exposure) via other mechanisms.

Identified Biomarkers of Exposure. Three identified gene fragments were consistently altered in the same direction in all treatment groups: cathepsin o, methionine-r-sulfoxide reductase, and muscle-specific protein. The relevance in metal exposure of the latter two was not described before. Thus, they could potentially serve as new biomarker of exposure after further investigation. In *Drosophila*, overexpression of methionine sulfoxide reductase was found predominantly in the nervous system, and it markedly extended lifespan. Therefore, the role of this gene on the life expectancy of *Daphnia* should be investigated. The observed down-regulation by Al, In, and the mixture might imply reduction of lifespan, and thus adverse outcome on organism or population level. The function of the muscle-specific protein and here observed transcriptional alterations of genes related to myogenesis are not well understood in *Daphnia*. It is suggested, that aluminum and indium target developing muscles.

Surprisingly, transcripts of metallothioneins (MTs) were not altered by Al and In. MTs are involved in transport and detoxification of heavy metals and serve as biomarkers of exposure to metals (Asselman et al., 2012; Poynton et al., 2007). In can induce MT mRNA expression in fish (Brun et al., 2014a), whereas in molluscs, Cd but not Al did increase MT concentrations (Desouky, 2012). Asselman et al. (2013) showed a time dependent transient induction of MT gene transcripts in *Daphnia* after four and eight days of exposure to Cd and Cu. Thus, either Al and In do not induce MT genes or the exposure duration of ten hours is suggested to be too short to capture MT induction by Al or In.

To this end, pathway analysis has not been done and therefore the discussion on biological gene functions is not complete. Furthermore, a multivariate analysis is planned in order to discriminate between molecular response of single compound and mixture treatment and to analyse the relationship between transcriptional and phenotypic response, considering that by far not all transcriptional alterations have functional implica-

tions. This study narrows down gene fragments with effects at higher biological level by comparing affected pathways and gene families to transcriptomic effects of other more commonly investigated metals.

Conclusion. Al, In, and their mixture induced dose-dependent adverse effects on growth and reproduction, which are related to reduced net energy in neonates, and thus has important ecological implications. The lowest added concentration (1.52 mg L^{-1}) is about four times higher than measured Al concentrations in contaminated aquatic environments. The here shown link between molecular effects with markers of overall health of individual organisms is important in order to understand the molecular basis of effects at higher biological levels and thus for ecological risk assessment. Although Al and ln targeted transcriptional alterations of different specific genes, they affected mostly the similar biological functions including exoskeleton maintenance, transmembrane transport, lipid and sugar metabolism. Transcriptional alterations of only 75 genes by In can be related to these important effects, while more genes are altered in their expression by Al, and particularly more by the mixture. Binary mixtures of Al and In exhibited synergistic activity on phenotypic responses and induced transcripts of additional genes, but belonging to the same functional group of genes. Therefore, the synergism of this metal mixture is probably related to different processes of Al and In that interact together for a higher than additive reaction. Furthermore, two new transcripts of potential interest were identified: the ageing related methionine-r-sulfoxide reductase and the muscle-related protein. Such expression patterns rarely related to metal exposure demonstrate the power of genomics and its aid in the identification of action of environmental contaminants.

5.5 Supplementary Information

Table S5.1 Constituents of Aachener Daphnien Medium (ADaM) according to Klüttgen et al. (1994) with modified selenium dioxide concentration according to (Ebert, 2006)

Chemical	Concentration [g L^{-1}]	Source
Sea Salt	0.333	Crystal Sea® Bioassay Formulation, Marine Enterprises International, Baltimore, USA
CaCl$_2$ x 2H$_2$O	117.6	Sigma, UK
NaHCO$_3$	25.2	Sigma, UK
SeO$_2$	0.07	Sigma, UK

Table S5.2 Calculated effective concentrations (EC) for acute immobility of *Daphnia magna* after 48 h exposure to aluminum and indium

EC	0.625	1.25	2.5	5	10	20	40	80
Aluminum (mg L^{-1})	24.05	25.45	26.94	28.54	30.31	32.36	35.02	40.46
Indium (mg L^{-1})	36.84	38.85	41.00	43.30	45.84	48.75	52.23	60.20
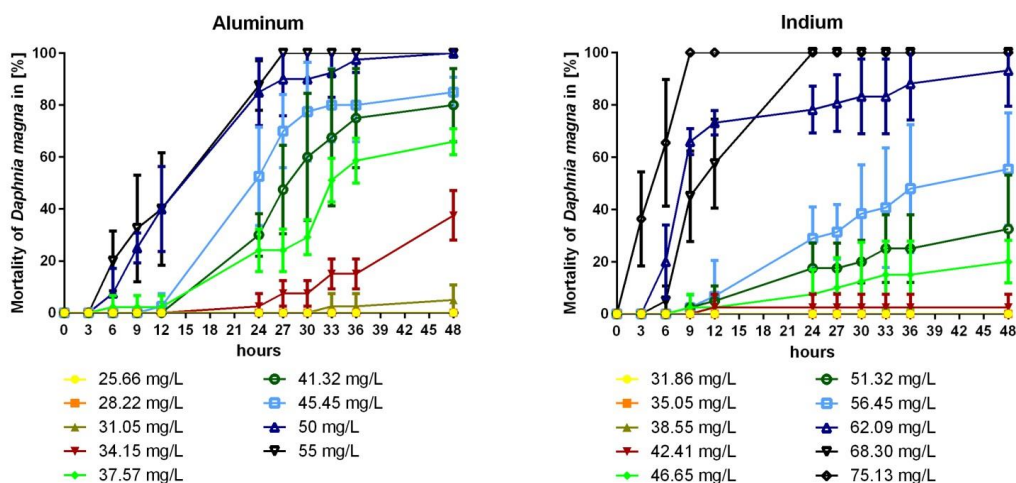
Figure S5.1 Time-course study showing the time points at which mortality started in single compound exposure for aluminum and indium.
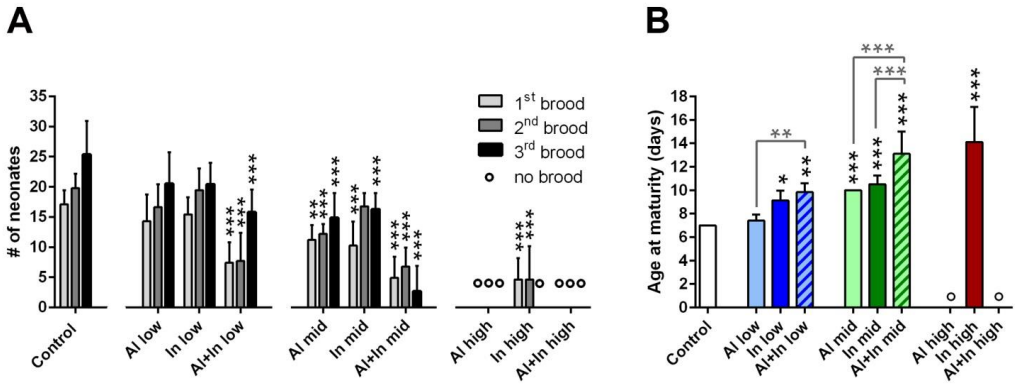
Figure S5.2 (A) Clutch sizes of 1st, 2nd, and 3rd brood in control and exposure groups. Circles indicate that none of the individuals in the produced neonates within 21 days and therefore were not included in statistical analysis. Statistics was done in comparison to control of the same brood (n=10). (B) Age at maturity of control and exposure groups. Age at maturity is the age (in days) when eggs first appear in the brood chamber. Black asterisks indicate significant difference to control, grey asterisks difference between single compound and equi-effective mixture (n=10). Circles indicate that none of the individuals in the group reached maturity within 21 days, and therefore were not included in statistical analysis. Nominal concentrations are for Al 1.52 (low), 3.03 (mid), 6.06 (high) mg L^{-1}, for In 2.29 (low), 4.58 (mid), 9.17 mg L^{-1} (high), and for Al + In 1.43 + 2.17 (low), 2.85 + 4.33 (mid), 5.71 + 8.66 mg L^{-1} (high).

The population growth rate (r) was calculated for all conditions according to the following formula (Lotka, 1913):

$$\sum_{i=1}^{21} l_x m_x e^{-rx} = 1$$

(1)

the formula takes into account the fraction surviving until age x (l_x), reproductive success represented by the amount of juveniles produced until age x (m_x), and the maximum age (x).

$$\sum_{i=1}^{21} l_x m_x e^{-rx} = 1$$

$$SGR = \frac{\ln(x_{t=21}) - \ln(x_{t=1})}{\# \ of \ days \ of \ experiment} \times 100\%$$
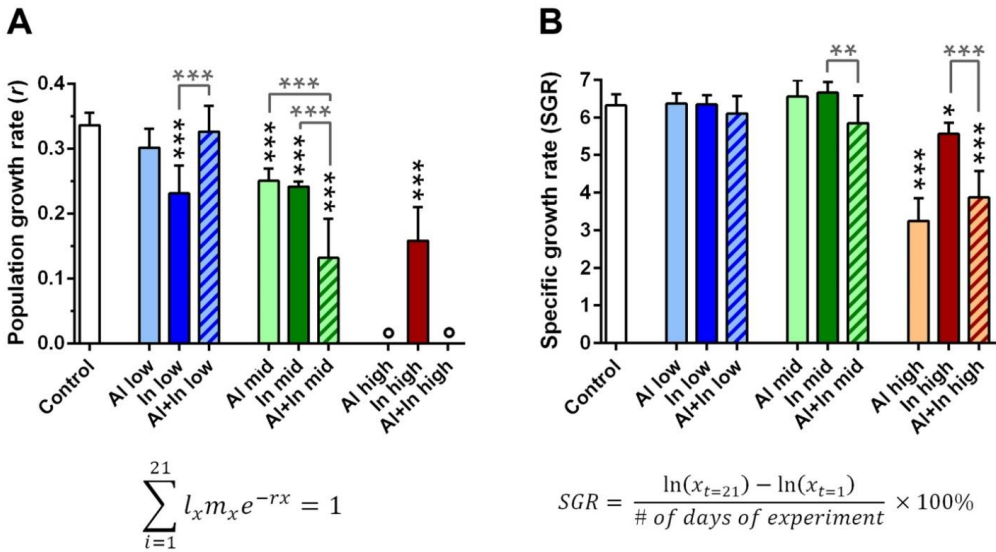
Figure S5.3. (A) Population growth rate (r) of daphnids in different exposure groups and control over 21 days. Intrinsic rate of increase per day is computed iteratively with the Lotka equation, where x is the maximum age, l_x is the fraction surviving until age x, and m_x is the amount of juveniles niles produced until age x. Black asterisks indicate significant difference to control, grey asterisks difference between single compound and equi-effective mixture (n=10). (B) Specific growth rate (SGR) of daphnids in different exposure groups and control over 21 days. Where $x_{t=21}$ is the carapace length of the daphnid at the end of the experiment and $x_{t=1}$ is the length of the daphnid at the start of the experiment. Black asterisks indicate significant difference to control, grey asterisks difference between single compound and equi-effective mixture (n=10). Nominal concentrations are for Al 1.52 (low), 3.03 (mid), 6.06 (high) mg L^{-1}, for In 2.29 (low), 4.58 (mid), 9.17 mg L^{-1} (high), and for Al + In 1.43 + 2.17 (low), 2.85 + 4.33 (mid), 5.71 + 8.66 mg L^{-1} (high).

6

CONCLUSIONS AND OUTLOOK

The overall goal of this work was to assess and improve the knowledge on ecotoxicological risk of organic photovoltaics (OPVs). A particular focus was set on effects of metals and metal nanoparticles (NPs) combining molecular techniques, phenotype characterization, and chemical analysis. In this chapter, I will briefly review the major results and important conclusions, extend it by a discussion of the advantages and main limitations of each study and compare it with current studies. Finally, some important points to be taken into account in future research directions will be given.

Comparison of Metal NP and Soluble Metal Effects. In this thesis, morphological and gene expressional effects of ZnO NPs and soluble zinc were compared in zebrafish early life stages. Both ZnO NPs and free zinc ions, Zn(II), showed a similar hatching delay, uptake, and distribution in zebrafish embryos and gene expressional alterations related to metallothionein, oxidative stress, as well as immune response. The conclusion was drawn that the biological activity can be mainly attributed to soluble Zn(II) rather than NPs. This is accordance with comparative global transcriptomic analyses of ZnO NPs and soluble Zn(II) in crustaceans, where strong similarities in gene expression suggested a response to Zn(II) at the cellular level in both cases (Adam et al., 2015b; Poynton et al., 2013). Interestingly, also the TNF receptor-associated protein was significantly down regulated in both ZnO NP and Zn(II) exposure. This corresponds to the significant alterations of inflammatory and immune-regulatory responses to Zn(II), which we demonstrated in zebrafish embryos (Chapter 2) and recently was shown in tilapia (Kaya et al., 2016). The TNF receptor-associated protein is highly conserved (Wajant et al., 2001) and the potential of ZnO NP triggering pro-inflammatory responses in human cells is well known (Giovanni et al., 2015;

Senapati et al., 2015). These findings are supporting our results showing an immune response to Zn(II) in fish as a novel potential effect not described before.

Although the findings indicate that observed effects are caused by Zn(II) ions rather than NPs, a potential of uncertainty remains. The dissolution of Zn(II) ions from NPs might add an additional layer of complexity and mask NP effects. NPs are extremely dynamic in their dissolution and aggregation behaviour upon contact with water and thus evaluation of ZnO NP toxicity represents a great challenge. In this study, the exposure method was specifically adjusted for NPs. Pilot experiments revealed that a medium of higher ionic strength together with the addition of alginic acid sodium salt reduced nanoparticle agglomeration in comparison to the standard zebrafish culture medium. Toxicity assessment of stable dispersed nanoparticle is the key to understand their potential risk. Besides a detailed characterisation of the particles in exposure media, a standardized guideline for adequate NP risk assessment would be required to bring all the results in line. As concentrations or released NPs under current disposal scenarios are expected to be much lower than concentrations used in laboratory studies and NP behaviour changes depending on its concentration (Xiao et al., 2015), the assessment of low concentrations is recommended. Not only is the toxicity assessment under lab conditions challenging, but moreover the behaviour and fate of NPs in the environment remains hypothetical. Quantitative NP-specific trace analytical methods are not yet available, hence assumptions on environmental fate rely on modelling (Batley et al., 2013; Nowack and Bucheli, 2007; Rodrigues et al., 2015). Pristine NPs used for product manufacturing may be transformed on their way to the environment (Lowry et al., 2012; Mitrano et al., 2015) or behave differently because of the dominant presence of natural NPs, colloidal materials, and other factors (Klaine et al., 2008). For instance, acidic pH conditions would stabilize ZnO NPs released from OPV in monodispersed form (Molina et al., 2011) and natural organic matter can adsorb to ZnO resulting in negative surface charges preventing aggregation (Zhang et al., 2009). Thus, data for pristine NPs may not be predictive for environmental scenarios (e.g. release of NPs from photovoltaics). In many cases, agglomeration and sedimentation of NPs in the environment is probable (Botta et al., 2011). This underlines the need for ecotoxicological assessment of NPs in benthic organisms and confirms that fish eggs and larvae (having their nursery habitat on the sediment) are an appropriate model for NP toxicity assessment.

A Novel Mode of Action of Indium - ER Stress. Cells respond to the presence of xenobiotics by inducing transcription of genes that are usually silent in unstressed condition. Often, a whole signalling pathway is switched on, eventually leading to physiological changes. For example, a compound inducing endoplasmic reticulum (ER) stress leads to activation of three distinct signal-transduction pathways collectively termed unfolded protein response (UPR). The major aim of these signalling cascades is to rescue ER protein processing capacity. In case of prolonged or massive ER stress, cell death (apoptosis) is induced either through activation of respective genes in the UPR or through excessive Ca^{2+} release from the ER followed by mitochondria mediated apoptosis (Sovolyova et al., 2014). Generally, apoptosis occurs during normal physiological functions to delete unwanted or potentially harmful cells. However, as apoptosis is an energy-dependent process (Elmore, 2007) an

increase in apoptotic cells triggered by ER stress subsequently decreases the organisms overall fitness.

We showed in chapter 3 that the OPV compound indium in its soluble form can induce ER stress associated with induction of transcripts of pro-apoptotic, pro-inflammatory, and oxidative stress related genes in the zebrafish liver cell line and to a lesser extent in zebrafish embryos. The study provided first evidence of this molecular mode of action related to indium toxicity, thus reqiores further investigation. It is of considerable importance to confirm gene expressional changes on protein level, as mRNA abundance not necessarily correlates with translation into proteins (Maier et al., 2009; Vogel et al., 2010). The discrepancy is commonly attributed to mRNA and protein decay (Varshavsky, 1996) and posttranscriptional mechanisms controlling the protein translation rate (Brockmann et al., 2007). In our study, we showed that the ER stress marker BiP is expressed on gene and protein level and thereby strengthened the evidence of cellular ER stress.

Further research needs to address impacts of the ER stress response induced by indium. Different fish organs could be compared to determine major targets. It is hypothesized that in addition to the liver, the brain would be affected as the ryanodine receptor involved in Ca^{2+} release plays a major role in this organ (Pessah et al., 2010). From an ecological and evolutionary perspective it would be of interest, if this stress response is found in different aquatic organisms and therefore could be used as general biomarker of indium or metal exposure. Daphnia exposed to indium did affect only one gene related to protein folding (Chapter 5), suggesting a minor impact on ER function. To confirm this, an assessment of different indium concentrations and later time points are recommended. Identifying signature patterns of altered gene expressions and relate it to physiological changes (i.e. growth or reproduction) is the next step and of current interest (Ankley et al., 2010; Pillai et al., 2014). Once established, it allows the prediction of chemical impacts on individuals and populations using molecular or biochemical endpoints.

Adverse outcome of ER stress in aquatic organism has rarely been explored, whereas in humans ER stress has been linked to several chronic metabolic diseases (e.g. obesity, type 2 diabetes; Schönthal, 2012). ER stress can play a critical role in lipid metabolism in mammalian liver (Bobrovnikova-Marjon et al., 2008; Lee et al., 2008; Rutkowski et al., 2008; Sriburi et al., 2004) and was related to reduced lipid accumulation in ER stressed catfish liver (Chen et al., 2015). The global transcription analysis in metal exposed *Daphnia* in Chapter 5 gives evidence of a connection between disturbed lipid homeostasis and protein folding in crustaceans. Disruption of ER function interferes with many different signalling pathways such as increased generation of reactive oxygen species, inflammation, and ultimately programmed cell death, all of which can influence energy metabolism (Alavian et al., 2011; Andersen and Kornbluth, 2013; Kominsky et al., 2010; Zhang, 2010) and have been shown in chapter 3 and 5. It is hypothesized that ER stress would interfere with the energy and lipid metabolism in fish and *Daphnia* and thus reduce the organisms overall fitness. To link this mode of action to physiological responses on organism level in fish, measurement of plasma glucose, lactate, and cortisol levels, lipogenic enzyme and ATPase

activity, histology of liver samples screened for relative areas of lipid droplets, or growth performance endpoints could be conducted.

ER Stress Response as Potential Biomarker for Metal Exposure. A major mechanism underlying metal toxicity is oxidative stress. Measurement of reactive oxygen species (ROS), genes related to oxidative stress, and additionally the abundance of metallothionein transcripts are frequently applied as biomarker of metal exposure. The data from chapter 3, 4, and 5 together support that ER stress is an additional mechanism affected by metal toxicity. Several investigations in mammalian or fish cells disclosed that ER stress response plays a critical role in metal toxicity including cadmium (Biagioli et al., 2008; Kitamura and Hiramatsu, 2010), manganese (Chun et al., 2001), mercury (Qian et al., 2001), lead (Shinkai et al., 2010), silver (Christen et al., 2013a), zinc (R. Chen et al., 2014), aluminum (Mustafa Rizvi et al., 2014), nickel, and cobalt (Hiramatsu et al., 2007). This is indicating that the ER stress mechanism is generally involved in metal-induced toxicity. Thus it is suggested here, that ER stress could be an early and sensitive biomarker for fish or *Daphnia* from metal contaminated sites. To confirm this, the transcriptional alterations need to be associated with other evidence of toxicity. And to gain further insights into responses to aqueous metal exposure, it is important to comparativley study wild species form contaminated sites. The jury is still out on the relationship between ER stress, oxidative stress, and metallothionein. Metallothioneins are well known to be induced by heavy metals, to bind metals, and effectively alleviate oxidative stress (Chen et al., 2007). Additionally, it can be overexpressed by ER stress inducer other than metals (Guo et al., 2009; Kondoh et al., 2004; Yang et al., 2014). Thus, the multifaceted role of metallothioneins, their interaction with different signalling pathways, and whether ER stress is an up-stream or down-stream effect remains to be further explored.

Metals Leaching from Photovoltaics Have Potential Ecotoxicological Implications. The implications of OPV weathering were assessed by producing leachates under different conditions: lake water, acidic rain water, and seawater. Under all three conditions zinc leached, whereas in acidic rain additionally copper was released, and in seawater it was silver. The ecotoxicological implications of these leachates were assessed in a comparative manner in zebrafish embryos using phenotypic and molecular endpoints. Table 6.1 summarises the findings described below.

The lake water leachate neither altered expression of selected target genes, nor affected embryo development. Therefore, the zinc present in the leachate was either not at effective concentration or not bioavailable. While the PEC for zinc in lake water is even lower. It is concluded that from this OPV dumping scenario close to lake water or leaching caused by non-acidic rain water the potential environmental risk is low.

The acidic rain water leachate significantly altered the *bip* and *chop* transcripts, indicating an ER stress response. However, this had no implication on the measured embryo development endpoints. Recently, Cu was shown to induce ER stress related genes predominantly in liver of the yellow catfish (Song et al., 2015) which was related to reduced lipid accumulation in liver of Cu exposed yellow catfish (Chen et al., 2015). Thus, the observed ER stress marker gene alterations caused by the OPV leachate from acidic rain could

have long-term fitness consequences, and therfore needs further investigations. Supposing that ER stress interferes with lipid and energy metabolism, embryo length should be included in future assessments of ER stress effects using zebrafish embryos.

Table 6.1 Summary of OPV metal leaching, observed effects, PECs (according to Zimmermann et al., 2013), and potential adverse outcome if environmental input is elevated.

Leachate	Metal concentration (µg L^{-1})[1]	Ecotoxicological effects[2]	PEC (µg L^{-1})[3]	Potential adverse effects[4]
Lake water	Zn = 63	- None observed	Zn = 4.4 ± 1	None expected
Acidic rain water	Cu = 14 Zn = 87	- genes altered involved in ER stress	Cu = n.a. Zn = 20.1 ± 1.4 (arid climate) 3.8 ± 1.4 (humid climate)	Reduced overall fitness
Seawater	Ag = 78 Zn = 17	- Reduced hatching success - Genes altered involved in metal binding, phase I enzyme activity, and ER stress	Ag = 14.6 ± 1.8 Zn = 0	Influence on population level

[1] in exposure media used in chapter 4

[2] based on zebrafish embryo development endpoints and target genes assessed in chapter 4

[3] according to Zimmermann et al., 2013 using the same experimental set up for leaching

[4] in case of environmental input is elevated due to increased OPV production or higher species sensitivity

The seawater leachate up-regulated genes involved in metal binding (*mt2*), phase I enzyme activity (*cyp1a*), and ER stress (*bip*), and reduced hatching success. These effects can be mainly attributed to silver present in the leachate. There is evidence that saline waters increase the bioavailability and toxicity of silver (Kataoka et al., 2015; Luoma et al., 1995) indicating that marine ecosystems are prone to be affected by silver contamination. The most bioavailable form of silver is Ag$^+$, and uptake is favoured through Cu transporter at higher salinity and through Na$^+$ channels in freshwater (Bertinato et al., 2010; Handy et al., 2002). Furthermore, in seawater the intestine of fish is the primary uptake site for silver, whereas in freshwater it is the gill (Bianchini et al., 2005; Hogstrand and Wood, 1998). With increasing salinity concentrations of Ag chloro complexes (AgCl^0, AgCl$_2^-$, AgCl$_3^{2-}$, AgCl$_4^{3-}$) increase, which were also the dominant speciation calculated for OPV leachate in seawater (Chapter 4; AgCl$_2^-$, AgCl$_3^{2-}$). Although complexation of Ag$^+$ by chloride, dissolved organic carbon, and sulphide generally hinders the recognition by the uptake transporters and therefore reduces bioavailability (Bianchini et al., 2002; Groh et al., 2014), rapid uptake of silver in marine organisms was described (Hogstrand and Wood, 1998; Luoma et al., 1995). More importantly, increasing salinity facilitated uptake of Ag chloro complexes into medaka eggs via the chorion due to decreased electrical resistance of the chorion

membrane and increased osmotic pressure (Kataoka et al., 2015). This results in the rec-
ommendation of taking silver toxicity into consideration to a higher extent in marine model
organisms (e.g. marine copepod, sea urchin, electric eel, or winter flounder) than in fresh-
water organisms. In terms of OPV leaching in seawater environments, the data indicates a
potential environmental risk, in particular, if OPV production and thus PEC increases. The
longer the embryo remains unhatched the longer it is an easy prey and it is prone to starva-
tion. Thus, this effect might influence population size.

Although metals such as Ag, Cu, and Zn did leach from OPV fragments, its PEC did
not exceed toxic values for aquatic organism (Zimmermann et al., 2013). For the PEC calcu-
lations the following assumptions were made: The amounts of metal(loid)s leaching from
OPV in laboratory experiments over four months were projected to a roof fully covered
with PV and then divided by the amount of rain precipitating on this area in the same
timespan for arid and humid climate zones. In environmental risk assessment the ratio of
the PEC to the predicted no-effect concentration (PNEC) indicates if a refined risk assess-
ment is needed. To derive a PNEC, toxicity data (e.g. no observed effect concentration:
NOEC, EC_{10}) of at least three taxonomic groups (e.g. algae, crustacea, and fish) are neces-
sary. An assessment factor addressing biological variance, chronic exposure extrapolation,
and laboratory data to field impact extrapolation is applied. One has to keep in mind, that
the use of NOEC is endpoint specific. For instance, no observed mortality does not neces-
sarily imply that there is no biological effect and thus is criticized manifold for being a poor
tool for data interpretation and decision making (Jager, 2012; Landis and Chapman, 2011;
Warne and Dam, 2008). The assessment of the OPV leachates using three different taxo-
nomic groups would go beyond the scope of this thesis. Nevertheless, chapter 5 brings in a
new organism to this risk assessment of metals from OPVs. Metal concentrations measured
in exposure leachates and induced effects in zebrafish embryos are only one order of mag-
nitude higher than the calculated PEC value (Table 6.1). For many toxic compounds,
zebrafish are among the least sensitive of the fishes (Braunbeck et al., 1992; Van den Belt et
al., 2003) and less sensitive in comparison to daphnids or algae (Griffitt et al., 2008;
Martins et al., 2007), also when exposed to Cu or Zn (Adam et al., 2015a). Thus it is recom-
mended to assess the biological activity of OPV leachates or Cu, Zn, Ag and the binary mix-
tures Cu/Zn and Ag/Zn in other taxonomic groups to refine this risk assessment.

Synergistic Toxic Effects of Aluminum and Indium. The aim of aluminum and indium
study in *Daphnia magna* was to gain insights on the molecular response of two rarely in-
vestigated metals and their mixture and to compare the gene expression profiles with ef-
fects at higher levels of biological organization. The reduced fitness (growth and reproduc-
tion) in exposed daphnids was related to higher energy consumption displayed in the tran-
scriptomic fingerprints. From similar acting compounds which produce similar gene tran-
scription profile, one would expect an equi-toxic mixture to result in an identical gene tran-
scription profile. However, the mixture exposure in chapter 5 affected a great sum of addi-
tional genes. This gene enrichment was found in the same functional groups as already af-
fected in the single metal exposures, thus could explain the faster and/or stronger pheno-
typic response. Multivariate analysis will be performed in a next step to compare mRNA
expression fingerprints of mixture to those of the single metal exposure. The RNA-seq data

will be available for other scientists and add up to the gene collection containing gene expression signatures of different heavy metals.

The transcriptional changes in this study were assessed in *Daphnia* neonates. The importance of life stages was shown by highly dynamic expression profiles over time in *Daphnia magna* exposed to genotoxic compounds or cadmium (David et al., 2011; Soetaert et al., 2007). Ideally, adult *Daphnia* from the chronic exposure would have been used to conduct RNA-seq analysis or to assess temporal expression of key genes. This would allow to identify and to confirm early response marker genes still affected in the adult animal and responsible for phenotypic effects. Furthermore, a large number of genes can be differentially expressed among control daphnids due to differences in molting stages (Vandegehuchte et al., 2010b). Thus, in global transcription assessment this unintended gene transcription patterns should be looked at and eliminated before further analysis. Knowledge on uptake and fate needs to be advanced to separate toxicokinetic from toxicodynamic response. Is it a time dependent effect due to increase in internal concentration or molecular interaction?

Toxicogenomics provide the possibility to examine the underlying molecular activity, which precede phenotypic effects (Powell, 2006). This study is the first of its kind using RNA-seq and thus providing a real global transcription analysis, whereas the microarray studies include a large set of selected genes. However, applying genomic tools such as RNA-seq to ecotoxicology will require further validation. The pitfall of the toxicogenomic approach on its own is that gene expression analysis may not represent a direct marker of functional response and it is a simple snapshot in time. As shown in this study, the connection of transcriptional changes to phenotypic or biochemical endpoints is necessary as proof of principle. Metabolic profiling could be performed to identify metabolites responsible for the observed effects. With the knowledge gained from the gene expression profiling in Chapter 5, it would be of interest to assess different biological responses including biochemical markers (i.e. glutathione-S-transferase to verify its reduced activity in the mixture and acetylcholinesterase to relate to the neuroactive gene fragments), behavioural response (i.e. locomotor activity to relate to the neuroactive gene fragments and feeding rate to relate to energy depletion), and available energy reserves (dividing between lipids, carbohydrates, and proteins).

Additionally, the here tested concentrations were quite high. A set of lower concentrations should be added to determine lowest effect levels on the transcription level and assess potential dose-response behaviour. The dose-response curve of *Daphnia* mortality resulted in a steep hill slope, which is not ideal for mixture experiments as EC_5 and EC_{10} are very close to each other. As the measured exposure concentrations were much lower than the nominal concentrations at EC_5 and EC_{10}, the solubility behaviour of these two metals should be investigated in more detail over a broader range of concentrations. It is hypothesized that the steep hill slope could be reasoned with changes in solubility.

Outlook. The knowledge gained in this thesis contributes to the advancement of the eco-toxicological risk assessment of photovoltaics and electronic devices in general. Overall, the results in this thesis are novel and provide first insights into mode of actions of single compounds, their binary mixture, and potential effects of photovoltaic leachates. Despite scientific findings of this thesis, research in this area of ecotoxicology should address and further investigate open questions such as:

- Are there distinct differences in laboratory NP behaviour and toxicity in comparison to aged NPs under environmental conditions? Are nanoparticles taken up and distributed in other cell compartments than the soluble metal? And are there differences in zebrafish regarding the molecular activity of nanoparticles versus the soluble metal if not just biomarker genes, but moreover a global gene expression analysis is conducted?

- Does ER stress lead to adverse outcome such as reduced lipid content and energy in aquatic organisms? In which tissues is ER stress prominent? And is this response to indium, aluminum, and other metals conserved across species?

- What toxic effects does silver have in marine organisms? And what is the toxic response to OPV leachates in organisms other than fish?

- Are the affected pathways of aluminum, indium, and their binary mixture in *Daphnia magna* only a snapshot of acute exposure response or are they manifested and thus can be used to predict adverse outcome occurring in chronic exposure? Which of the few genes altered by indium, are the key genes for reduced reproduction and growth?

The production of photovoltaics will continue to rise in the next years. At the United Nations Climate Change Conference 2015 (COP 21) meeting in December 2015, twenty countries, including the United States and China, committed themselves to double funding for energy research and development over the next five years, in partnership with major investors (Tollefson, 2015). The present knowledge is not sufficient for a comprehensive hazard and risk assessment of OPVs or other PVs. However, the leaching studies showed that released metal concentrations strongly depend on the environmental condition. In the marine dumping scenario silver is likely to play a critical role. Thus it is highly recommended to stakeholders and producers to reduce and substitute inorganic content in PVs and for governments to promote take-back programs and metal recycling from PVs and e-waste in general. Some of the raw materials used in OPVs such as indium are expensive, scarce, and prone to supply shortage. E-waste represents, together with incineration ashes, slags, and red mud, a novel secondary source to be tapped. Thus, innovation is required such as bio-metallurgy (Hennebel et al., 2013) or nanofiltration (Zimmermann et al., 2014) for metal recovery from and recycling of photovoltaic waste. This development is likely to be driven by economic reasons but the environment will gratefully profit thereof.

In comparison to other photovoltaics, OPV was shown to be of lesser environmental concern (chapter 4). And with restrictions on photovoltaics containing cadmium likely to come into force in the near future (by the RoHS), OPVs might increase its market share or other PVs decrease their hazardous content. Thus, the future development is steering towards a more sustainable PV production.

REFERENCES

Abràmoff, M.D., Magalhães, P.J., Ram, S.J., 2004. Image Processing with ImageJ. Biophotonics Int. 11, 36–42.

Adam, N., Schmitt, C., Bruyn, L. De, Knapen, D., Blust, R., 2015a. Aquatic acute species sensitivity distributions of ZnO and CuO nanoparticles. Sci. Total Environ. 526, 233–242.

Adam, N., Vergauwen, L., Blust, R., Knapen, D., 2015b. Gene transcription patterns and energy reserves in *Daphnia magna* show no nanoparticle specific toxicity when exposed to ZnO and CuO nanoparticles. Environ. Res. 138, 82–92.

Adams, J.M., 1998. The Bcl-2 protein family: Arbiters of cell survival. Science. 281, 1322–1326.

Aerle, R. Van, Lange, A., Moorhouse, A., Paszkiewicz, K., Ball, K., Johnston, B.D., Booth, T., Tyler, C.R., Santos, E.M., 2013. Molecular mechanisms of toxicity of silver nanoparticles in zebrafish embryos. Environ. Sci. Technol. 47, 8005–8014.

Ahn, S., Lee, S., Lee, H., 2012. Toward commercialization of triple-junction thin-film silicon solar panel with > 12% efficiency, in: 27th European Photovoltaic Solar Energy Conference. Frankfurt.

Akira, S., Uematsu, S., Takeuchi, O., 2006. Pathogen recognition and innate immunity. Cell. 124, 783–801.

Alavian, K.N., Li, H., Collis, L., Bonanni, L., Zeng, L., Sacchetti, S., Lazrove, E., Nabili, P., Flaherty, B., Graham, M., Chen, Y., Messerli, S.M., Mariggio, M.A., Rahner, C., McNay, E., Shore, G.C., Smith, P.J.S., Hardwick, J.M., Jonas, E.A., 2011. Bcl-xL regulates metabolic efficiency of neurons through interaction with the mitochondrial F1FO ATP synthase. Nat. Cell Biol. 13, 1224–1233.

Aleström, P., Holter, J.L., Nourizadeh-Lillabadi, R., 2006. Zebrafish in functional genomics and aquatic biomedicine. Trends Biotechnol. 24, 15–21.

Amsterdam, A., Nissen, R.M., Sun, Z., Swindell, E.C., Farrington, S., Hopkins, N., 2004. Identification of 315 genes essential for early zebrafish development. Proc. Natl. Acad. Sci. USA. 101, 12792–12797.

Anastas, P.T., Bickart, P.H., Kirchhoff, M.M., 2000. Designing safer polymers. John Wiley & Sons, New York.

Anderegg, G., 1977. Critical survey of stability constans of EDTA complexes. IUPAC Chem. Data Ser. No. 14. Pergamon Press, London.

Andersen, J.L., Kornbluth, S., 2013. The tangled circuitry of metabolism and apoptosis. Mol. Cell. 49, 399–410.

Ankley, G.T., Bennett, R.S., Erickson, R.J., Hoff, D.J., Hornung, M.W., Johnson, R.D., Mount, D.R., Nichols, J.W., Russom, C.L., Schmieder, P.K., Serrrano, J. a, Tietge, J.E., Villeneuve, D.L., 2010. Adverse outcome pathways: a conceptual framework to support ecotoxicology research and risk assessment. Environ. Toxicol. Chem. 29, 730–741.

Asselman, J., Glaholt, S.P., Smith, Z., Smagghe, G., Janssen, C.R., Colbourne, J.K., Shaw, J.R., De Schamphelaere, K.A.C., 2012. Functional characterization of four metallothionein genes in *Daphnia pulex* exposed to environmental stressors. Aquat. Toxicol. 110-111, 54–65.

Asselman, J., Shaw, J.R., Glaholt, S.P., Colbourne, J.K., De Schamphelaere, K. a C., 2013. Transcription patterns of genes encoding four metallothionein homologs in *Daphnia pulex* exposed to copper and cadmium are time- and homolog-dependent. Aquat. Toxicol. 142-143, 422–430.

Auffan, M., Rose, J., Bottero, J.-Y., Lowry, G. V, Jolivet, J.-P., Wiesner, M.R., 2009. Towards a definition of inorganic nanoparticles from an environmental, health and safety perspective. Nat. Nanotechnol. 4, 634–641.

Bai, W., Zhang, Z., Tian, W., He, X., Ma, Y., Zhao, Y., Chai, Z., 2010. Toxicity of zinc oxide nanoparticles to zebrafish embryo: a physicochemical study of toxicity mechanism. J. Nanoparticle Res. 12, 1645–1654.

Baird, D.J., Barber, I., Bradley, M., Soares, A., Calow, P., 1991. A comparative study of genotype sensitivity to acute toxic stress using clones of *Daphnia magna* straus. Ecotoxicol. Environ. Saf. 21, 257–265.

Banni, M., Chouchene, L., Said, K., Kerkeni, A., Messaoudi, I., 2011. Mechanisms underlying the protective effect of zinc and selenium against cadmium-induced oxidative stress in zebrafish *Danio rerio*. Biometals 24, 981–992.

Bao, Q., Liu, X., Xia, Y., Gao, F., Kauffmann, L.-D., Margeat, O., Ackermann, J., Fahlman, M., 2014. Effects of ultraviolet soaking on surface electronic structures of solution processed ZnO nanoparticle films in polymer solar cells. J. Mater. Chem. A 2, 17676–17682.

Barata, C., Baird, D.J., Markich, S.J., 1998. Influence of genetic and environmental factors on the tolerance of *Daphnia magna* Straus to essential and non-essential metals. Aquat. Toxicol. 42, 115–137.

Barata, C., Varo, I., Navarro, J.C., Arun, S., Porte, C., 2005. Antioxidant enzyme activities and lipid peroxidation in the freshwater cladoceran *Daphnia magna* exposed to redox cycling compounds. Comp. Biochem. Physiol. C. Toxicol. Pharmacol. 140, 175–186.

Barnes, D.K.A., Galgani, F., Thompson, R.C., Barlaz, M., 2009. Accumulation and fragmentation of plastic debris in global environments. Philos. Trans. R. Soc. London 364, 1985–1998.

Baršienė, J., Bjornstad, A., Rybakovas, A., Šyvokienė, J., Andreikėnaitė, L., 2010. Environmental genotoxicity and cytotoxicity studies in mussels and fish inhabiting northern Atlantic zones impacted by aluminum industry. Ekologija. 56, 116–123.

Basha, P.S., Rani, A.U., 2003. Cadmium-induced antioxidant defense mechanism in freshwater teleost *Oreochromis mossambicus* (Tilapia). Ecotoxicol. Environ. Saf. 56, 218–221.

Batley, G.E., Kirby, J.K., McLaughlin, M.J., 2013. Fate and risks of nanomaterials in aquatic and terrestrial environments. Acc. Chem. Res. 46, 854–862.

Baun, A., Sørensen, S.N., Rasmussen, R.F., Hartmann, N.B., Koch, C.B., 2008. Toxicity and bioaccumulation of xenobiotic organic compounds in the presence of aqueous suspensions of aggregates of nano-C(60). Aquat. Toxicol. 86, 379–387.

Becker, S.J., 2013. Imaging of metals in biological tissue by laser ablation inductively coupled plasma mass spectrometry (LA-ICP-MS): state of the art and future developments. J. mass Spectrom. 48, 255–268.

Benn, T.M., Westerhoff, P., 2008. Nanoparticle silver released into water from commercially available sock fabrics. Environ. Sci. Technol. 42, 4133–4139.

Bertinato, J., Cheung, L., Hoque, R., Plouffe, L.J., 2010. Ctr1 transports silver into mammalian cells. J. Trace Elem. Med. Biol. 24, 178–184.

Betz, U., Kharrazi Olsson, M., Marthy, J., Escolá, M.F., Atamny, F., 2006. Thin films engineering of indium tin oxide: Large area flat panel displays application. Surf. Coatings Technol. 200, 5751–5759.

Biagioli, M., Pifferi, S., Ragghianti, M., Bucci, S., Rizzuto, R., Pinton, P., 2008. Endoplasmic reticulum stress and alteration in calcium homeostasis are involved in cadmium-induced apoptosis. Cell Calcium. 43, 184–195.

Bianchini, A., Bowles, K.C., Brauner, C.J., Gorsuch, J.W., Kramer, J.R., Wood, C.M., 2002. Evaluation of the effect of reactive sulfide on the acute toxicity of silver (I) to *Daphnia magna*. Part 2: toxicity results. Environ. Toxicol. Chem. 21, 1294–1300.

Bianchini, A., Playle, R.C., Wood, C.M., Walsh, P.J., 2005. Mechanism of acute silver toxicity in marine invertebrates. Aquat. Toxicol. 72, 67–82.

Bielmyer, G.K., Bell, R. a, Klaine, S.J., 2002. Effects of ligand-bound silver on *Ceriodaphnia dubia*. Environ. Toxicol. Chem. 21, 2204–2208.

Blaise, C., Gagné, F., Fe, J.F., 2008. Ecotoxicity of selected nano-materials to aquatic organisms. Environ. Toxicol. 23, 591–598.

Blechinger, S.R., Kusch, R.C., Haugo, K., Matz, C., Chivers, D.P., Krone, P.H., 2007. Brief embryonic cadmium exposure induces a stress response and cell death in the developing olfactory system followed by long-term olfactory deficits in juvenile zebrafish. Toxicol. Appl. Pharmacol. 224, 72–80.

Blinova, I., Ivask, A., Heinlaan, M., Mortimer, M., Kahru, A., 2010. Ecotoxicity of nanoparticles of CuO and ZnO in natural water. Environ. Pollut. 158, 41–47.

Bliss, C.I., 1939. The toxicity of poisons applied jointly. Ann. Appl. Biol. 26, 585–615.

Bobrovnikova-Marjon, E., Hatzivassiliou, G., Grigoriadou, C., Romero, M., Cavener, D.R., Thompson,

C.B., Diehl, J.A., 2008. PERK-dependent regulation of lipogenesis during mouse mammary gland development and adipocyte differentiation. Proc. Natl. Acad. Sci. USA. 105, 16314–16319.

Boerger, C.M., Lattin, G.L., Moore, S.L., Moore, C.J., 2010. Plastic ingestion by planktivorous fishes in the North Pacific Central Gyre. Mar. Pollut. Bull. 60, 2275–2278.

Borm, P., Klaessig, F.C., Landry, T.D., Moudgil, B., Pauluhn, J., Thomas, K., Trottier, R., Wood, S., 2006. Research strategies for safety evaluation of nanomaterials, part V: role of dissolution in biological fate and effects of nanoscale particles. Toxicol. Sci. 90, 23–32.

Botta, C., Labille, J., Auffan, M., Borschneck, D., Miche, H., Cabié, M., Masion, A., Rose, J., Bottero, J.Y., 2011. TiO_2-based nanoparticles released in water from commercialized sunscreens in a life-cycle perspective: Structures and quantities. Environ. Pollut. 159, 1543–1550.

Boughriet, A., Proix, N., Billon, G., Recourt, P., Ouddane, B., 2007. Environmental impacts of heavy metal discharges from a smelter in Deûle-canal sediments (Northern France): concentration levels and chemical fractionation. Water Air Soil Pollut. 180, 83–95.

Brabec, C.J., Gowrisanker, S., Halls, J.J.M., Laird, D., Jia, S., Williams, S.P., 2010. Polymer-fullerene bulk-heterojunction solar cells. Adv. Mater. 22, 3839–3856.

Braunbeck, T., Burkhardt-Holm, P., Görge, G., Nagel, R., Negele, R., Storch, V., 1992. Rainbow trout and zebrafish, two models for continuous toxicity tests: relative sensitivity, species and organ specificity in cytopathologic reaction of liver and intestines to atrazine. Schriftenr. Ver. Wasser. Boden. Lufthyg. 89, 109–145.

Brockmann, R., Beyer, A., Heinisch, J.J., Wilhelm, T., 2007. Posttranscriptional expression regulation: What determines translation rates? PLoS Comput. Biol. 3, 531–539.

Browne, M.A., Dissanayake, A., Galloway, T.S., Lowe, D.M., Thompson, R.C., 2008. Ingested microscopic plastic translocates to the circulatory system of the mussel, *Mytilus edulis* (L.). Environ. Sci. Technol. 42, 5026–5031.

Brun, N.R., Christen, V., Furrer, G., Fent, K., 2014a. Indium and indium tin oxide induce endoplasmic reticulum stress and oxidative stress in zebrafish (*Danio rerio*). Environ. Sci. Technol. 48, 11679–11687.

Brun, N.R., Lenz, M., Wehrli, B., Fent, K., 2014b. Comparative effects of zinc oxide nanoparticles and dissolved zinc on zebrafish embryos and eleuthero-embryos: Importance of zinc ions. Sci. Total Environ. 476-477, 657–666.

Brun, N.R., Wehrli, B., Fent, K., 2016. Ecotoxicological assessment of solar cell leachates: Copper indium gallium selenide (CIGS) cells show higher activity than organic photovoltaic (OPV) cells. Sci. Total Environ. 543, 703–714.

Brunauer, S., Emmet, P.H., Teller, E., 1938. Adsorption of gases in multimolecular layers. J Am Chem Soc. 60, 309–319.

Buerki-Thurnherr, T., Xiao, L., Diener, L., Arslan, O., Hirsch, C., Maeder-Althaus, X., Grieder, K., Wampfler, B., Mathur, S., Wick, P., Krug, H.F., 2013. In vitro mechanistic study towards a better understanding of ZnO nanoparticle toxicity. Nanotoxicology. 4, 402–415.

Buffle, J., Altmann, R.S., Filella, M., Tessier, A., 1990. Complexation by natural heterogeneous compounds: Site occupation distribution functions, a normalized description of metal complexation. Geochim. Cosmochim. Acta. 54, 1535–1553.

Cano, M., Wang, L., Wan, J., Barnett, B.P., Ebrahimi, K., Qian, J., Handa, J.T., 2014. Oxidative stress induces mitochondrial dysfunction and a protective unfolded protein response in RPE cells. Free Radic. Biol. Med. 69, 1–14.

Cao, L., Huang, W., Shan, X., Xiao, Z., Wang, Q., Dou, S., 2009. Cadmium toxicity to embryonic-larval development and survival in red sea bream *Pagrus major*. Ecotoxicol. Environ. Saf. 72, 1966–1974.

Chan, P.K., Cheng, S.H., 2003. Cadmium-induced ectopic apoptosis in zebrafish embryos. Arch. Toxicol. 77, 69–79.

Chang, Z., Lu, M., Lee, K.W., Oh, B.S., Bae, M.J., Park, J.S., 2011. Influence of divalent metal ions on E2-induced ER pathway in goldfish (*Carassius auratus*) hepatocytes. Ecotoxicol. Environ. Saf. 74, 2233–2239.

Chapin, D.M., Fuller, C.S., Pearson, G.L., 1954. A new silicon p-n junction photocell for converting

solar radiation into electrical power. J. Appl. Phys. 25, 676–677.

Chen, D., Zhang, D., Yu, J.C., Chan, K.M., 2011. Effects of Cu$_2$O nanoparticle and CuCl$_2$ on zebrafish larvae and a liver cell-line. Aquat. Toxicol. 105, 344–354.

Chen, H., Hu, J., Yang, J., Wang, Y., Xu, H., Jiang, Q., Gong, Y., Gu, Y., Song, H., 2010. Generation of a fluorescent transgenic zebrafish for detection of environmental estrogens. Aquat. Toxicol. 96, 53–61.

Chen, K.L., Mylon, S.E., Elimelech, M., 2006. Aggregation kinetics of nanoparticles in monovalent and divalent electrolytes. Environ. Sci. Technol. 40, 1516–1523.

Chen, Q.-L., Wu, K., Huang, C., Mei-Qin, Z., Song, Y.-F., Hu, W., 2015. Differential effects of dietary copper deficiency and excess on lipid metabolism in yellow catfish *Pelteobagrus fulvidraco*. Comp. Biochem. Physiol. Part B. 184, 19-28.

Chen, R., Huo, L., Shi, X., Bai, R., Zhang, Z., Zhao, Y., Chang, Y., Chen, C., 2014. Endoplasmic reticulum stress induced by zinc oxide nanoparticles is an earlier biomarker for nanotoxicological evaluation. ACS Nano. 8, 2562–2574.

Chen, W.-Y., John, J.A.C., Lin, C.-H., Chang, C.-Y., 2007. Expression pattern of metallothionein, MTF-1 nuclear translocation, and its DNA-binding activity in zebrafish (*Danio rerio*) induced by zinc and cadmium. Environ. Toxicol. Chem. 26, 110–117.

Chen, W.-Y., John, J.A.C., Lin, C.-H., Lin, H.-F., Wu, S.-C., Lin, C.-H., Chang, C.-Y., 2004. Expression of metallothionein gene during embryonic and early larval development in zebrafish. Aquat. Toxicol. 69, 215–227.

Chen, Y.Y., Zhu, J.Y., Chan, K.M., 2014. Effects of cadmium on cell proliferation, apoptosis, and proto-oncogene expression in zebrafish liver cells. Aquat. Toxicol. 157, 196–206.

Cheng, S., Wai, A., 2000. Cellular and molecular basis of cadmium induced deformities in zebrafish embryos. Environ. Toxicol. Chem. 19, 3024–3031.

Cheuk, W.K., Chan, P.C.Y., Chan, K.M., 2008. Cytotoxicities and induction of metallothionein (MT) and metal regulatory element (MRE)-binding transcription factor-1 (MTF-1) messenger RNA levels in the zebrafish (*Danio rerio*) ZFL and SJD cell lines after exposure to various metal ions. Aquat. Toxicol. 89, 103–112.

Christen, V., Camenzind, M., Fent, K., 2014a. Silica nanoparticles induce endoplasmic reticulum stress response, oxidative stress and activate the mitogen-activated protein kinase (MAPK) signaling pathway. Toxicol. Reports. 1, 1143-1151.

Christen, V., Crettaz, P., Fent, K., 2014b. Additive and synergistic antiandrogenic activities of mixtures of azol fungicides and vinclozolin. Toxicol. Appl. Pharmacol. 279, 455-466.

Christen, V., Capelle, M., Fent, K., 2013a. Silver nanoparticles induce endoplasmatic reticulum stress response in zebrafish. Toxicol. Appl. Pharmacol. 272, 519–528.

Christen, V., Meili, N., Fent, K., 2013b. Microcystin-LR induces endoplasmatic reticulum stress and leads to induction of NFκB, interferon-alpha, and tumor necrosis factor-alpha. Environ. Sci. Technol. 47, 3378–3385.

Christen, V., Crettaz, P., Oberli-Schrämmli, A., Fent, K., 2012. Antiandrogenic activity of phthalate mixtures: validity of concentration addition. Toxicol. Appl. Pharmacol. 259, 169–176.

Christen, V., Fent, K., 2012. Silica nanoparticles and silver-doped silica nanoparticles induce endoplasmatic reticulum stress response and alter cytochrome P4501A activity. Chemosphere. 87, 423–434.

Christen, V., Oggier, D.M., Fent, K., 2009. A microtiter-plate-based cytochrome P450 3A activity assay in fish cell lines. Environ. Toxicol. Chem. 28, 2632–2638.

Chun, H.S., Lee, H., Son, J.H., 2001. Manganese induces endoplasmic reticulum (ER) stress and activates multiple caspases in nigral dopaminergic neuronal cells, SN4741. Neurosci. Lett. 316, 5–8.

Colbourne, J.K., Pfrender, M.E., Gilbert, D., Thomas, W.K., Tucker, A., Oakley, T.H., … Boore, J.L., 2011. The ecoresponsive genome of *Daphnia pulex*. Science. 331, 555–561.

Conner, E.A., Yamauchi, H., Fowler, B.A., 1995. Alterations in the heme biosynthetic pathway from the III-V semiconductor metal, indium arsenide (InAs). Chem. Biol. Interact. 96, 273–285.

Connon, R., Hooper, H.L., Sibly, R.M., Lim, F.L., Heckmann, L.H., Moore, D.J., Watanabe, H., Soetaert, A., Cook, K., Maund, S.J., Hutchinson, T.H., Moggs, J., De Coen, W., Iguchi, T., Callaghan, A., 2008.

Linking molecular and population stress responses in *Daphnia magna* exposed to cadmium. Environ. Sci. Technol. 42, 2181–2188.

Cooper, N.L., Bidwell, J.R., Kumar, A., 2009. Toxicity of copper, lead, and zinc mixtures to *Ceriodaphnia dubia* and *Daphnia carinata*. Ecotoxicol. Environ. Saf. 72, 1523–1528.

Craig, P.M., Wood, C.M., McClelland, G.B., 2007. Oxidative stress response and gene expression with acute copper exposure in zebrafish (*Danio rerio*). Am. J. Physiol. Regul. Integr. Comp. Physiol. 293, R1882–1892.

Cullough, K.D.M.C., Martindale, J.L., Klotz, L., Aw, T.-Y., Holbrook, N.J., 2001. Gadd153 sensitizes cells to endoplasmic reticulum stress by down-regulating Bcl2 and perturbing the cellular redox state. Mol. Cell. Biol. 21, 1249–1259.

Cyrs, W.D., Avens, H.J., Capshaw, Z.A., Kingsbury, R.A., Sahmel, J., Tvermoes, B.E., 2014. Landfill waste and recycling: Use of a screening-level risk assessment tool for end-of-life cadmium telluride (CdTe) thin-film photovoltaic (PV) panels. Energy Policy. 68, 524–533.

Dara, L., Ji, C., Kaplowitz, N., 2011. The contribution of endoplasmic reticulum stress to liver diseases. Hepatology. 53, 1752–1763.

David, R.M., Dakic, V., Williams, T.D., Winter, M.J., Chipman, J.K., 2011. Transcriptional responses in neonate and adult *Daphnia magna* in relation to relative susceptibility to genotoxicants. Aquat. Toxicol. 104, 192–204.

De Boeck, G., van der Ven, K., Hattink, J., Blust, R., 2006. Swimming performance and energy metabolism of rainbow trout, common carp and gibel carp respond differently to sublethal copper exposure. Aquat. Toxicol. 80, 92–100.

De Coen, W.M., Janssen, C.R., 2003. The missing biomarker link: relationships between effects on the cellular energy allocation biomarker of toxicant-stressed *Daphnia magna* and corresponding population characteristics. Environ. Toxicol. Chem. 22, 1632–1641.

De Samber, B., Silversmit, G., Evens, R., De Schamphelaere, K., Janssen, C., Masschaele, B., Van Hoorebeke, L., Balcaen, L., Vanhaecke, F., Falkenberg, G., Vincze, L., 2008. Three-dimensional elemental imaging by means of synchrotron radiation micro-XRF: Developments and applications in environmental chemistry. Anal. Bioanal. Chem. 390, 267–271.

De Schamphelaere, K. a C., Canli, M., Van Lierde, V., Forrez, I., Vanhaecke, F., Janssen, C.R., 2004. Reproductive toxicity of dietary zinc to *Daphnia magna*. Aquat. Toxicol. 70, 233–244.

De Schamphelaere, K.A.C., Vandenbrouck, T., Muyssen, B.T.A., Soetaert, A., Blust, R., De Coen, W., Janssen, C.R., 2008. Integration of molecular with higher-level effects of dietary zinc exposure in *Daphnia magna*. Comp. Biochem. Physiol. - Part D Genomics Proteomics. 3, 307–314.

Deng, J., Lu, P.D., Zhang, Y., Scheuner, D., Kaufman, R.J., Sonenberg, N., Harding, H.P., Ron, D., 2004. Translational repression mediates activation of nuclear factor kappa b by phosphorylated translation initiation factor 2. Mol. Cell. Biol. 24, 10161–10168.

Deniaud, A., Sharaf el dein, O., Maillier, E., Poncet, D., Kroemer, G., Lemaire, C., Brenner, C., 2008. Endoplasmic reticulum stress induces calcium-dependent permeability transition, mitochondrial outer membrane permeabilization and apoptosis. Oncogene. 27, 285–299.

Denier, X., Hill, E.M., Rotchell, J., Minier, C., 2009. Estrogenic activity of cadmium, copper and zinc in the yeast estrogen screen. Toxicol. Vitr. 23, 569–573.

Desouky, M.M.A., 2012. Metallothionein is up-regulated in molluscan responses to cadmium, but not aluminum, exposure. J. Basic Appl. Zool. 65, 139–143.

Daphnia Genomics Consortium, DGC, 2015. Retrieved from: http://daphnia.cgb.indiana.edu/. Accessed on November 16 2015.

Dineley, K.E., Votyakova, T. V., Reynolds, I.J., 2003. Zinc inhibition of cellular energy production: implications for mitochondria and neurodegeneration. J. Neurochem. 85, 563–570.

Driscoll, C.T., Lawrence, G.B., Bulger, A.J., Butler, T.J., Cronan, C.S., Eagar, C., Lambert, K.F., Likens, G.E., Stoddard, J.L., Weathers, K.C., 2001. Acidic deposition in the northeastern United States: Sources and inputs, ecosystem effects, and management strategies. Bioscience. 51, 180–198.

Duong, F.H.T., Filipowicz, M., Tripodi, M., La Monica, N., Heim, M.H., 2004. Hepatitis C virus inhibits interferon signaling through up-regulation of protein phosphatase 2A. Gastroenterology. 126, 263–277.

Ebert, D., 2005. Ecology, Epidemiology, and Evolution of Parasitism in *Daphnia* [Internet]. Bethesda

(MD): National Center for Biotechnology Information (US), Bethesda (MD).

Ebert, D., 2006. Artifical Daphnia medium: ADaM. Retrieved from: http://www.biomedcentral.com/cont-ent/supplementary/2041-9139-5-12-S1.pdf

Edoff, M., 2012. Thin film solar cells: research in an industrial perspective. Ambio. 41 (Suppl 2), 112–118.

Eide, M., Rusten, M., Male, R., Jensen, K.H.M., Goksøyr, A., 2014. A characterization of the ZFL cell line and primary hepatocytes as *in vitro* liver cell models for the zebrafish (*Danio rerio*). Aquat. Toxicol. 147, 7–17.

El Chaar, L., Lamont, L.A., El Zein, N., 2011. Review of photovoltaic technologies. Renew. Sustain. Energy Rev. 15, 2165–2175.

Elmore, S., 2007. Apoptosis: a review of programmed cell death. Toxicol. Pathol. 35, 495–516.

Emmott, C.J.M., Urbina, A., Nelson, J., 2012. Environmental and economic assessment of ITO-free electrodes for organic solar cells. Sol. Energy Mater. Sol. Cells. 97, 14–21.

Endo, S., Takizawa, R., Okuda, K., Takada, H., Chiba, K., Kanehiro, H., Ogi, H., Yamashita, R., Date, T., 2005. Concentration of polychlorinated biphenyls (PCBs) in beached resin pellets: Variability among individual particles and regional differences. Mar. Pollut. Bull. 50, 1103–1114.

Engeszer, R.E., Patterson, L.B., Rao, A. a, Parichy, D.M., 2007. Zebrafish in the wild: a review of natural history and new notes from the field. Zebrafish. 4, 21–40.

Eo, Y.S., Rhee, H.W., Chin, B.D., Yu, J.-W., 2009. Influence of metal cathode for organic photovoltaic device performance. Synth. Met. 159, 1910–1913.

Fabrega, J., Luoma, S.N., Tyler, C.R., Galloway, T.S., Lead, J.R., 2011. Silver nanoparticles: behaviour and effects in the aquatic environment. Environ. Int. 37, 517–531.

Farkas, J., Peter, H., Christian, P., Gallego Urrea, J.A., Hassellöv, M., Tuoriniemi, J., Gustafsson, S., Olsson, E., Hylland, K., Thomas, K.V., 2011. Characterization of the effluent from a nanosilver producing washing machine. Environ. Int. 37, 1057–1062.

Feltis, B.N., Okeefe, S.J., Harford, A.J., Piva, T.J., Turney, T.W., Wright, P.F.A., 2012. Independent cytotoxic and inflammatory responses to zinc oxide nanoparticles in human monocytes and macrophages. Nanotoxicology. 6, 757–765.

Fent, K., Chew, G., Li, J., Gomez, E., 2014. Benzotriazole UV-stabilizers and benzotriazole: Antiandrogenic activity in vitro and activation of aryl hydrocarbon receptor pathway in zebrafish eleuthero-embryos. Sci. Total Environ. 482-483, 125–136.

Fent, K., Sumpter, J.P., 2011. Progress and promises in toxicogenomics in aquatic toxicology: Is technical innovation driving scientific innovation? Aquat. Toxicol. 105, 25–39.

Fent, K., 2010. Ecotoxicology of engineered nanoparticles, in: Frimmel, F.H., Niessner, R. (Eds.), Nanoparticles in the Water Cycle. Springer-Verlag, Berlin Heidelberg, pp. 183–205.

Fent, K., Weisbrod, C.J., Wirth-Heller, A., Pieles, U., 2010. Assessment of uptake and toxicity of fluorescent silica nanoparticles in zebrafish (*Danio rerio*) early life stages. Aquat. Toxicol. 100, 218–228.

Fernández, D., García-Gómez, C., Babín, M., 2013. *In vitro* evaluation of cellular responses induced by ZnO nanoparticles, zinc ions and bulk ZnO in fish cells. Sci. Total Environ. 452-453, 262–574.

Fernández-Dávila, M.L., Razo-Estrada, A.C., García-Medina, S., Gómez-Oliván, L.M., Piñón-López, M.J., Ibarra, R.G., Galar-Martínez, M., 2012. Aluminum-induced oxidative stress and neurotoxicity in grass carp (Cyprinidae—*Ctenopharingodon idella*). Ecotoxicol. Environ. Saf. 76, 87–92.

Finkel, T., Holbrook, N.J., 2000. Oxidant, oxidative stress and the biology of ageing. Nature. 408, 239–247.

Finne, E.F., Cooper, G.A., Koop, B.F., Hylland, K., Tollefsen, K.E., 2007. Toxicogenomic responses in rainbow trout (*Oncorhynchus mykiss*) hepatocytes exposed to model chemicals and a synthetic mixture. Aquat. Toxicol. 81, 293–303.

Franklin, N.M., Rogers, N.J., Apte, S.C., Batley, G.E., Gadd, G.E., Casey, P.S., 2007. Comparative toxicity of nanoparticulate ZnO , bulk ZnO , and $ZnCl_2$ to a freshwater microalga (*Pseudokirchneriella subcapitata*): The importance of particle solubility. Environ. Sci. Technol. 41, 8484–8490.

Fraunhofer ISE, 2015. Current and future cost of photovoltaics - Long-term scenarios for market development, system prices and LCOE of utility-scale PV systems. Study on behalf of Agora En-

ergiewende. Retrieved from: www. agora-energiewende.de. Accessed on October 2 2015.

Fraysse, B., Mons, R., Garric, J., 2006. Development of a zebrafish 4-day embryo-larval bioassay to assess toxicity of chemicals. Ecotoxicol. Environ. Saf. 63, 253–267.

Fthenakis, V., 2009. Sustainability of photovoltaics: The case for thin-film solar cells. Renew. Sustain. Energy Rev. 13, 2746–2750.

Fthenakis, V.M., 2004. Life cycle impact analysis of cadmium in CdTe PV production. Renew. Sustain. Energy Rev. 8, 303–334.

Funk, A.E., Day, F.A., Brady, F.O., 1987. Displacement of zinc and copper from copper-induced metallothionein by cadmium and by mercury: *in vivo* and *ex vivo* studies. Comp. Biochem. Physiol. C. 86, 1–6.

Furlong, E.E.M., 2011. Molecular biology: A fly in the face of genomics. Nature. 471, 458–459.

Gaither, L.A., Eide, D.J., 2001. The human ZIP1 transporter mediates zinc uptake in human K562 erythroleukemia cells. J. Biol. Chem. 276, 22258–22264.

Galagan, Y., Andriessen, R., 2012. Organic photovoltaics: Technologies and manufacturing. Third Gener. Photovoltaics. 61–91.

Galán, A., García-Bermejo, L., Troyano, A., Vilaboa, N.E., Fernández, C., de Blas, E., Aller, P., 2001. The role of intracellular oxidation in death induction (apoptosis and necrosis) in human promonocytic cells treated with stress inducers (cadmium, heat, X-rays). Eur. J. Cell Biol. 80, 312–320.

García-Medina, S., Angélica Núñez-Betancourt, J., Lucero García-Medina, A., Galar-Martínez, M., Neri-Cruz, N., Islas-Flores, H., Manuel Gómez-Oliván, L., 2013. The relationship of cytotoxic and genotoxic damage with blood aluminum levels and oxidative stress induced by this metal in common carp (*Cyprinus carpio*) erythrocytes. Ecotoxicol. Environ. Saf. 96, 191–197.

Garcia-Reyero, N., Lavelle, C.M., Escalon, B.L., Martinović, D., Kroll, K.J., Sorensen, P.W., Denslow, N.D., 2011. Behavioral and genomic impacts of a wastewater effluent on the fathead minnow. Aquat. Toxicol. 101, 38–48.

Garcia-Reyero, N., Poynton, H.C., Kennedy, A.J., Guan, X., Escalon, B.L., Chang, B., Varshavsky, J., Loguinov, A. V, Vulpe, C.D., Perkins, E.J., 2009. Biomarker discovery and transcriptomic responses in *Daphnia magna* exposed to munitions constituents. Environ. Sci. Technol. 43, 4188–4193.

García-Valverde, R., Cherni, J.A., Urbina, A., 2010. Life cycle analysis of organic photovoltaic technologies. Prog. Photovoltaics Res. Appl. 18, 535–558.

Gensemer, R.W., Playle, R.C., 1999. The bioavailability and toxicity of aluminum in aquatic environments. Crit. Rev. Environ. Sci. Technol. 29, 315–450.

Geoghegan, F., Katsiadaki, I., Williams, T.D., Chipman, J.K., 2008. A cDNA microarray for the three-spined stickleback, Gasterosteus aculeatus L., and analysis of the interactive effects of oestradiol and dibenzanthracene exposures. J. Fish Biol. 72, 2133–2153.

George, S., Lin, S., Ji, Z., Thomas, C.R., Li, L., Mecklenburg, M., Meng, H., Wang, X., Zhang, H., Xia, T., Hohman, J.N., Lin, S., Zink, J.I., Weiss, P.S., Nel, A.E., 2012. Surface defects on plate-shaped silver nanoparticles contribute to its hazard potential in a fish gill cell line and zebrafish embryos. ACS Nano. 6, 3745–3759.

George, S., Xia, T., Rallo, R., Zhao, Y., Ji, Z., Lin, S., Wang, X., Zhang, H., France, B., Schoenfeld, D., Damoiseaux, R., Liu, R., Lin, S., Bradley, K. a, Cohen, Y., Nel, A.E., 2011. Use of a high-throughput screening approach coupled with in vivo zebrafish embryo screening to develop hazard ranking for engineered nanomaterials. ACS Nano. 5, 1805–1817.

Ghosh, C., Zhou, Y.L., Collodi, P., 1994. Derivation and characterization of a zebrafish liver cell line. Cell Biol. Toxicol. 10, 167–176.

Giovanni, M., Yue, J., Zhang, L., Xie, J., Ong, C.N., Leong, D.T., 2015. Pro-inflammatory responses of RAW264.7 macrophages when treated with ultralow concentrations of silver, titanium dioxide, and zinc oxide nanoparticles. J. Hazard. Mater. 297, 146–152.

Gloeckler, M., Sankin, I., Zhao, Z., 2013. CdTe solar cells at the threshold to 20% efficiency. IEEE J. Photovoltaics 3, 1389–1393.

Godon, C., Lagniel, G., Lee, J., Buhler, J.-M., Kieffer, S., Perrot, M., Boucherie, H., Toledano, M.B., Labarre, J., 1998. The H_2O_2 stimulon in *Saccharomyces cerevisiae.* J. Biol. Chem. 273, 22480–

22489.

Gojova, A., Guo, B., Kota, R.S., Rutledge, J.C., Kennedy, I.M., Barakat, A.I., 2007. Induction of inflammation in vascular endothelial cells by metal oxide nanoparticles: effect of particle composition. Environ. Health Perspect. 115, 403–409.

Gottschalk, F., Sonderer, T., Scholz, R.W., Nowack, B., 2009. Modeled environmental concentrations of engineered nanomaterials (TiO_2, ZnO, Ag, CNT, fullerenes) for different regions. Environ. Sci. Technol. 43, 9216–9222.

Gottschling, B.C., Maronpot, R.R., Hailey, J.R., Peddada, S., Moomaw, C.R., Klaunig, J.E., Nyska, A., 2001. The role of oxidative stress in indium phosphide-induced lung carcinogenesis in rats. Toxicol. Sci. 64, 28–40.

Grassie, C., Braithwaite, V. a, Nilsson, J., Nilsen, T.O., Teien, H.-C., Handeland, S.O., Stefansson, S.O., Tronci, V., Gorissen, M., Flik, G., Ebbesson, L.O.E., 2013. Aluminum exposure impacts brain plasticity and behavior in Atlantic salmon (*Salmo salar*). J. Exp. Biol. 216, 3148–3155.

Grayfer, L., Belosevic, M., 2012. Cytokine regulation of teleost inflammatory responses, in: Türker, H. (Ed.), New Advances and Contributions to Fish Biology. pp. 59–96.

Gregory, M.R., 2009. Environmental implications of plastic debris in marine settings - entanglement, ingestion, smothering, hangers-on, hitch-hiking and alien invasions. Philos. Trans. R. Soc. London. 364, 2013–2025.

Griffith, M.J., Cooling, N.A., Vaughan, B., O'Donnell, K.M., Al-Mudhaffer, M.F., Al-Ahmad, A., Noori, M., Almyahi, F., Belcher, W.J., Dastoor, P.C., 2015. Roll-to-roll sputter coating of aluminum cathodes for large-scale fabrication of organic photovoltaic devices. Energy Technol. 6102, 428–436.

Griffitt, R.J., Feswick, A., Weil, R., Hyndman, K., Carpinone, P., Powers, K., Denslow, N.D., Barber, D.S., 2011. Investigation of acute nanoparticulate aluminum toxicity in zebrafish. Environ. Toxicol. 26, 541–551.

Griffitt, R.J., Luo, J., Gao, J., Bonzongo, J.-C., Barber, D.S., 2008. Effects of particle composition and species on toxicity of metallic nanomaterials in aquatic organisms. Environ. Toxicol. Chem. 27, 1972–1978.

Groh, K.J., Dalkvist, T., Piccapietra, F., Behra, R., Suter, M.J.-F., Schirmer, K., 2014. Critical influence of chloride ions on silver ion-mediated acute toxicity of silver nanoparticles to zebrafish embryos. Nanotoxicology. 5390, 1–11.

Guo, R., Ma, H., Gao, F., Zhong, L., Ren, J., 2009. Metallothionein alleviates oxidative stress-induced endoplasmic reticulum stress and myocardial dysfunction. J. Mol. Cell. Cardiol. 47, 228–237.

Gwinn, W.M., Qu, W., Shines, C.J., Bousquet, R.W., Taylor, G.J., Waalkes, M.P., Morgan, D.L., 2013. Macrophage solubilization and cytotoxicity of indium-containing particles in vitro. Toxicol. Sci. 135, 414–424.

Hallare, A.V., Schirling, M., Luckenbach, T., Köhler, H.R., Triebskorn, R., 2005. Combined effects of temperature and cadmium on developmental parameters and biomarker responses in zebrafish (*Danio rerio*) embryos. J. Therm. Biol. 30, 7–17.

Hamilton, S.J., Buhl, K.J., 1990. Acute toxicity of boron, molybdenum, and selenium to fry of chinook salmon and coho salmon. Arch. Environ. Contam. Toxicol. 19, 366–373.

Handy, R.D., Owen, R., Valsami-Jones, E., 2008a. The ecotoxicology of nanoparticles and nanomaterials: current status, knowledge gaps, challenges, and future needs. Ecotoxicology. 17, 315–325.

Handy, R.D., von der Kammer, F., Lead, J.R., Hassellöv, M., Owen, R., Crane, M., 2008b. The ecotoxicology and chemistry of manufactured nanoparticles. Ecotoxicology. 17, 287–314.

Handy, R.D., Eddy, F.B., Baines, H., 2002. Sodium-dependent copper uptake across epithelia: a review of rationale with experimental evidence from gill and intestine. Biochim. Biophys. Acta. 1566, 104–115.

Harding, H.P., Zhang, Y., Zeng, H., Novoa, I., Lu, P.D., Calfon, M., Sadri, N., Yun, C., Popko, B., Paules, R., Stojdl, D.F., Bell, J.C., Hettmann, T., Leiden, J.M., Ron, D., 2003. An integrated stress response regulates amino acid metabolism and resistance to oxidative stress. Mol. Cell. 11, 619–633.

Hart, B.A., Potts, R.J., Watkin, R.D., 2001. Cadmium adaptation in the lung - A double-edged sword? Toxicology. 160, 65–70.

Haye, S., Slaveykova, V.I., Payet, J., 2007. Terrestrial ecotoxicity and effect factors of metals in life cycle assessment (LCA). Chemosphere. 68, 1489–1496.

Hecht, D.S., Hu, L., Irvin, G., 2011. Emerging transparent electrodes based on thin films of carbon nanotubes, graphene, and metallic nanostructures. Adv. Mater. 23, 1482–1513.

Heckmann, L.-H., Sibly, R.M., Connon, R., Hooper, H.L., Hutchinson, T.H., Maund, S.J., Hill, C.J., Bouetard, A., Callaghan, A., 2008. Systems biology meets stress ecology: linking molecular and organismal stress responses in *Daphnia magna*. Genome Biol. 9, R40.

Heng, B.C., Zhao, X., Xiong, S., Ng, K.W., Boey, F.Y.-C., Loo, J.S.-C., 2010. Toxicity of zinc oxide (ZnO) nanoparticles on human bronchial epithelial cells (BEAS-2B) is accentuated by oxidative stress. Food Chem. Toxicol. 48, 1762–1766.

Hennebel, T., Boon, N., Maes, S., Lenz, M., 2013. Biotechnologies for critical raw material recovery from primary and secondary sources: R&D priorities and future perspectives. N. Biotechnol. 32, 121–127.

Henry, T.B., Menn, F.-M., Fleming, J.T., Wilgus, J., Compton, R.N., Sayler, G.S., 2007. Attributing effects of aqueous C60 nano-aggregates to tetrahydrofuran decomposition products in larval zebrafish by assessment of gene expression. Environ. Health Perspect. 115, 1059–1065.

Herkovits, J., Castañaga, L.A., D'Eramo, J.L., Jourani, V.P., 2015. Living organisms influence on environmental conditions: pH modulation by amphibian embryos versus aluminum toxicity. Chemosphere 139, 210–215.

Hernández, P.P., Moreno, V., Olivari, F.A., Allende, M.L., 2006. Sub-lethal concentrations of waterborne copper are toxic to lateral line neuromasts in zebrafish (*Danio rerio*). Hear. Res. 213, 1–10.

Herrmann, D., Kratzert, P., Weeke, S., Zimmer, M., Djordjevic-reiss, J., Lindberg, P., Wallin, E., Lundberg, O., Stolt, L., Gmbh, S.H., Thalheim, B.O.T., 2014. CIGS module manufacturing with high deposition rates and efficiencies. IEEE Pvsc. 40; 2–4.

Hetz, C., 2012. The unfolded protein response: controlling cell fate decisions under ER stress and beyond. Nat. Rev. Mol. Cell Biol. 13, 89–102.

Heymann, D., 1996. Solubility of fullerenes C60 and C70 in seven normal alcohols and their deduced solubility in water. Fuller. Sci. Technol. 4, 509–515.

Hiramatsu, N., Kasai, A., Du, S., Takeda, M., Hayakawa, K., Okamura, M., Yao, J., Kitamura, M., 2007. Rapid, transient induction of ER stress in the liver and kidney after acute exposure to heavy metal: evidence from transgenic sensor mice. FEBS Lett. 581, 2055–2059.

Hogstrand, C., Wood, C.M., 1998. Toward a better understanding of the bioavailability , physiology , and toxicity of dilver in fish: Implications for water quality criteria. Environ. Toxicol. Chem. 17, 547–561.

Holcombe, G.W., Phipps, G.L., Fiandt, J.T., 1983. Toxicity of selected priority pollutants to various aquatic organisms. Ecotoxicol. Environ. Saf. 7, 400–409.

Homma, S., Miyamoto, A., Sakamoto, S., Kishi, K., Motoi, N., Yoshimura, K., 2005. Pulmonary fibrosis in an individual occupationally exposed to inhaled indium-tin oxide. Eur. Respir. J. 25, 200–204.

Hong, S., Kim, Y., Han, J., 2008. Development of ultrafine indium tin oxide (ITO) nanoparticle for ink-jet printing by low-temperature synthetic method. IEEE Trans. Nanotechnol. 7, 172–176.

Howe, K., Clark, M.D., Torroja, C.F., Torrance, J., Berthelot, C., Muffato, M., … Stemple, D.L., 2013. The zebrafish reference genome sequence and its relationship to the human genome. Nature. 496, 498–503.

Hu, P., Han, Z., Couvillon, A.D., Kaufman, R.J., Exton, J.H., 2006. Autocrine tumor necrosis factor alpha links endoplasmic reticulum stress to the membrane death receptor pathway through IRE1a - mediated NF-κB activation and down-regulation of TRAF2 expression. Mol. Cell. Biol. 26, 3071–3084.

Hu, X., Cook, S., Wang, P., Hwang, H.-M., 2009. *In vitro* evaluation of cytotoxicity of engineered metal oxide nanoparticles. Sci. Total Environ. 407, 3070–3072.

Hua, J., Vijver, M.G., Ahmad, F., Richardson, M.K., Peijnenburg, W.J.G.M., 2014. Toxicity of different-sized copper nano- and submicron particles and their shed copper ions to zebrafish embryos. Environ. Toxicol. Chem. 33, 1774–1782.

Hung, J.-H., Su, I.-J., Lei, H.-Y., Wang, H.-C., Lin, W.-C., Chang, W.-T., Huang, W., Chang, W.-C., Chang, Y.-S., Chen, C.-C., Lai, M.-D., 2004. Endoplasmic reticulum stress stimulates the expression of cyclooxygenase-2 through activation of NF-kappaB and pp38 mitogen-activated protein kinase. J. Bol. Chem. 279, 46384–46392.

Hwang, P., Tsail, Y., Tung, Y., 1994. Calcium balance in embryos and larvae of the freshwater-adapted teleost , *Oreochromis mossambicus*. Fish Physiol. Biochem. 13, 325–333.

Hwang, U.G., Kagawa, N., Mugiya, Y., 2000. Aluminium and cadmium inhibit vitellogenin and its mRNA induction by estradiol-17 beta in the primary culture of hepatocytes in the rainbow trout *Oncorhynchus mykiss*. Gen. Comp. Endocrinol. 119, 69–76.

Hyung, H., Fortner, J.D., Hughes, J.B., Kim, J.-H., 2007. Natural organic matter stabilizes carbon nanotubes in the aqueous phase. Environ. Sci. Technol. 41, 179–184.

International Energy Agency, IEA, 2015. Renewable energy medium-term market report 2015. Market Analysis and Forecasts to 2020. 266pp.

Ip, T.Y., Davis, R.J., 1998. Signal transduction by the c-Jun N-terminal kinase (JNK) - from inflammation to development. Curr. Opin. Cell Biol. 10, 205–219.

IPCC, 2007. Summary for policymakers. In: Climate Change 2007: The Physical Science Basis. Contribution of Working Group I to the Fourth Assessment Report of the Intergovernmental Panel on Climate Change [Solomon, S., D. Qin, M. Manning, Z. Chen, M. Marquis, K.B. Averyt, M. Tignor and H.L. Miller (eds.)]. Cambridge University Press, Cambridge, United Kingdom and New York, NY, USA.

IPCC, 2014. Summary for policymakers. In: Climate Change 2014: Impacts,Adaptation, and Vulnerability. Part A: Global and Sectoral Aspects. Contribution of Working Group II to the Fifth Assessment Report of the Intergovernmental Panel on Climate Change [Field, C.B., V.R. Barros, D.J. Dokken, K.J. Mach, M.D. Mastrandrea, T.E. Bilir, M. Chatterjee, K.L. Ebi, Y.O. Estrada, R.C. Genova, B. Girma, E.S. Kissel, A.N. Levy, S. MacCracken, P.R. Mastrandrea, and L.L.White (eds.)]. Cambridge University Press, Cambridge, United Kingdom and New York, NY, USA, pp. 1-32.

Isidori, M., Cangiano, M., Palermo, F.A., Parrella, A., 2010. E-screen and vitellogenin assay for the detection of the estrogenic activity of alkylphenols and trace elements. Comp. Biochem. Physiol. Part C Toxicol. Pharmacol. 152, 51–56.

Jager, T., 2012. Bad habits die hard: The NOEC's persistence reflects poorly on ecotoxicology. Environ. Toxicol. Chem. 31, 228–229.

Jager, T., Vandenbrouck, T., Baas, J., De Coen, W.M., Kooijman, S.A.L.M., 2010. A biology-based approach for mixture toxicity of multiple endpoints over the life cycle. Ecotoxicology 19, 351–361.

Jancula, D., Mikula, P., Marsalek, B., 2011. Effects of polyaluminium chloride on the freshwater invertebrate *Daphnia magna*. Chem. Ecol. 27, 351–357.

Johnson, A., Carew, E., Sloman, K.A., 2007. The effects of copper on the morphological and functional development of zebrafish embryos. Aquat. Toxicol. 84, 431–438.

Kamunde, C., MacPhail, R., 2011. Subcellular interactions of dietary cadmium, copper and zinc in rainbow trout (*Oncorhynchus mykiss*). Aquat. Toxicol. 105, 518–527.

Kaneko, M., Ishiguro, M., Niinuma, Y., Uesugi, M., Nomura, Y., 2002. Human HRD1 protects against ER stress-induced apoptosis through ER-associated degradation. FEBS Lett. 532, 147–152.

Karagiannidis, P.G., Kassavetis, S., Pitsalidis, C., Logothetidis, S., 2011. Thermal annealing effect on the nanomechanical properties and structure of P3HT:PCBM thin films. Thin Solid Films. 519, 4105–4109.

Kataoka, C., Ariyoshi, T., Kawaguchi, H., 2015. Salinity increases the toxicity of silver nanocolloids to Japanese medaka embryos. Environ. Sci. Nano. 2, 94–103.

Kaya, H., Aydın, F., Gürkan, M., Yılmaz, S., Ates, M., Demir, V., Arslan, Z., 2016. A comparative toxicity study between small and large size zinc oxide nanoparticles in tilapia (*Oreochromis niloticus*): Organ pathologies, osmoregulatory responses and immunological parameters. Chemosphere. 144, 571–582.

Kermanizadeh, A., Pojana, G., Gaiser, B.K., Birkedal, R., Bilaničová, D., Wallin, H., Jensen, K.A., Sellergren, B., Hutchison, G.R., Marcomini, A., Stone, V., 2013. *In vitro* assessment of engineered nanomaterials using a hepatocyte cell line: cytotoxicity, pro-inflammatory cytokines and

functional markers. Nanotoxicology. 7, 301–313.

Kester, D.R., Duedall, I.W., Connors, D.N., Pytkowicz, R.M., 1967. Preparation of artificial seawater. Limnol. Oceanogr. 12, 176–179.

Kim, J.-W., Chang, K.-H., Isobe, T., Tanabe, S., 2011. Acute toxicity of benzotriazole ultraviolet stabilizers on freshwater crustacean (*Daphnia pulex*). J. Toxicol. Sci. 36, 247–251.

Kim, R., Emi, M., Tanabe, K., Murakami, S., 2006. Role of the unfolded protein response in cell death. Apoptosis 11, 5–13.

Kitamura, M., Hiramatsu, N., 2010. The oxidative stress: endoplasmic reticulum stress axis in cadmium toxicity. Biometals. 23, 941–950.

Klaine, S.J., Alvarez, P.J., Batley, G.E., Fernandes, T.F., Handy, R.D., Lyon, D.Y., Mahendra, S., McLaughlin, M.J., Lead, J.R., 2008. Nanomaterials in the environment: behavior, fate, bioavailability, and effects. Environ. Toxicol. Chem. 27, 1825–1851.

Klüttgen, B., Dülmer, U., Engels, M., Ratte, H.T., 1994. ADaM, an artifical freshwater for the culture of zooplankton. Water Res. 28, 743–746.

Knops, M., Altenburger, R., Segner, H., 2001. Alterations of physiological energetics, growth and reproduction of *Daphnia magna* under toxicant stress. Aquat. Toxicol. 53, 79–90.

Kominsky, D.J., Campbell, E.L., Colgan, S.P., 2010. Metabolic shifts in immunity and inflammation. J. Immunol. 184, 4062–4068.

Komjarova, I., Blust, R., 2008. Multi-metal interactions between Cd, Cu, Ni, Pb and Zn in water flea *Daphnia magna*, a stable isotope experiment. Aquat. Toxicol. 90, 138–144.

Komjarova, I., Blust, R., 2009. Multimetal interactions between Cd, Cu, Ni, Pb, and Zn uptake from water in the zebrafish *Danio rerio*. Environ. Sci. Technol. 43, 7225–7229.

Komjarova, I., Bury, N.R., 2014. Evidence of common cadmium and copper uptake routes in zebrafish *Danio rerio*. Enviromental Sci. Technol. 48, 12946–12951.

Kondoh, M., Tsukada, M., Kuronaga, M., Higashimoto, M., Takiguchi, M., Himeno, S., Watanabe, Y., Sato, M., 2004. Induction of hepatic metallothionein synthesis by endoplasmic reticulum stress in mice. Toxicol. Lett. 148, 133–139.

Kumar, V., Bal, A., Gill, K.D., 2009. Susceptibility of mitochondrial superoxide dismutase to aluminium induced oxidative damage. Toxicology 255, 117–123.

Kunz, P.Y., Fent, K., 2009. Estrogenic activity of ternary UV filter mixtures in fish (*Pimephales promelas*) - An analysis with nonlinear isobolograms. Toxicol. Appl. Pharmacol. 234, 77–88.

Kupsco, A., Schlenk, D., 2014. Mechanisms of selenomethionine developmental toxicity and the impacts of combined hypersaline conditions on japanese medaka (*Oryzias latipes*). Environ. Sci. Technol. 48, 7062–7068.

Kwong, R.W.M., Hamilton, C.D., Niyogi, S., 2013. Effects of elevated dietary iron on the gastrointestinal expression of Nramp genes and iron homeostasis in rainbow trout (*Oncorhynchus mykiss*). Fish Physiol. Biochem. 39, 363–372.

Laleman, R., Albrecht, J., Dewulf, J., 2011. Life cycle analysis to estimate the environmental impact of residential photovoltaic systems in regions with a low solar irradiation. Renew. Sustain. Energy Rev. 15, 267–271.

Lampert, W., 2011. *Daphnia*: Development of a model organism in ecology and evolution, Excellence. ed. International Ecology Institute, Oldendorf/Luhe.

Landis, W.G., Chapman, P.M., 2011. Well past time to stop using NOELs and LOELs. Integr. Environ. Assess. Manag. 7, 7–9.

Larese, F.F., D'Agostin, F., Crosera, M., Adami, G., Renzi, N., Bovenzi, M., Maina, G., 2009. Human skin penetration of silver nanoparticles through intact and damaged skin. Toxicology. 255, 33–37.

Leal Filho, W., Kotter, R., 2015. E-mobility in europe. Trends and Good Practice. Springer International Publishing.

Lee, A.-H., Scapa, E.F., Cohen, D.E., Glimcher, L.H., 2008. Regulation of hepatic lipogenesis by the transcription factor XBP1. Science. 320, 1492–1497.

Lee, K.J., Nallathamby, P.D., Browning, L.M., Osgood, C.J., Xu, X.-H.N., 2007. *In vivo* imaging of transport and biocompatibility of single silver nanoparticles in early development of zebrafish embryos. ACS Nano 1, 133–143.

Li, L.-Z., Zhou, D.-M., Peijnenburg, W.J.G.M., van Gestel, C.A.M., Jin, S.-Y., Wang, Y.-J., Wang, P., 2011.

Toxicity of zinc oxide nanoparticles in the earthworm, *Eisenia fetida* and subcellular fractionation of Zn. Environ. Int. 37, 1098–1104.

Li, M., Czymmek, K.J., Huang, C.P., 2011. Responses of *Ceriodaphnia dubia* to TiO_2 and Al_2O_3 nanoparticles: A dynamic nano-toxicity assessment of energy budget distribution. J. Hazard. Mater. 187, 502–508.

Li, P., Nijhawan, D., Budihardjo, I., Srinivasula, S.M., Ahmad, M., Alnemri, E.S., Wang, X., 1997. Cytochrome c and dATP-dependent formation of Apaf-1/caspase-9 complex initiates an apoptotic protease cascade. Cell. 91, 479–489.

Li, S., Irin, F., Atore, F.O., Green, M.J., Cañas-Carrell, J.E., 2013. Determination of multi-walled carbon nanotube bioaccumulation in earthworms measured by a microwave-based detection technique. Sci. Total Environ. 445-446, 9–13.

Li, S., Wallis, L.K., Ma, H., Diamond, S. a, 2014. Phototoxicity of TiO_2 nanoparticles to a freshwater benthic amphipod: are benthic systems at risk? Sci. Total Environ. 466-467, 800–808.

Liang, X., Wang, M., Chen, X., Zha, J., Chen, H., Zhu, L., Wang, Z., 2014. Endocrine disrupting effects of benzotriazole in rare minnow (*Gobiocypris rarus*) in a sex-dependent manner. Chemosphere. 112, 154–162.

Lin, C.-F., Liu, S.-W., Hsu, W.-F., Zhang, M., Chiu, T.-L., Wu, Y., Lee, J.-H., 2010. Modification of silver anode and cathode for a top-illuminated organic photovoltaic device. J. Phys. D. Appl. Phys. 43, 7pp.

Lin, J.H., Li, H., Yasumura, D., Cohen, H.R., Zhang, C., Panning, B., Shokat, K.M., Lavail, M.M., Walter, P., 2007. IRE1 signaling affects cell fate during the unfolded protein response. Science. 318, 944–949.

Lin, W.-C., Chuang, Y.-C., Chang, Y.-S., Lai, M.-D., Teng, Y.-N., Su, I.-J., Wang, C.C.C., Lee, K.-H., Hung, J.-H., 2012. Endoplasmic reticulum stress stimulates p53 expression through NF-κB activation. PLoS One. 7, e39120.

Linnik, P.N., Zhezherya, V.A., Linnik, R.P., Ivanechko, Y.S., 2012. Concentrations of aluminium, iron, and copper in water of some Shatskiye Lakes and specificity of their distribution among different forms of occurrence. Russ. J. Gen. Chem. 82, 2226–2238.

Lison, D., Laloy, J., Corazzari, I., Muller, J., Rabolli, V., Panin, N., Huaux, F., Fenoglio, I., Fubini, B., 2009. Sintered indium-tin-oxide (ITO) particles: a new pneumotoxic entity. Toxicol. Sci. 108, 472–481.

Lizin, S., Van Passel, S., De Schepper, E., Maes, W., Lutsen, L., Manca, J., Vanderzande, D., 2013. Life cycle analyses of organic photovoltaics: a review. Energy Environ. Sci. 6, 3136-3149.

Loewe, S., Muischnek, H., 1926. Über Kombinationswirkungen. Arch. Exp. Pathol. Pharmakol. 114, 313–326.

Lopes, S., Ribeiro, F., Wojnarowicz, J., Lojkowski, W., Jurkschat, K., Crossley, A., Soares, A.M.V.M., Loureiro, S., 2014. Zinc oxide nanoparticles toxicity to *Daphnia magna*: Size-dependent effects and dissolution. Environ. Toxicol. Chem. 33, 190–198.

Lotka, A.J., 1913. A natural population norm. J Washingt. Acad Sci. 3, 241–248.

Lowry, G. V, Gregory, K.B., Apte, S.C., Lead, J.R., 2012. Transformations of Nanomaterials in the Environment. Environ. Sci. Technolgy. 46, 6893–6899.

Luoma, S.N., Ho, Y.B., Bryan, G.W., 1995. Fate, bioavailability and toxicity of silver in estuarine environments. Mar. Pollut. Bull. 31, 44–54.

Lyche, J.L., Gutleb, A.C., Bergman, A., Eriksen, G.S., Murk, A.J., Ropstad, E., Saunders, M., Skaare, J.U., 2009. Reproductive and developmental toxicity of phthalates. J. Toxicol. Environ. Health. B. Crit. Rev. 12, 225–249.

Maier, T., Güell, M., Serrano, L., 2009. Correlation of mRNA and protein in complex biological samples. FEBS Lett. 583, 3966–3973.

Malhotra, J.D., Kaufman, R.J., 2007. Endoplasmic reticulum stress and oxidative stress: a vicious cycle or a double-edged sword? Antioxid. Redox Signal. 9, 2277–2293.

Malhotra, J.D., Miao, H., Zhang, K., Wolfson, A., Pennathur, S., Pipe, S.W., Kaufman, R.J., 2008. Antioxidants reduce endoplasmic reticulum stress and improve protein secretion. Proc. Natl. Acad. Sci. USA. 105, 18525–18530.

Manceau, M., Rivaton, A., Gardette, J.-L., Guillerez, S., Lemaître, N., 2011. Light-induced degradation

of the P3HT-based solar cells active layer. Sol. Energy Mater. Sol. Cells. 95, 1315–1325.

Martell, A.E., Smith, R.M., 1977. Critical stability constants. Plenum Press, New York.

Martin, R.B., 1986. The chemistry of aluminum as related to biology and medicine. Clin. Chem. 32, 1797–806.

Martinon, F., Glimcher, L.H., 2011. Regulation of innate immunity by signaling pathways emerging from the endoplasmic reticulum. Curr. Opin. Immunol. 23, 35–40.

Martins, J., Oliva Teles, L., Vasconcelos, V., 2007. Assays with *Daphnia magna* and *Danio rerio* as alert systems in aquatic toxicology. Environ. Int. 33, 414–425.

Mattos, L.S., Scully, S.R., Syfu, M., Olson, E., Yang, L., Ling, C., Kayes, B.M., He, G., 2012. New module efficiency record: 23.5% under 1-sun illumination using thin-film single-junction GaAs solar cells. Conf. Rec. IEEE Photovolt. Spec. Conf. 3187–3190.

Mengubas, K., Riordan, F.A., Hoffbrand, A.V., Wickremasinghe, R.G., 1996. Co-ordinated downregulation of bcl-2 and bax expression during granulocytic and macrophage-like differentiation of the HL60 promyelocytic leukaemia cell line. FEBS Lett. 394, 356–360.

Meyer, J.S., Ranville, J.F., Pontasch, M., Gorsuch, J.W., Adams, W.J., 2015. Acute toxicity of binary and ternary mixtures of Cd, Cu, and Zn to *Daphnia magna*. Environ. Toxicol. Chem. 34, 799–808.

Miles, R.W., Hynes, K.M., Forbes, I., 2005. Photovoltaic solar cells: An overview of state-of-the-art cell development and environmental issues. Prog. Cryst. Growth Charact. Mater. 51, 1–42.

Miner, B.E., De Meester, L., Pfrender, M.E., Lampert, W., Hairston, N.G., 2012. Linking genes to communities and ecosystems: *Daphnia* as an ecogenomic model. Proc. R. Soc. B Biol. Sci. 279, 1873–1882.

Mitrano, D.M., Motellier, S., Clavaguera, S., Nowack, B., 2015. Review of nanomaterial aging and transformations through the life cycle of nano-enhanced products. Environ. Int. 77, 132–147.

Mohd Omar, F., Abdul Aziz, H., Stoll, S., 2014. Aggregation and disaggregation of ZnO nanoparticles: Influence of pH and adsorption of Suwannee River humic acid. Sci. Total Environ. 468-469, 195–201.

Molina, R., Al-Salama, Y., Jurkschat, K., Dobson, P.J., Thompson, I.P., 2011. Potential environmental influence of amino acids on the behavior of ZnO nanoparticles. Chemosphere. 83, 545–51.

Monteiro, D.A., Rantin, F.T., Kalinin, A.L., 2009. The effects of selenium on oxidative stress biomarkers in the freshwater characid fish matrinxã, *Brycon cephalus* (Günther, 1869) exposed to organophosphate insecticide Folisuper 600 BR (methyl parathion). Comp. Biochem. Physiol. Part C 149, 40–49.

Moore, M.N., 2006. Do nanoparticles present ecotoxicological risks for the health of the aquatic environment? Environ. Int. 32, 967–976.

Mortazavi, A., Williams, B. a, McCue, K., Schaeffer, L., Wold, B., 2008. Mapping and quantifying mammalian transcriptomes by RNA-Seq. Nat. Methods. 5, 621–628.

Mosmann, T., 1983. Rapid colorimetric assay for celular growth and survival: Application to proliferation and cytotoxicity assays. J. Immunol. Methods. 65, 135–147.

Mudunkotuwa, I.A., Grassian, V.H., 2011. The devil is in the details (or the surface): impact of surface structure and surface energetics on understanding the behavior of nanomaterials in the environment. J. Environ. Monit. 13, 1135–1144.

Muller, E.B., Lin, S., Nisbet, R.M., 2015. Quantitative adverse outcome pathway analysis of hatching in zebrafish with CuO nanoparticles. Environ. Sci. Technol. 49, 11817-11824.

Murphy, C.A., Rose, K.A., Thomas, P., 2005. Modeling vitellogenesis in female fish exposed to environmental stressors: Predicting the effects of endocrine disturbance due to exposure to a PCB mixture and cadmium. Reprod. Toxicol. 19, 395–409.

Muthukrishnan, S., Merzendorfer, H., Arakane, Y., Kramer, K.J., 2012. Chitin metabolism in insects, Insect Molecular Biology and Biochemistry. Academic Press, London.

Nakata, H., Murata, S., Filatreau, J., 2009. Occurrence and concentrations of benzotriazole UV stabilizers in marine organisms and sediments from the Ariake Sea, Japan. Environ. Sci. Technol. 43, 6920-6926.

Nel, A., Xia, T., Mädler, L., Li, N., 2006. Toxic potential of materials at the nanolevel. Science. 311, 622–627.

Nicholson, J.W., 2012. The chemistry of polymers, 4th ed. The Royal Society of Chemistry,

Cambridge.

Nikinmaa, M., Rytkönen, K.T., 2011. Functional genomics in aquatic toxicology—Do not forget the function. Aquat. Toxicol. 105, 16–24.

Niyogi, S., Nadella, S.R., Wood, C.M., 2015. Interactive effects of waterborne metals in binary mixtures on short-term gill–metal binding and ion uptake in rainbow trout (*Oncorhynchus mykiss*). Aquat. Toxicol. 165, 109–119.

Nowack, B., Bucheli, T.D., 2007. Occurrence, behavior and effects of nanoparticles in the environment. Environ. Pollut. 150, 5–22.

National Renewable Energy Laboratory, NREL, 2015. Retrieved from: http://www.nrel.gov/ncpv/images/ efficiency_chart.jpg. Accessed on October 20 2015.

Nunes, F., Spiering, D., Wolf, M., Wendler, A., Pirow, R., Paul, R.J., 2005. Sequencing of hemoglobin gene 4 (dmhb4) and southern blot analysis provide evidence of more than four members of the *Daphnia magna* globin family. Biosci. Biotechnol. Biochem. 69, 1193–1197.

Nys, C., Asselman, J., Hochmuth, J.D., Janssen, C.R., Blust, R., Smolders, E., De Schamphelaere, K.A.C., 2015. Mixture toxicity of nickel and zinc to *Daphnia magna* is noninteractive at low effect sizes but becomes synergistic at high effect sizes. Environ. Toxicol. Chem. 34, 1091–1102.

Oberdörster, E., 2004. Manufactured nanomaterials (fullerenes, C60) induce oxidative stress in the brain of juvenile largemouth bass. Environ. Health Perspect. 112, 1058–1062.

Ong, K., Zhao, X., Thistle, M., Maccormack, T.J., Clark, R.J., Ma, G., Martinez-Rubi, Y., Simard, B., Loo, J., Veinot, J.G., Goss, G.G., 2013. Mechanistic insights into the effect of nanoparticles on zebrafish hatch. Nanotoxicology. 8, 295-304.

Pahl, H.L., Baeuerle, P.A., 1995. A novel signal transduction pathway from the endoplasmic reticulum to the nucleus is mediated by transcription factor NF-κB. EMBO J. 14, 2580–2588.

Palermo, F.A., Mosconi, G., Angeletti, M., Polzonetti-Magni, A.M., 2008. Assessment of water pollution in the Tronto River (Italy) by applying useful biomarkers in the fish model *Carassius auratus*. Arch. Environ. Contam. Toxicol. 55, 295–304.

Paton, C., Hellstrom, J., Paul, B., Woodhead, J., Hergt, J., 2011. Iolite: Freeware for the visualisation and processing of mass spectrometric data. J. Anal. At. Spectrom. 26, 2508–2518.

Patton, E.E., Zon, L.I., 2001. The art and design of genetic scrSt Johnston, Danieleens: zebrafish. Nat. Rev. Genet. 2, 956–966.

Paules, R., 2003. Phenotypic anchoring: linking cause and effect. Environ. Health Perspect. 111, 338–339.

Pereira, S., Cavalie, I., Camilleri, V., Gilbin, R., Adam-Guillermin, C., 2013. Comparative genotoxicity of aluminium and cadmium in embryonic zebrafish cells. Mutat. Res. - Genet. Toxicol. Environ. Mutagen. 750, 19–26.

Pessah, I.N., Cherednichenko, G., Lein, P.J., 2010. Minding the calcium store: Ryanodine receptor activation as a convergent mechanism of PCB toxicity. Pharmacol. Ther. 125, 260–285.

Pillai, S., Behra, R., Nestler, H., Suter, M.J.-F., Sigg, L., Schirmer, K., 2014. Linking toxicity and adaptive responses across the transcriptome, proteome, and phenotype of Chlamydomonas reinhardtii exposed to silver. Proc. Natl. Acad. Sci. USA. 111, 3490–3495.

Powell, C.L., 2006. Phenotypic anchoring of acetaminophen-induced oxidative stress with gene expression profiles in rat liver. Toxicol. Sci. 93, 213–222.

Poynton, H.C., Lazorchak, J.M., Impellitteri, C. a, Smith, M.E., Rogers, K., Patra, M., Hammer, K. a, Allen, H.J., Vulpe, C.D., 2011. Differential gene expression in *Daphnia magna* suggests distinct modes of action and bioavailability for ZnO nanoparticles and Zn ions. Environ. Sci. Technol. 45, 762–768.

Poynton, H.C., Lazorchak, J.M., Impellitteri, C.A., Blalock, B., Smith, M.E., Struewing, K., Unrine, J., Roose, D., 2013. Toxicity and transcriptomic analysis in *hyalella azteca* suggests increased exposure and susceptibility of epibenthic organisms to zinc oxide nanoparticles. Environ. Sci. Technol. 47, 9453–9460.

Poynton, H.C., Loguinov, A. V, Varshavsky, J.R., Chan, S., Vulpe, C.D., 2008. Gene expression profiling in *Daphnia magna* Part I : Concentration-dependent profiles provide support for the no observed transcriptional effect level. Environ. Sci. Technol. 42, 6250–6256.

Poynton, H.C., Varshavsky, J.R., Chang, B., Cavigiolio, G., Chan, S., Holman, P.S., Loguinov, A. V, Bauer,

D.J., Komachi, K., Theil, E.C., Perkins, E.J., Hughes, O., Vulpe, C.D., 2007. *Daphnia magna* ecotoxicogenomics provides mechanistic insights into metal toxicity. Environ. Sci. Technol. 41, 1044–1050.

Pyati, U.J., Gjini, E., Carbonneau, S., Lee, J.-S., Guo, F., Jette, C.A., Kelsell, D.P., Look, A.T., 2011. p63 mediates an apoptotic response to pharmacological and disease-related ER stress in the developing epidermis. Dev. Cell. 21, 492–505.

Qian, Y., Falahatpisheh, M.H., Zheng, Y., Ramos, K.S., Tiffany-Castiglioni, E., 2001. Induction of 78 kD glucose-regulated protein (GRP78) expression and redox-regulated transcription fator activity by lead and mercury in C6 rat glioma cells. Neurotox. Res. 3, 581–589.

Quiroz-Vázquez, P., Sigee, D.C., White, K.N., 2010. Bioavailability and toxicity of aluminium in a model planktonic food chain (*Chlamydomonas–Daphnia*) at neutral pH. Limnol. - Ecol. Manag. Inl. Waters. 40, 269–277.

Quiroz-Vazquez, P., White, K.N., Sigee, D.C., 2008. Aluminium, silicon and transition metal dynamics in a non-polluted lake: aquatic concentrations and phytoplankton uptake. Hydrobiologia. 607, 131–142.

Rao, R. V, Castro-Obregon, S., Frankowski, H., Schuler, M., Stoka, V., del Rio, G., Bredesen, D.E., Ellerby, H.M., 2002. Coupling endoplasmic reticulum stress to the cell death program. An Apaf-1-independent intrinsic pathway. J. Biol. Chem. 277, 21836–21842.

Ratte, H.T., 1999. Bioaccumulation and toxicity of silver compounds: A review. Environ. Toxicol. Chem. 18, 89–108.

Raugei, M., Fthenakis, V., 2010. Cadmium flows and emissions from CdTe PV: Future expectations. Energy Policy 38, 5223–5228.

Razo-Estrada, A.C., García-Medina, S., Madrigal-Bujaidar, E., Gómez-Oliván, L.M., Galar-Martínez, M., 2013. Aluminum-induced oxidative stress and apoptosis in liver of the common carp, *Cyprinus carpio*. Water, Air, Soil Pollut. 224, 1510, 1-9.

Razykov, T.M., Ferekides, C.S., Morel, D., Stefanakos, E., Ullal, H.S., Upadhyaya, H.M., 2011. Solar photovoltaic electricity: Current status and future prospects. Sol. Energy. 85, 1580–1608.

Reed, R.B., Ladner, D. a, Higgins, C.P., Westerhoff, P., Ranville, J.F., 2012. Solubility of nano-zinc oxide in environmentally and biologically important matrices. Environ. Toxicol. Chem. 31, 93–99.

Reichle, R.A., McCurdy, K.G., Hepler, L.G., 1975. Zinc hydroxide: solubility product and hydroxy-complex stability constants from 12.5-75 °C. Can. J. Chem. 53, 3841–3845.

Rizvi, S.H.M., Parveen, A., Verma, A.K., Ahmad, I., Arshad, M., Mahdi, A.A., 2014. Aluminium induced endoplasmic reticulum stress mediated cell death in SH-SY5Y neuroblastoma cell line is independent of p53. PLoS One. 9, e98409.

Rocha, J.B.T., Tuerlinckx, S.M., Schetinger, M.R.C., Folmer, V., 2004. Effect of Group 13 metals on porphobilinogen synthase *in vitro*. Toxicol. Appl. Pharmacol. 200, 169–176.

Rodrigues, S.M., Trindade, T., Duarte, A.C., Pereira, E., Koopmans, G.F., Römkens, P.F.A.M., 2015. A framework to measure the availability of engineered nanoparticles in soils: trends in soil tests and analytical tools. Trends Anal. Chem. 75, 129-140.

Rodríguez Moreno, P.A., Medesani, D.A., Rodríguez, E.M., 2003. Inhibition of molting by cadmium in the crab *Chasmagnathus granulata* (Decapoda Brachyura). Aquat. Toxicol. 64, 155–164.

Roes, A.L., Alsema, E.A., Blok, K., Patel, M.K., 2009. Ex-ante environmental and economic evaluation of polymer photovoltaics. Prog. Photovoltaics Res. Appl. 17, 372–393.

Rola, R.C., Marins, L.F., Nery, L.E.M., da Rosa, C.E., Sandrini, J.Z., 2014. Responses to ROS inducer agents in zebrafish cell line: differences between copper and UV-B radiation. Fish Physiol. Biochem. 40, 1817–1825.

Ron, D., Walter, P., 2007. Signal integration in the endoplasmic reticulum unfolded protein response. Nat. Rev. Mol. Cell Biol. 8, 519–529.

Routledge, E.J., Sumpter, J.P., 1996. Estrogenic activity of surfactants and some of their degradation products assessed using a recombinant yeast screen. Environ. Toxicol. Chem. 15, 241–248.

Routtu, J., Hall, M.D., Albere, B., Beisel, C., Bergeron, R., Chaturvedi, A., Choi, J.-H., Colbourne, J., De Meester, L., Stephens, M.T., Stelzer, C.-P., Solorzano, E., Thomas, W., Pfrender, M.E., Ebert, D., 2014. An SNP-based second-generation genetic map of *Daphnia magna* and its application to QTL analysis of phenotypic traits. BMC Genomics 15, 1033.

Routtu, J., Jansen, B., Colson, I., De Meester, L., Ebert, D., 2010. The first-generation *Daphnia magna* linkage map. BMC Genomics 11, 508.

Roy, R., Campbell, P.G.C., 1995. Survival time modeling of exposure of juvenile atlantic salmon (*Salmo Salar*) to mixtures of aluminum and zinc in soft water at low pH. Aquat. Toxicol. 33, 155–176.

Russell, W.M.S., Burch, R.L., 1959. The principles of humane experimental techniques. Methuen, London.

Rutkowski, D.T., Wu, J., Back, S.H., Callaghan, M.U., Ferris, S.P., Iqbal, J., Clark, R., Miao, H., Hassler, J.R., Fornek, J., Katze, M.G., Hussain, M.M., Song, B., Swathirajan, J., Wang, J., Yau, G.D.Y., Kaufman, R.J., 2008. UPR pathways combine to prevent hepatic steatosis caused by ER stress-mediated suppression of transcriptional master regulators. Dev. Cell 15, 829–840.

Sabaliauskas, N.A., Foutz, C.A., Mest, J.R., Budgeon, L.R., Sidor, A.T., Gershenson, J.A., Joshi, S.B., Cheng, K.C., 2006. High-throughput zebrafish histology. Methods 39, 246–254.

Saga, T., 2010. Advances in crystalline silicon solar cell technology for industrial mass production. NPG Asia Mater. 2, 96–102.

Sandrini, J.Z., Bianchini, A., Trindade, G.S., Nery, L.E.M., Marins, L.F.F., 2009. Reactive oxygen species generation and expression of DNA repair-related genes after copper exposure in zebrafish (*Danio rerio*) ZFL cells. Aquat. Toxicol. 95, 285–291.

Sant'Anna, M.C.B., de Soares, V.M., Seibt, K.J., Ghisleni, G., Rico, E.P., Rosemberg, D.B., de Oliveira, J.R., Schröder, N., Bonan, C.D., Bogo, M.R., 2011. Iron exposure modifies acetylcholinesterase activity in zebrafish (*Danio rerio*) tissues: Distinct susceptibility of tissues to iron overload. Fish Physiol. Biochem. 37, 573–581.

Sauer, G.R., Watabe, N., 1988. The effects of heavy metals and metabolic inhibitors on calcium uptake by gills and scales of Fundulus hetroclitus in bitro. Comp. Biochem. Physiol. 9.

Sayer, M.D., Reader, J.P., Morris, R., 1991. Effects of six trace metals on calcium fluxes in brown trout (*Salmo trutta L.*) in soft water. J. Comp. Physiol. B. 161, 537–542.

Schartl, M., 2014. Beyond the zebrafish: diverse fish species for modeling human disease. Dis. Model. Mech. 7, 181–192.

Schönthal, A.H., 2012. Endoplasmic reticulum stress: its role in disease and novel prospects for therapy. Scientifica (Cairo). 1, 1-26.

Schröder, M., Kaufman, R.J., 2005. The mammalian unfolded protein response. Annu. Rev. Biochem. 74, 739–789.

Schwarz, G., Mendel, R.R., Ribbe, M.W., 2009. Molybdenum cofactors, enzymes and pathways. Nature. 460, 839–847.

Senapati, V.A., Kumar, A., Gupta, G.S., Pandey, A.K., Dhawan, A., 2015. ZnO nanoparticles induced inflammatory response and genotoxicity in human blood cells: A mechanistic approach. Food Chem. Toxicol. 1–10.

Sensi, S.L., Yin, H.Z., Carriedo, S.G., Rao, S.S., Weiss, J.H., 1999. Preferential Zn2+ influx through Ca^{2+}-permeable AMPA/kainate channels triggers prolonged mitochondrial superoxide production. Proc. Natl. Acad. Sci. USA. 96, 2414–2419.

Sharma, V., Anderson, D., Dhawan, A., 2012. Zinc oxide nanoparticles induce oxidative DNA damage and ROS-triggered mitochondria mediated apoptosis in human liver cells (HepG2). Apoptosis 17, 852–870.

Shaw, B., Handy, R., 2006. Dietary copper exposure and recovery in Nile tilapia, *Oreochromis niloticus*. Aquat. Toxicol. 76, 111–121.

Shaw, B.J., Handy, R.D., 2011. Physiological effects of nanoparticles on fish: A comparison of nanometals versus metal ions. Environ. Int. 37, 1083–1097.

Shinkai, Y., Yamamoto, C., Kaji, T., 2010. Lead induces the expression of endoplasmic reticulum chaperones GRP78 and GRP94 in vascular endothelial cells via the JNK-AP-1 pathway. Toxicol. Sci. 114, 378–386.

Shockley, W., Queisser, H.J., 1961. Detailed balance limit of efficiency of p-n junction solar cells. J. Appl. Phys. 32, 510-519.

Silva, E., Lopez-Espinosa, M.J., Molina-Molina, J.-M., Fernández, M., Olea, N., Kortenkamp, A., 2006. Lack of activity of cadmium in in vitro estrogenicity assays. Toxicol. Appl. Pharmacol. 216, 20–

28.

Şişman, T., 2009. Early life stage and genetic toxicity of stannous chloride on zebrafish embryos and adults: toxic effects of tin on zebrafish. Environ. Toxicol. 26, 240–249.

Sivakumar, S., Khatiwada, C.P., Sivasubramanian, J., 2012. Bioaccumulations of aluminum and the effects of chelating agents on different organs of *Cirrhinus mrigala*. Environ. Toxicol. Pharmacol. 34, 791–800.

Smith, E.J., Davison, W., Hamilton-Taylor, J., 2002. Methods for preparing synthetic freshwaters. Water Res. 36, 1286–1296.

Snape, J.R., Maund, S.J., Pickford, D.B., Hutchinson, T.H., 2004. Ecotoxicogenomics: the challenge of integrating genomics into aquatic and terrestrial ecotoxicology. Aquat. Toxicol. 67, 143–154.

Soetaert, A., Vandenbrouck, T., van der Ven, K., Maras, M., van Remortel, P., Blust, R., De Coen, W.M., 2007. Molecular responses during cadmium-induced stress in *Daphnia magna*: integration of differential gene expression with higher-level effects. Aquat. Toxicol. 83, 212–222.

Song, W., Zhang, J., Guo, J., Zhang, J., Ding, F., Li, L., Sun, Z., 2010. Role of the dissolved zinc ion and reactive oxygen species in cytotoxicity of ZnO nanoparticles. Toxicol. Lett. 199, 389–397.

Song, Y.-F., Luo, Z., Huang, C., Chen, Q.-L., Pan, Y.-X., Xu, Y.-H., 2015. Endoplasmic reticulum stress-related genes in yellow catfish *Pelteobagrus fulvidraco*: Molecular characterization, tissue expression, and expression responses to dietary copper deficiency and excess. G3. 5, 2091–2104.

Sovolyova, N., Healy, S., Samali, A., Logue, S.E., 2014. Stressed to death - mechanisms of ER stress-induced cell death. Biol. Chem. 395, 1–13.

Sriburi, R., Jackowski, S., Mori, K., Brewer, J., 2004. XBP1: a link between the unfolded protein response, lipid biosynthesis, and biogenesis of the endoplasmic reticulum. J. Cell Biol. 167, 35–41.

Stratakis, E., Kymakis, E., 2013. Nanoparticle-based plasmonic organic photovoltaic devices. Mater. Today 16, 133–146.

Stumm, W., Morgan, J.J., 1981. Aquatic Chemistry. John Wiley & Sons, Chichester, NY.

Sumiya, E., Ogino, Y., Miyakawa, H., Hiruta, C., Toyota, K., Miyagawa, S., Iguchi, T., 2014. Roles of ecdysteroids for progression of reproductive cycle in the fresh water crustacean. Front. Zool. 11, 60, 1-12.

Tanaka, A., Hirata, M., Omura, M., Inoue, N., Ueno, T., Homma, T., Sekizawa, K., 2002. Pulmonary toxicity of indium-tin oxide and indium phosphide after intratracheal instillations into the lung of hamsters. J. Occup. Health. 99–102.

Tang, S., Wu, Y., Ryan, C.N., Yu, S., Qin, G., Edwards, D.S., Mayer, G.D., 2014. Distinct expression profiles of stress defense and DNA repair genes in *Daphnia pulex* exposed to cadmium, zinc, and quantum dots. Chemosphere. 120C, 92–99.

Thastrup, O., Cullen, P.J., Drøbak, B.K., Hanley, M.R., Dawson, A.P., 1990. Thapsigargin, a tumor promoter, discharges intracellular Ca^{2+} stores by specific inhibition of the endoplasmic reticulum Ca^{2+}-ATPase. Proc. Natl. Acad. Sci. USA. 87, 2466–2470.

Todd, D.J., Lee, A.-H., Glimcher, L.H., 2008. The endoplasmic reticulum stress response in immunity and autoimmunity. Nat. Rev. Immunol. 8, 663–674.

Tolcin, A.C., 2013. Indium - Mineral Commodity Summaries, U.S. Geological Survey.

Tollefson, J., 2015. Billion-dollar boost for clean energy kicks off UN climate talks. Natuer News. Accessed on December 10 2015.

Tsang, M.P., Sonnemann, G.W., Bassani, D.M., 2016. A comparative human health, ecotoxicity, and product environmental assessment on the production of organic and silicon solar cells. Prog. Photovoltaics Res. Appl. 24, 1–11.

Tsoutsos, T., Frantzeskaki, N., Gekas, V., 2005. Environmental impacts from the solar energy technologies. Energy Policy 33, 289–296.

United Nations Environment Programme UNEP, Secretariat of the Basel Convention, 2011. Ban Amendment to the Basel Convention on the Control of Transboundary Movements of Hazardous Wastes and their Disposal Geneva, 22 September 1995. Retrieved from: http://www.basel.int/Countries/Statusof-RatificationsBan/ Amendment/tabid/1344/Default.aspx. Accessed on October 7 2015.

Valavanidis, A., Vlahogianni, T., Dassenakis, M., Scoullos, M., 2006. Molecular biomarkers of oxidative stress in aquatic organisms in relation to toxic environmental pollutants. Ecotoxicol. Environ. Saf. 64, 178–189.

Valdiglesias, V., Costa, C., Kiliç, G., Costa, S., Pásaro, E., Laffon, B., Teixeira, J.P., 2013. Neuronal cytotoxicity and genotoxicity induced by zinc oxide nanoparticles. Environ. Int. 55, 92–100.

Van den Belt, K., Verheyen, R., Witters, H., 2003. Comparison of vitellogenin responses in zebrafish and rainbow trout following exposure to environmental estrogens. Ecotoxicol. Environ. Saf. 56, 271–281.

Van der Heijden, A., Van der Meij, J., Flik, G., Wendelaar Bonga, S., 1999. Ultrastructure and distribution dynamics of chloride cells in tilapia larvae in fresh water and sea water. Cell Tissue Res. 297, 119–130.

Vandegehuchte, M.B., Lemière, F., Vanhaecke, L., Vanden, W., Janssen, C.R., Vanden Berghe, W., Janssen, C.R., Vanden, W., Janssen, C.R., Vanden Berghe, W., Janssen, C.R., 2010a. Direct and transgenerational impact on *Daphnia magna* of chemicals with a known effect on DNA methylation. Comp. Biochem. Physiol. C. Toxicol. Pharmacol. 151, 278–285.

Vandegehuchte, M.B., Vandenbrouck, T., Coninck, D. De, De Coen, W.M., Janssen, C.R., 2010b. Can metal stress induce transferable changes in gene transcription in *Daphnia magna*? Aquat. Toxicol. 97, 188–195.

Vandegehuchte, M.B., Vandenbrouck, T., De Coninck, D., De Coen, W.M., Janssen, C.R., 2010c. Gene transcription and higher-level effects of multigenerational Zn exposure in *Daphnia magna*. Chemosphere 80, 1014–1020.

Vandenbrouck, T., Soetaert, A., van der Ven, K., Blust, R., De Coen, W., 2009. Nickel and binary metal mixture responses in *Daphnia magna*: molecular fingerprints and (sub)organismal effects. Aquat. Toxicol. 92, 18–29.

Vanduyn, N., Settivari, R., Levora, J., Zhou, S., Unrine, J., Nass, R., 2013. The metal transporter SMF-3/DMT-1 mediates aluminum-induced dopamine neuron degeneration. J. Neurochem. 124, 147–157.

Varshavsky, A., 1996. The N-end rule: functions, mysteries, uses. Proc. Natl. Acad. Sci. USA. 93, 12142–12149.

Vieira, V.A.R.O., Correia, T.G., Moreira, R.G., 2013. Effects of aluminum on the energetic substrates in neotropical freshwater *Astyanax bimaculatus* (Teleostei: Characidae) females. Comp. Biochem. Physiol. Part C 157, 1–8.

Vogel, C., de Sousa Abreu, R., Ko, D., Le, S.-Y., Shapiro, B.A., Burns, S.C., Sandhu, D., Boutz, D.R., Marcotte, E.M., Penalva, L.O., 2010. Sequence signatures and mRNA concentration can explain two-thirds of protein abundance variation in a human cell line. Mol. Syst. Biol. 6, 1–9.

Wajant, H., Henkler, F., Scheurich, P., 2001. The TNF-receptor-associated factor family - Scaffold molecules for cytokine receptors, kinases and their regulators. Cell. Signal. 13, 389–400.

Walton, R.C., McCrohan, C.R., Livens, F., White, K.N., 2010. Trophic transfer of aluminium through an aquatic grazer-omnivore food chain. Aquat. Toxicol. 99, 93–99.

Wan, G., Cheuk, W.K., Chan, K.M., 2009. Differential regulation of zebrafish metallothionein-II (zMT-II) gene transcription in ZFL and SJD cell lines by metal ions. Aquat. Toxicol. 91, 33–43.

Wang, D., Hu, J., Forthaus, B.E., Wang, J., 2011. Synergistic toxic effect of nano-Al_2O_3 and As(V) on *Ceriodaphnia dubia*. Environ. Pollut. 159, 3003–3008.

Wang, H., Ho, K.T., Scheckel, K.G., Wu, F., Cantwell, M.G., Katz, D.R., Horowitz, D.B., Boothman, W.S., Burgess, R.M., 2014. Toxicity, bioaccumulation, and biotransformation of silver nanoparticles in marine organisms. Environ. Sci. Technol. 48, 13711–13720.

Wang, K., Gross, A., Waksman, G., Korsmeyer, S.J., 1998. Mutagenesis of the BH3 domain of BAX identifies residues critical for dimerization and killing. Mol. Cell. Biol. 18, 6083–6089.

Wang, Y., Fang, J., Leonard, S.S., Rao, K.M.K., 2004. Cadmium inhibits the electron transfer chain and induces reactive oxygen species. Free Radic. Biol. Med. 36, 1434–1443.

Wang, Z., Gerstein, M., Snyder, M., 2009. RNA-Seq: a revolutionary tool for transcriptomics. Nat. Rev. Genet. 10, 57–63.

Warby, R. a F., Johnson, C.E., Driscoll, C.T., 2008. Changes in aluminum concentrations and speciation in lakes across the northeastern U.S. following reductions in acidic deposition.

Environ. Sci. Technol. 42, 8668–8674.

Ward, R.J.S., McCrohan, C.R., White, K.N., 2006. Influence of aqueous aluminium on the immune system of the freshwater crayfish *Pacifasticus leniusculus*. Aquat. Toxicol. 77, 222–228.

Warheit, D.B., Sayes, C.M., Reed, K.L., 2009. Nanoscale and fine zinc oxide particles: can *in vitro* assays accurately forecast lung hazards following inhalation exposures? Environ. Sci. Technol. 43, 7939–7945.

Warne, M.S.J., Dam, R. Van, 2008. NOEC and LOEC data should no longer be generated or used. Australas. J. Ecotoxicol. 14, 1–5.

Webb, P.A., Orr, C., 1997. Analytical methods in fine particle technology. Micromeritics Instrument Corporation.

Westerfield, M., 1995. The zebrafish book. A guide for the laboratory use of zebrafish (*Danio rerio*), 3rd Editio. ed. University of Oregon Press, Eugene, OR.

White, S.J.O., Hemond, H.F., 2012. The anthrobiogeochemical cycle of indium: a review of the natural and anthropogenic cycling of indium in the environment. Crit. Rev. Environ. Sci. Technol. 42, 155–186.

Wiecinski, P.N., Metz, K.M., Heiden, T.C.K., Louis, K.M., Mangham, A.N., Hamers, R.J., Heideman, W., Peterson, R.E., Pedersen, J.A., 2013. Toxicity of oxidatively degraded quantum dots to developing zebrafish (*Danio rerio*). Environ. Sci. Technol. 47, 9132–9138.

Wilhelm, B.T., Landry, J.-R., 2009. RNA-Seq—quantitative measurement of expression through massively parallel RNA-sequencing. Methods. 48, 249–257.

Williams, T.D., Diab, A.M., George, S.G., Godfrey, R.E., Sabine, V., Conesa, A., Minchin, S.D., Watts, P.C., Chipman, J.K., 2006. Development of the GENIPOL European flounder (*Platichthys flesus*) microarray and determination of temporal transcriptional responses to cadmium at low dose. Environ. Sci. Technol. 40, 6479–6488.

Wood, S.A., Samson, I.M., 2006. The aqueous geochemistry of gallium, germanium, indium and scandium. Ore Geol. Rev. 28, 57–102.

Xia, T., Kovochich, M., Liong, M., Mädler, L., Gilbert, B., Shi, H., Yeh, J.I., Zink, J.I., Nel, A.E., 2008. Comparison of the mechanism of toxicity of zinc oxide and cerium oxide nanoparticles based on dissolution and oxidative stress properties. ACS Nano 2, 2121–2134.

Xia, T., Zhao, Y., Sager, T., George, S., Pokhrel, S., Li, N., Schoenfeld, D., Meng, H., Lin, S., Wang, X., Wang, M., Ji, Z., Zink, J.I., Mädler, L., Castranova, V., Lin, S., Nel, A.E., 2011. Decreased dissolution of ZnO by iron doping yields nanoparticles with reduced toxicity in the rodent lung and zebrafish embryos. ACS Nano. 5, 1223–1235.

Xia, X.R., Monteiro-Riviere, N. a, Riviere, J.E., 2010. Intrinsic biological property of colloidal fullerene nanoparticles (nC60): lack of lethality after high dose exposure to human epidermal and bacterial cells. Toxicol. Lett. 197, 128–134.

Xiao, Y., Vijver, M.G., Chen, G., Peijnenburg, W.J.G.M., 2015. Toxicity and Accumulation of Cu and ZnO Nanoparticles in *Daphnia magna*. Environ. Sci. Technol. 49, 4657–4664.

Yamasaki, S., Yagishita, N., Nishioka, K., Nakajim, T., 2007a. The roles of synoviolin in crosstalk between endoplasmic reticulum stress-induced apoptosis and p53 pathway. Cell Cycle 1319–1323.

Yamasaki, S., Yagishita, N., Sasaki, T., Nakazawa, M., Kato, Y., Yamadera, T., Bae, E., Toriyama, S., Ikeda, R., Zhang, L., Fujitani, K., Yoo, E., Tsuchimochi, K., Ohta, T., Araya, N., Fujita, H., Aratani, S., Eguchi, K., Komiya, S., Maruyama, I., Higashi, N., Sato, M., Senoo, H., Ochi, T., Yokoyama, S., Amano, T., Kim, J., Gay, S., Fukamizu, A., Nishioka, K., Tanaka, K., Nakajima, T., 2007b. Cytoplasmic destruction of p53 by the endoplasmic reticulum-resident ubiquitin ligase "Synoviolin". EMBO J. 26, 113–122.

Yamazaki, H., Hiramatsu, N., Hayakawa, K., Tagawa, Y., Okamura, M., Ogata, R., Huang, T., Nakajima, S., Yao, J., Paton, A.W., Paton, J.C., Kitamura, M., 2009. Activation of the Akt-NF-κB pathway by subtilase cytotoxin through the ATF6 branch of the unfolded protein response. J. Immunol. 183, 1480–1487.

Yang, L., Hu, N., Jiang, S., Zou, Y., Yang, J., Xiong, L., Ren, J., 2014. Heavy metal scavenger metallothionein attenuates ER stress-induced myocardial contractile anomalies: role of autophagy. Toxicol. Lett. 225, 333–341.

Yin, H., Casey, P.S., McCall, M.J., Fenech, M., 2010. Effects of surface chemistry on cytotoxicity, genotoxicity, and the generation of reactive oxygen species induced by ZnO nanoparticles. Langmuir 26, 15399–15408.

You, J., Dou, L., Yoshimura, K., Kato, T., Ohya, K., Moriarty, T., Emery, K., Chen, C.-C., Gao, J., Li, G., Yang, Y., 2013. A polymer tandem solar cell with 10.6% power conversion efficiency. Nat. Commun. 4, 1446.

Zhang, K., 2010. Integration of ER stress, oxidative stress and the inflammatory response in health and disease. Int. J. Clin. Exp. Med. 3, 33–40.

Zhang, K., Kaufman, R.J., 2008. From endoplasmic-reticulum stress to the inflammatory response. Nature 454, 455–462.

Zhang, Y., Chen, Y., Westerhoff, P., Crittenden, J., 2009. Impact of natural organic matter and divalent cations on the stability of aqueous nanoparticles. Water Res. 43, 4249–4257.

Zhao, C.-M., Wang, W.-X., 2012. Size-dependent uptake of silver nanoparticles in *Daphnia magna*. Environ. Sci. Technol. 46, 11345–11351.

Zhao, X., Wang, S., Wu, Y., You, H., Lv, L., 2013. Acute ZnO nanoparticles exposure induces developmental toxicity , oxidative stress and DNA damage in embryo-larval zebrafish. Aquat. Toxicol. 136-137, 49–59.

Zhao, Y., Castiglioni, S., Fent, K., 2015. Synthetic progestins medroxyprogesterone acetate and dydrogesterone and their binary mixtures adversely affect reproduction and lead to histological and transcriptional alterations in zebrafish (*Danio rerio*). Environ. Sci. Technol. 49, 4636–4645.

Zhou, D., Keller, A. a, 2010. Role of morphology in the aggregation kinetics of ZnO nanoparticles. Water Res. 44, 2948–2956.

Zhu, B., Wu, Z.F., Li, J., Wang, G.X., 2011. Single and joint action toxicity of heavy metals on early developmental stages of Chinese rare minnow (*Gobiocypris rarus*). Ecotoxicol. Environ. Saf. 74, 2193–2202.

Zhu, X., Tian, S., Cai, Z., 2012. Toxicity assessment of iron oxide nanoparticles in zebrafish (*Danio rerio*) early life stages. PLoS One. 7, e46286.

Zhu, X., Wang, J., Zhang, X., Chang, Y., Chen, Y., 2009. The impact of ZnO nanoparticle aggregates on the embryonic development of zebrafish (*Danio rerio*). Nanotechnology. 20, 195103 (9pp).

Zimmermann, Y.-S., Niewersch, C., Lenz, M., Kül, Z.Z., Corvini, P.F.-X., Schäffer, A., Wintgens, T., 2014. Recycling of indium from CIGS photovoltaic cells: Potential of combining acid-resistant nanofiltration with liquid–liquid extraction. Environ. Sci. Technol. 48, 13412–13418.

Zimmermann, Y.-S., Schaeffer, A., Corvini, P.F.-X., Lenz, M., 2013. Thin-film photovoltaic cells: Long-term metal(loid) leaching at their end-of-life. Environ. Sci. Technol. 47, 13151–13159.

Zimmermann, Y.-S., Schäffer, A., Hugi, C., Fent, K., Corvini, P.F.-X., Lenz, M., 2012. Organic photovoltaics: potential fate and effects in the environment. Environ. Int. 49, 128–140.

Zotina, T., Köster, O., Jüttner, F., 2003. Photoheterotrophy and light-dependent uptake of organic and organic nitrogenous compounds by Planktothrix rubescens under low irradiance. Freshw. Biol. 48, 1859–1872.

Zucchi, S., Castiglioni, S., Fent, K., 2012. Progestins and antiprogestins affect gene expression in early development in zebrafish (*Danio rerio*) at environmental concentrations. Environ. Sci. Technol. 46, 518351–518392.

Zucchi, S., Mirbahai, L., Castiglioni, S., Fent, K., 2014. Transcriptional and physiological responses induced by binary mixtures of drospirenone and progesterone in zebrafish (*Danio rerio*). Environ. Sci. Technol. 48, 3523–3531.

Zurita, J.L., Jos, A., del Peso, A., Salguero, M., Cameán, A.M., López-Artíguez, M., Repetto, G., 2007. Toxicological assessment of indium nitrate on aquatic organisms and investigation of the effects on the PLHC-1 fish cell line. Sci. Total Environ. 387, 155–65.

CURRICULUM VITAE

Nadja Rebecca Brun

Born on September 16, 1984 in Baden, Switzerland

2011 - 2015	Doctoral thesis at FHNW and ETH
	in the Ecotoxicology group of Prof. Karl Fent, Switzerland
2014 - 2015	Research visit at the University of Birmingham, UK
2008 - 2010	Master studies in Environmental Geosciences
	at the University of Basel, Switzerland
	Master thesis: *"Assessing the fishtoxicity of sewage system biofilm and river sediment in the catchment area of the sewage treatment plant Mittleres Wynental, Switzerland"*
2005 - 2008	Bachelor studies in Geosciences with major in Environmental Geosciences and in-depth module in Biogeography
	at the University of Basel, Switzerland
2007	Exchange student at the University of Iceland in Reykjavík, Iceland
2002 - 2005	Gymnasium in Wettingen, Switzerland